EXPERIMENTAL AND NUMERICAL ANALYSIS OF THE EFFECTS OF TEST VARIABLES ON AUTO-IGNITION IN A RAPID COMPRESSION MACHINE

By

Chaitanya Wadkar

A DISSERTATION

Submitted to
Michigan State University
in partial fulfillment of the requirements
for the degree of

Mechanical Engineering - Doctor of Philosophy

2021

ABSTRACT

EXPERIMENTAL AND NUMERICAL ANALYSIS OF THE EFFECTS OF TEST VARIABLES ON AUTO-IGNITION IN A RAPID COMPRESSION MACHINE

By

Chaitanya Wadkar

Ignition delay measurements are frequently carried out in Rapid Compression Machines (RCMs). When data is compared from different RCM facilities, the ignition delay times are often inconsistent for any particular fuel at a specific compressed condition. The literature has attributed the discrepancy to experimental uncertainties and/or facility effects; however, this issue has yet to be examined more thoroughly. Due to the limited studies on understanding the effect of "facility-dependent" factors on low-temperature reactions and the subsequent ignition of the fuel, one of the main goals of this work is to determine the root cause of the discrepancy. Further analyzing the impact of these factors would facilitate the comparison of ignition delay results across RCM facilities. Additionally, validating chemical kinetic mechanisms against experimental data with these effects in mind would help yield more accurate and consistent ignition delay predictions. Different RCM facilities employ various combinations of compression ratio, initial temperature, initial pressure, diluent gas composition, etc., to achieve the same compressed conditions. Therefore, this work aims to determine the effects of different compression ratios, mixture preparation methods, and diluent gas composition on the measured ignition delay.

First, experiments and 0-D CHEMKIN simulations were carried out for stoichiometric mixtures of ethanol and air. To study the effect of diluent gas composition, two different mixtures, one consisting of nitrogen as the diluent gas and other consisting of argon were used. Additionally, this study also examined the effect of compression ratio and mixture preparation methods.

Furthermore, 3-D CFD simulations were carried out to investigate the consistent top-to-bottom flame propagation behavior observed in the optical experiments of ethanol auto-ignition.

Once a strong fundamental understanding of the factors causing discrepancies in ignition delay measurements of a simple fuel like ethanol was achieved, the study then moved on to a more complex fuel, iso-octane, which exhibits two-stage ignition delay and has a pronounced negative temperature coefficient (NTC) region. The iso-octane studies were focused on the effect of compression ratio; therefore, experiments and 0-D CHEMKIN simulations were carried out for rich mixtures (ϕ = 1.3) of iso-octane and air, using five different compression ratios. Using numerical analysis, the sensitivity of ignition delay to changes in compression ratio at different equivalence ratios and using different diluent gases was also studied.

The results show that the method used to obtain the compressed condition, particularly the use of different compression ratios and diluent gas compositions, can strongly influence the ignition delay times, especially under two-stage ignition conditions. Changes in compression ratio and/or diluent gas composition leads to changes in initial conditions and post-compression heat loss. It was observed that a reduction in post-compression heat losses led to shorter ignition delay times. Furthermore, changing the compression ratio also changes the value of t_{50}, defined as the duration of the last 50% pressure rise during compression. For conditions at which the ignition delay time is short (<15 ms), a longer t_{50} initiates reactivity prior to the end of the compression stroke, thus reducing the ignition delay time. This range of simulation and experimental conditions helps provide a diverse array of auto-ignition results, involving single-stage and two-stage auto-ignition fuels.

ACKNOWLEDGEMENTS

I would first like to thank my advisor Dr. Elisa Toulson for giving me this opportunity to pursue a PhD degree under her guidance. She has been a great supervisor and a mentor, and I would not be where I am today without her guidance. Thank you for sharing your expertise and assisting me in growing and becoming a better researcher along the way.

I am incredibly grateful to my committee members, Dr. Indrek Wichman, Dr. Patton Allison and Dr. Christopher Saffron, for their constructive feedback and guidance over all these years.

The friendship and collaboration I received from my research tema has been another important factor in completing my PhD. Thank you to Dr. Prasanna Chinnathambi, Berk Can Duva and Tom Stueken; their willingness to assist me with any and every aspect over the course of my PhD did not go unnoticed. I also would like to acknowledge Shashank Gowda for his help with post-processing the RCM data and I wish him all the best for his future.

Thank you to all my students for allowing me to guide you through your engineering studies, even though it was just for a short time. They all helped me develop a lot of confidence in my engineering skillset, for which I am truly grateful.

I also wanted to thank my Master's adviser, Dr. Bassem Ramadan of Kettering University, for encouraging and inspiring me to pursue a PhD degree. I appreciate all the guidance he has provided me so far.

Thank you to my family and friends, both near and far, for forcing me to have some fun every now and then and for helping me come out of this experience with a sound mind. I value them for sticking by my side through it all, whether they could fully comprehend the complexity of my research or simply understood the stress that the graduate school had to offer.

Finally, I am eternally grateful to my parents and immediate family for their constant efforts and sacrifices. My deepest gratitude goes to them for always believing in me and being supportive of my ventures.

TABLE OF CONTENTS

LIST OF TABLES

LIST OF FIGURES

KEY TO ABBREVIATIONS

$(dP/dt)_{max}$	Maximum Rate of Pressure Rise
0-D	Zero Dimensional
2-D	Two Dimensional
3-D	Three Dimensional
Ar	Argon
BDC	Bottom Dead Center
CFD	Computational Fluid Dynamics
CFL	Courant–Friedrichs–Lewy numbers
CH_2O	Formaldehyde
CH4	Methane
CO	Carbon Monoxide
CO_2	Cabon Dioxide
$C_{p, a}$	Heat capacity of the gas ’a’
$C_{p, mix}$	Heat capacity of the mixture
CR	Compression Ratio
deg. C	degree Celsius
DME	Dimethyl Ether
dP/dt	Rate of Pressure Rise
DRGEPSA	Direct Relation Graph with Error Propagation and Sensitivity Analysis
DTC	Direct Test Chamber
EOC	End of Compression
FSID	First-stage Ignition Delay

GC/MS	Gas Chromatography–Mass Spectrometry
GC-FID	Gas Chromatography–Flame Ionization Detector
GC-TCD	Gas Chromatography-Thermal Conductivity Detector
GDI	Gasoline Direct Injection
H_2	Hydrogen
H_2O_2	Hydrogen Peroxide
HO_2	Hydroperoxyl radical
HRR	Heat Release Rate
IDT	Ignition Delay Time
J	Joule
JSR	Jet Stirred Reactor
K	Kelvin
L	Litre
LES	Large Eddy Simulation
LLNL	Lawrence Livermore National Laboratory
m	metre
mm	milli-metre
mol	mole
ms	milli-second
M	third-body
MSU	Michigan State University
N_2	Nitrogen
NTC	Negative Temperature Coefficient
O_2	Oxygen
OH/OH*	Hydroxyl Radical

P_c	Compressed Pressure
PISO	Pressure Implicit with Splitting of Operators
$QOOHO_2$	Alkyl peroxide radicals
RANS	Reynolds-Averaged Navier-Stokes
RCM	Rapid Compression Machine
RO_2	Alkylperoxy radical
rpm	revolutions per minute
s	seconds
SA/V	surface area-to-volume ratio
t	time
t_{50}	Time for the last 50% of the pressure rise to occur during the compression phase
T_c	Compressed Temperature
TDC	Top Dead Center
TTL	Transistor-Transistor Logic
U.S	United States
W	Watts
γ	ratio of specific heats
η	chemical effect
$\eta_{\text{post-compression heat loss, first-stage}}$	Effect of post-compression heat loss on first-stage ignition delay time
$\eta t_{50,\text{ first-stage}}$	Effect of t_{50} on first-stage ignition delay time
$\eta_{\text{post-compression heat loss, pressure rise}}$	Effect of post-compression heat loss on pressure rise due to first-stage ignition
$\eta_{\text{post-compression heat loss, second-stage}}$	Effect of post-compression heat loss on second stage ignition delay time

$\eta_{\text{post-compression heat loss, total ignition delay}}$	Effect of post-compression heat loss on total ignition delay time
$\eta_{\text{post-compression heat loss}}$	Effect of post-compression heat loss
$\eta t_{50,\text{ pressure rise}}$	Effect of t_{50} on pressure rise due to first-stage ignition
$\eta t_{50,\text{ second-stage}}$	Effect of t_{50} on second-stage ignition delay time
$\eta t_{50,\text{ total ignition delay}}$	Effect of t_{50} on total ignition delay time
σ_{Pc}	Standard deviation of normal distribution of compressed pressure
σ_{Ti}	Standard deviation of normal distribution of initial temperature
τ	Total ignition delay time
τ_1	First-stage Ignition Delay time
τ_2	Second-stage Ignition Delay time
τ_{Ar}	Total ignition delay time with argon as diluent
$\tau_{\text{modified N2}}$	Total ignition delay time with the heat capacity of nitrogen set to the same value as that of argon
τ_{N2}	Total ignition delay time with nitrogen as diluent
ϕ	Equivalence Ratio
P_i	Initial Pressure
T_i	Initial Temperature
χ_a	mole fraction of gas 'a'

Chapter 1. INTRODUCTION

1.1. Background and Motivation

Fundamental combustion research typically starts from chemical ignition studies and flame-speed measurements. Chemical ignition experiments are most commonly carried out using one of three testing methods which allow the exploration of ignition properties without the use of an internal combustion engine: flow reactors, shock tubes and Rapid Compression Machines (RCMs). Ignition delay time data provide valuable benchmark results for validation and refinement of the chemical reaction mechanisms used in many combustion simulations. An excellent apparatus to isolate the auto-ignition process from the complex in-cylinder engine flow conditions is an RCM. RCMs are used for studying the ignition behavior of fuels at low to moderate temperature conditions relevant to existing and future combustion technologies [1]. An RCM simulates a single stroke of an internal combustion engine by rapidly compressing a piston into a cylinder containing a reactive fuel and oxidizer mixture. As a result, RCMs enable combustion studies at elevated pressure (compressed pressure ~5-40 bar) and intermediate temperatures (compressed temperature ~600-1100 K) [2]. In an RCM, the experimental duration is limited on the high end by the adiabatic core hypothesis losing validity above ~100 ms [3] and on the low end by pre-compression reactions influencing very short ignition delays (<3 ms) [4]. RCM ignition delay measurements help to validate chemical kinetic mechanisms which are made up of elementary reactions. Kinetic mechanisms are developed to predict what happens during combustion. These mechanisms can be used to predict the chemical behavior and the products of chemical reactions through numerical simulations while using fewer resources than physical experiments and offering additional insight into the combustion process. Although RCMs are an excellent tool to study auto-ignition, limited

information can be extracted from the pressure profiles. Using optical measurements can provide supplemental information and aid in a better understanding of the ignition characteristics in detail.

All RCMs would ideally provide identical data for similar test conditions. However, a huge scatter in the reported ignition delay data has been observed across past studies involving various fuels. With RCMs being increasingly used to investigate the ignition behavior of fuels, there is an urgent need to address the disagreement in the ignition delay times reported by different RCMs at near-identical conditions. The parameters inherent to RCM design, such as the geometry of the RCM, piston crevice design, compression time, etc., are often the attributable factors responsible for the inconsistencies in auto-ignition delay measurements. These inherent parameters contribute to unique heat loss characteristics of the RCM and differ from facility to facility. Furthermore, the different methods adopted to achieve a given compressed condition, such as changing the diluent gas composition, preheating, compression ratio, etc., change the initial conditions needed, affecting the thermodynamic conditions and thereby influencing the ignition event. To date, however, there have only been limited studies that have investigated facility effects including participants in the 1st RCM Characterization Initiative [1,5], which concentrated on assessing iso-octane ignition delay due to the large variability in the literature data [6], especially in the negative temperature coefficient (NTC) region. However, the complications of NTC and multi-stage ignition behavior of iso-octane made the data analysis difficult and these challenges motivated a 2nd Characterization Initiative, this time focused on measuring ethanol ignition delay times, due to the lack of NTC behavior with ethanol. The current study was partially motivated by the participation of MSU in the 2nd RCM characterization initiative where an effort was made to contribute to understanding the differences in separate rapid compression machine facilities and to make experimental data reliable and easier to compare across facilities. While participating,

several test variables that affected ignition delay times at the same compressed conditions within the facility itself were encountered and an independent investigation was performed and is discussed in this work.

1.1.1. Current status of ethanol auto-ignition research

Ignition delay studies have already been performed with the help of shock tubes [7–9] and RCMs [10,11], for stoichiometric ethanol-air mixtures with pressures greater than 10 atm and temperatures ranging from 750 K to 1400 K. Numerous studies have also focused on chemical kinetics of ethanol combustion using various methods such as laminar flames [11–14], shock tubes [7–9,15–17], flow reactors [18–20], jet-stirred reactors [21,22] and RCMs [7,10,23–26]. Ethanol auto-ignition has been studied in shock tubes, for argon diluted mixtures with equivalence ratios (ϕ) of 0.5, 1 and 2, mostly at high temperatures (greater than 1100 K) and at pressures ranging between 1 to 10 atm [7–9,15–17,27]. Ignition delay measurements of ethanol at ϕ= 0.3 and 1.0, temperatures in the range of 770–1250 K and pressure ranging from 10 bar to 40 bar were performed by Cancino et al. [9] in a shock tube. A study by Lee et al. [7] focused on determining IDTs for stoichiometric ethanol-air mixtures in a shock tube at temperatures in the range of 775–1000 K and at 80 bar pressure and also in an RCM at a pressure of 35 bar. Lee et al. [7] also obtained Schlieren images of ethanol auto-ignition in the shock tube, which showed deflagrative behavior. The corresponding pressure measurements and emission signals recorded also showed strong pre-ignition behavior as pressure increased by more than 100% in some cases prior to auto-ignition. However, no such pre-ignition pressure rise was reported by Cancino et al. [9]. In a recent study by Büttgen et al. [25], a gradual increase in pressure about 20 ms after the end of compression (EOC) until auto-ignition was observed. They also observed pre-ignition flame kernels in a few of their tests that shortened the ignition delay considerably. Many numerical and experimental studies

on various fuels have concluded that two distinct ignition regimes are observable; the first described with various terms, such as volumetric, ideal, or strong as seen in the case of homogeneous ignition and the second one being the propagation of a reaction front prior to volumetric ignition or, in other words, mild/deflagration regime as seen in the case of inhomogeneous ignition [23,28–31]. In a high speed OH* luminescence study by Büttgen et al. [25] using an RCM, they observed 4 fronts namely, the flame kernel, ignition front, and reaction fronts α and β, all of which differed in their propagation speed. Barraza-Botet and Wooldridge [23,24] investigated pure and blended ethanol mixtures using a high-speed camera, observing only homogeneous ignitions. Despite ethanol's long existence and well-known relevance and benefits, there remains limited experimental studies on ethanol auto-ignition behavior at engine relevant conditions. For this purpose, the auto-ignition of ethanol was studied at conditions that not only complement but also expand on prior studies in the literature.

In Figure 1-1, there is a clear demonstration of the discrepancy in the ignition delay time (IDT) values of ethanol at identical compressed conditions from different facilities. The data shown in the plot was obtained only from RCMs and was reported in the works of Mittal et al. [10], Lee et al. [7], Barazza-Botet et al. [24], Büttgen et al. [25] and Lee et al. [26]. It should be noted that all of the data shown in Figure 1-1 is presented as it was reported in the literature and no scaling was used for the literature data or for the data from the current study, in the creation of this figure.

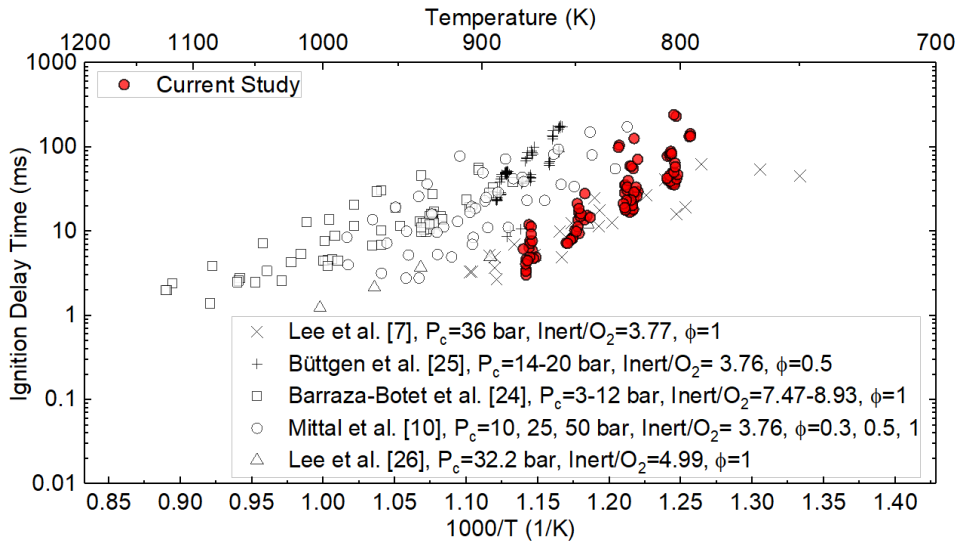

Figure 1-1: Summary of ethanol ignition delay time from RCMs without any scaling studied in this work and available in the literature [7,10,24–26].

1.1.2. Current status of iso-octane auto-ignition research

Iso-octane, or 2,2,4-trimethyl pentane, has been used for many years as a primary reference fuel and also as a simple chemical surrogate for gasoline. For fuels with an octane number less than 100, the octane number is defined by comparison with a mixture of iso-octane (assigned an octane rating of 100) and n-heptane (octane rating of 0) which has the same anti-knock capacity as the fuel [32,33]. For fuels with an octane number above 100, the antiknock quality of the fuel is determined in terms of iso-octane plus milliliters of the antiknock additive, tetraethyl lead, per U.S gallon [32,33]. As a model compound for branched alkane species found not only in gasoline [34], but also in diesel [35] and jet fuels [36], iso-octane has attracted considerable attention and due to its relevance to practical liquid fuels, it has been the subject of numerous experimental and kinetic modeling studies [6,28,35–72]. Various experimental methods have been adopted to study the chemical kinetics of iso-octane combustion, such as shock tubes [37–43], flames [44–54], jet stirred reactors [55–57], and flow reactors [58,59]. A variety of kinetic measurements have been made in these studies, including ignition times, species concentrations and flame-speeds.

Additionally, several modeling studies have been reported in recent years, involving the development of detailed and reduced mechanisms [44,60–63] and the adoption of these mechanisms to study the iso-octane ignition behavior via chemical kinetics [6,28,39,64–68]. Iso-octane has been studied previously in numerous RCMs, [28,64–66,69,71–75] and a selection of this data for stoichiometric mixtures of iso-octane and air at different pressures and levels of dilution is shown in Figure 1-2. From the figure, it can be seen that there is some scatter in the ignition delay times measured in different facilities but at identical compressed conditions. Goldsborough et al. [6] developed a correlation for iso-octane that involves dependencies for equivalence ratio, pressure, oxygen percentage and activation energy. The authors of that study plotted the raw data obtained from several RCMs and shock tubes [28,37–39,41,66,71,72,75–84] and observed that the spread in data is more pronounced in the low-temperature regime of 645–870 K. Even after data normalization using the developed correlation, a standard deviation of ±34% was observed. The authors attribute the departures from the correlation to an incomplete description of the functional dependencies, some inconsistencies about diluent composition, experimental uncertainties, and facility-influenced phenomena. This implies that there are factors other than those considered in the correlation that cause the discrepancy in the data.

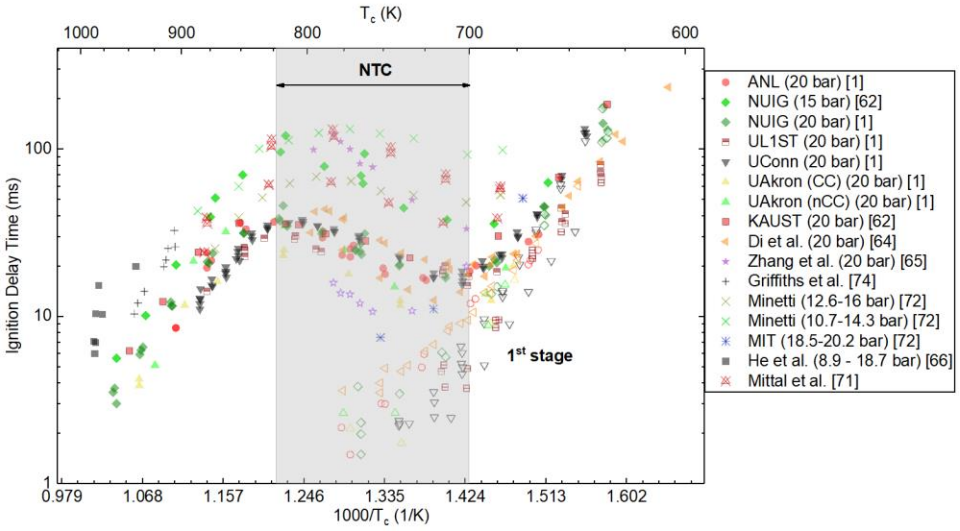

Figure 1-2: Results comparing several RCM ignition delay data for stoichiometric mixtures of iso-octane and air at different levels of dilution, as reported in [1,62,64–66,71,72,74].

1.1.3. Current status of research addressing the discrepancy in auto-ignition delay data

Across the studies reviewed earlier, it can be observed that the inert/O_2 ratios varied from 3.76 to as high as 12. Diluent gas composition is often varied to achieve different compressed temperatures while maintaining the same compression ratio. Depending on the heat capacity requirements needed to achieve the desired compressed temperatures, the diluent gas composition can be adjusted by adding or substituting part of the non-reactive mixture with inert gases such as argon, carbon dioxide, nitrogen, etc. However, using different diluent gases can affect the IDTs of the mixture at same compressed conditions, primarily by altering the heat loss characteristics and also by changing the third body efficiencies [64]**.** There have been a number of studies that have addressed the influence of diluent gases on iso-octane ignition delay measurements. Up to a 50% difference in ignition delay time, depending on the reaction mechanism used, was shown in a modeling study of auto-ignition of iso-octane with argon and nitrogen as buffer gases by Davidson and Hanson [85]. Würmel et al. [67] concluded that, because of the longer time scales observed in

an RCM as compared to shock tubes, argon retarded the ignition process in an RCM but accelerated it in a shock tube. Shen et al. [39] also observed 20% shorter IDTs using argon as a diluent for iso-octane mixtures, when compared to nitrogen. The primary reason for the behavior was attributed to the difference in post-compression heat losses governed by the thermal capacities of the various diluent gases. Wagnon and Wooldridge [68] found that the buffer gases had a significantly higher effect on total ignition delay times during two-stage ignition on fuels exhibiting NTC behavior. Di et al. [64] observed that at conditions exhibiting two-stage ignition within the NTC region, the buffer gas composition significantly influenced the ignition. However, the first-stage ignition was found to be less affected by the buffer gas composition. The difference in heat capacities of CO_2 and N_2 caused a difference in the first-stage heat release and the subsequent pressure and temperature rise during the first-stage ignition. Di et al. [64] also investigated and found that higher collision efficiency reduced ignition delay times. Zhang et al. [65] explored two-stage ignition in the NTC region for stoichiometric mixtures of iso-octane/O_2/N_2/Ar and concluded that the first-stage ignition delay was sensitive to O_2 concentration but was insensitive to the dilution gas composition and fuel concentration. Chinnathambi et al. [69] investigated the dilution effect of CO_2 on iso-octane for various equivalence ratios at engine relevant conditions. The NTC region temperature range was not altered with increasing CO_2 dilution levels, for each equivalence ratio. However, at a compressed pressure (P_c) of 20 bar the ignition delay times increased by a factor of 3 for 30% CO_2 dilution levels as compared to 15% dilution. Part of the data presented by Chinnathambi et al. [69], specifically for ϕ=1.3 and 0% CO_2 dilution at compressed temperature (T_c) of 835 K and 880 K using a compression ratio (CR) of 17.1, has been used for comparisons made in this study as the data was collected in the same rapid compression machine that was used in the current study.

Recent RCM review papers by Sung et al. [87], Goldsborough et al. [1] and Kéromnès et al. [88] have focused on facility dependence. The review by Goldsborough et al. [1] examines the experimental and computational approaches that help in understanding the role of physical-chemical interactions; while those by Sung and Curran [87] focus primarily on the operational principles and design features of RCMs which help suppress roll-up vortices and support the assumption of the adiabatic core hypothesis. The significance of modeling RCM experiments to account for the compression stroke and post-compression heat losses is discussed in detail by Sung and Curran [87]. Mittal et al. [89] also demonstrated the importance of modeling the full RCM compression stroke when comparing experiments to kinetic simulations. The significance has been attributed to the radical initiation processes that begin just before the EOC and is also found to be one of the factors affecting the ignition delay times in this study depending on the compression characteristics (compression ratio and compression speed).

The discrepancy observed in the auto-ignition delay data has also been attributed to the temperature inhomogeneities in the combustion chamber that is unique to each facility depending on the RCM configuration. Several computational fluid dynamics (CFD) studies have been carried out to characterize flow fields for various RCMs. The main emphasis has been on optimizing the piston crevice design to suppress the roll-up vortex [3,71,90–93] and the characterization of turbulent flow in an RCM [94–99]. Several studies have been focused on the suppression of the roll-up vortex as it is the main reason for the temperature inhomogeneities observed in an RCM. The need for a crevice piston to support the adiabatic core led to several CFD studies focused on optimization of the crevice design [71,90,91,100]. Furthermore, in order to eliminate gas flows into the crevice during multi-stage ignition, recent works have aimed at investigating the crevice containment strategy [101–104]. The technique of `crevice containment' aims to mitigate the

unintended mass transfer from the reaction chamber to the crevice, especially during the first-stage of the two-stage ignition, by engaging a physical partition between the combustion chamber and the piston crevice at the end of the compression. The review by Kéromnès et al. [88] discusses the different types of designs employed in RCM ignition studies, which helps to achieve a basic understanding of the possible factors that influence ignition delay measurements. Recent works by Yousefian et al. [100,105] aid in predicting temperature inhomogeneities in any RCM configuration and gas mixture using computational efforts based on a dimensionless measure that is primarily dependent on the Peclet number, aspect ratio (i.e., bore radius divided by stroke), and crevice volume in order of decreasing importance. Bourgeois et al. [106,107] presented a process to validate a crevice design based on the parameters that influence the suppression of roll-up vortices which involves predicting the critical mass that is needed to be transferred to the crevice in order to guarantee its efficiency and whether a specific crevice volume is likely to absorb this mass during the compression stroke. In a recent study by Ezzell et al. [108], it was shown through simulations that faster compression time and larger crevice volumes both increased the rate of heat loss from the crevice which in turn led to longer ignition delay times. Furthermore, varying the initial conditions or the RCM configurations was observed to have a greater effect on the ignition delay of the fuels exhibiting two-stage ignition behavior as compared to those showing only single-stage ignition. The study by Ezzel et al. [108] focused on the role of crevice volume and compression times, as a result of which the rate of heat loss was observed to be affecting the ignition delay times.

These works [1,39,64,67,68,71,85,87–91,100–108] provide significant insight into how fluid flow and heat losses impact the reaction chamber conditions and homogeneity, which in turn affect ignition delay measurements.

1.2. Research Objectives

Under ideal conditions, all RCMs would provide identical data for similar experiments; however, data discrepancies have been observed across past studies involving various fuels, as observed in Figure 1-1 and Figure 1-2. In RCMs, the same compressed conditions can be reached by a variety of combinations of compression ratio, initial temperature, initial pressure, diluent gas composition, etc. The literature review shows that to date, there have been only limited studies on understanding the effect that these parameters have on the distribution of the fuel in the combustion chamber, temperature homogeneity, low-temperature reactions, and the subsequent ignition of the fuel. It has previously been assumed that the value of ignition delay for a given fuel and at a given set of compressed conditions, would be the same, irrespective of the variety of the above-mentioned combinations that were used to achieve the compressed conditions. In an effort to address this assumption, the objective of this work is to determine which components of RCM testing have the strongest connection to the data discrepancy. Additionally, it can be difficult to understand the complex processes going on inside the combustion chamber through only experiments, and numerical analysis can aid in our understanding of these processes. In this study, experimental and numerical analysis in the form of chemical kinetic model predictions of the effects that different compression ratios, diluent gases and charge preparation method have on ignition delay was performed. Efforts were made to study the sensitivity of ignition delay to the charge preparation method, diluent gases and compression ratio that would help determine which parameter would have the greatest effect on the ignition delay. Moreover, changing the compression ratio, in turn, changes many other operating parameters, such as the initial conditions required to achieve the same compressed conditions, compression time, surface-area-to-volume ratio and another operating parameter called t_{50}. The influence of each of these parameters on the

ignition delay times was isolated and studied for a mixture of various equivalence ratios and diluent gas compositions. The surface-area-to-volume ratio can be used as a measure of the post-compression heat losses observed in RCM experiments.

The aim of this project is to answer the following research questions:

- What are the reasons behind the discrepancies in measured auto-ignition delay data at identical compressed conditions? Which components of RCM testing have the strongest connection to the data discrepancy?
- Do the post-compression heat loss and t_{50} have a larger impact on ignition delay times at certain equivalence ratios?
- Do the post-compression heat loss and t_{50} affect ignition delay times more for a particular diluent gas?
- Do the post-compression heat loss and t_{50} affect the first-stage of the two-stage ignition process? Does a given factor affect a particular stage more than the other?
- Is this discrepancy also observed during numerical analysis of RCM experiments? What other factors can potentially contribute other than those observed experimentally?

In order to answer the research questions, the following objectives were set:

1.2.1. Experimental Objectives

- Examine the effects of mixture preparation methods, compression ratios and diluent gas composition on ethanol and iso-octane IDTs and heat release rates for various equivalence ratios.

1.2.2. Modeling Objectives

- Generate volume profiles, to accurately simulate an RCM, derived from the non-reactive experiments conducted at different compression ratios, consisting of different diluent gases.
- Use these volume profiles to conduct 0-dimensional (0-D) analysis with the help of validated kinetic mechanisms and support the experimental results to confirm the effects of compression ratios, diluent gas composition on ethanol and iso-octane IDTs for various equivalence ratios.
- Gain further insight into the reasons behind discrepancies in IDTs of ethanol and iso-octane that cannot be observed through experiments.

1.3. Structure of the Dissertation

This thesis aims at identifying the factors causing a discrepancy in auto-ignition delay data at identical compressed conditions using an RCM. An overview of the current research status of auto-ignition of ethanol, iso-octane and factors affecting ignition delay times in RCMs is provided in the present chapter. Lastly, the research questions and main objectives are summarized. Chapter 2 provides an overview of the Michigan State University (MSU) RCM facility and modifications that were required to conduct the auto-ignition experiments. Chapter 3 discusses the details of the numerical modeling required to simulate auto-ignition experiments. The fourth and sixth chapters present the experimental results of ethanol and iso-octane, respectively. In Chapter 4, the ignition characteristics and heat release rates of ethanol under a variety of combinations of compression ratio, mixture preparation method and diluent gas composition are discussed. This chapter also investigates the optimum mixing time required to prepare a homogeneous charge mixture in a mixing tank. A factor that was determined to be important in consistent ignition delay

measurements was the cleanliness of the combustion chamber and some discussion on the suggested protocol is also included. Chapter 6 investigates the effects of changing the compression ratio on the two-stage ignition and also in the NTC region of iso-octane. Model predictions validated against experimental data are presented and compared in Chapter 5 and Chapter 7. Chapter 5 analyzes and discusses the kinetic modeling results of ethanol and further investigates the chemical and thermal effect of diluent gases. Additionally, CFD modeling results are presented in an attempt to explain the ignition behavior of ethanol observed in the optical experiments. Chapter 7 analyzes and discusses the kinetic modeling results of iso-octane and expands on the experimental results to study the sensitivity of the factors affecting ignition delay time to various diluent gases and equivalence ratios. The final chapter summarizes the research conclusions and achievements in addition to providing recommendations for future research.

The research that is presented in this work has been compiled from previously published papers and from manuscripts that are currently in preparation. For convenience, these publications are referenced here, and the reader is directed to them for additional information:

- Ferliga, F., Dooley, S., Horward, M., Leahy, L., [and 24 others, including **Wadkar, C.**], "Rapid Compression Machine Workshop 2nd Characterization Initiative – Ethanol Ignition", poster presentation at the 37th International Symposium on Combustion, 2018.
- Wadkar, C., Chinnathambi, P., and Toulson, E., "An Experimental Study on the factors affecting Ignition Delay of Ethanol in a RCM," SAE Technical Paper 2019-01-0576, 2019.
- Wadkar, C., Chinnathambi, P., and Toulson, E., "Analysis of rapid compression machine facility effects on the auto-ignition of ethanol", Fuel 2020; 264.

- Wadkar, C., Chinnathambi, P., and Toulson, E., “Effect of Changing Compression Ratio on Ignition Delay Times of Iso-Octane in a Rapid Compression Machine”, SAE Technical Paper 2020-01-0338, 2020.
- Wadkar, C., and Toulson, E., “A numerical study of the effect of changing compression ratio on the auto-ignition of iso-octane in an RCM”, Fuel 2021; 291.
- Wadkar, C., and Toulson, E., “A CFD Study of the effect of initial temperature inhomogeneities and buoyancy on the auto-ignition behavior of ethanol in an RCM”, Energy and Fuels, manuscript under review.

Chapter 2. EXPERIMENTAL SETUP

2.1. Rapid Compression Machine

The experiments completed for this research were performed in an RCM which was designed, built and characterized at MSU [109–112]. The RCM consists of a 2-inch diameter combustion chamber in which an air/fuel mixture is rapidly compressed by piston motion to engine relevant conditions. This piston is pneumatically driven and hydraulically stopped with an optimized pin and groove mechanism [112]. The RCM consists of three pistons that are all mounted on the same shaft: the pneumatic piston, hydraulic piston and combustion chamber piston. The pressurized air acting on the pneumatic piston serves as the driving force, while the high-pressure oil in the hydraulic reservoir provides a holding force for the system, during operation. A solenoid valve vents the high-pressure oil from the hydraulic chamber when triggered. The no longer restrained piston system is now driven forward until the hydraulic piston is stopped due to a mechanical interference towards the end of the hydraulic chamber. The hydraulic piston governs the motion of the RCM piston. Depending on where the hydraulic piston touches the stroke adjustment shim, the starting position of the stroke is determined. Additionally, the end of the stroke occurs when the hydraulic piston strikes the stopping ring. The RCM piston assembly is hydraulically stopped by a cupped piston that enters a groove filled with oil to generate hydraulic pressure and decelerate the piston. A schematic of the RCM and the various components that makeup the RCM facility is shown in Figure 2-1.

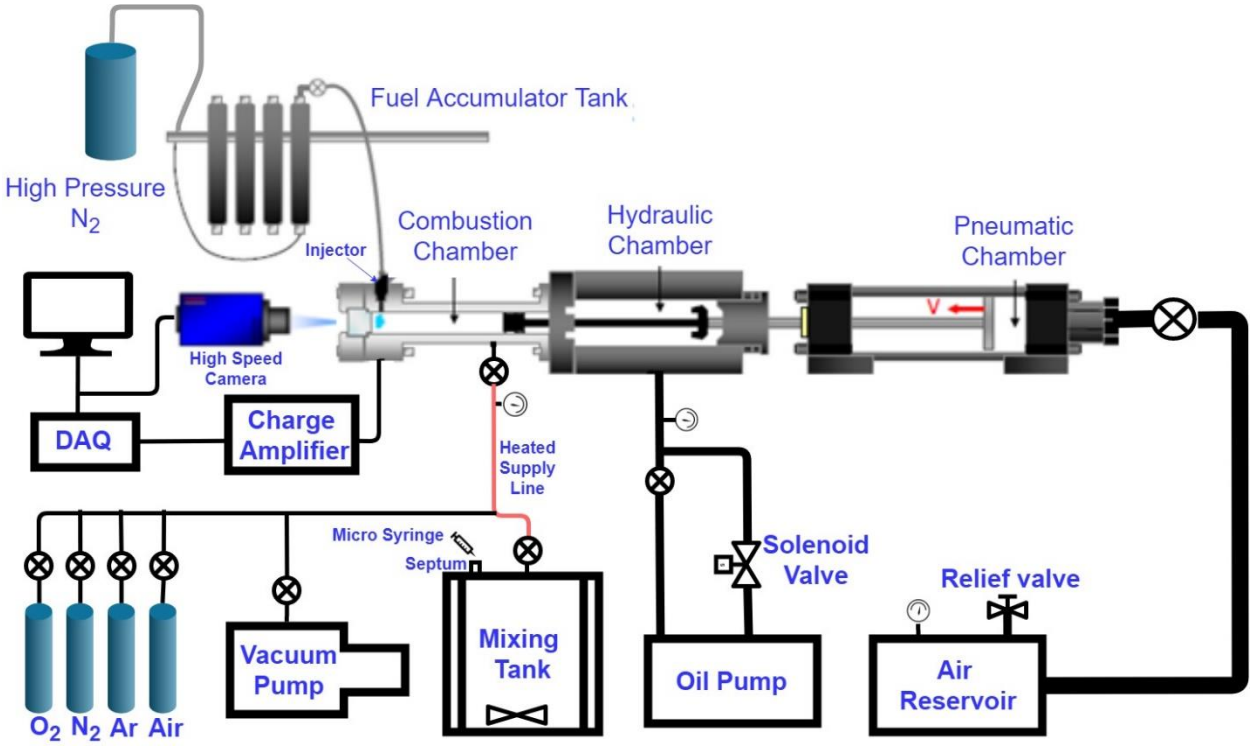

Figure 2-1: RCM test facility at MSU.

The CR can be varied by adjusting the stroke length, which in turn is achieved by adding shims either in the back or the front of the hydraulic chamber. Adding shims behind the hydraulic chamber changes the Bottom Dead Center (BDC) volume but the Top Dead Center (TDC) volume remains the same, increasing the CR. On the other hand, adding shims in the front of the hydraulic chamber maintains the same stroke length but changes both the TDC and BDC volume, thereby reducing the CR. Additionally, a stepped metal window, as shown in Figure 2-2 and Figure 2-3 (b), consisting of a step on one of its faces, can be used to alter the TDC volume. The additional step decreases the TDC and BDC volume when introduced into the test chamber, thereby increasing the CR for a given stroke length. The RCM head can be equipped with either a metal window or a quartz window. The quartz window enables optical access to the entire combustion chamber, Figure 2-3 (a). However, the quartz window does not have a step because incorporating a step reduced the structural integrity of the window to withstand the combustion pressure, Figure

2-3 (c); hence optical results were achieved only for the compression ratios achievable by adding or removing shims in front of and/or in the back of the hydraulic chamber. A Photron SA4 high-speed camera along with a 105 mm, 1:2.8G, AF-S Micro Nikkor lens was used for the high-speed imaging of the ignition process. A frame rate of 10,000 frames per second with a shutter speed of 1/(2 x frame rate) was used. The resolution was set at 512 x 512. No wavelength filter or laser excitation was used.

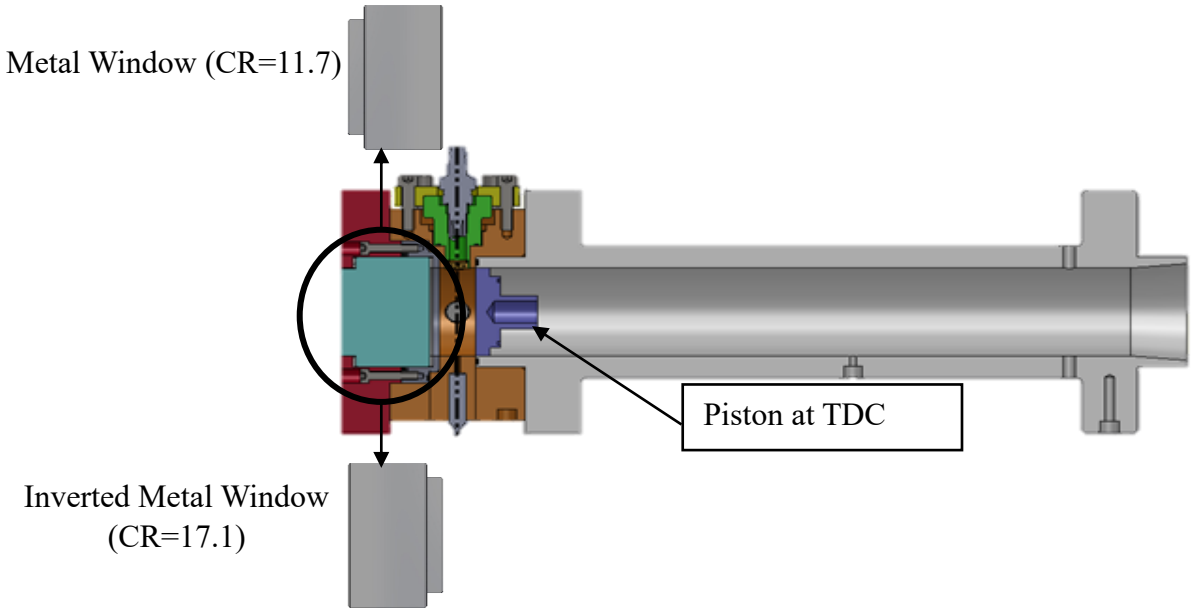

Figure 2-2: Schematic of the RCM showing the configuration of the stepped metal window used for increasing or decreasing TDC volume.

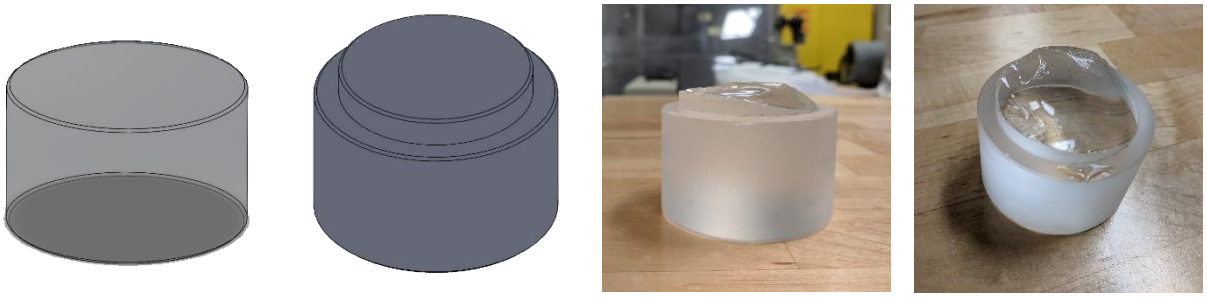

(a) (b) (c)

Figure 2-3: (a) Optical Window without the step, (b) Stepped Metal Window and (c) Broken Optical Windows with step.

The compression process takes approximately 30 ms. Once the piston reaches TDC, the air/fuel mixture is compressed to an elevated pressure and temperature suitable for combustion. The piston is held in place by the driving force of the air, which remains greater than the force of compressed/burning mixture and hence allows for combustion to occur at constant volume conditions.

The piston consisted of a crevice design to avoid roll-up vortices during compression and ensure a homogeneous temperature field in the combustion chamber [92]. The geometry of the creviced is based on the optimized design of Mittal and Sung [71], and can be seen in Figure A-1 of Appendix.

National Instruments® hardware and LabVIEW® VIs were used for controlling and acquiring data from the RCM. The dynamic pressure during and after compression was measured at 100 kHz sampling frequency using a piezoelectric pressure transducer (Kistler 6125B) and a charge amplifier (Kistler Type 5010 Dual-Mode Amplifier). The temperature of the combustion chamber and the manifold was maintained using 6 heating bands with feedback provided by 6 type T thermocouples as shown in Figure 2-4. The results confirmed a uniform initial temperature along the combustion chamber within a standard deviation of ±0.5 K. Furthermore, an insulation jacket is used to minimize the heat transfer to the surroundings.

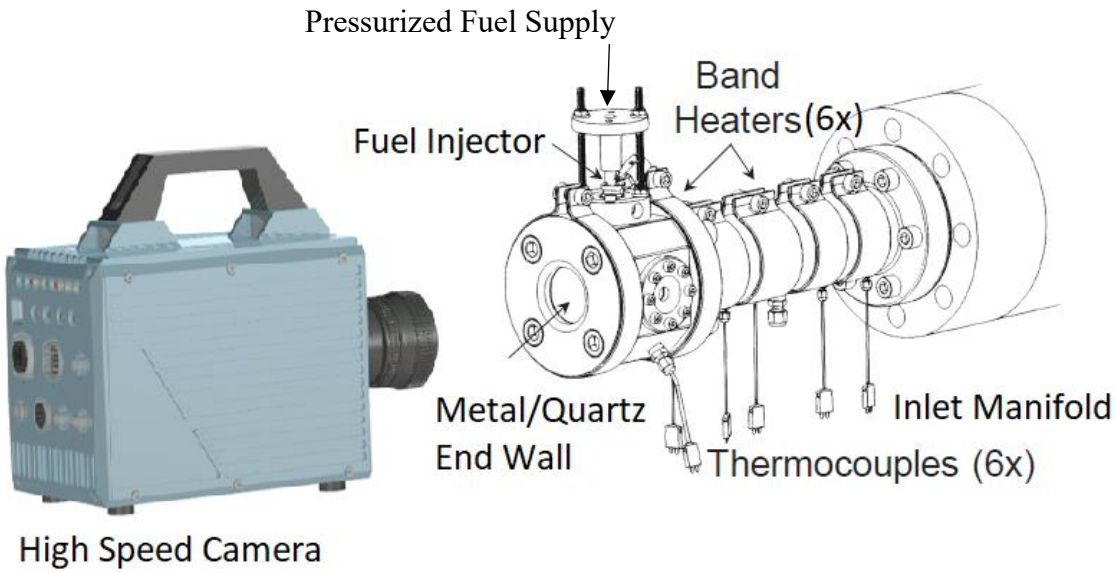

Figure 2-4: View of RCM combustion cylinder with component locations and connections for auto-ignition studies.

2.2. Mixture Preparation

Prior to performing auto-ignition tests, the combustion chamber is evacuated of all gasses using a vacuum pump through a small port at the bottom of the combustion cylinder. The fuel/air mixture is then added from the mixing tank to the cylinder using metering valves and heated supply lines, or the mixture is prepared directly inside the combustion chamber using the Direct Test Chamber (DTC) approach by injecting the fuel directly into the heated RCM. An absolute pressure manometer (MKS Instruments Baratron 626B) is installed onto a small manifold that is connected to the inlet port that allows the cylinder pressure as well as the mixing tank pressure to be measured. This provides the partial pressure of the air to be measured, based on which the amount of fuel to be injected either in the mixing tank or in the combustion chamber can then be calculated and confirmed by measuring the final pressure after injection.

2.2.1. Direct Test Chamber Method

Typically, RCM setups consist of a mixing tank in which the charge is initially prepared and allowed to mix homogeneously before supplying it to the RCM for compression. At MSU, a DTC technique was developed by Allen et al. [110] in which the fuel is directly injected into the RCM test chamber. This enables quick and convenient preparation of various equivalence ratio mixtures inside the combustion chamber while also reducing the risks associated with traditional techniques, such as thermal decomposition of the fuel and condensation of the fuel in the lines connecting the mixing vessel to the combustion chamber. Furthermore, the partial pressure requirement of the fuel and the wall temperature needed to ensure complete evaporation is lowered, because the total initial pressure in the RCM itself is between 0.4 to 2 bar. Fuel is metered into the RCM using a production water-cooled 7-hole GDI injector manufactured by Bosch and the mixture stoichiometry is controlled by varying the pulse width and number of pulses of the injector via LabVIEW by sending Transistor-Transistor Logic (TTL) pulses to a custom-made driver box. A hydraulic accumulator pressurized to 30 bar was used to pressurize the fuel line. Using the method of partial pressures, the mixture is prepared directly inside the combustion chamber and 5 minutes wait time is allowed so that the fuel can evaporate and mix before compression. When argon was used as a diluent, due to its lower heat capacity, the initial temperatures needed to be maintained to achieve the same compressed conditions were much lower as compared to when nitrogen was used as a diluent. Since the required initial temperature was lower than the boiling point of ethanol, a wait time of 10 minutes was allowed to ensure fuel evaporation and mixing. Studies by Allen et al. [113] and Chinnathambi et al. [114] have validated this mixture preparation approach by withdrawing gas samples from the RCM and analyzing the contents by GC/MS. It was verified by Chinnathambi et al. [114] that a wall temperature of 80 deg. C is adequate to ensure evaporation

of fuel blend gasoline components (without thermal decomposition or condensation) and 2 minutes of mixture preparation time is enough to achieve a homogeneous mixture. Allen et al. [113] verified that all of the components of JP-8/air mixture fully vaporized and a homogeneous charge was prepared within two minutes and at a temperature of 105 deg. C. A full description of the direct test chamber fuel preparation approach can be found in [110,113].

2.2.1.1. Fuel Calibration

The fuel injector used for this study for all purposes was a seven-hole Bosch injector (P/N: 62806) for high-pressure direct-injection applications. The injector was mounted such that its axis was perpendicular to that of the piston as can be seen in Figure 2-1. The distribution of the seven nozzle holes can be seen in Figure 2-5. For each fuel, the injector was calibrated by pulsing the injector 10 times into the vacuumed combustion chamber of the RCM, maintained at 80 °C. The injector is controlled using LabVIEW by sending TTL pulses to a custom-made driver box. After fuel injection, the pressure rise measured using an absolute pressure sensor was used to calculate the mass injected using the ideal gas law. This procedure was performed for a pulse width ranging from 0.5 ms to 1.0 ms. Each test was repeated 5 times, and the partial pressure recorded across the tests displayed a negligible standard deviation in the range of 1.5%. This highlights the repeatability of the injectors, even for a very small number of injections in the pulse width range. The resulting linear fit from the injector calibration procedure is shown in Figure 2-6. Since the calibration utilizes as high as 20 pulses and the DTC tests employed for the spray analysis used only a single pulse, a GC/MS study by Allen et al. [113] indicated that the actual mass loaded by the injector matches the injector calibration curve which implies that the linear fit obtained is applicable to any number of pulses and pulse widths as long as they are within the range maintained during the calibration.

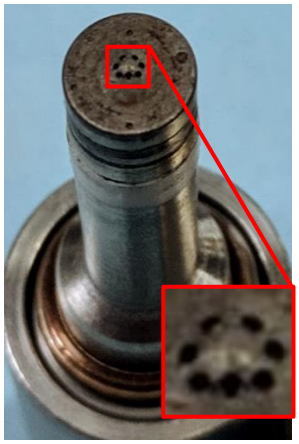

Figure 2-5: Image showing the distribution of the seven nozzle holes of the Bosch injector.

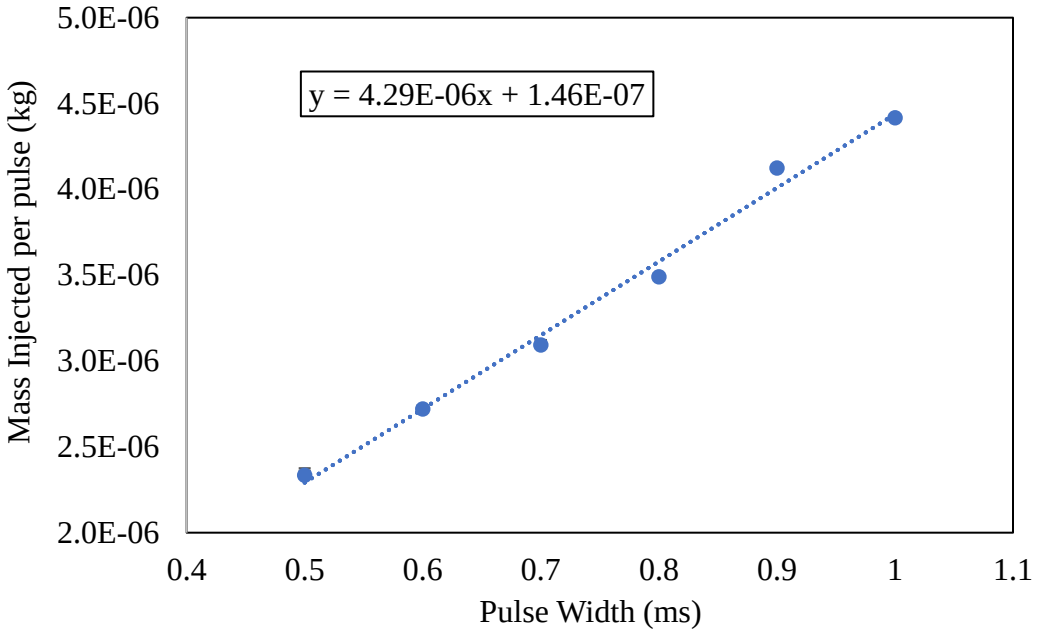

Figure 2-6: Fuel injector calibration curve of ethanol showing pulse width vs mass injected information.

2.2.2. Mixing Tank

In order to investigate the effect of charge preparation method on ignition delay measurements, the traditional mixing tank technique was also adopted for this study. The mixing tank was used to prepare either the fuel/air mixture or the oxygen/argon mixture when the DTC approach was used. All mixtures were prepared in a 15.9 L stainless steel tank equipped with a

magnetic stirrer that mixes the reactants for the entire duration of the experiments. Both, the mixing tank and RCM can be evacuated to sub-torr pressures using a vacuum pump. An insulating jacket around the tank ensures uniform heating and a feedback from thermocouple inside the mixing tank ensures temperature maintenance. The mixing tank temperature is set above the saturation temperature of ethanol to ensure complete vaporization of the fuel. Furthermore, it has been shown that if the fuel partial pressure is sufficiently lower than the fuel vapor pressure, complete vaporization is guaranteed and the loss of fuel to wall adsorption is negligible [115,116]. Since ethanol is a liquid at room temperature, it was injected using a gas-tight syringe via a septum located at the top of the heated tank. The determined amount of fuel was added based on its appropriate weight and the partial pressure of fuel and air was measured using an absolute pressure manometer (MKS Instruments Baratron 626B). The saturated vapor pressure dependence of ethanol on temperature is taken from the Chemical Properties Handbook by Yaws [117]. An investigation was carried out to determine the optimum mixing time and it was found that a mixing time of 2 hours was sufficient and longer duration had no benefits in terms of IDTs and optical images. Further details on this investigation are discussed in Section 4.4.2.1. Therefore, all mixtures were allowed to mix for at least two hours with the help of a magnetic stirrer rotating at 600 rpm, before use in the RCM, to ensure homogeneous charge composition. The fuel/air mixture was supplied to the RCM through a supply line that was heated with the help of heating tape to ensure the fuel did not condense while transferring the mixture. Once supplied to the RCM, the temperature of the combustion chamber was allowed to stabilize for two minutes prior to the start of the experiment.

Several previous studies have validated this mixture preparation approach by withdrawing gas samples from the mixing tank and analyzing the contents by GC/MS [118], GC-FID [119],

and GC-TCD [120]. It was verified by Weber et al. [118] that the fuel mole fraction was within 5% of the expected value and the study of Das et al. [120] verified the water mole fraction to be within 2% of the expected value. In addition, works by Kumar et al. [119] on n-decane and the study of Weber et al. [118] on n-butanol confirmed that no fuel decomposed in the mixing tank over the course of a typical set of experiments.

2.3. Adiabatic Core Hypothesis

It is not possible to measure reactant gas temperatures directly once the RCM is fired as one cannot readily obtain information about instantaneous spatial variation of temperature using thermocouples. Additionally, correction of the measured temperature due to slow time response of the thermocouple requires the knowledge of velocity field inside the chamber [2]. The use of non-intrusive absorption techniques also becomes challenging due to high-pressure conditions prevalent within the reaction cylinder [114]. The compressed temperature can be predicted by assuming isentropic compression of the core region of a pure vapor charge. The compressed temperature was therefore calculated using an adiabatic core hypothesis given by Equation 2-1, as previous CFD simulations have shown that the core gas, away from the thermal boundary layer and for short time scales, has an almost adiabatic temperature at the end of the compression process [121]. This approach also assumes that there is no significant chemical heat release during the compression stroke and the assumption is also validated in previous studies [71,89,91,118,119,122–124]. Mittal and Sung also experimentally demonstrated that the use of a creviced piston supports this hypothesis [3].

$$\int_{T_i}^{T_c} \frac{\gamma}{\gamma - 1} \frac{dT}{T} = \ln\left[\frac{P_c}{P_i}\right] \tag{2-1}$$

Here, P_i and T_i are the initial pressure and temperature, γ is the ratio of specific heats of the mixture, and P_c and T_c are the compressed pressure and temperature. It should be noted that the T_c in

Equation 2-1 is not the temperature of an adiabatically compressed charge. Heat loss is occurring during the compression process and is accounted for by the experimentally measured pressure P_c.

2.4. Experimental Uncertainties

All test conditions were repeated a minimum of three times for both, spray and auto-ignition experiments. Total ignition delay measurements were repeatable to within ±5%. The detailed procedure to determine the standard deviation of each component of the RCM can be found in a study conducted by Weber et al. [125] on the uncertainty of temperature estimation in an RCM. Although not as much in detail, a similar method is adopted for this study and is discussed briefly in this section. The manufacturer's quoted uncertainty is assumed to represent a normal distribution with a coverage factor of two, unless otherwise specified. The uncertainty is divided by the coverage factor to determine the standard deviation, as recommended by the British Measurement and Testing Association Measurement Good Practice Guide No. 36 [126]. As can be seen from Equation 2-1, the compressed temperature estimation depends upon the compressed pressure and initial temperature and pressure. Hence, the uncertainties that would affect the compressed temperature would depend upon the accuracy of the pressure measurements and in measuring the initial conditions.

The thermocouples had the standard limits of error as "greater of 2.2 deg. C or 0.75%". The maximum temperature possible with the heaters on the present RCM is 175 deg. C, so the maximum uncertainty in the temperature is 2.2 deg. C. Assuming the tolerance is given with a coverage factor of two, the standard deviation of the normal distribution is σ_{Ti}= 1.1 deg. C.

According to the manufacturer's calibration, the deviation of the full-scale output of the pressure transducer from linearity is less than 0.1% over the pressure range 0 bar to 50 bar, indicating that the uncertainty in the compressed pressure is $2\sigma_{Pc}$ = 0.05 bar, since the uncertainty

of the pressure transducers is typically specified as a percentage of the full-scale range. The uncertainty of the compressed pressure is thus assumed to be normally distributed with mean at the measured value and standard deviation of one half of the specified value, i.e. σ_{Pc} = 0.025 bar. The absolute pressure manometer had an accuracy of ±0.25% of the reading, which led to a maximum deviation of ±0.002 bar.

Other than the manufacturer provided uncertainties, the standard deviation of the tests carried out at a given condition was calculated for initial temperature (±5 K), initial pressure (±0.005 bar) and compressed pressure (±0.4 bar). As discussed in Section 2.2.1.1, the uncertainty in injected fuel mass was ±1.5%.

Additional sources of uncertainties include the cold junction compensation, A/D converter and the uncertainty in the signal acquisition equipment—including the charge amplifier and the data acquisition through LabView. These uncertainties are negligible compared to the above-calculated uncertainties [125]. All these uncertainties together affect the estimation of the compressed temperature and although this study does not investigate that effect, the study by Weber et al. [125] found that the maximum deviation in compressed temperature estimation using the adiabatic core hypothesis and accounting only random errors is ±6 K. Another study by Allen et al. [113] calculated the uncertainty in the calculation of compressed temperature to be ±1.25% (±8-9 K). Although difficult to quantify experimentally, systematic uncertainties inherent to the design and operation of RCMs such as diluent gas composition, thermophysical properties of gases, piston velocity, piston crevice design, compressed pressure etc. may also affect the assumption of the adiabatic core and in turn, play a role in determining the uncertainty of the EOC temperature estimation.

Chapter 3. NUMERICAL PROCEDURE

3.1 Chemical Kinetic Modeling

Combustion modeling of RCM data is an important step in assessing the accuracy of the chemical kinetic models by comparing experimental results with chemical kinetic predictions. At the most fundamental level, combustion modeling involves a reaction mechanism or a kinetic mechanism. Chemical kinetic mechanisms provide the time-dependent progression of chemical reactions in a system, consisting of various chemical species and elementary reactions. The specific chemical species and the number of elementary reactions in a particular kinetic mechanism vary. However, they are all developed to predict the fundamental combustion process. Predictive modeling makes use of these chemical kinetic mechanisms to predict the chemical behavior and the products of chemical reactions through numerical simulations while using fewer resources than physical experiments. The purpose of a comprehensive mechanism is to have a generalized reaction mechanism that can reproduce all of the available experimental data and predict with some confidence the kinetics of systems for which experimental data is not available. This also helps in understanding the chemical kinetics at conditions that are infeasible to achieve experimentally. Details regarding the reaction mechanisms used for each of the fuels studied in this work are provided in Chapter 5 and Chapter 7.

ANSYS CHEMKIN-PRO was used to conduct the chemical kinetics simulations as part of this work. For modeling the RCM, a Closed Homogeneous Reactor model is utilized along with specifications of initial conditions (temperature, pressure, mole fraction, etc.), the time-dependent effective volume profile (obtained from the corresponding non-reactive experimental pressure trace) and a reaction mechanism. The specification of an effective volume profile that accounts for the heat losses from the RCM combustion chamber during the compression and post-compression

periods is another important element of the modeling. The approach for specifying the effective volume profile is summarized in [113]. Due to the evolving reactions and conditions in the combustion chamber, a reactive test cannot be used to create an effective volume profile. Therefore, the volume profile for a given test is created by running a separate non-reactive test in which all the oxygen is replaced by the corresponding diluent gas that is used for the reactive tests (nitrogen and argon in this study) in order to eliminate oxidation reactions and at the same time, maintain a similar heat capacity ratio. All the other non-reactive test conditions mimic those of the reactive test. A non-reactive experiment also ensures that no significant heat release occurs during the compression stroke.

Default values from CHEMKIN were used for the solver tolerances and solver time-steps. The energy equation over a specified time interval is then solved to calculate system temperatures, pressure, and species concentrations.

The approach outlined in [113] has also been used to calculate all the effective volume profiles used for predictive modeling purposes in this work. As an example, two of the calculated profiles are shown in Figure 3-1, with each for a unique compression ratio. A rapid change in volume during the compression process leading up to TDC is depicted by the profiles. Once the piston reaches TDC, the piston is locked in position during the experiments. However, the derived volume profile shows a slow volume expansion process which is representative of the additional heat lost to the surroundings. Figure 3-2 depicts a volume profile and the non-reactive pressure data in the corresponding time interval for a compression ratio of 11.7. The heat loss in the post-compression period is evident by the loss in pressure that occurs after TDC.

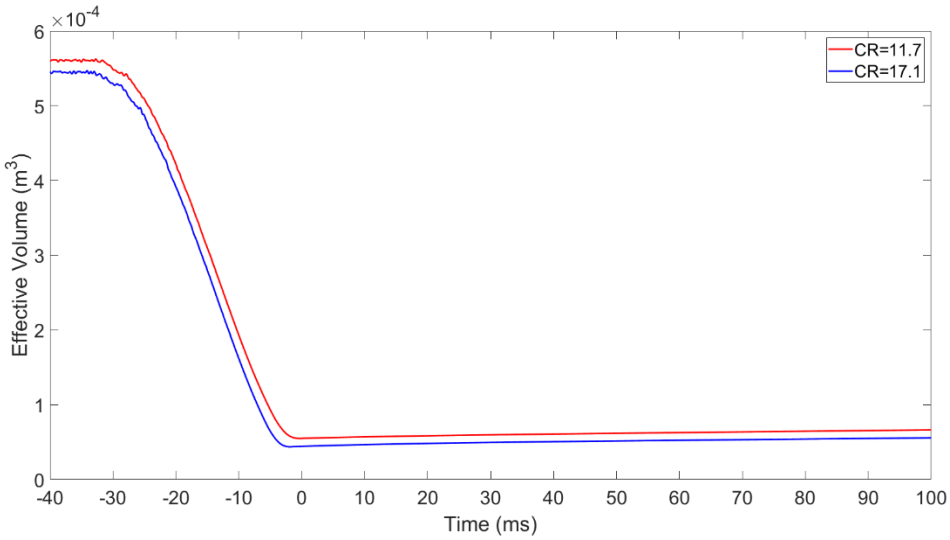

Figure 3-1: Sample effective volume profiles (stoichiometric mixture of ethanol and air, T_c=825 K, P_c=20 bar).

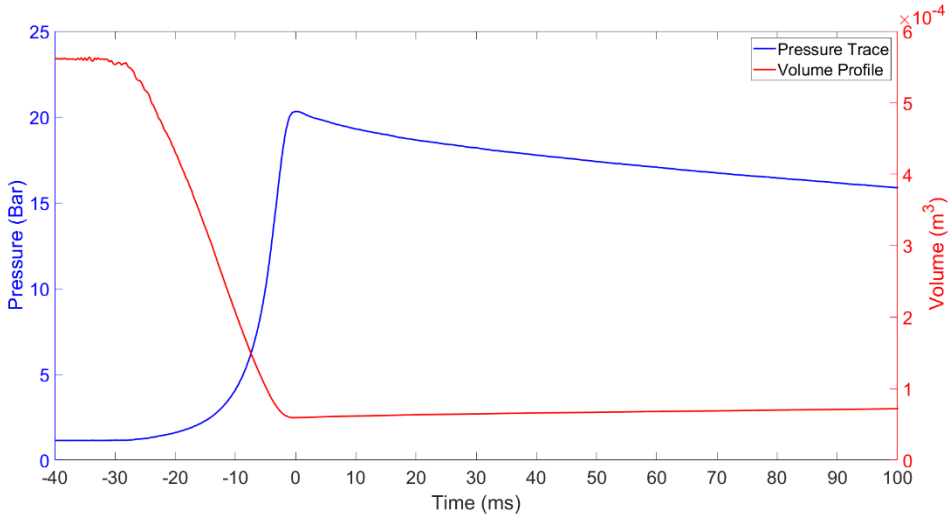

Figure 3-2: Comparison of effective volume profile with the corresponding pressure data over the same time interval (stoichiometric mixture of ethanol and air, T_c=825 K, P_c=20 bar and CR=11.7).

The derived effective volume profiles are then used as an input to the kinetic 0-D simulations. A typical kinetic modeling result for a single operating condition is shown in Figure 3-3 where it is compared with reactive experimental data and the corresponding non-reactive test that was used to construct the effective volume profile. The data and simulation predictions are

results obtained as part of the ethanol study presented in Chapter 4 and Chapter 5. It can be clearly observed that the heat loss characteristics of the non-reactive case also resemble the heat loss behavior for the reactive experimental test.

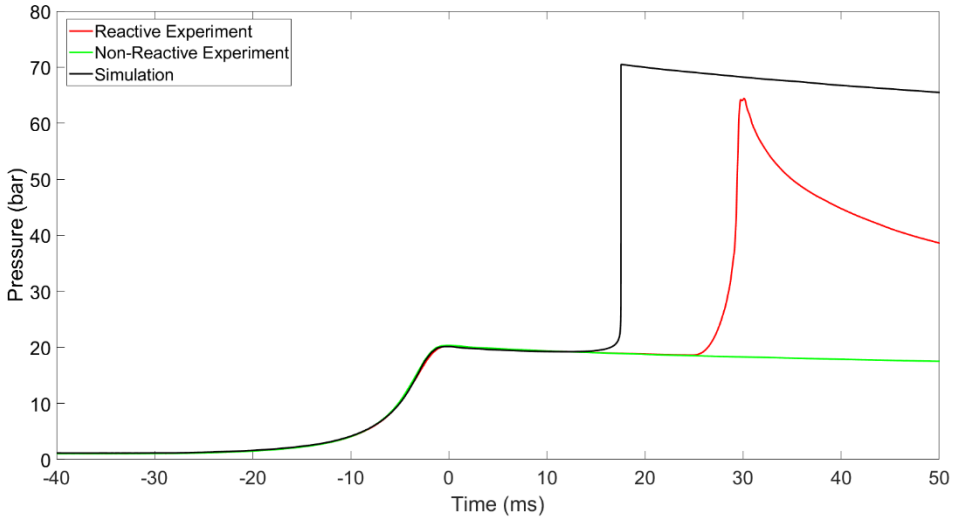

Figure 3-3: Comparison of the pressure evolution for a reactive experiment, a non-reactive test used to create an effective volume profile, and a kinetic simulation based on the effective volume profile (stoichiometric mixture of ethanol and air, T_c=825 K, P_c=20 bar, CR=17.1).

3.2 Computational Fluid Dynamics Modeling

Computational Fluid Dynamics (CFD) simulation is an efficient method to study the temperature and the aerodynamics in an RCM comprehensively. Three-dimensional (3-D) CFD simulations were carried out to investigate the consistent top-to-bottom flame propagation behavior observed in the optical experiments of ethanol auto-ignition. Simulations were conducted for the RCM geometry using Converge CFD software. Each transient simulation starts with the initial temperature, pressure, velocity and species concentrations, obtained through a steady-state solution. The mesh is then compressed based on a piston trajectory which specifies the piston position at a given time. The piston displacement history is prescribed as a polynomial fit to the numerically derived piston profile from non-reactive pressure-time data obtained from experiments. Figure 3-4 demonstrates that the simulation closely matches the experiment, except

near the TDC, where a slight discrepancy is observed. The simulations and experiments both had a compression time of 32 ms. In simulations, to accommodate for various dead volumes in experiments, the clearance volume at TDC is considered slightly larger than the geometric volume. This was also done because the compressed pressure obtained using simulations was slightly higher than those observed in experiments. The discrepancy near TDC could be due to overcompensation for dead volumes. Nevertheless, the overall agreement is fairly good. The time taken for the last 50% rise in pressure (5.4 ms) was also in good agreement with those observed in experiments (5.2 ± 0.1 ms). Furthermore, it was observed that as long as the compression time is kept constant, the resulting flow field is insensitive to reasonable changes in the velocity profile [127,128]. Another important prerequisite to any reactive simulation is that the simulated and experimental non-reactive pressure traces agree, which is the case here (Figure 3-4). This suggests that the wall-heat transfer, during and after compression, is captured by the simulations and is in reasonable agreement with those observed in experiments. The simulation continues until ignition occurs after the piston is compressed.

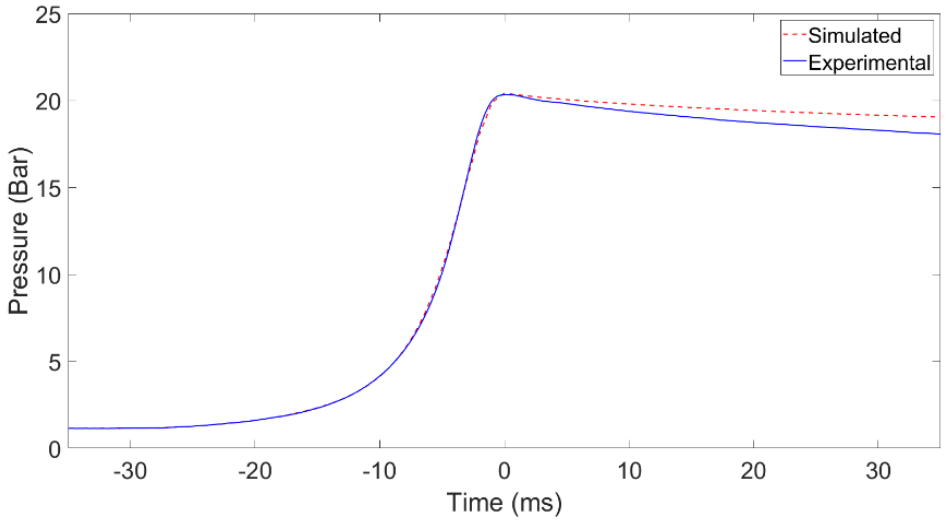

Figure 3-4: Comparison of experimental (blue line) and Converge-simulated (red line) non-reactive pressure trace.

Pressure Implicit with Splitting of Operators (PISO) method is used to solve the transport equations implicitly. Converge utilizes a variable time step governed by the convective, speed of sound, and diffusive Courant–Friedrichs–Lewy (CFL) numbers and the grid spacing. The minimum and maximum allowable time steps for the simulations are 10^{-8} s and 10^{-4} s, respectively. Momentum, energy, and species equations were solved considering mixture-averaged diffusion coefficients. A laminar solver was used since it has been shown to achieve the best agreement with experimental results [129,130]. Furthermore, a laminar CFD model has been proven to adequately predict compression and the post-compression flow field in comparison to the LES models [97] and the overly dissipative RANS models [128,131,132].

3.2.1 Simulation Geometry and Computational Grid

The CFD simulations were run for half or 180 degrees of the MSU RCM geometry. A symmetry boundary condition is applied to the tangential boundary, while a temperature boundary condition of varying values and a no-slip boundary condition is applied to the piston and cylinder walls.

A base grid size of 0.8 mm was used. Additionally, the simulations in this analysis use temperature and velocity-based adaptive mesh refinement to achieve a more refined grid in areas with large temperature and velocity gradients. As an example, the cell is divided into multiple cells, each of 1/16th the size of the original cell, if the sub-grid temperature of that cell is greater than 1.5 K and/or the velocity is greater than 1 m/s. The embedding is released and the original cell is restored if the sub-grid value of the refined cell falls below 1/5. The maximum cell limit is 4,500,000 cells. To capture the gradients in temperature near the walls caused due to the heat loss to the boundaries, permanent refinement or fixed embedding is applied near the wall boundaries. The refinement is such that three layers of base grid size 0.4 mm extend from the wall boundary

into the mesh. It is worth noting that the adaptive mesh refinement also works in the embedded areas. Mesh independence was confirmed by changing the base grid size and the fixed embedding levels near the boundaries until further refinement yielded less than a 5% change in the ignition delay.

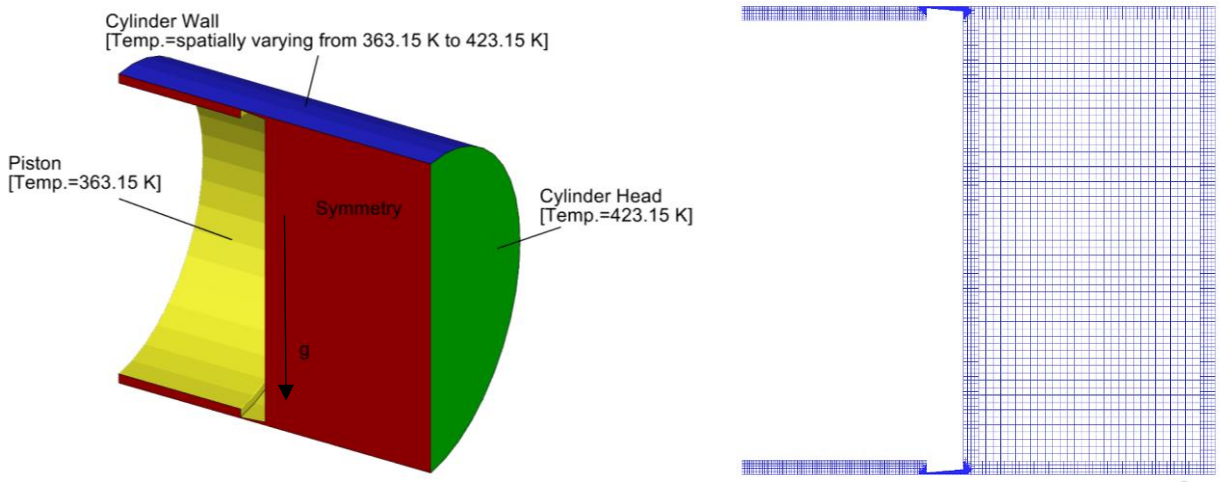

(a) (b)

Figure 3-5: (a) Combustion Chamber geometry and boundary conditions and (b) computational grid at the end of compression (without AMR).

Illustration of the CFD grid at the end of compression along with the geometry of the main combustion chamber with boundary conditions specified is shown in Figure 3-5.

3.2.2 Combustion Modeling

The simulations use the ethanol mechanism by Mittal et al. [10] containing 113 species and 710 reactions. However, since the computational time taken to obtain a numerical solution is linearly proportional to the square of the number of species or the number of reactions [133] a mechanism reduction was performed using the zero-dimensional utility tools in Converge. Converge uses a Direct Relation Graph with Error Propagation [134] and Sensitivity Analysis (DRGEPSA) to generate reduced mechanisms. Ignition delay analysis was performed to ensure that the reduction technique does not affect the results. The final reduced mechanism had 34

species and 175 reactions with a maximum of a 5% deviation in ignition delay from the originally predicted values for constant volume simulations. The primary objective of this paper is to study the effect of temperature inhomogeneities as a result of buoyancy and non-isothermal boundary conditions on the auto-ignition behavior of ethanol. For this reason, the mechanism by Mittal et al. and the resulting reduced mechanism are not fine-tuned to match with the experimental auto-ignition delay times of ethanol. The SAGE detailed chemistry solver along with a two-dimensional multi-zone model that solves chemistry in temperature and equivalence ratio bins of 2 K and 0.05, respectively, is used for combustion modeling.

The simulations are carried out in two parts. First, a steady-state CFD simulation is performed to obtain the initial gas temperature and velocity fields with the piston at BDC. The gas temperature and velocity are calculated for a given set of boundary temperatures, wherein the piston temperature is 60 K cooler than the rest of the boundaries. Along with the "cool" piston, a spatially varying temperature along the length of the cylinder wall, starting at the piston and increasing in temperature to about quarter the length of the combustion chamber, is applied. The remaining 3/4 length of the combustion chamber wall has a uniform temperature of 423.15 K applied. The feedback from the thermocouple close to the piston showing a 60 K cooler temperature indicates that the heat exchange with the cooler piston face is more dominant than the heating effect of the band heater close to the piston. Furthermore, there is a gap of about 1 inch between the bottom of the cylinder and the point where the last heating band ends. Therefore, such a boundary condition is representative of the gap between the band heaters seen in typical experimental RCM configurations. This in turn would cause the mixture close to the piston to be cooler, as will be shown in the section 5.3.1. Finally, the steady-state solution is used as the initial temperature and pressure fields during the transient simulation of the RCM compression stroke.

The same mesh, simulation and modeling parameters are used for the steady-state as well as the transient RCM compression simulations.

Chapter 4. EXPERIMENTAL RESULTS – ETHANOL

4.1 Introduction

Ignition delay measurements are most frequently carried out in RCMs and shock tubes, each of which require a means to prepare mixtures of fuel, oxidizer and diluent gases. As mentioned earlier, the same compressed conditions can be reached by a variety of combinations of compression ratio, initial temperature, initial pressure, diluent gas composition, etc. in an RCM. In an effort to address the assumption that IDTs are insensitive to the above-mentioned combinations used to achieve the compressed conditions, the objective of this work is to determine which components of RCM testing the ignition delay time is most sensitive to.. In this chapter, experimental and numerical analysis of the effects that post-compression heat losses and initial conditions affected by different compression ratios and diluent gas compositions have on ethanol ignition delay was performed.

4.2 Experimental Test Conditions

Experiments were conducted for stoichiometric ethanol/oxygen/diluent mixtures over a temperature range of 800 K-875 K and at a pressure of 20 bar. Two diluent gases differing in their thermal capacities, nitrogen and argon, were used to study the effect of diluent gases on IDTs. The diluent/O_2 ratio, however, was kept constant at 3.76 to simulate normal air. In order to study the effects of post-compression heat losses, experiments were conducted at two compression ratios of 11.7 and 17.1 for the same range of temperature with nitrogen as the diluent. All the possible configurations of the compression ratios of the MSU RCM were evaluated to cover the temperature range of interest without having to use a variety of compression ratios and/or change the diluent gas composition. Compression ratios of 11.7 and 17.1 were each found to cover the entire temperature range while maintaining the use of nitrogen as a diluent with a diluent/O_2 ratio of 3.76.

The compressed conditions thereby achieved are similar to those that prevail in piston engines. To study the effect of diluent gases, tests were carried out only at CR=11.7 using pure nitrogen and argon as buffer gases. Argon and oxygen mixture was prepared in the mixing tank, while ethanol was injected directly into the combustion chamber (DTC) method. This study also investigates whether the ignition delay measurements are sensitive to changes in preparation methods: (1) directly injecting the fuel in the combustion chamber and allowing it to mix for a certain amount of time before compressing it and (2) using a mixing tank in which the fuel and air are pre-mixed and then supplied to the combustion chamber for compression. Tests were carried out at both the compression ratios using each mixture preparation method to investigate whether the post-compression heat losses are dependent on the mixture preparation method. The effect that both charge preparation methods have on the concentration and temperature homogeneities, as well as the ignition delay characteristics, are discussed.

Figure 4-1 depicts a summary of IDT data for stoichiometric mixtures of ethanol obtained from past shock tube and RCM studies together with the test conditions investigated in this study highlighted in green. It should be noted that all of the data shown in Figure 4-1 is presented as it was reported in the literature and no scaling was used for the literature data, in the creation of this figure. In Figure 4-1 it can be seen that there was minimal data in the literature for the temperature range of the current study (800 K-875 K). Also, data presented by Lee et al. [7], Huefer et al. [8] and Cancino et al. [9] show a deviation from Arrhenius behavior for the temperature range of 800 K-875 K. Referring to these shock tube results, the shorter IDTs and the deviation from Arrhenius behavior for lower temperatures (<900 K) are the result of pre-ignition and also due to the temperature and pressure gradients caused by shock attenuation [8]. Based on the Figure 4-1, it can be seen that the tests are focused on the low temperature region and are at a moderate pressure.

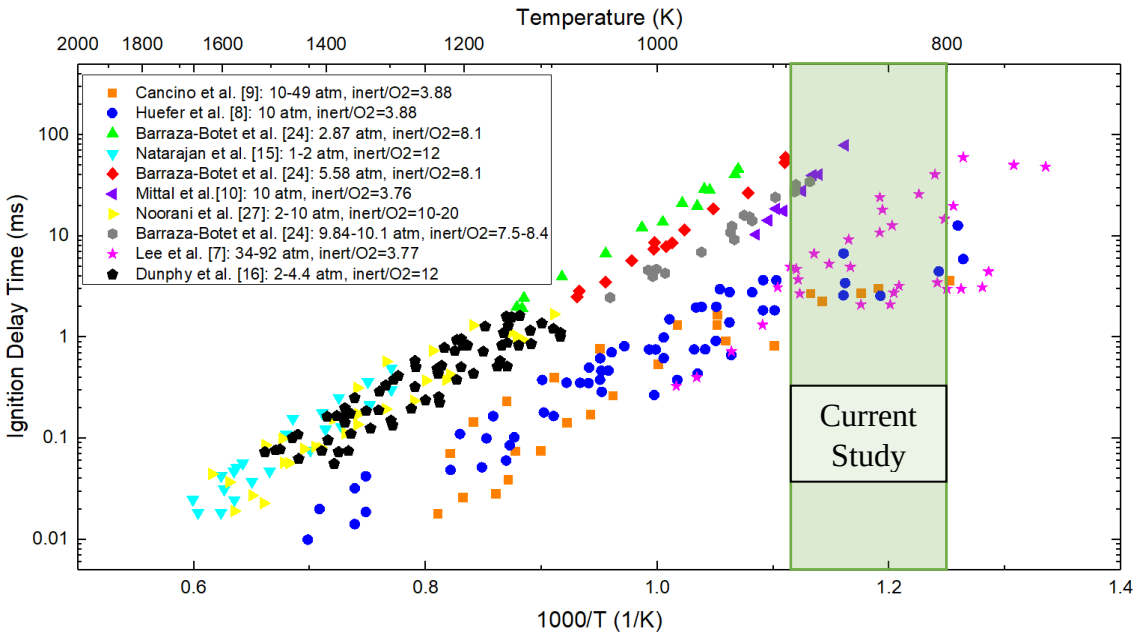

Figure 4-1: Summary of IDT results for stoichiometric mixtures of ethanol studied in the past and highlighting the test conditions investigated in this work, adapted from [24].

Table 4-1 shows the test matrix and also shows the compression ratios and the mixture preparation methods that were employed in order to achieve the corresponding compressed conditions. A minimum of three combustion tests and two non-reactive tests were carried out for each case. The ethanol used for the experiments was obtained from KOPTEC, which was 200 Proof (100% absolute ethyl alcohol), while all gases were supplied by Airgas. A Photron SA4 high-speed camera was used to image record the auto-ignition event.

Table 4-1: Test Conditions for which IDTs were measured.

	Molar Composition				**Pc (bar)**	**Tc (K)**	**CR**	**Mixture Preparation Method**
	Ethanol	O_2	N_2	Ar				
1	1	3.00	11.28	-	20	800	11.7 & 17.1	DTC & Mixing Tank
2						825		
3						850		
4						875		
5	1	3.00	-	11.28	20	800	11.7	DTC
6						825		
7						850		
8						875		

4.3 Data Interpretation

A typical pressure trace encountered in this study is shown in Figure 4-2. The measured pressure and evaluated temperature at the EOC (t=0) are P_c=20.3 bar and T_c=806 K, respectively. The duration of the compression stroke is approximately 32 ms. The ignition delay time (τ) is defined as the time from the end of the compression stroke (t=0 ms) to the point of the maximum pressure rise rate due to ignition (inflection point, $(dP/dt)_{max}$). EOC, when the piston reaches top TDC, is identified as the time when dP/dt falls below zero past the start of compression; this also corresponds to the maximum of the pressure trace (P_c) prior to the ignition point. The corresponding non-reactive pressure trace is also shown in green in Figure 4-2. In addition to the reactive experiments, a non-reactive experiment was performed at each compressed condition, to ensure that no significant heat release occurs during the compression stroke. Furthermore, the non-

reactive pressure profiles also aid in developing volume profiles for chemical modeling. The non-reactive tests were conducted at conditions identical to the reactive tests, except that the oxygen in the mixture was replaced by argon (or nitrogen) in order to eliminate oxidation reactions and at the same time, maintain a similar heat capacity ratio to those observed in reactive experiments. Ideally, if the RCM was perfectly insulated, the pressure would not drop after the EOC and the compressed conditions would remain constant until ignition occurs. In reality, due to heat transfer to the walls, the pressure of the gas mixture decreases slightly after the EOC as can be seen in Figure 4-2. Simulations [19,71] have found that the adiabatic core of the gas mixture attains a temperature similar to that observed at the EOC for at least 100 ms after the EOC. Therefore, IDTs are reported for pressure and volume conditions determined at the EOC. It should also be noted that post-compression heat losses can vary between facilities but as the core region remains similar to the compressed conditions for 100 ms the compressed temperature and pressure are used to compare measurements between facilities. Figure 4-2 also illustrates the time at which the camera was triggered to record the images, which is ~10 ms before the EOC.

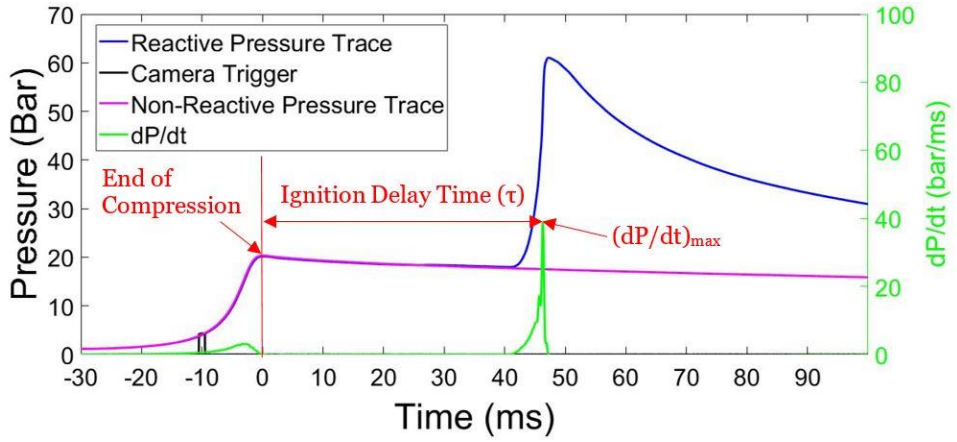

Figure 4-2: Typical pressure trace for a reactive and non-reactive case at 20 bar and 800 K for stoichiometric ethanol-air mixture.

4.4 Effect of Mixture Preparation Method

In order to investigate the effect of the charge preparation method on the ignition delay measurements, the traditional mixing tank technique was also adopted for this study and the results were compared with those obtained using the DTC method.

4.4.1 Analysis of Optical Images using DTC Method

As discussed in Chapter 2, Section 2.2.1, the DTC method enabled the preparation of fuel and air mixtures directly inside the combustion chamber, by first supplying air and then injecting ethanol, the amounts of both are calculated using the method of partial pressures. The mixture is then allowed to homogenize for 5 minutes before compressing it, with this duration determined experimentally through GC/MS testing [113,114].

4.4.1.1 Maintenance of a Clean Combustion Chamber

Irrespective of the mixture preparation method employed, in order to avoid contamination through substances absorbed in oil layers, O-rings and other surfaces, the interior of the RCM combustion chamber was cleaned after each test at a given operating condition and also conducting oxygen runs in between individual tests. This methodology was effective in providing reproducible results and preventing contamination and pre-ignition, which are known problems in these types of studies. Figure 4-3 (b) shows an example of an auto-ignition event that can be observed if the cleaning protocol is not followed correctly. In this case, multiple flame kernels were observed. Figure 4-3 (a) shows a typical case at similar conditions when the combustion chamber was cleaned.

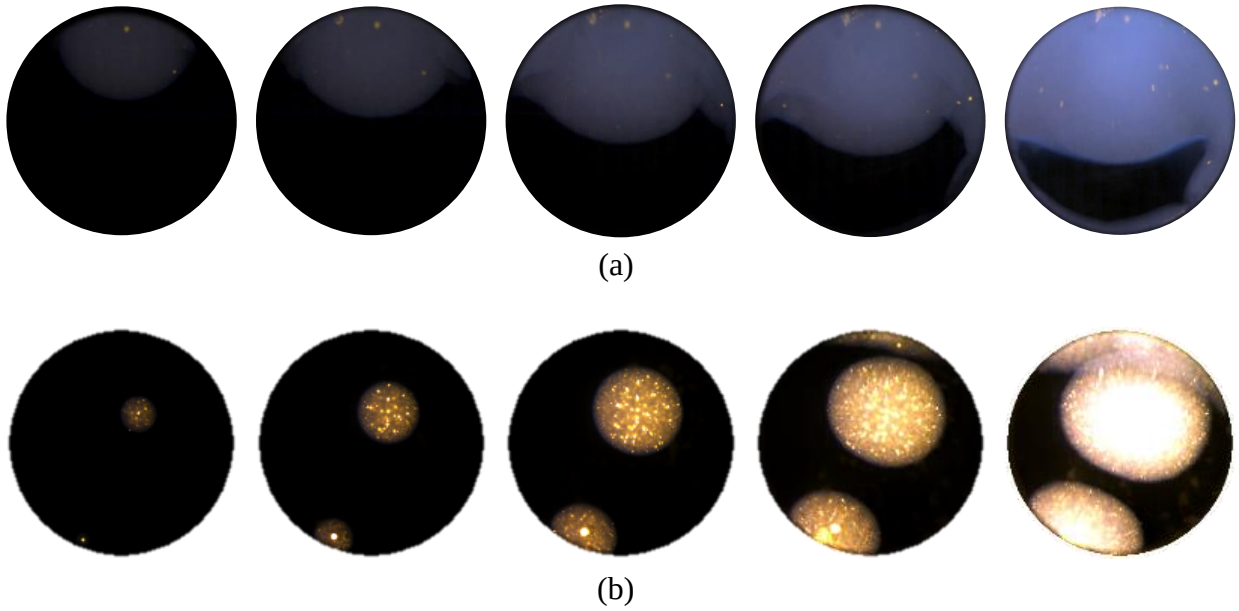

Figure 4-3: Optical images using DTC approach at Tc = 850 K for (a) clean combustion chamber and (b) when cleaning protocol was not followed.

In Figure 4-3 it can also be seen that the flame kernels exhibited different colors in both cases. This could be because of the effect of different impurities present in the combustion chamber, as the observed yellow flames can indicate the presence of soot particles or solid contaminants. In the chemiluminescence study by Büttgen et al. [25], the authors also observed multiple flame kernels at 20 bar and 875 K and stated that there is no clear pattern regarding the amount and size of the flame kernels. They claimed that this was not “pre-ignition” since the flame kernels did not shorten the IDTs significantly as they appeared only a few milliseconds before the actual ignition.

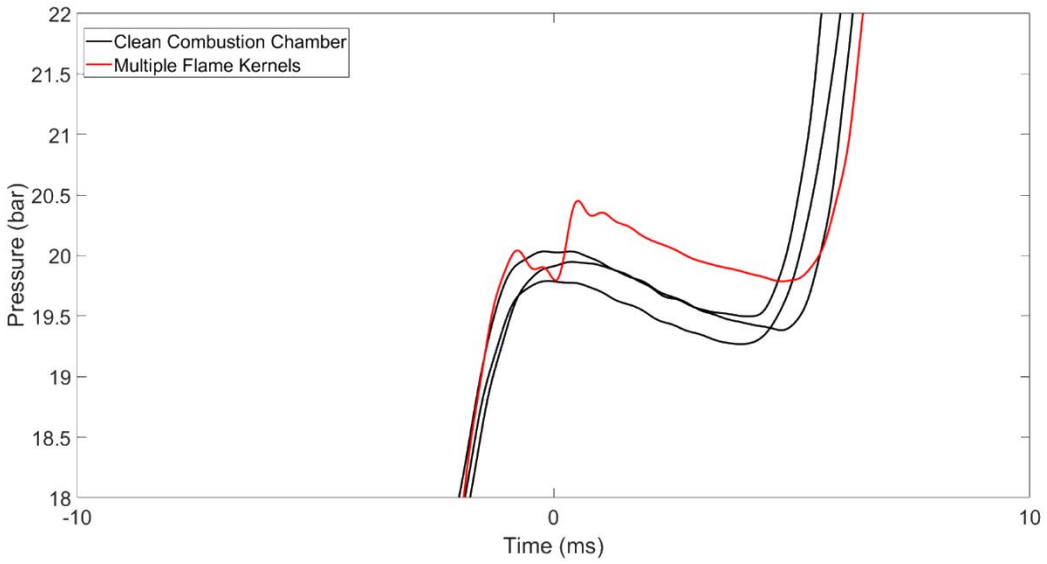

Figure 4-4: Pressure traces for T_c = 850 K and P_c=20 bar for clean combustion chamber and when multiple flame kernels were observed.

Figure 4-4 shows pressure traces of the cases mentioned in Figure 4-3, including the case shown in Figure 4-3 (b) (red line) and all three runs of the clean combustion chamber case (black lines), for repeatability. It is observed that the multiple flame kernels do not affect the IDT significantly, but we do observe a pressure increase of about 0.5 bar only a couple of milliseconds after the EOC; even though no flame kernels were seen until a millisecond before the actual auto-ignition event. The slight pressure rise before the actual ignition event could be because of some minor small-scale chemical reactions taking place at multiple locations where the flame kernels are later observed to develop. In the case where the clean combustion protocol was followed, no rise in pressure was observed before the actual ignition event. This could be due to the fact that there was only a single flame developing and the volume over which these minor small-scale reactions took place was small compared to the case in which multiple flame kernels were observed. Although this does not qualify as a pre-ignition case, the compression process was affected, as can be seen in the pressure trace. It should also be noted that similar events were

observed in other initial testing where the combustion cleaning protocol was not yet established. Pre-ignition or not, in order to eliminate any reasons for doubt regarding the ignition delay data, a strict combustion chamber cleaning protocol was followed to reduce, if not eliminate, the chances of multiple flame kernels occurring and provide more reliable and accurate data regarding the ignition delay measurements.

4.4.1.2 Results and Discussion

Figure 4-5 shows the pressure traces from the experiments carried out using the optical window at a compression ratio of 11.7 for the compressed conditions of 800, 825 and 850 K at 20 bar. The numbers 1-6 in Figure 4-5 are the points at which the optical images are shown in Figure 4-6. An interesting trend that was observed was that the first test carried out always had the shortest ignition delay followed by tests 2, 3 and 4. A possible reason for this could be that even after cleaning the combustion chamber following each set of compressed conditions and performing oxygen runs between every test, there were still impurities that may have played a role in the ignition event, however, this has been reduced significantly with the cleaning protocol. These impurities can be seen as bright spots, see Figure 4-6, and may result from residues left behind by the chem-wipes, soot, etc. The impurities did not appear to affect the IDT significantly as they appeared after the first flame kernel was observed. In the highest temperature case shown in Figure 4-6 (c), more bright spots appear and eventually are consumed. As can be observed, only a single spherical flame kernel that propagated across the chamber, most often from top to bottom, was observed in all the tests that were performed with the cleaning protocol. Büttgen et al. [25] mentioned in their study that the front propagating from the top to the bottom could be due to minor temperature gradients present in the combustion chamber. Note that the brightness and contrast of some images were optimized to improve visibility. Also, for brevity, only the optical

images of the second test run for each compressed condition are shown, although images were similar for all runs. The apparent propagating speeds of these flame fronts were calculated to be between 5-8 m/s. A similar propagating flame front was observed by Büttgen et al. [25] for a 20 bar, 875 K and ϕ=0.5 case. In contrast to their study, no slight pressure rise was observed after the EOC for any of the cases. For the experiments presented here, the flame kernels were first observed at the start of the pressure rise during the main ignition event, and not at any earlier time. Additionally, the light intensity of the optical images increased to a maximum at the point that also corresponded to the time of the maximum pressure rise rate ($(dP/dt)_{max}$). The IDTs for these cases are tabulated in Table 4-2. As can be seen, the repeatability of the RCM improves at higher temperatures.

Table 4-2: IDT for compression ratio=11.7 at 20 bar and ϕ =1.

T_c (K)	800	825	850
IDT (ms)	45.1 ± 3.4	29.8 ± 2.8	7.1 ± 0.38

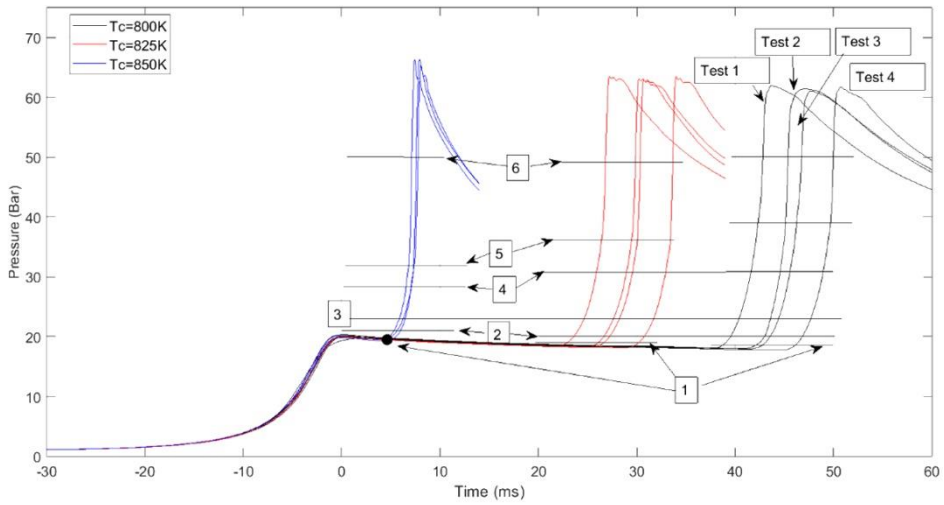

Figure 4-5: Pressure traces of stoichiometric ethanol ignition at 20 bar for compression ratio=11.7 using the optical window. Note that the numbers 1-6 correspond to the locations at which the optical images are shown in Figure 4-6.

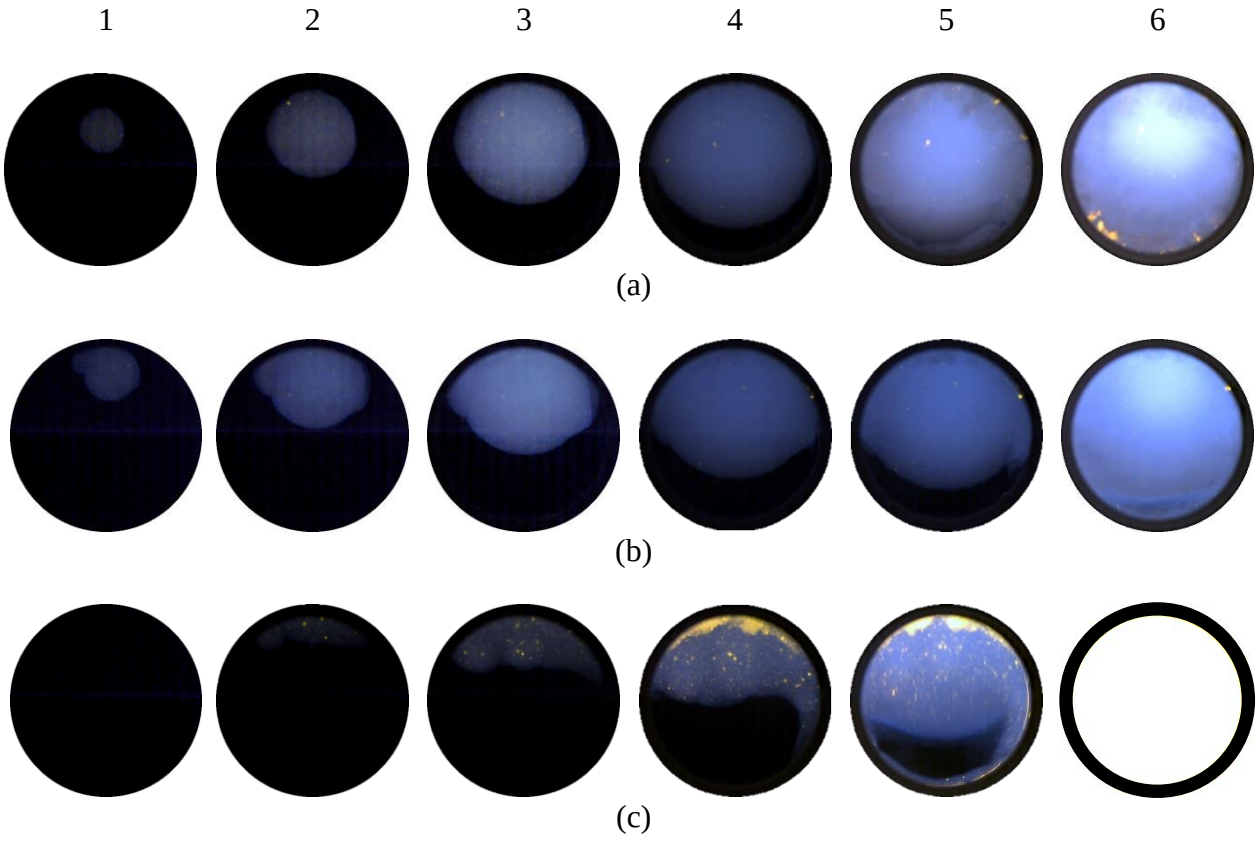

Figure 4-6: Optical Images showing flame propagation corresponding to the numbers in Figure 4-5 at (a) T_c=800 K, (b) T_c=825 K and (c) T_c=850 K and 20 bar pressure.

Images in Figure 4-7 show a single flame kernel at the start of ignition corresponding to location 1 in Figure 4-5 and the propagation of the flame towards the bottom of the chamber, corresponding to location 6 in Figure 4-5. Note that all the test runs were conducted at a given test condition. It can be concluded that performing the oxygen runs and cleaning the combustion chamber routinely helps in obtaining more accurate results as only a single flame kernel was consistently observed to originate at the top of the chamber and propagate towards the bottom in all the test runs at all the compressed conditions.

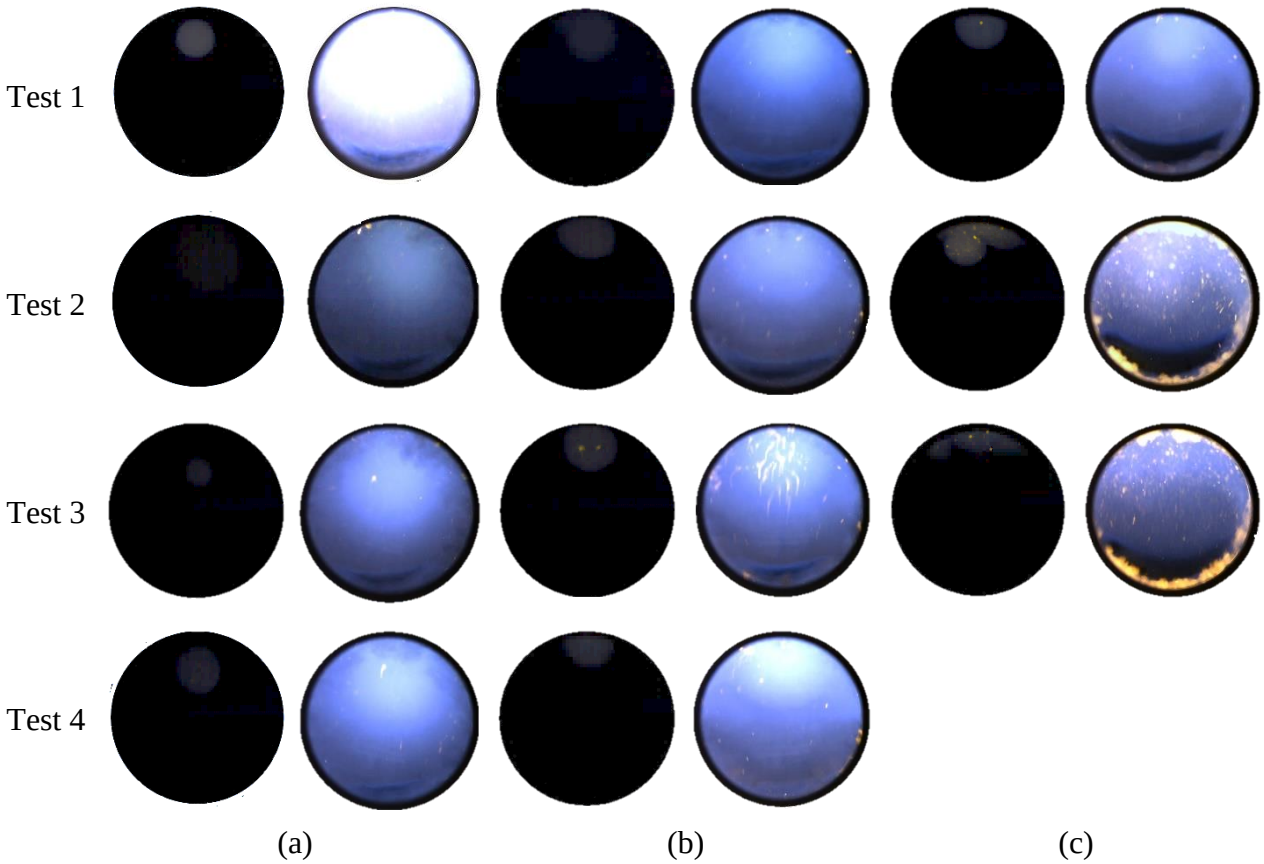

Figure 4-7: Optical Images of all tests conducted at (a) Tc=800 K, (b) Tc=825 K and (c) Tc=850 K and 20 bar pressure, consistently showing a single flame kernel propagating from top to bottom.

4.4.2 Analysis of Optical Images using Mixing Tank

4.4.2.1 Optimum Mixing Time

As discussed in Chapter 2, Section 2.2.2, the fuel and air mixture is prepared in a 15.9 L stainless steel tank equipped with a magnetic stirrer. In order to determine the minimum amount of mixing time required to obtain a homogeneous mixture, an investigation was carried out in which the mixture was allowed to mix for up to 20 hours and tests were run at regular intervals to compare the ignition delay results. Optical images, along with pressure measurements, aided in obtaining a better understanding of the events taking place in the combustion chamber.

Preliminary results from pressure data showed that the ignition delay measurements obtained after 1, 2, 4 and 6 hours of mixing were similar. However, ignition delay measurements taken after 17 and 20.5 hours of mixing were longer. Overall, the IDTs were shorter as compared to the DTC results at CR=11.7, T_c=800 K and P_c=20 bar. The results are tabulated in Table 4-3.

Table 4-3: Comparison of DTC IDTs for compression ratio = 11.7 at P_c=20 bar, T_c=800 K and ϕ = 1 with mixing tank results at different time intervals of mixing (NOTE: these results were later determined to be invalid due to inadequate mixing and tests were repeated and results are shown in Table 4-4).

Mixing Time	**Average IDT (ms) using Mixing Tank**	**Average DTC IDT (ms)**
1 hour	19.9 ± 2.6	46.4 ± 3.4 (5 minutes of mixing inside the combustion chamber)
2 hours	20.2 ± 1.1	
4 hours	20.4 ± 0.6	
6 hours	23.8 ± 2.1	
17 hours	35.8 ± 3.2	
20.5 hours **(Metal Window)**	32.3 ± 1.6	

Looking at the results in Table 4-3, one may conclude that 17 hours of mixing time would be required in order to achieve accurate ignition delay measurements. However, looking at the optical images gave further insight into these results. Figure 4-8 shows the optical images obtained from the ignition delay tests carried out after the mixing times mentioned in Table 4-3. At first glimpse, a trend common with the DTC results can be observed, which is, a single flame originating at the top and propagating downwards. This flame propagation behavior was consistent in all mixing time tests, which also ensures that the clean combustion protocol is working well as no pre-ignition events and only a single flame kernel was observed in all the tests.

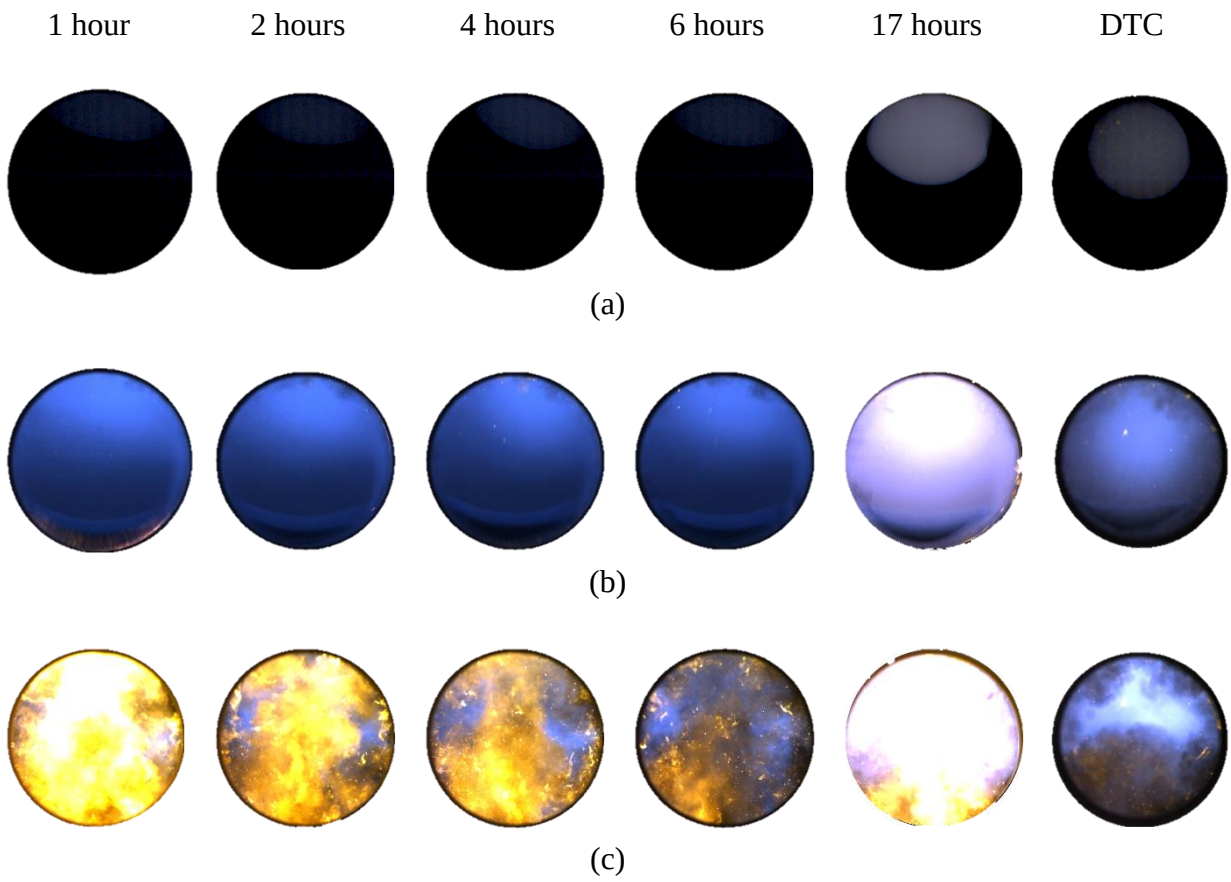

Figure 4-8: Comparison of optical images obtained after various mixing times using a mixing tank versus DTC method at T_c=800 K and P_c=20 bar, (a) 3 ms before the flame kernel has just reached the bottom of the combustion chamber, (b) reference image when flame just reached the bottom and (c) 3 ms after flame had reached the bottom.

The temporal distribution of the images in Figure 4-8 is such that the images in row (a) are 3 ms before the flame front has just reached the bottom of the combustion chamber, the images just as the flame reaches the bottom of the chamber are in row (b); and the images in row (c) are 3 ms after the flame front had finished propagating across the combustion chamber. The difference in flame intensities in the case of 17 hours of mixing could be because of stratification taking place due to such prolonged mixing times. As a result of this, due to the supply port being at the top of the mixing tank, a lean mixture (since air is lighter than ethanol vapor at a given temperature and pressure because of its lower molecular weight than ethanol) is supplied to the RCM for

measurements that causes the bright intensity in burning and saturation of the optical images. Due to the large scatter of IDTs using the mixing tank, it is clear that the mixture is not homogeneous even after 4 hours of mixing and by 17 hours of mixing the mixture may have begun to stratify.

4.4.2.1.1 Modifications to Stirrer Magnet and Optical Head

Based on the above results, it was determined that the two-inch long stirrer that was originally inside the mixing tank was not adequate for the 15.9 L tank even at 600 rpm. It was suspected that the stirrer was too short in height to cause appropriate turbulence for proper mixing. In order to improve mixing, the stirrer was modified by using aluminum pieces to increase its height. Figure 4-9 (a) shows the original stirrer magnet and Figure 4-9 (b) shows the modification that was made by attaching an aluminum foil that was one inch in height.

(a) (b)

Figure 4-9: (a) Original stirrer magnet (b) aluminum foil attached to the stirrer magnet.

In the preliminary optical tests using the mixing tank, the images in Figure 4-8 show a clean blue flame propagating downward and after reaching the bottom, a yellow sooty flame starts to develop and propagate upwards which later on consumes the whole combustion chamber. This implies that there are some impurities that lie at the bottom of the combustion chamber, which start burning with a yellow flame once the ethanol flame reaches the bottom. It was, therefore, difficult to determine the optimum mixing time as all images showed a yellow sooty flame even after 17 hours of mixing. It was later discovered that during the oxygen runs that were performed as part of the clean combustion chamber protocol, the Teflon ring that stays in direct contact with the

combustion chamber seemed to burn and as a result would get chipped which introduced white particles in the combustion chamber. Performing a combustion test after this would result in the smaller lighter particles burning and showing up as bright spots along with the ethanol flame. Once this flame has propagated to the bottom, the bigger heavier of the particles that lie at the bottom would start to burn with a yellow sooty flame. Since these particles were heavy, they were not removed with the RCM vacuum pump. As a remedy, the Teflon ring was replaced with a combination of a metal and an O-ring that served a similar purpose to the Teflon ring but had better flame resistance as only the metal ring would be in direct contact with the combustion chamber.

The results with the modifications to the optical head and the stirrer magnet can be seen in Figure 4-10 and show the usual blue flame propagating downward, but this time no yellow flame is observed from the bottom up. The temporal distribution of the images in Figure 4-10 is identical to the images in Figure 4-8, i.e. the images in row (a) are 3 ms before the flame front has just reached the bottom of the combustion chamber, the images as the flame reaches the bottom are in row (b), and the images in row (c) are 3 ms after the flame front had just propagated across the combustion chamber. Additionally, bright spots are no longer observed appearing within the flames. Also, the optical images after 1 hour of mixing look similar to those after 4 hours of mixing and the same can be said regarding the IDTs, the results of which are tabulated in Table 4-4. Comparing the mixing tank images with those obtained using the DTC method, we see that a homogeneous mixture is achieved using the DTC method with just 5 minutes of mixing time within the combustion chamber. Again, yellow flames are observed at the bottom in those cases, which are due to the Teflon ring impurities as the DTC tests were performed before the mixing tank tests and the effect of these impurities was not as drastic as can be observed in the optical results already

discussed in Section 4.4.1 of this chapter. The apparent propagating speeds of these flame fronts at T_c=800 K were also calculated to be identical to those seen in the DTC results.

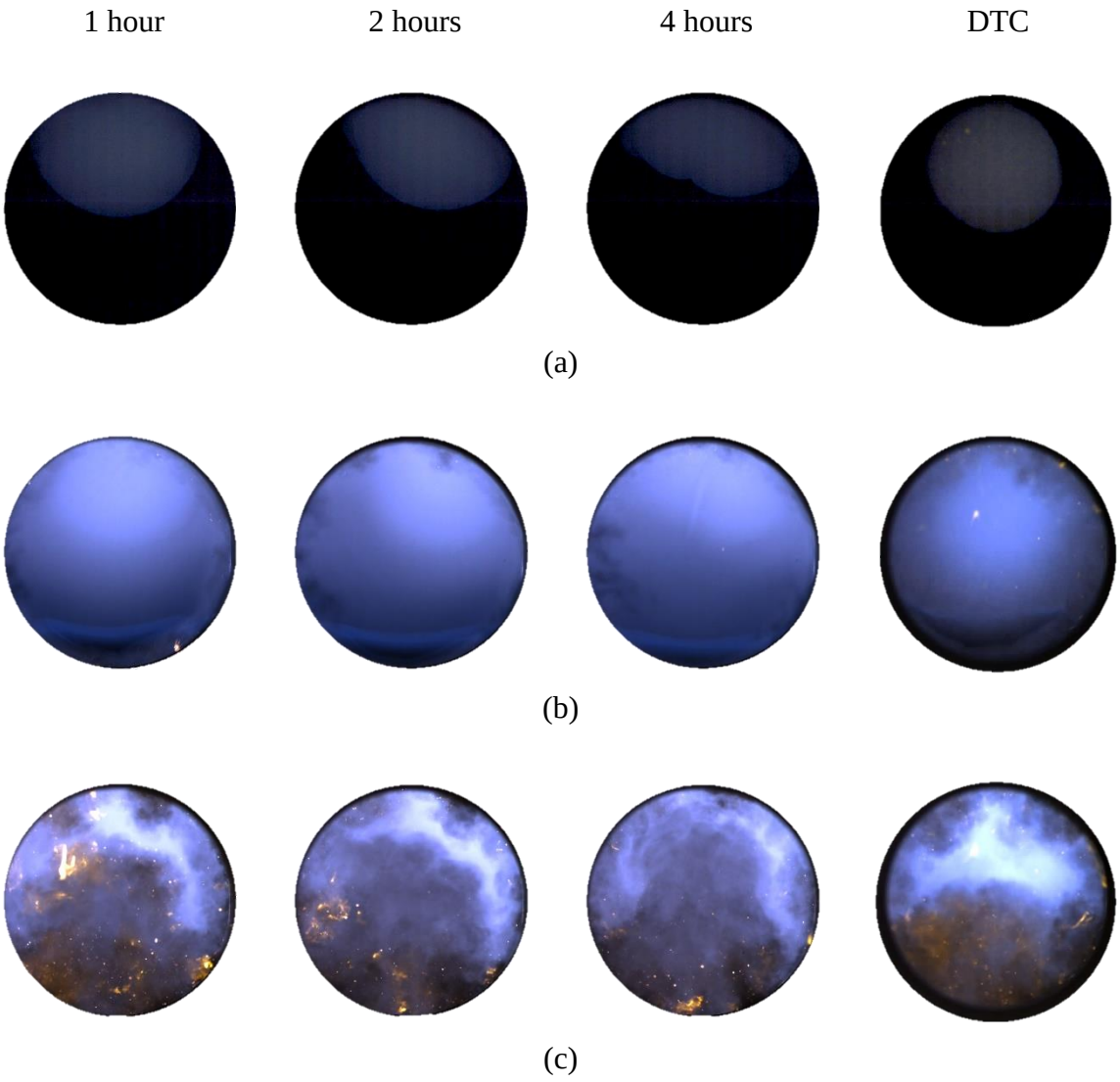

Figure 4-10: Comparison of optical images obtained after various mixing times using a mixing tank with modifications to the stirrer and optical head versus DTC method at T_c=800 K and P_c=20 bar, (a) 3 ms before the flame kernel has just reached the bottom of the combustion chamber, (b) reference image when flame just reached the bottom and (c) 3 ms after flame had reached the bottom.

Table 4-4: Comparison of ethanol IDTs at different mixing times for compression ratio=11.7 at 20 bar and ϕ =1 for the two mixture preparation methods.

Mixing Time	**Average IDT (ms) using Mixing Tank**	**Average DTC IDT (ms)**
1 hour **(with Teflon Ring)**	34.8 ± 3.6	46.4 ± 3.4 (5 minutes of mixing inside the combustion chamber)
1 hour	35.6 ± 3.6	
2 hours	35.7 ± 4.2	
4 hours	38.9 ± 4.1	
7 hours **(Metal Window)**	35.7 ± 1.4	

In order to show that the DTC results were accurate and that the Teflon ring particles do not affect the IDTs; the Mixing Tank tests were re-run with the modified stirrer and the metal ring was replaced with the Teflon ring. The results in Table 4-4 show that the IDTs after 1 hour of mixing are similar to those obtained from the tests in which the metal and O-rings were used. This confirmed that the particles from the Teflon ring did not affect the IDTs. Furthermore, a test using the metal window was conducted after 7 hours of mixing and the IDTs obtained from that mixture were similar to those obtained after 1, 2 and 4 hours of mixing. This confirmed that the ignition delay data obtained using the optical end wall and the metal end wall for the same compression ratio of 11.7 is identical and also implies that as a result of the modifications done to the stirrer magnet, the mixing is more effective and just 1 hour of mixing would be enough to get accurate test data. However, a minimum of 2 hours of mixing time was allowed for all mixtures.

Due to improper functioning of the stirrer prior to the modification, the results in Table 4-3 and the corresponding optical images depicted in Figure 4-8 were considered invalid and were not used for comparison of results in the following sections.

In Figure 4-11, it can be observed that only a single spherical flame kernel propagates across the chamber, most often from top to bottom, in all the tests that were performed with the cleaning protocol. For the experiments presented here, the flame kernels were first observed at the start of the pressure rise during the main ignition event, and not at any earlier time. Additionally, the light intensity of the optical images increased to a maximum at the point that also corresponded to the time of the maximum pressure rise rate ($(dP/dt)_{max}$). The temporal distribution of the images in Figure 4-11 is such that the first image corresponds to 0.5 ms after the start of ignition event ($dP/dt>0$) and the subsequent images were optimized to improve visibility. Also, for brevity, only the optical images of the second test run for each compressed condition are shown, although images were similar for all runs. The apparent propagating speeds of these flame fronts were calculated to be between 5–8 m/s, which was also observed by Büttgen et al. [25] for a 20 bar, 875 K and ϕ=0.5 case. However, in contrast to their study, no slight pressure rise was observed after the end of compression for any of the cases. Overall, it can be concluded that there is a good agreement between the optical images and the IDTs of ethanol obtained from the mixing tank and the DTC method, where the average deviation between the two is about 12%. From the optical images obtained using the mixing tank and with the metal plate in Figure 4-10, it can be concluded that the flame propagation is not affected by the injector. This also validates the DTC method and makes it a much more convenient mixture preparation method relative to the mixing tank, for ignition delay measurements using an RCM.

In order to ensure that using premixed air did not affect the ignition delay measurements due to the presence of small quantities of water vapor, carbon dioxide, etc., a few tests were conducted at 825 K and 20 bar compressed conditions, by preparing a mixture of nitrogen, oxygen and ethanol in the mixing tank. The results are plotted as black squares in Figure 4-18, and it can be observed that the ignition delay times were similar to those obtained using premixed air and ethanol; the same can be said for the optical images shown in Figure 4-12.

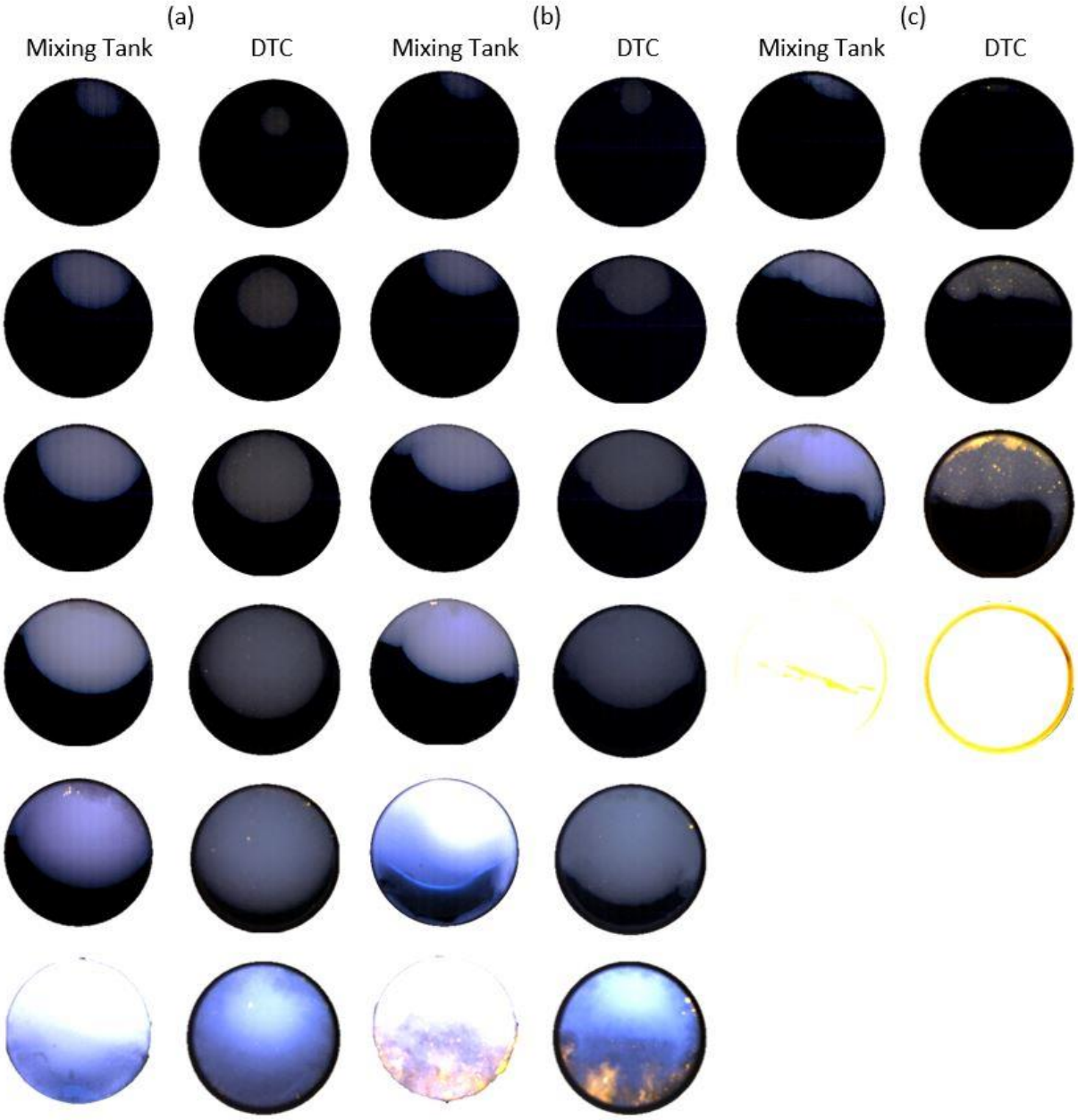

Figure 4-11: Comparison of optical images obtained from Mixing Tank and DTC tests at (a) T_c =800 K, (b) T_c =825 K and (c) T_c =850 K and 20 bar pressure.

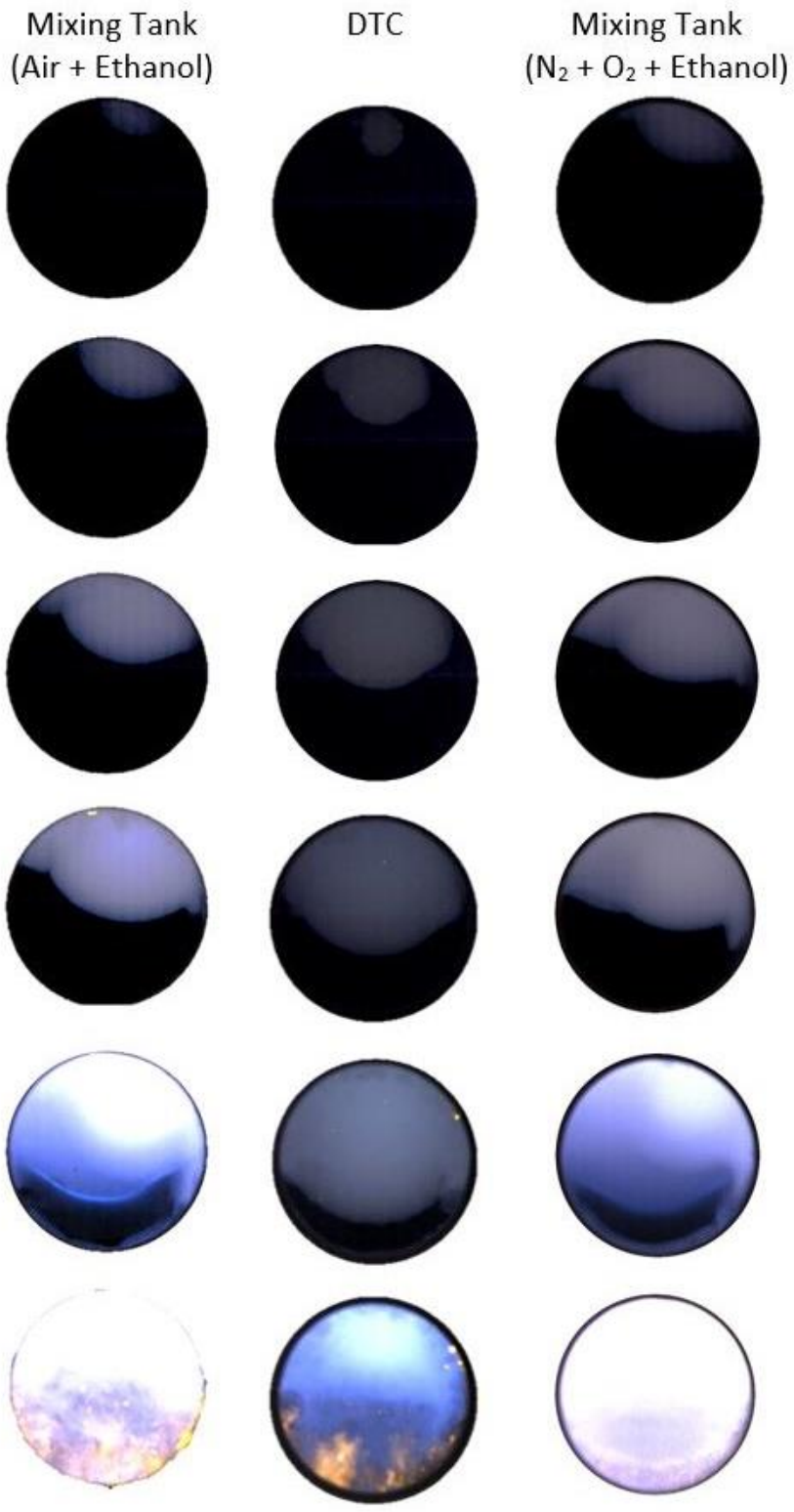

Figure 4-12: Comparison of optical images obtained from Mixing Tank and DTC tests at T_c =825 K and 20 bar pressure.

4.4.3 Results and Discussion

Once the optimum time was set and the necessary modifications were done to the RCM, tests were conducted to study the effects of mixture preparation method on IDTs. Tests were conducted at both the compression ratios to see if the post-compression heat losses were sensitive to the mixture preparation method. Since it was established earlier that ignition delay data using an optical end wall and metal end wall for a given compression ratio was identical, comparisons were made from data obtained from tests that employed both the optical and metal windows in each mixture preparation method.

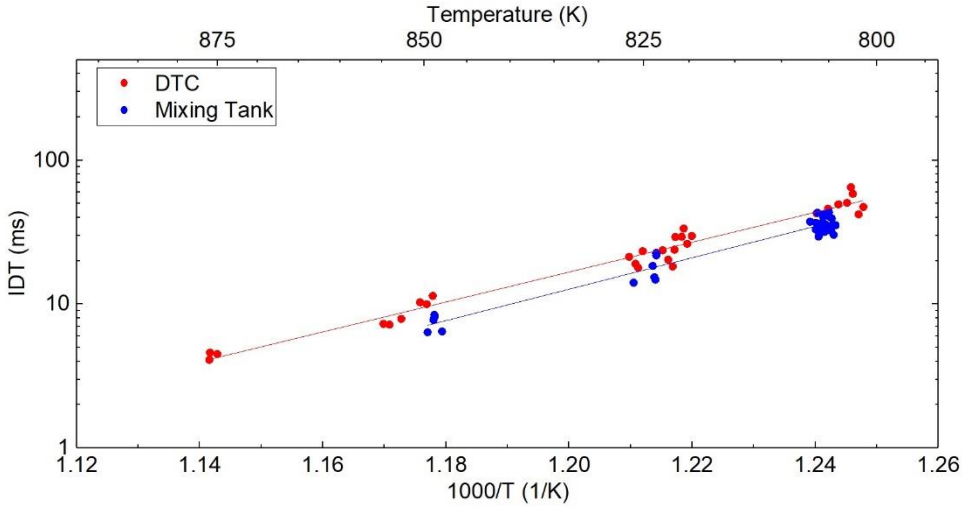

Figure 4-13: Comparison of Mixing Tank (blue) and DTC (red) results at CR=11.7, P_c=20 bar.

Figure 4-13 compares the ignition delay results obtained at CR=11.7 using both the mixing tank and DTC methods. The IDTs obtained using the mixing tank are consistently shorter than the DTC results. However, the results are in reasonable agreement as the difference in ignition delay is about 10 ms at T_c=800 K and 825 K and are almost similar at 850 K.

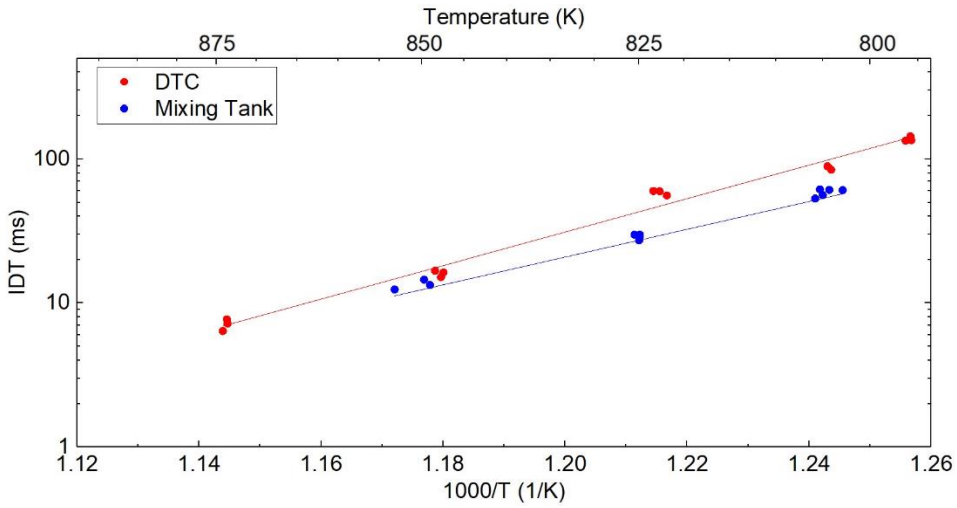

Figure 4-14: Comparison of Mixing Tank (blue) and DTC (red) results at CR=17.1, P_c=20 bar.

At CR=17.1, the difference in ignition delay between the mixture preparation methods is the highest at low temperature as compared to that at CR=11.7, as can be observed in Figure 4-14. The reason for the mixing tank results being consistently shorter than those obtained using the DTC method is attributed to the fact that the use of the mixing tank results in replacing the injector and the water jacket that is needed to protect the injector from high temperatures, with a metal plate as can be seen in Figure 4-15. The water jacket is otherwise in direct contact with the combustion chamber and as a result, affects the insulation of the RCM, which in turn affects the rate of heat exchange. Replacing the water jacket with a metal plate improves the insulation and hence the heat losses are less. However, the difference in heat loss is not distinct enough to be reflected in the pressure traces. The reduced heat losses do, however, lead to a shorter IDT for the mixing tank tests compared to those completed with the DTC method.

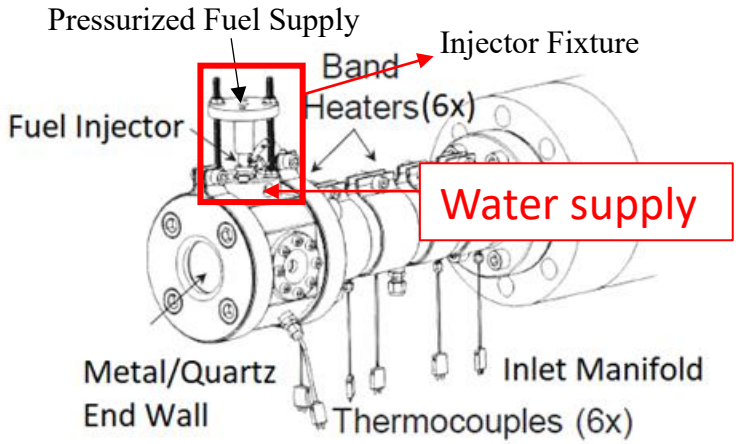

Figure 4-15: Combustion chamber setup using DTC method, highlighting the injector fixture and water supply.

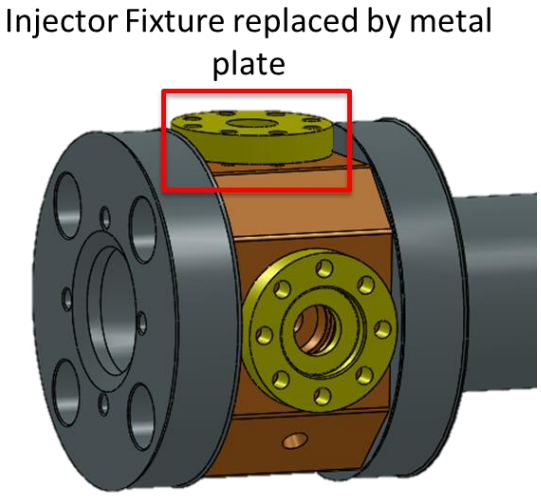

Figure 4-16: Combustion chamber setup using a mixing tank, injector fixture replaced by a metal plate.

It is anticipated that the water jacket would have amplified the heat loss effect when the compression ratio was increased to CR=17.1 as the fraction of surface-to-volume ratio that is in contact with the jacket is comparatively greater and hence the heat losses would be greater as well. Therefore, we observe a bigger difference in IDTs at CR=17.1 using the two mixture preparation methods, as compared to those at CR=11.7.

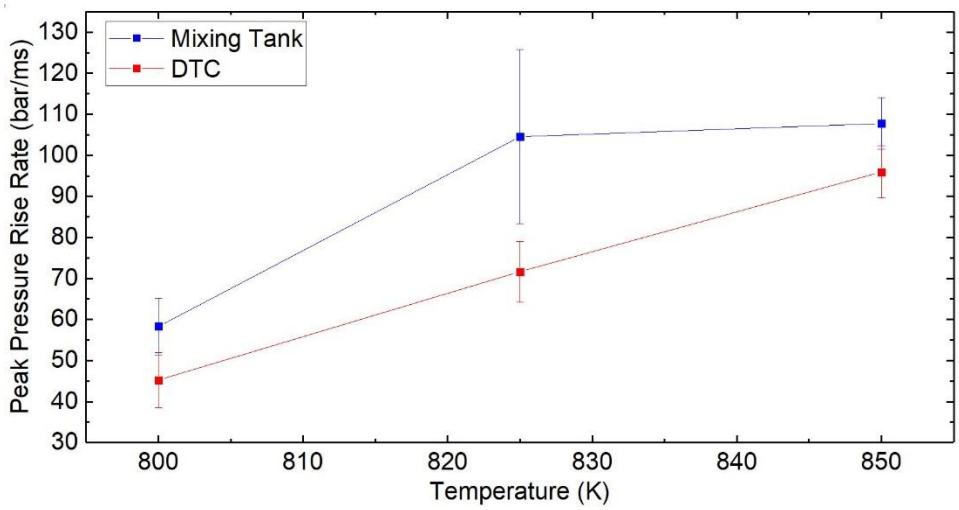

(a)

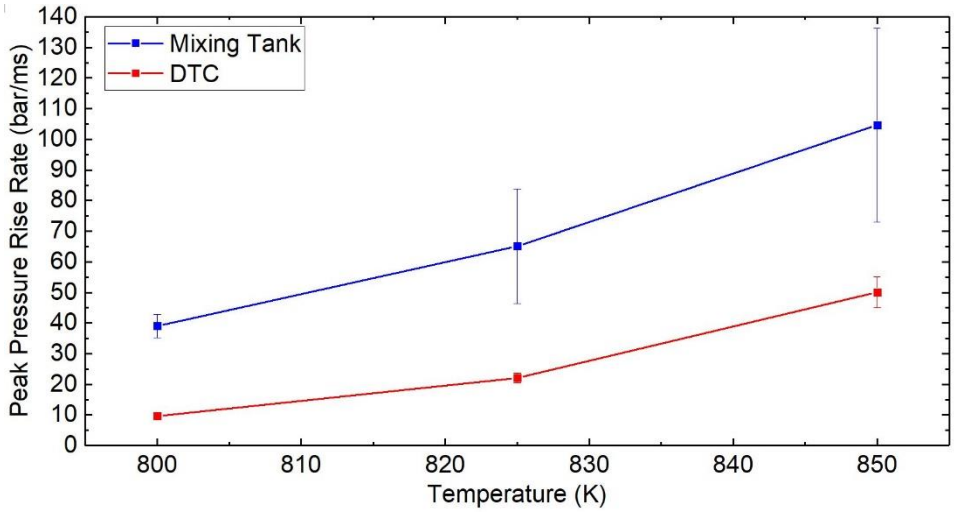

(b)

Figure 4-17: Comparison of Heat Release Rates at (a) CR=11.7 and (b) CR=17.1, for stoichiometric ethanol air mixture at 20 bar using the two mixture preparation methods.

As can be observed from Figure 4-17, experiments conducted using the mixing tank have higher heat release rates (HRR) as compared to those conducted using the DTC method, at both the compression ratios. This is also attributed to the injector fixture along with the water supply being replaced by the metal plate. This causes comparatively lesser heat losses and hence, makes it easier to heat the mixture (rate of pressure rise is faster).

Therefore, experiments were then conducted by preparing the fuel/air mixture in the mixing tank while keeping the injector fixture in place with water supplied through the jacket to keep the configurations between the two methods as similar as possible. This helped keep the rate of pressure rise rates identical in both methods and enabled a better comparison in ignition delay measurements.

Figure 4-18 compares the ignition delay results obtained at CR=11.7 and CR=17.1 using both the mixing tank (with the injector fixture and water supply) and DTC methods. The IDTs obtained using the mixing tank are in agreement with the DTC results. As can be observed from Figure 4-19, experiments conducted using the mixing tank have similar peak pressure rise rates and identical trends as temperature increases to that observed using DTC method. Therefore, it can be said that for a given configuration of the RCM, diluent gas composition, initial conditions and at a given compressed condition, the ignition delay times would be shorter if the peak pressure rise rates are higher.

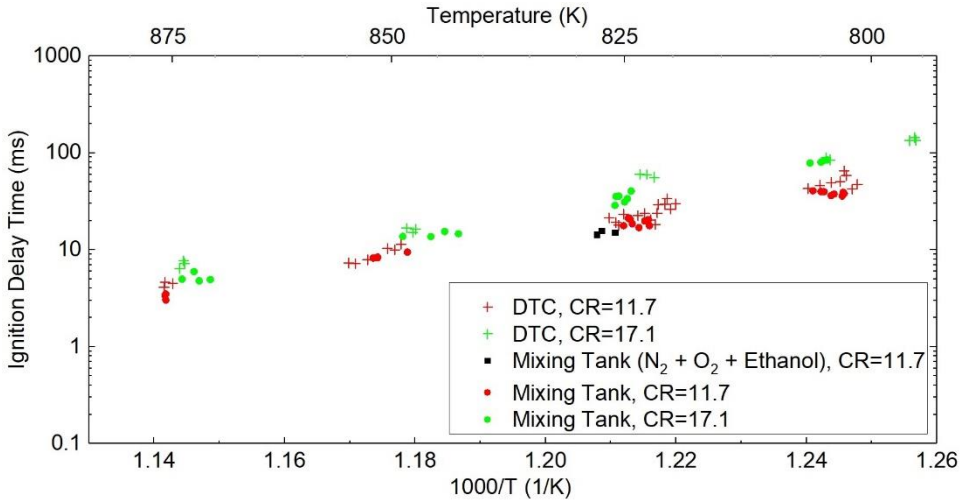

Figure 4-18: Comparison of IDTs using the two mixture preparation methods at CR=11.7 and 17.1, for a stoichiometric ethanol air mixture at 20 bar.

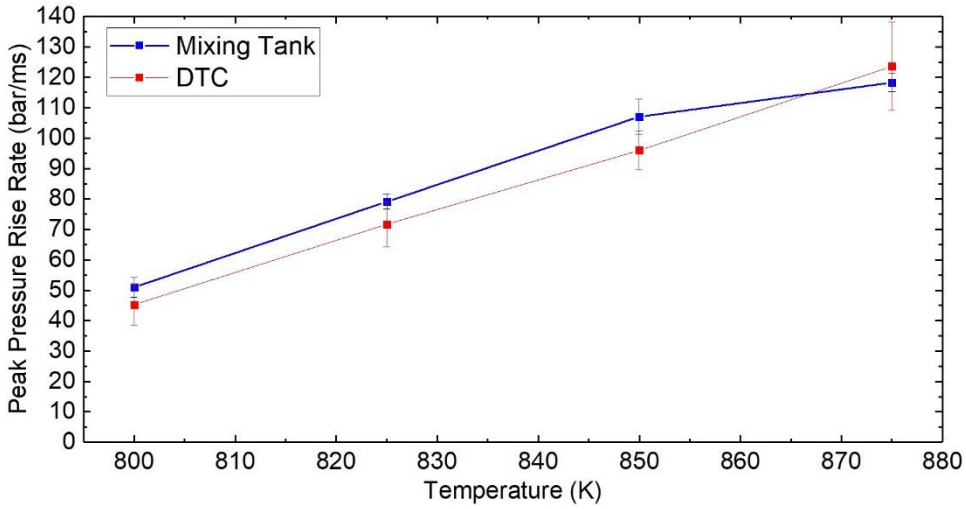

(a)

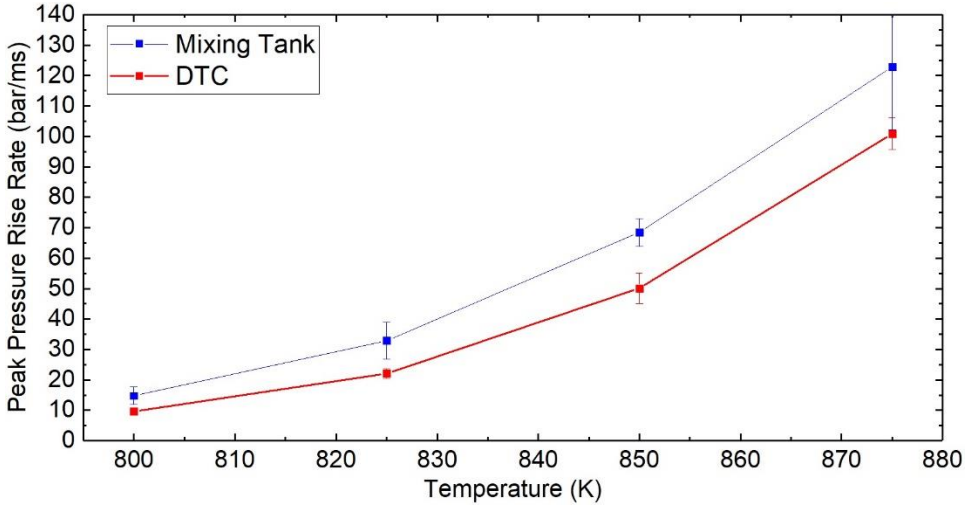

(b)

Figure 4-19: Comparison of Peak Pressure Rise Rates using the two mixture preparation methods at (a) CR=11.7 and (b) CR=17.1, respectively, for stoichiometric ethanol air mixture at 20 bar.

4.5 Effect of post-compression heat losses

4.5.1 Comparison of DTC Results

It is a well-known fact that the same set of compressed conditions can be achieved using different compression ratios. When using different compression ratios, the initial conditions needed to achieve the same compressed conditions change accordingly. For example, in the present

study, the above-mentioned compressed conditions of 20 bar and 800, 825 and 850 K were achieved by using two different compression ratios of 11.7 and 17.1. As mentioned previously, the higher compression ratio was achieved by flipping the metal end wall, as shown in Figure 2-2, thereby reducing the clearance volume while maintaining the same stroke length. In order to eliminate the difference in heat losses due to the material (metal or quartz) of the end wall, the tests that were run with the optical end wall were repeated using the metal end wall at the same compression ratio of 11.7.

Figure 4-20 depicts a plot of IDT vs 1000/T (K) for all the DTC tests that were carried out, using the optical as well as the metal end walls. It can be derived from the plot that the IDTs for a compression ratio of 17.1 are higher than those for a compression ratio of 11.7 for all cases. However, in both compression ratio cases, Arrhenius behavior is observed.

In Figure 4-20, it can be seen that the IDT for T_c=800 K and compression ratio of 17.1, is greater than 100 ms. It has been previously shown that the growth of the thermal boundary layer limits the maximum test time to about 100 ms, as beyond this, the adiabatic core hypothesis breaks down prior to ignition [26]. It was also shown in a study by Mittal et al. [3] that longer IDTs can cause larger low-temperature zones that can have temperature deviations of up to 100 K relative to the adiabatic core temperature, which are potentially caused by corner vortices which can interfere with the core region. It is also clear from Figure 4-20 that the difference in IDTs for different compression ratios at the same compressed conditions reduces as T_c increases. This is most likely due to the shorter ignition delay in these cases, which allows less time for heat losses to affect the ignition delay time.

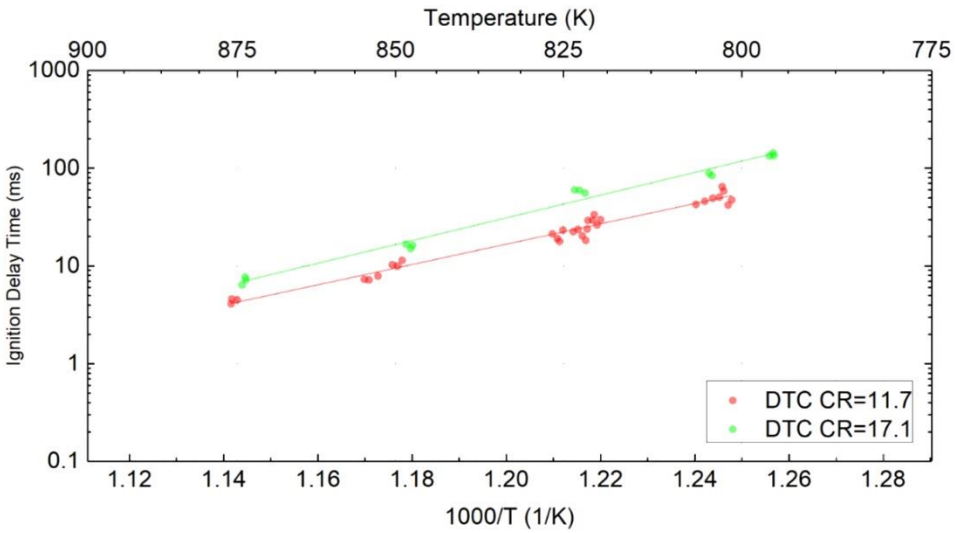

Figure 4-20: Plot of IDT vs 1000/T (K) for compression ratio 11.7 and compression ratio 17.1 at 20 bar pressure and ϕ=1, using DTC method.

There are several possible reasons that contribute to the differences observed in IDTs for different compression ratios, even when the compressed temperature and pressure conditions are the same:

1. Heat Losses:

It can be seen in Figure 4-21 and Figure 4-22 that the heat losses for the CR=17.1 case are greater than that for the CR=11.7 case. Referring to Figure 4-21, the pressure in the 11.7 CR case drops from 19.9 bar to 15.3 bar (4.6 bar) after 100 ms, whereas in the 17.1 CR case, the pressure drops by 5.5 bar. This is due to the higher surface-to-volume ratio in the higher compression ratio case, which causes heat transfer to occur at a faster rate to the cylinder walls and eventually lead to a longer ignition delay. The surface area-to-volume ratio for CR=17.1 is 265.43 m^{-1} and for CR=11.7 is 203.39 m^{-1}, which is about 30% more.

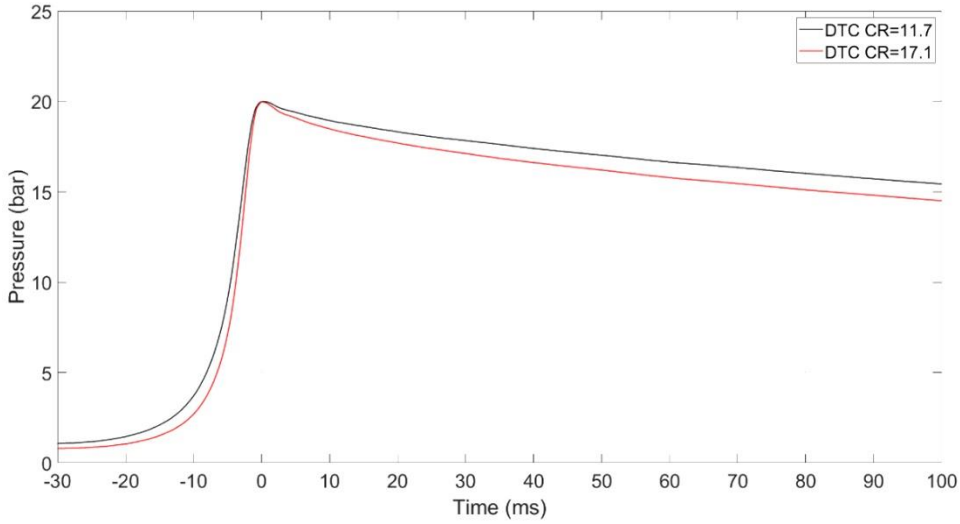

Figure 4-21: Non-reactive pressure traces for compression ratios of 11.7 and 17.1 at T_c = 875 K and 20 bar pressure (also note the decrease in compression time for the higher compression ratio case).

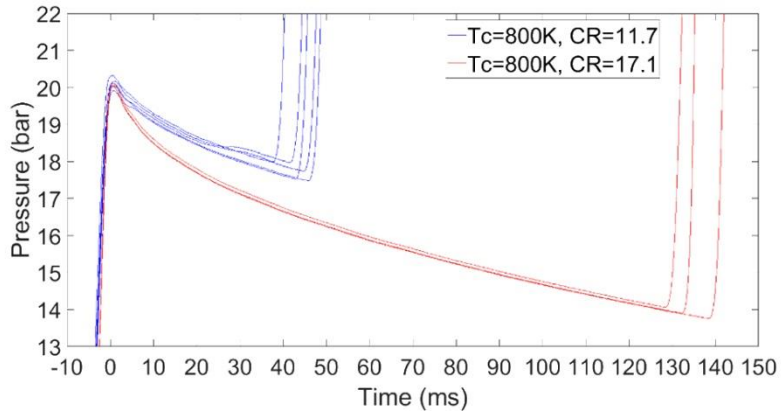

(a)

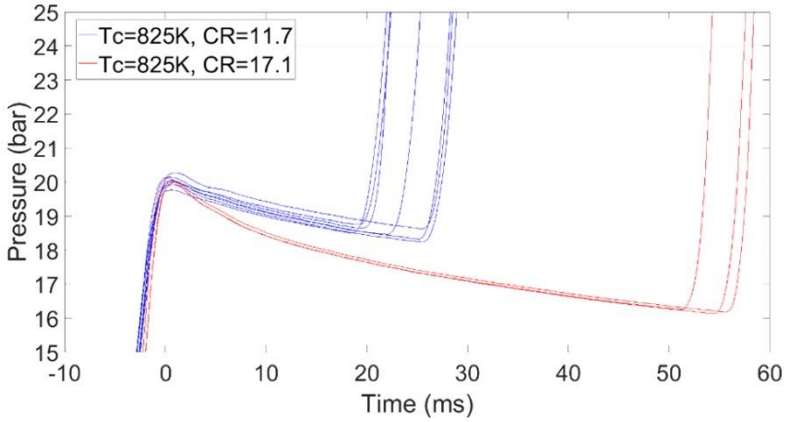

(b)

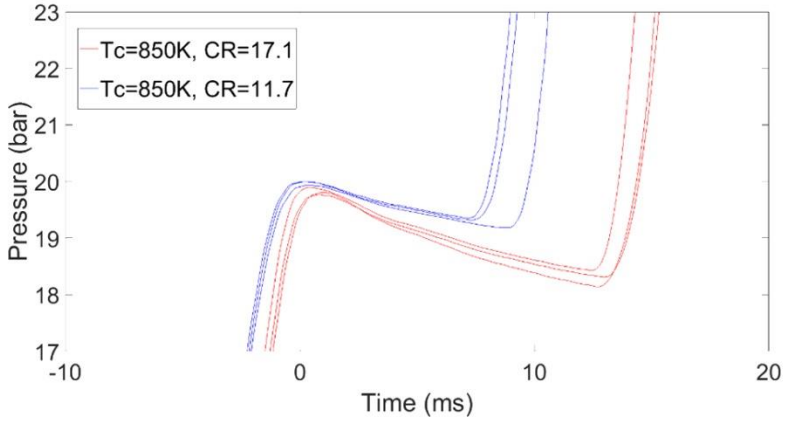

(c)

Figure 4-22: Plot comparing the pressure traces of the two compression ratios representing the difference in ignition delay at 20 bar and (a) T_c=800 K, (b) T_c=825 K, (c) T_c=850 K and (d) T_c=875 K, using DTC method (blue lines indicate compression ratio of 11.7, red lines indicate CR=17.1).

Figure 4-22 (cont'd)

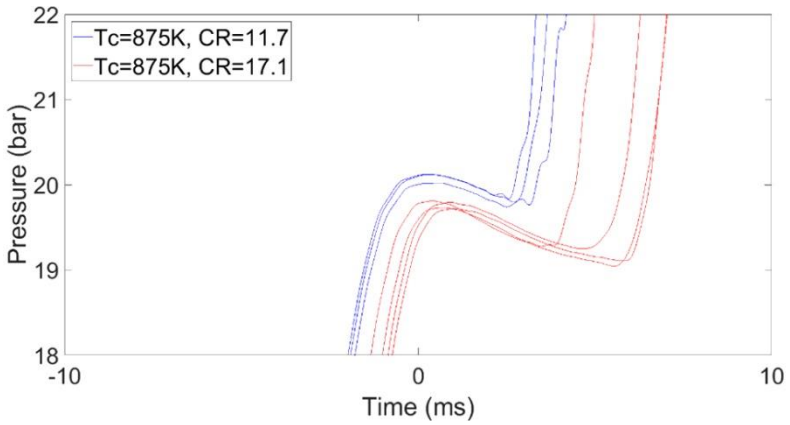

(d)

The heat transfer rate also depends on several other parameters that are facility dependent; such as the insulation around the RCM, the cylinder head and piston configuration, etc. In other words, across facilities, higher compression ratio does not necessarily mean there is a higher rate of heat transfer. However, it does imply that higher heat transfer rates would lead to longer IDTs. In Chapter 5, it will be shown through simulations that keeping the heat transfer rate constant across both compression ratio configurations leads to the same IDT for a given set of compressed conditions. Figure 4-23 compares the peak dP/dt, which is representative of heat release rates during the ignition event at two different compression ratios but for same compressed conditions. It is clear that the heat release rate is consistently higher at CR=11.7 as compared to that at CR=17.1. This difference in heat release rates is attributed to the surface-to-volume ratio. Since CR=17.1 has a higher surface-to-volume ratio, it loses heat to the surrounding at a faster rate and hence the rate of pressure rise is slower as compared to CR=11.7. This is confirmed from the chemical heat release plot in Figure 4-23. In other words, for the same combustion duration, the pressure would rise faster as a result of combustion in CR=11.7 because of lesser heat exchange with the walls due to lesser surface-to-volume ratio. This trend was also observed using the Mixing Tank method to prepare the mixture as can be seen in Figure A-2 of the Appendix.

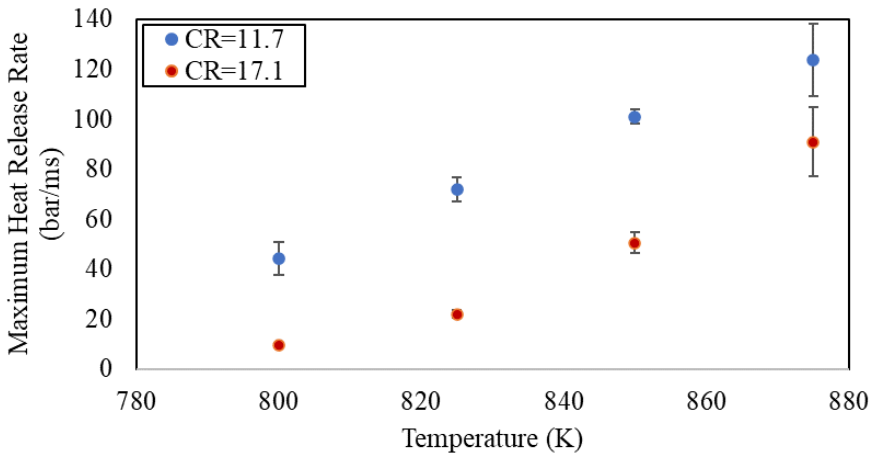

Figure 4-23: Plot comparing the maximum heat release rates during ignition at same compressed conditions of the two compression ratios, using DTC method.

2. Initial Conditions:

In order to achieve the same compressed conditions using different compression ratios, the required initial conditions need to be different. Maintaining a higher initial pressure and temperature can lead to increased low-temperature reactions taking place during the compression stroke, which can result in a shorter ignition delay. Additionally, as can be seen in Figure 4-21, a lower compression ratio leads to a slightly longer compression time (30 ms for a compression ratio of 17.1 vs 32 ms for a compression ratio of 11.7), which increases the potential for reactions to occur during the compression stroke. In the experiments presented here for the 11.7 compression ratio case the initial pressure was 1.04 bar and the initial temperature ranged from 403-448 K, whereas for the 17.1 compression ratio case the initial pressure was maintained at 0.79 bar and the initial temperature ranged from 373 K-418 K. The higher initial pressure and temperature conditions required for the lower compression ratio case, combined with the longer compression time are most likely the cause of the shorter IDTs. Presently there is no experimental way to confirm whether low-temperature reactions took place on a small scale during the compression stroke for this compression ratio case. The results in Chapter 5 show that HO_2 and H_2O_2 radicals

for CR=11.7 begin to form in low concentrations approximately 3ms before the end of compression. By the end of compression, results show that the concentration of these species is approximately double for the lower compression ratio case. This implies that the fuel is more reactive at the end of compression in the lower compression ratio case relative to the higher compression ratio case. However, the mole fractions of these species were not high enough to reflect a chemical heat release during the compression period.

4.5.2 Comparison of Mixing Tank Results

In order to test the effect of premixing the reactants, the same tests conditions as discussed above were now carried out by preparing the fuel and air mixture in the mixing tank and allowing it to mix for at least 2 hours, as was already discussed in Section 4.4.2.1. The results in Figure 4-24 and Figure 4-25 confirm that changing the compression ratio has an effect on the IDTs as a result of the change in the rate of heat losses due to the different surface-to-volume ratio. Figure 4-24 also confirms the Arrhenius behavior that was earlier observed and that the effect of heat losses is independent of the mixture preparation method.

Additionally, as can be seen in Figure 4-25, a lower compression ratio leads to a slightly longer compression time (30 ms for a compression ratio of 17.1 vs 32 ms for a compression ratio of 11.7). In the study by Ezzell et al. [108] it was observed through simulations that the compression times influence ignition delay times by affecting the heat loss characteristics, especially at temperatures when the ignition delay times are longer. Although the compression times compared differed by a factor of 2, the simulations using ethanol as fuel showed that even with the same compressed temperature and crevice volume, the heat loss rate through the crevice is significantly enhanced by decreasing the compression time. Two reasons were given for this behavior: 1-accelerated flow into the crevice due to greater pressure difference which in turn

increases the convection coefficient causing greater rates of heat transfer and 2- increased crevice temperature due to shorter compression time which contributes to an increased rate of heat loss.

In a study by Mittal et al. [89], it was demonstrated through modeling of the compression process in the RCM using dimethyl ether as the fuel that the induction chemistry occurring during compression can result in substantive changes in the ignition delays observed after compression. These chemical reactions are the establishment of the initial radical pool but show negligible changes in the chemical energy release of the mixture. As mentioned earlier, the lower compression ratio had longer compression time, which increases the potential for these reactions to occur during the compression stroke. Additionally, in the experiments presented here for the 11.7 compression ratio case the initial pressure was 1.04 bar and the initial temperature ranged from 403 K–448 K, whereas for the 17.1 compression ratio case the initial pressure was maintained at 0.74 bar and the initial temperature ranged from 370 K–412 K. The higher pressure and temperature initial conditions needed for the lower compression ratio case, coupled with longer compression time are also the probable causes for shorter ignition delay times, in addition to the post-compression heat losses. There is currently no experimental way to verify whether low temperature reactions occur on a small scale during the compression stroke. Therefore, it will be shown in Section 4.5 using chemical modeling that HO_2, H_2O_2 and CH_2O begin to form in low concentrations approximately 5–7 ms before the end of compression. Results show that the concentration of these species by the end of compression is significantly higher for the lower compression ratio case. This implies that the fuel is more reactive at the end of compression in the lower compression ratio case relative to the higher compression ratio case. The increased rate of heat losses and the fuel being less reactive in the higher compression ratio case as compared to

lower compression ratio case are the two contributing reasons for the longer ignition delays observed for CR=17.1 at identical compressed conditions.

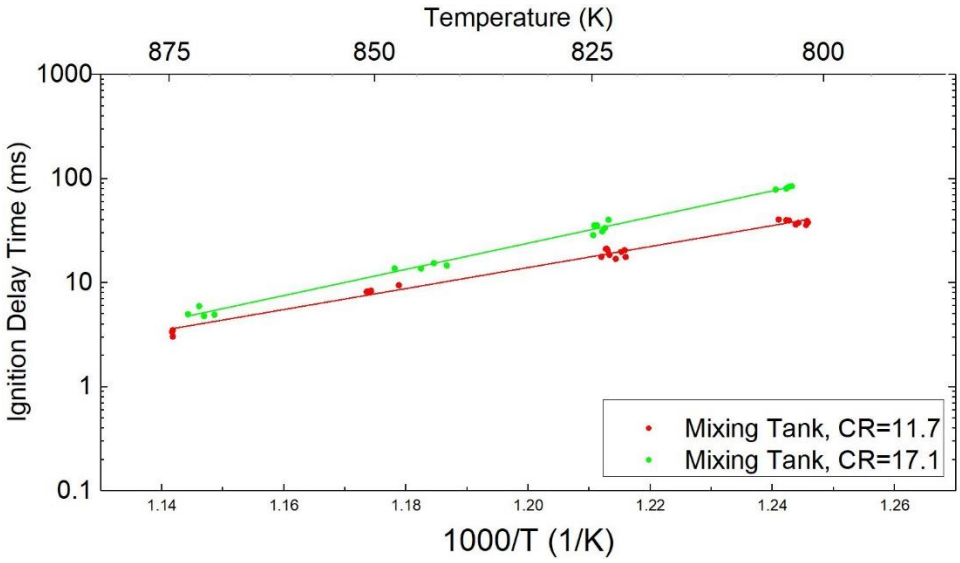

Figure 4-24: Plot of IDT vs. 1000/T (K) for compression ratio 11.7 and compression ratio 17.1 at 20 bar pressure and $\phi = 1$, using Mixing Tank.

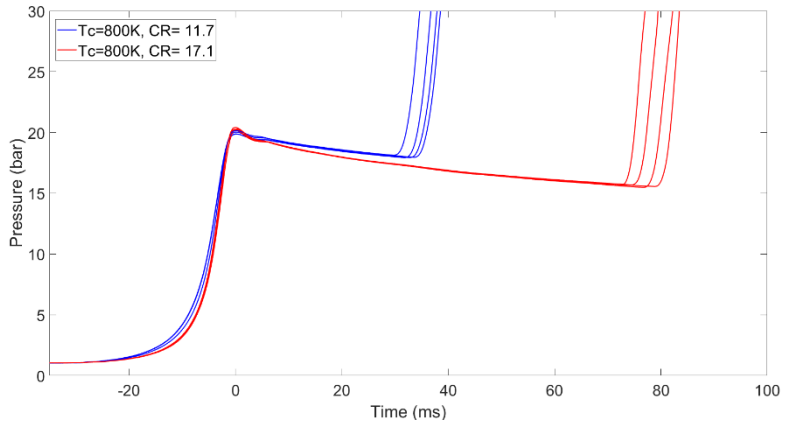

(a)

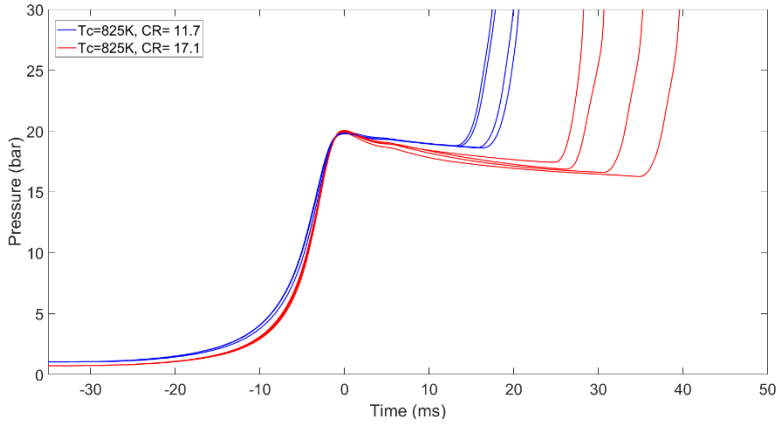

(b)

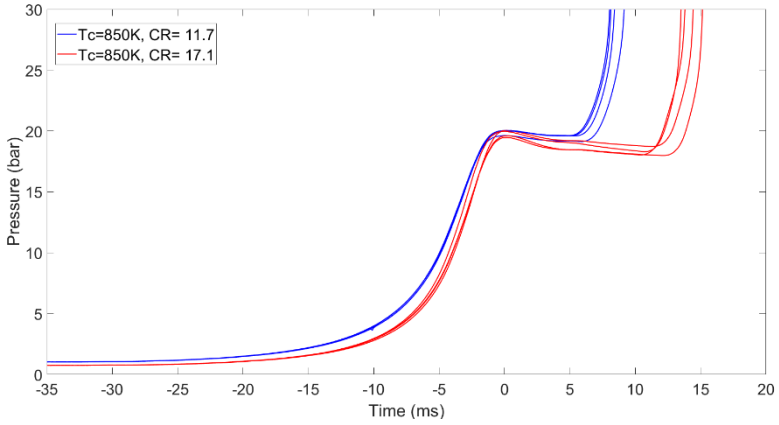

(c)

Figure 4-25: Plot comparing the pressure traces of the two compression ratios representing the difference in ignition delay at 20 bar and (a) Tc=800 K, (b) Tc=825 K, (c) Tc=850 K and (d) Tc=875 K, using Mixing Tank (blue lines indicate compression ratio of 11.7, red lines indicate CR=17.1).

Figure 4-25 (cont'd)

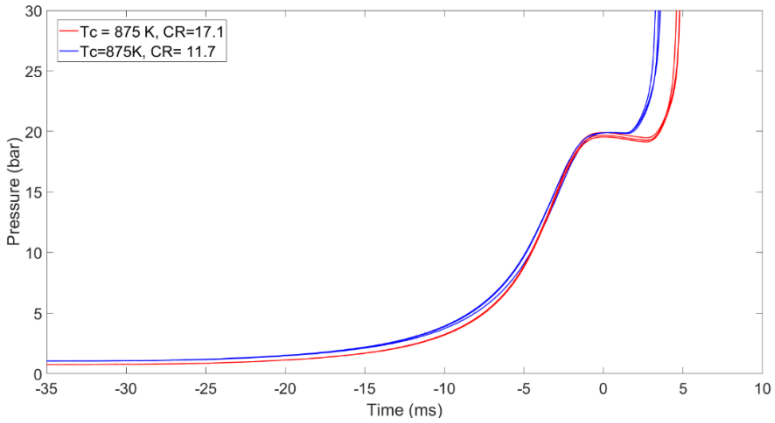

(d)

Table 4-5 tabulates all the results at different conditions using the two mixture preparation methods, with both compression ratio configurations. It can be seen that for both mixture preparation methods, the IDTs for the two compression ratios at the same compressed conditions are different. This shows that the post-compression heat losses are independent of the mixture preparation method but vary with different compression ratios, which affects the IDT.

Table 4-5: Ethanol IDTs at 20 bar and ϕ = 1 using Mixing Tank and DTC method for CR=11.7 and 17.1.

	Mixing Tank		**DTC**	
	CR=11.7	**CR=17.1**	**CR=11.7**	**CR=17.1**
800 K	38.4 ± 1.6	81.7 ± 2.5	50.2 ± 7.4	86.6 ± 2.5
825 K	19.3 ± 1.6	34.2 ± 3.7	24.2 ± 4.7	58.5 ± 1.9
850 K	8.5 ± 0.5	14.4 ± 0.7	9.0 ± 1.6	16.0 ± 0.7
875 K	3.3 ± 0.2	5.2 ± 0.5	4.4 ± 0.2	7.1 ± 0.5

Another trend that is common between both mixture preparation methods is that the difference in IDTs at different compression ratios is more or less the same when normalized. The percentage difference in IDTs when using the mixing tank at CR=17.1 and CR=11.7 was similar at all compressed temperatures and was 43 ± 7 % when normalized with respect to the IDTs at CR=17.1. This difference is similar to the 46 ± 6 % difference observed in the DTC method. However, the highest difference was at 800 K of 53% (46% using DTC) and the least was at 875 K of 36% (38% using DTC). It is clear from Figure 4-26 that the difference in ignition delay times for different compression ratios, but the same compressed conditions decreases as T_c increases, irrespective of the mixture preparation method used. This is most likely due to the shorter ignition delay in these cases, which allows less time for heat losses to affect the ignition delay time. Figure 4-26 is a plot of averaged IDTs vs averaged Tc obtained using both the compression ratios and the two mixture preparation methods. The good agreement of data between the two mixture preparation methods can be observed as the standard deviations of the IDT measurements overlap. The repeatability of the MSU RCM also improves at higher temperatures as the deviation in the IDTs is reduced. The effect of post-compression heat losses is clearly visible at the lower temperatures of 800 K and 825 K as there is a larger scatter of IDTs using both the mixture preparation methods.

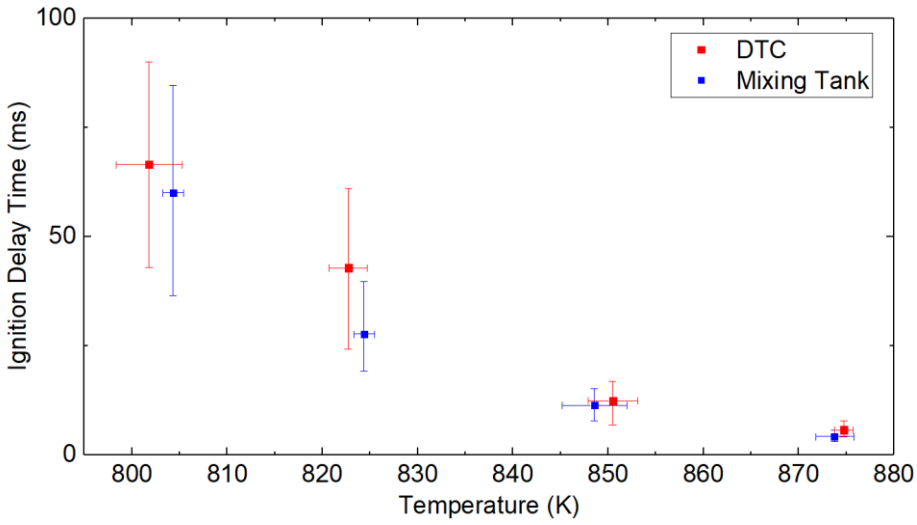

Figure 4-26: Comparison of the deviation in ignition delay times obtained from both compression ratios using the two mixture preparation methods at identical compressed conditions.

4.6. Effect of diluent gases

As discussed in Chapter 1, different compressed temperatures can be achieved while maintaining the same compression ratio by adding or replacing part of the non-reactive mixture with inert gases such as argon, carbon dioxide, nitrogen, etc. The proportions of these gases are adjusted based on the heat capacity demands needed to achieve the desired compressed temperatures. The diluent gas used in the preparation of test fuel/oxygen mixtures is inert and does not take part in the chemical reaction. However, the use of these different diluent gases can alter IDTs of the mixture mainly by changing heat loss properties and also by changing the third body efficiencies. To investigate the diluent gas effect, the tests were repeated with the nitrogen replaced by argon, while maintaining the diluent-to-oxygen ratio of 3.76:1. The remainder of the RCM configuration was kept the same; a compression ratio of 11.7 was employed and the DTC method was used to prepare the fuel/air mixture. The argon and oxygen mixture was prepared in the mixing tank described in Chapter 2 and the mixture was allowed to homogenize for 2 hours before beginning the tests. Due to the lower thermal capacity of argon relative to nitrogen, the initial

conditions needed to achieve the same set of compressed conditions were much lower compared to what were needed for nitrogen, at a given compression ratio. For example, using a CR=11.7, in order to achieve compressed temperature range of 800 K-850 K with argon as the diluent, the initial temperature required was in the range of 320 K-340 K as compared to 403 K-433 K needed when nitrogen was used as the diluent. As a result, more time was allowed for the ethanol to vaporize and mix with the air as initial temperatures were lower than the saturation temperature. When nitrogen was used as a diluent, 5 minutes was allowed for the ethanol to evaporate and mix; whereas with argon, 10 minutes was allowed for the same purpose. However, since the fuel partial pressure was sufficiently less than the fuel vapor pressure at the initial temperatures mentioned earlier, complete vaporization was guaranteed and the loss of fuel to wall adsorption was negligible [115,116]. In order to ensure that ethanol was evaporating and had sufficient time for mixing at initial temperatures lower than the saturation temperature, the combustion chamber was first filled with argon and oxygen mixture to the desired pressure needed to achieve 20 bar compressed pressure and ethanol was injected. The increase in pressure as ethanol evaporated was measured and monitored through the absolute pressure manometer and the time to reach the calculated final pressure (partial pressure of fuel + partial pressure of argon and oxygen) was measured as well. It was observed that the desired final pressure was reached well within 10 minutes allowing for homogeneous mixing to take place and implying that all the injected ethanol had evaporated. Additionally, the repeatability of the experiments ensures evaporation and homogeneous mixing of fuel and air. As mentioned earlier, since the initial temperatures required were already much lower with argon at CR=11.7, using a CR=17.1 to attain the same compressed conditions was not feasible as even lower initial temperatures would be needed which were either not realistic or would not ensure ethanol evaporation. For instance, in order to achieve a compressed condition of

20 bar and 800 K using CR=17.1, an initial pressure of ~0.58 bar and temperature of 283.15 K (10 deg. C) is needed. The partial pressure of ethanol at this condition would be ~0.038 bar and the saturated vapor pressure of ethanol at 283.15 K is 0.031 bar [117] which implies that ethanol would not evaporate at this condition. However, achieving higher temperatures would require increasing the initial temperatures which in turn would mean the ethanol would evaporate at those temperatures, but the feasibility of maintaining those initial temperatures was still not possible, at least up to 825 K (initial temperature of 19 deg. C). Therefore, comparisons were made only at CR=11.7 as higher compressed temperatures (>850 K) were observed to give similar IDTs, irrespective of the diluent gas composition.

A non-reactive experiment was performed to ensure that no significant heat release occurred during the compression stroke. The non-reactive tests were conducted at identical initial conditions to which the reactive tests were carried out, except that the oxygen in the mixture was replaced by argon in order to eliminate oxidation reactions and at the same time, maintain a similar heat capacity ratio.

The results shown in Figure 4-27 indicate that for T_c =800 K and 825 K with argon as a diluent, the IDTs were greater than 100 ms. Since the adiabatic core hypothesis is only valid until 100 ms [3,71], these measurements are not valid. However, the results are included as they show that the IDTs at T_c =800 K and 825 K when using argon as diluent are longer compared to when using nitrogen as a diluent. This is because of the lower heat capacity (12.5 J/K at 300 K [117]) of argon compared to nitrogen (20.6 J/K at 300 K [117]). This is because of the lower heat capacity (12.5 J/K at 300 K [117]) of argon compared to nitrogen (20.6 J/K at 300 K [117]). The lower heat capacity causes the mixture to lose heat with the walls at a faster rate, thereby leading to greater heat losses as can be observed from the non-reactive pressure trace in Figure 4-28 and from the

reactive pressure traces in Figure 4-29. However, this effect is minimized at T_c=850 K and 875 K due to the shorter ignition delays, and the IDTs are in reasonable agreement with those obtained using nitrogen as diluent. Arrhenius behavior is still valid for these sets of experiments.

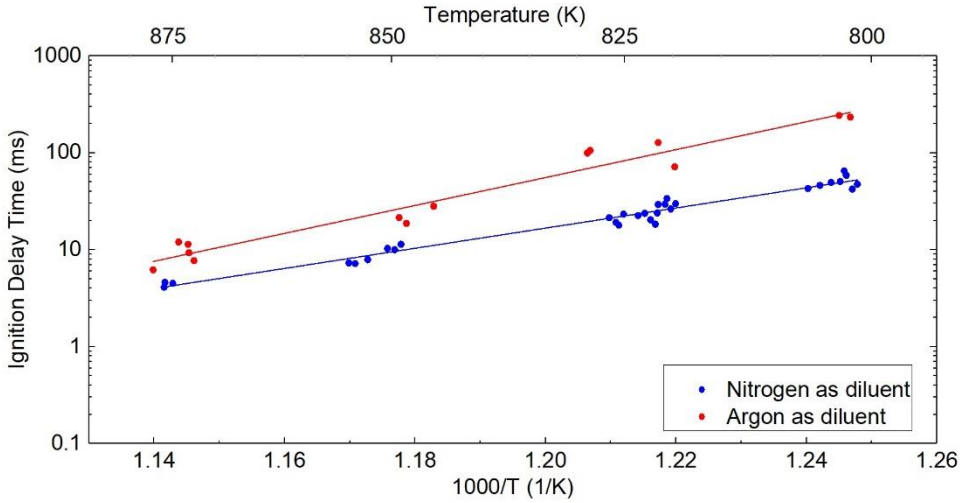

Figure 4-27: Comparison of IDT vs. 1000/T (K) for compression ratio 11.7 at 20 bar pressure and ϕ = 1, using nitrogen as diluent vs when using argon as diluent.

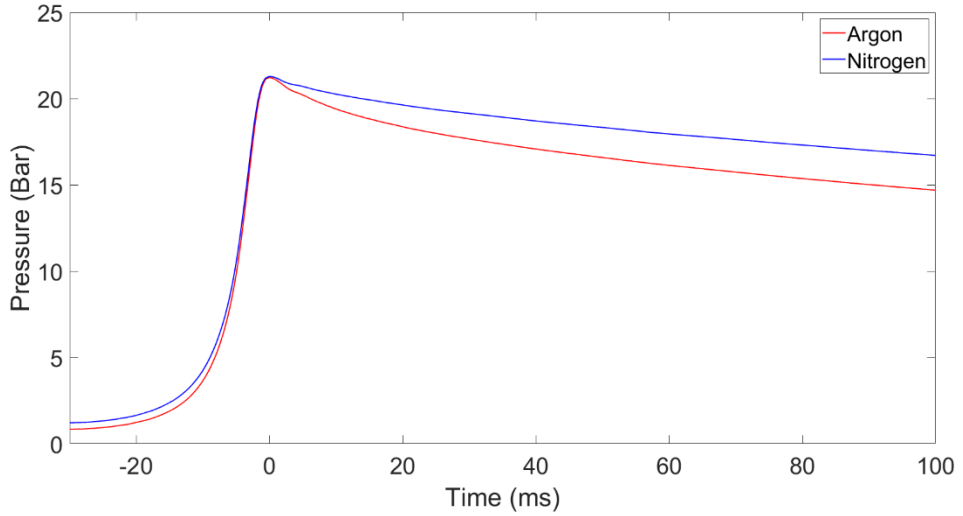

Figure 4-28: Comparison of non-reactive pressure traces when using nitrogen as a diluent (blue) vs when using argon as a diluent (red) for a compression ratio of 11.7, T_c = 825 K and 20 bar pressure.

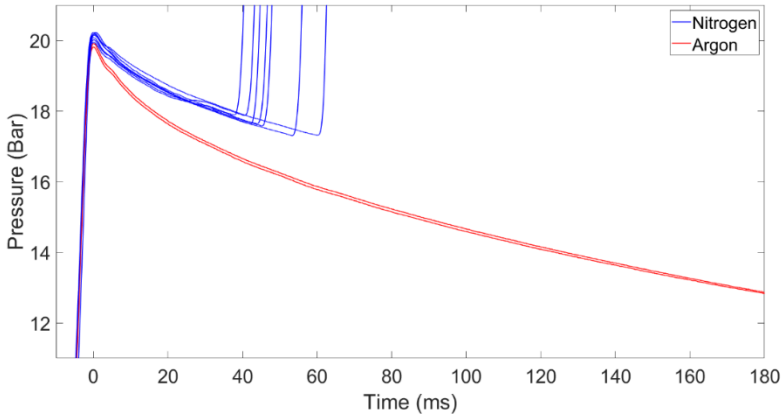

(a)

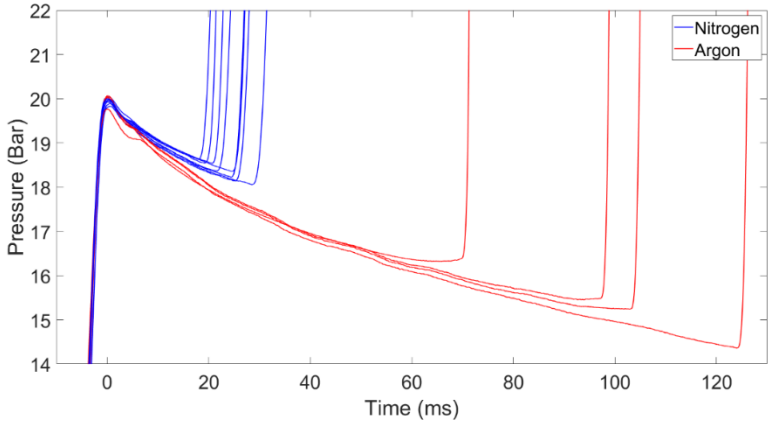

(b)

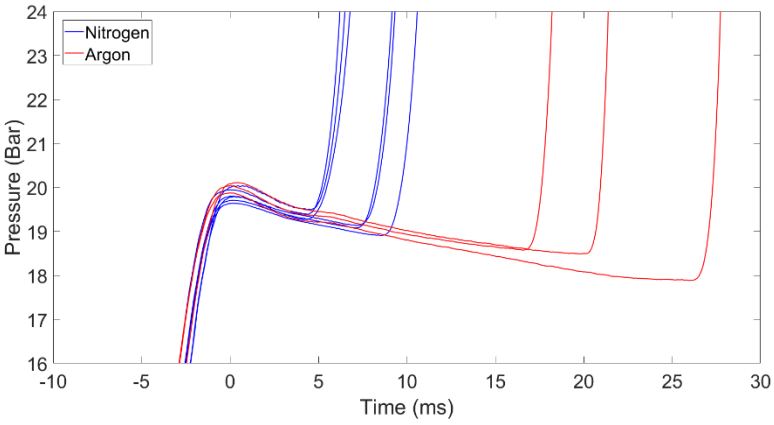

(c)

Figure 4-29: Comparison of the pressure traces using two diluent gases, argon (red) and nitrogen (blue), representing the difference in ignition delay at P_c=20 bar and (a) T_c=800 K, (b) T_c=825 K and (c) T_c=850 K.

Figure 4-29 (cont'd)

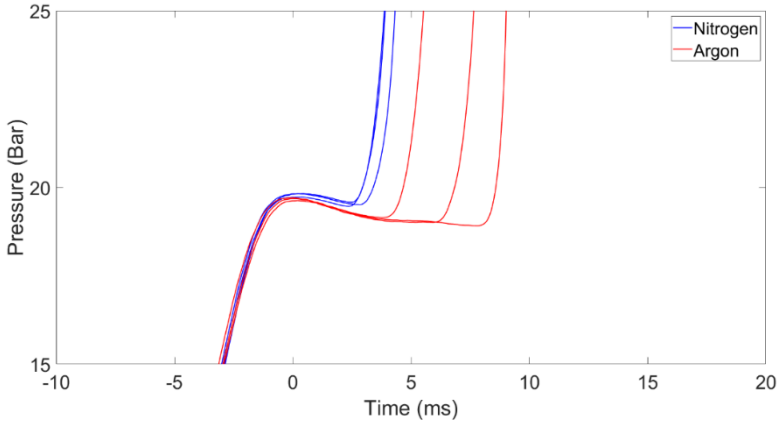

(d)

Comparing the heat release rates in Figure 4-30, it is observed that when argon was used as a diluent, the heat release rate was consistently higher at all compressed temperatures as compared to when nitrogen was used as the diluent. The higher HRR when argon is used as diluent is again attributed to its lower thermal capacity as compared to nitrogen. The lower heat capacity of argon causes the mixture to heat up and cool quickly, which in turn leads to shorter combustion durations as compared to nitrogen [135].

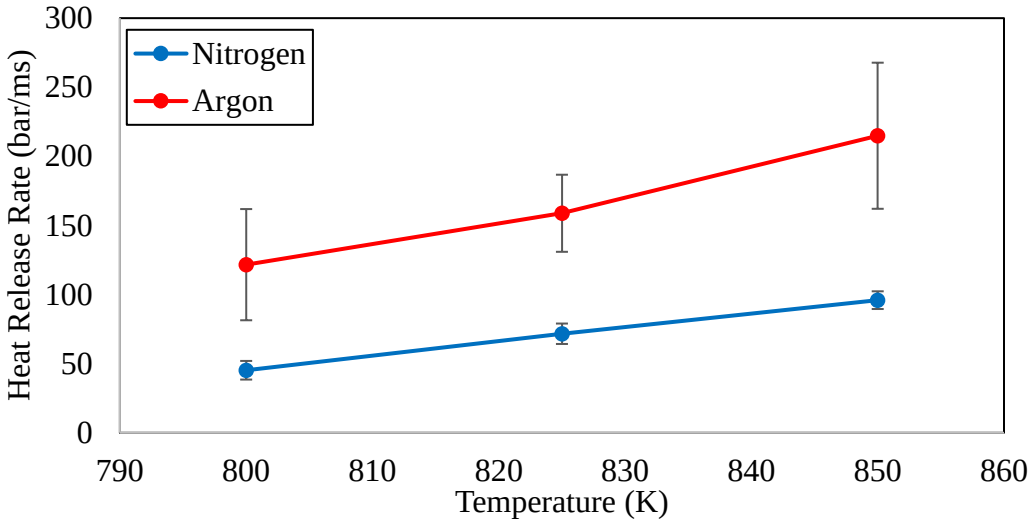

Figure 4-30: Comparison of the maximum heat release rates when using argon as a diluent (red) vs when using nitrogen as a diluent (blue), during ignition at same compressed conditions.

This is confirmed by calculating the time duration of the dP/dt rise and fall during the ignition event. From the first derivative of the pressure data, i.e. dP/dt, it can be determined if the pressure is rising or falling by considering if the sign is positive or negative. As mentioned earlier, the change in sign of the first derivative is useful in determining when the EOC occurs by considering the transition from a positive dP/dt to a negative value, where the pressure is no longer rising and is starting to fall. This same technique can be used to determine the end of combustion when there is no longer any significant generation of pressure due to combustion. The time duration of the dP/dt rise and fall during the ignition event can be considered to be representative of the combustion duration. When nitrogen was used as the diluent, the combustion duration was about 5.4 ms and when argon was used, the duration was 4.5 ms at 825 K and 20 bar as can be seen in Figure 4-31. The shorter combustion duration causes the pressure rise rate to be much faster in the tests where argon was used as the diluent (165.2 bar/ms), as compared to the tests in which nitrogen was used as the diluent (68.7 bar/ms). The faster PRR when argon is used as diluent is attributed to its lower heat capacity as compared to nitrogen. The lower heat capacity of argon causes the mixture to heat up and cool quickly, which in turn leads to shorter combustion durations as compared to nitrogen [135]. This trend was consistent at all compressed temperatures. Despite nitrogen and argon having identical thermal diffusivities (2.2×10^{-5} m^2/s at 300 K [117]) and nitrogen having a higher thermal conductivity (0.026 W/(m-K) at 300 K [117]) than argon (0.0177 W/(m-K) at 300 K [117]), heat losses and HRR were higher when using argon as diluent. This implies that heat capacity plays a more significant role as compared to thermal conductivities and diffusivities in post-compression heat losses.

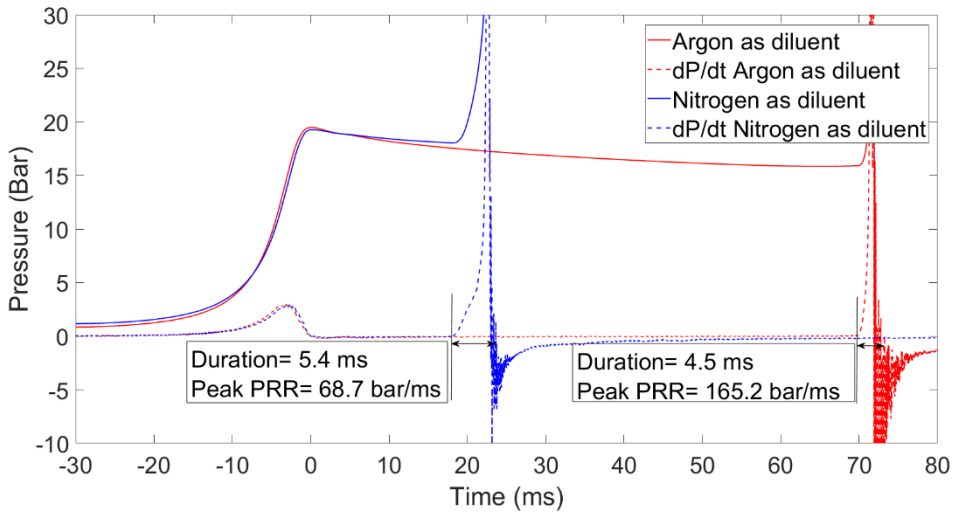

Figure 4-31: Comparison of combustion duration using argon as the diluent vs using nitrogen as the diluent at T_c=825 K and P_c=20 bar.

Another reason behind the shorter ignition delays when using nitrogen as the diluent is the higher initial temperature that needs to be maintained when using nitrogen as the diluent to achieve the same compressed conditions due to its higher thermal capacity, which makes the mixture comparatively more reactive by the end of compression. The results in Chapter 5 show that HO_2, H_2O_2 and CH_2O begin to form in low concentrations by the end of compression. In the cases when nitrogen was used as the diluent, results show that the concentration of these species is higher by orders of magnitude, implying the mixture is more reactive. However, in both cases, the mole fractions of intermediate species were not high enough to reflect a substantial chemical heat release during the compression period.

4.7. Chapter Summary

The ignition characteristics of stoichiometric ethanol/air mixtures at 20 bar and for a temperature range of 800 K-875 K were studied with the help of optical images obtained from a high-speed camera. By following a cleaning protocol, it was observed that multiple flame kernels and pre-ignition events could be minimized, which can help in obtaining more accurate ignition

delay data. In this study the flame kernels propagated with a speed of 5.6 m/s, 6.2 m/s and 8.1 m/s at temperatures of 800 K, 825 K and 850 K, respectively; which is in agreement with the flame speeds for spherical propagating flames. For the majority of cases, the flame originated near the top of the combustion chamber and spread towards the bottom, which implies that the ignition was not completely homogeneous.

The results of the present study aid in gaining a better understanding of how ignition delay data needs to be measured and compared. Several test variables can affect the IDT for the same compressed temperature and pressure conditions. Several of these factors can vary between different RCM facilities (heat losses, geometry, piston design, duration of compression etc.) while others can be observed with different initial conditions in a single RCM (compression ratio, initial temperature, initial pressure, diluent gas composition, mixture preparation method). Due to the variety of factors that have the potential to affect the IDT, it would be prudent to make an effort to determine the impact of these factors when comparing ignition delay results across RCM facilities and even within a single facility, particularly if a wide variety of initial conditions were employed when gathering data. A comparison between the optical images from both fueling methods provided further insight into the effect of impurities in the mixture on the ignition delay and burn characteristics of ethanol. The effects of different test variables on auto-ignition delay times of ethanol were successfully studied and the main observations are outlined as follows:

- Using a mixing tank to prepare the air/fuel mixture resulted in shorter IDTs as compared to the DTC method. The difference in IDTs of the two mixture preparation methods was greater for a higher compression ratio of 17.1. More accurate comparison needs to be made by maintaining the injector fixture along with the water jacket even when conducting tests using the mixing tank and this is a part of the ongoing research.

- In both charge preparation methods, increasing the compression ratio from 11.7 to 17.1 resulted in longer IDTs due to increased rate of post-compression heat losses. This increase was smaller in the case of the mixing tank as compared to the DTC method and hence the difference in IDTs between the two compression ratios was less in the case of the mixing tank experiments.
- Using argon as a diluent resulted in longer IDTs compared to using nitrogen as the diluent at same compression ratio of 11.7 and diluent/oxygen ratio of 3.76. This was because of the lower heat capacity of argon which causes an increased rate of post-compression heat losses and a shorter combustion duration.
- The difference in IDTs of the various combinations of compression ratio and diluent gas collapsed around one value as the compressed temperature increased. This is due to the shorter ignition delay durations which were less affected by the post-compression heat losses.

Chapter 5. NUMERICAL RESULTS – ETHANOL

5.1. 0-D CHEMKIN Analysis

The purposes of the chemical kinetics simulations are to (1) emphasize the importance of post-compression heat losses and confirm the effects on ignition delay that were observed experimentally, (2) study the effect of maintaining higher initial conditions in lower compression ratio to achieve identical compressed conditions on ignition delay, by studying the mole fraction of species that are responsible for chain initiation reactions, (3) study the chemical effect of the difference in third body efficiencies of nitrogen and argon on ignition delay at identical compressed conditions and (4) show that a mechanism that is validated for a given volume profile obtained for a specific compression ratio and diluent gas composition will not necessarily accurately predict the ignition delay for a different configuration of compression ratio and diluent gas composition which would have a different rate of heat losses. These factors would be otherwise difficult to notice experimentally and it was needed to bring them under consideration.

Ignition time measurements from this study are compared to the predictions of the three kinetic mechanisms shown in

Table 5-1, each of which has been validated against ignition delay data from RCM for pressure and temperature range that is identical to this study. The mechanisms mainly differed in the number of species and the number of reactions they consisted of. In their study, Mittal et al. [10] investigated the predictions of two other mechanisms, that of Marinov et al. [136] and Li et al. [137] with both mechanisms overpredicting the IDTs mainly because the mechanisms were validated for high-temperature oxidation of ethanol. Therefore, these mechanisms were not used for this study. The mechanism of Mittal et al. [10] is derived from the Aramco Mech v1.3, which includes the H_2 /CO/O_2 sub-mechanism developed by Kéromnès et al. [138] and the C1 –C2 sub-

mechanism established by Metcalfe et al. [139], with refinements to the rate constant for the reaction of ethanol and the hydroperoxyl radical and by analogy the reaction of ethanol and methyl peroxy radicals [10]. In addition, the branching ratio of the abstraction from each of the three sites on the ethanol molecule by radicals was changed to improve the agreement for ethylene concentration profiles in the Jet Stirred Reactors and flow reactor studies [10].

In addition to the mechanism by Mittal et al. [10], a mechanism by Zhang et al. [140] that uses dimethyl ether (DME) as a radical initiator to explore the low-temperature reactivity of ethanol is also considered for this study. Zhang et al.'s [140] mechanism is also based on the Aramco Mech 1.3 and uses the same ethanol mechanism as Mittal et al. [10] as a sub-mechanism and also includes a DME sub-mechanism that was adopted from the work of Burke et al. [141]. Zhang et al.'s [140] model showed very good agreement with the experimental data, for both fuel in air mixtures and fuel in argon mixtures, at both lower and higher pressures.

The final mechanism that was used is the Aramco Mech. V3.0 [142], which is also based on a series of previous studies which include the H_2/O_2 sub-mechanism of Kéromnès et al. [138], the C1–C2 sub-mechanism from Metcalfe et al. [139], the propene/allene/propyne sub-mechanism from Burke et al. [143,144], the CH_4/DME sub-mechanism from Burke et al. [141], the isobutene sub-mechanism development by Zhou et al. [145] and the 1- and 2-butene sub-mechanism developed by Li et al. [146,147]. As a result, this is a detailed mechanism with about 3000 reactions. The reactions updated are all part of the generally well-known low-temperature reaction scheme describing the oxidation of alkanes [142].

All three of chemical kinetic mechanisms have been validated by comparing against experimental data taken in multiple devices including IDTs, JSR and flow reactor species profiles, over a wide range of pressure, temperature, and fuel/oxidizer conditions.

Table 5-1: Mechanisms used in the ethanol study for CHEMKIN simulations.

Mechanism	No. of species	No. of Reactions	Citation
Mittal et al.	113	710	[10]
Aramco Mech v3.0	581	3034	[142]
Zhang et al.	433	1004	[140]

The plots in Figure 5-1 shows a comparison of predicted ignition delay results using each of the abovementioned mechanisms with the experimental data. The mechanism of Mittal et al. [10] consistently over-predicted the IDTs at all compressed conditions, irrespective of the compression ratio and diluent gas employed. The Aramco Mech. V3.0 was a better predictor of the IDT than the mechanism of Mittal et al. [10]; however, it still over predicted the IDT.

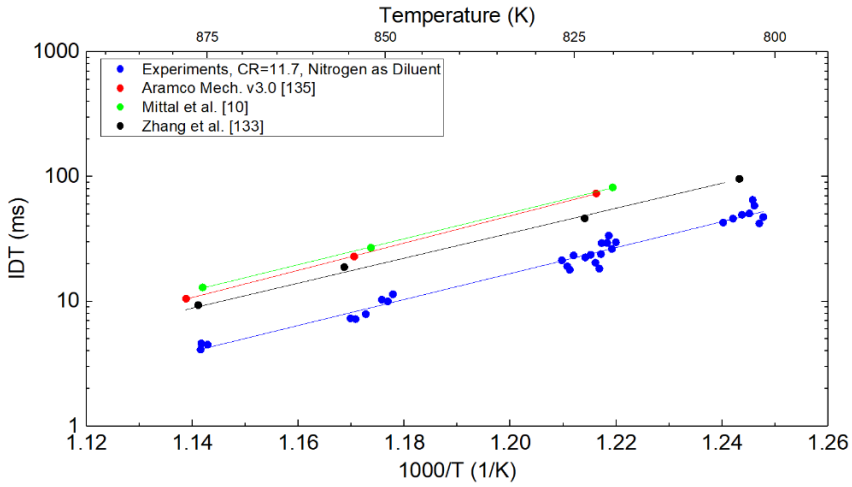

(a)

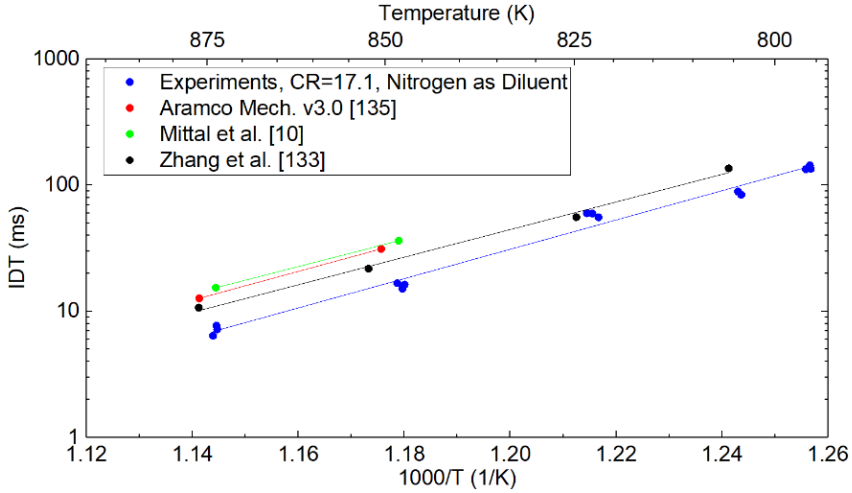

(b)

Figure 5-1: Comparison of IDT vs 1000/T plot of experimental data with model predictions using the three mechanisms by Mittal et al. [10], Zhang et al. [140] and Aramco Mech v3.0.; (a) Using nitrogen as diluent at CR=11.7, (b) Using nitrogen as diluent at CR=17.1 and (c) using argon as diluent at CR=11.7, all at P_c=20 bar.

Figure 5-1 (cont'd)

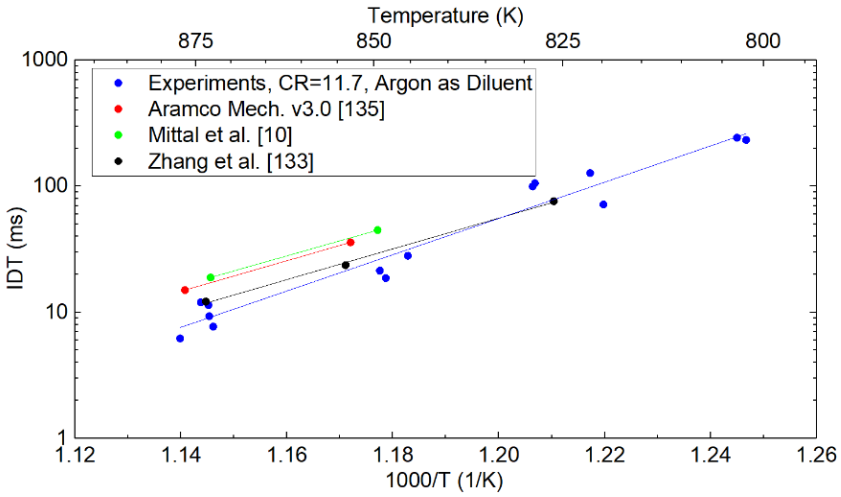

(c)

It can be seen that the fuel did not burn at T_c=800 K using both of these mechanisms at either compression ratio. Additionally, there was no ignition in the simulations with these mechanisms at T_c=825 K for the 17.1 compression ratio case and also when argon was used as the diluent for CR=11.7, as can be seen in Figure 5-1. It can be seen that all three mechanisms had the closest agreement at CR=17.1 when nitrogen was used as the diluent which was maybe due to the original data that was used to validate the mechanisms. It should be noted that Arrhenius behavior was observed using all three mechanisms at all the various test conditions. The percentage deviation of IDTs for a given mechanism at a given compressed condition using different compression ratios and diluent gases varied between 14% and 25%. In numbers, the percentage difference between experimental and simulation data was the least (~20%) for CR=11.7 with argon as a diluent and the most for CR=11.7, with nitrogen as a diluent (~73%). Although the compression ratios and the compressed conditions were identical, the mechanism failed to give an accurate prediction for CR=11.7 with nitrogen as diluent. Furthermore, the developers of the mechanism [140] have mentioned that the updated models can predict ignition times for ethanol/air

mixtures at temperatures above 850 K, which was close to the upper limit of the temperature range studied and hence the agreement is not observed at lower temperatures. While validating against Mittal et al.'s [10] experimental data, the model underpredicted the ignition delay times in the temperature range of 820 K–960 K. This may be due to the difference in post-compression heat losses of the RCM of the two facilities as a result of different compression ratios employed (NUI Galway and University of Akron); and also due to the difference in the diluent gas composition that would, in turn, change the third body efficiencies, post-compression heat losses and initial pressure and temperature. This means that a mechanism that is validated for a given volume profile obtained for a specific compression ratio and diluent gas composition, will not necessarily accurately predict the ignition delay for a different configuration of compression ratio and diluent gas composition which would have different rates of heat losses. This implies that even within the facility itself, a mechanism may give a scatter of predictions for a range of compression ratio or diluent gas compositions, making it difficult to develop a mechanism that would not only give reasonable predictions. The mechanism by Zhang et al. [140] gives predictions that are in reasonable agreement with the experimental results. For this purpose, this mechanism was used for further investigations in this study.

As was discussed briefly in Section 4.5.1, the simulations showed that keeping the heat transfer rate constant across both compression ratio configurations and diluent gases leads to similar IDTs for a given set of compressed conditions. The plots in Figure 5-1 show that even though the rate of compression was different in both the compression ratios, the IDTs were similar with the maximum percentage deviation being 6%. The simulations showed that keeping the heat transfer rate constant across both compression ratio configurations and both diluent gas mixtures

leads to similar IDTs for a given set of compressed conditions, implying that the IDTs are more sensitive to post-compression heat losses than the compression time and initial conditions.

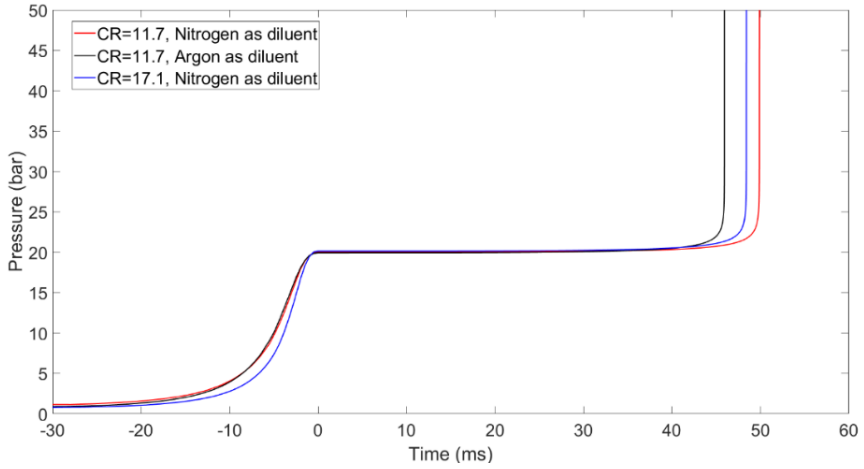

(a)

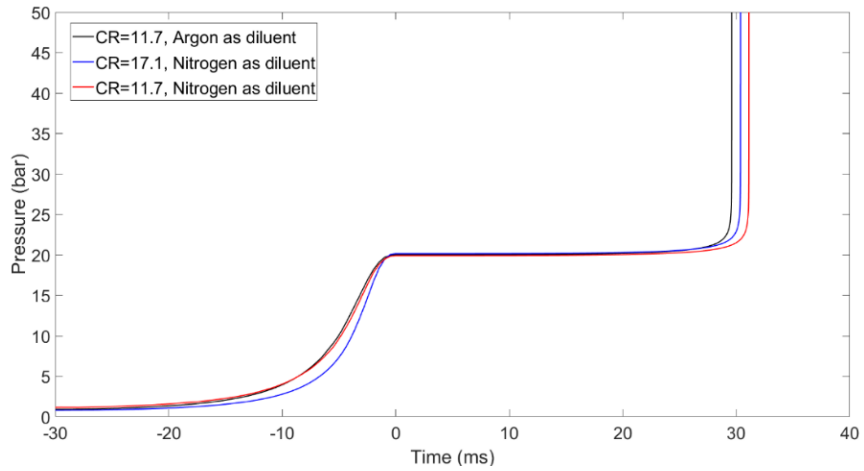

(b)

Figure 5-1: CHEMKIN results, using mechanism by Zhang et al. [140], when there is no post-compression heat loss for P_c=20 bar and (a) T_c=800 K, (b) T_c=825 K, (c) T_c=850 K and (d) T_c=875 K.

Figure 5-1 (cont'd)

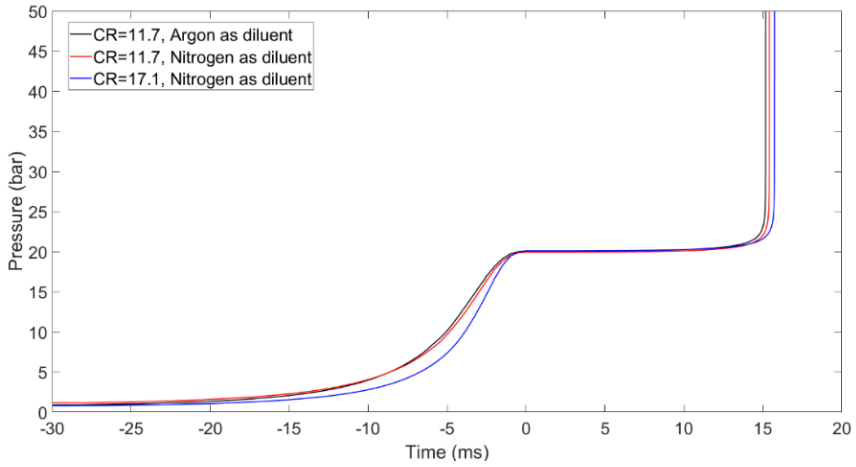

(c)

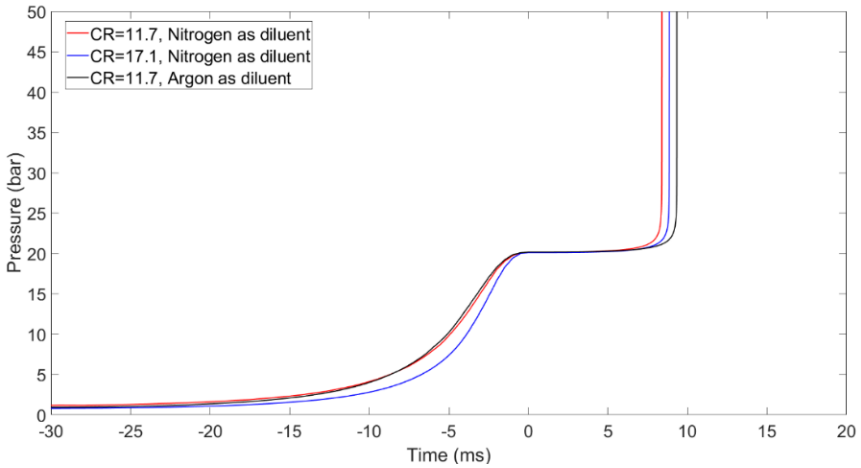

(d)

Efforts were taken in this study to isolate the chemical effects of the diluent gas composition from the thermal effects. Sensitivity analysis was performed by Barraza-Botet et al. [24] for ethanol in the 880–1150 K temperature range for stoichiometric ethanol-air mixtures with varying buffer gas compositions, and also by Mittal et al. [10] in the temperature range of 825-985 K and 10-50 bar pressure. The propene mechanism used by Barraza-Botet et al. [24] consists of an ethanol sub-mechanism developed by Mittal et al. [10] and hence the propene mechanism was

not used in this study as it gave similar results. The results showed one reaction involving third-body collisions that could have an impact on the predicted ignition delays:

$$H_2O_2(+M) \leftrightarrow 2OH(+M) \quad (5\text{-}1)$$

In order to further quantify the chemical effects on IDTs, numerical calculations were conducted using the constant volume adiabatic modeling approach, with the heat capacity of nitrogen set to the same value as that of argon, so that they would only differ in terms of third-body collision efficiencies. Figure 5-2 shows the simulation results for conditions of 20 bar, 800 K, ϕ = 1, buffer gas/O_2 = 3.76 using the modified nitrogen heat capacity data, along with the original data for argon and nitrogen. The difference between the results for 100% nitrogen with the modified specific heats with the argon data represents the chemical effects on the ignition process. As seen in the figure, the ignition delay with Ar-modified N_2 is shorter than that with argon.

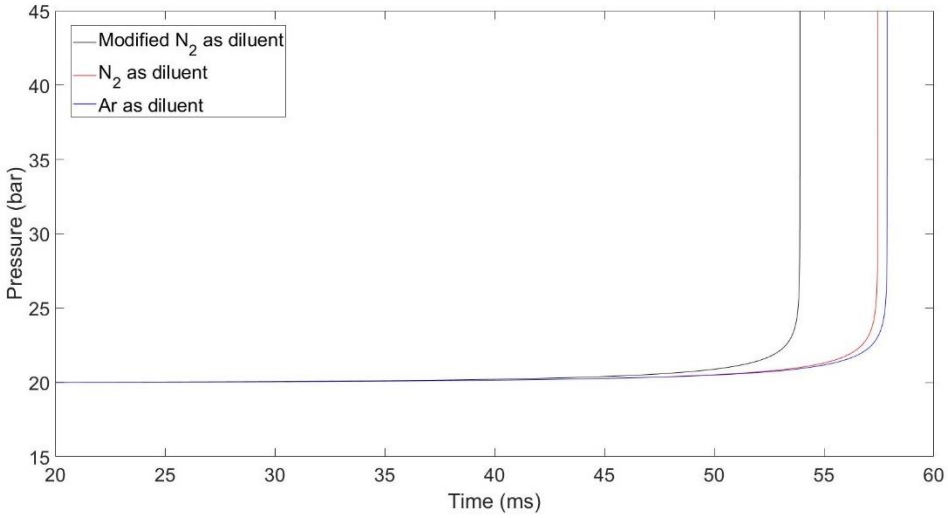

Figure 5-2: Zhang et al. [140] model predictions considering the chemical effects on ethanol ignition at P=20.0 bar, T=800 K.

The longer argon ignition delay is due to the lower collision efficiency of argon compared to nitrogen (where, in the mechanism used, nitrogen has a third body collision efficiency of 1.5,

whereas argon has 1.0 for the reaction mentioned earlier). Higher collision efficiency promotes the ignition process and thus reduces the ignition delay. A similar trend was observed in a study by Di et al. [64] on the effects of buffer gas composition on low-temperature ignition of iso-octane and n-heptane. CO_2-modified N_2 had longer overall ignition delay as compared to CO_2 because CO_2 has third-body collision efficiency that is 3.8 times that of N_2. There was a negligible chemical effect when comparing argon and nitrogen at 720 K, but the effect increased as the temperature was increased. For the temperature range investigated in the current study, however, the chemical effect remained more or less consistent as seen in Figure 5-3, where the chemical effect (η) is defined by ($\tau_{\text{modified N2}} - \tau_{\text{Ar}}$) and is then normalized with respect to the originally predicted ignition delay for argon. Although results using the mechanism by Zhang et al. [140] are shown and discussed here, this trend was also observed using the Mittal et al. [10] and Aramco Mech. V3.0 mechanisms [142]. However, the numerically determined thermal effect, defined as ($\tau_{\text{modified N2}} - \tau_{\text{N2}}$) and normalized with respect to the IDTs of original N_2, was negligible (0.06) at all temperatures. Nevertheless, experimentally (Section 4.5 and 0) it was observed that using argon as the diluent had greater post-compression heat losses (thermal effect) as compared to nitrogen; and together with the chemical effect of third-body collision efficiencies, the diluent gases can have a significant impact on the IDTs at same compressed conditions.

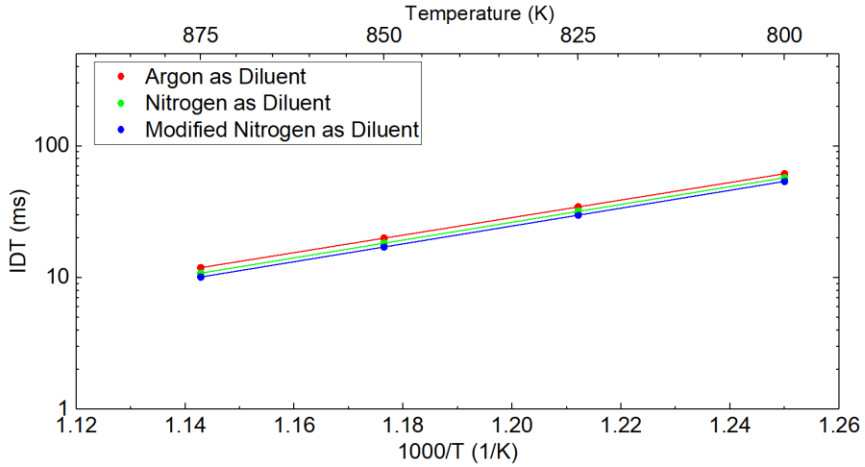

(a)

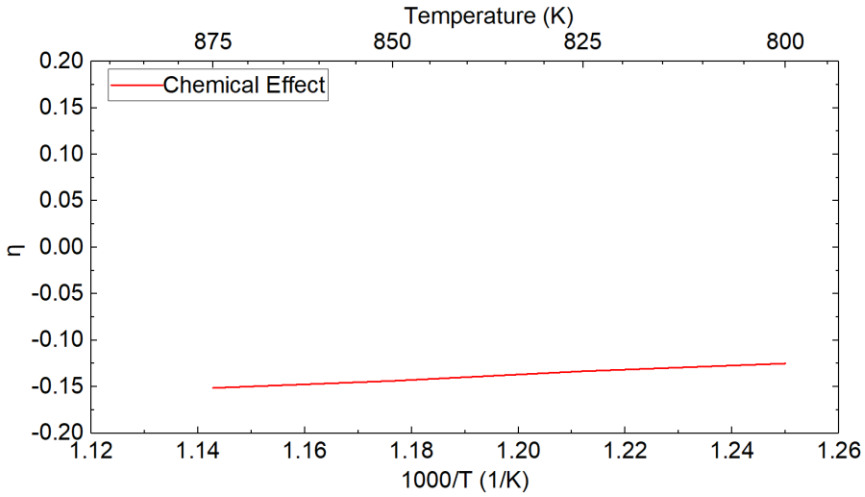

(b)

Figure 5-3: Comparison of the predicted chemical effects of argon on the total ignition delay time, mechanism by Zhang et al. [140]. ((a) total ignition delay, (b) Normalized chemical effect).

It can also be seen by looking at the IDT vs 1000/T plot in Figure 5-3 (a) which shows the constant volume simulation results and Figure 5-4 which shows the simulation results using a volume profile with the Zhang et al. mechanism at CR=11.7 that using argon as diluent had the longest IDTs, followed by CR=17.1 with nitrogen as the diluent and CR=11.7 with nitrogen as the diluent had the shortest IDTs. The same can be said for the experimental results as well as can be

seen in Figure 5-4. However, as the compressed temperature increased, the deviation in the IDTs reduced, which was also observed in the experimental part of this study. The reason for this deviation as T_c increases is that as the IDTs reduce, there is less time for post-compression heat losses to affect the IDTs.

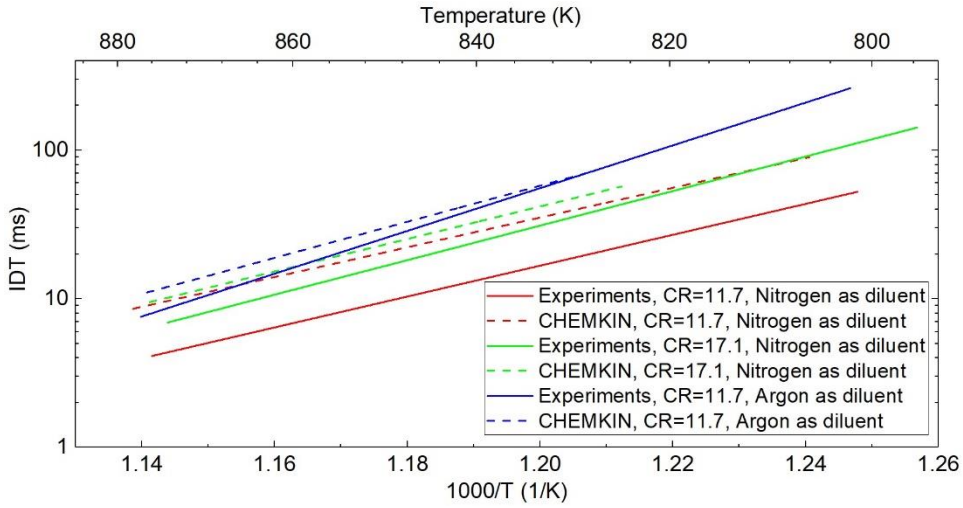

Figure 5-4: Plot of IDT vs 1000/T comparing results from CHEMKIN simulations for various combination of compression ratio and diluent gas composition and the mechanism by Zhang et al. [140] with corresponding experimental data using DTC method.

As was discussed briefly in Section 4.5.1, in order to achieve the same compressed conditions using different compression ratios, the required initial conditions need to be different. Maintaining a higher initial pressure and temperature can lead to increased low-temperature reactions taking place during the compression stroke, which can result in a shorter ignition delay. It should be noted that the initial conditions maintained during the experiments were specified for the simulations as well. The higher initial pressure and temperature required for the lower compression ratio case, combined with the longer compression time are most likely the cause of the shorter ignition delay times when comparing the IDTs of different compression ratios when using nitrogen as the diluent. Similarly, use of argon as diluent led to the maintenance of lower initial conditions of temperature and pressure as compared to when nitrogen was used as the

diluent, which again led to shorter ignition times when nitrogen was used as the diluent. Presently, there is no experimental way to confirm if low-temperature reactions took place on a small scale during the compression stroke for this compression ratio case.

The combustion of hydrocarbon species follows a basic series of steps, starting with initiation decomposition reactions, followed by radical attack on the fuel, generation of intermediates that generally are smaller, and finally a chain of aldehyde → CO → CO_2 reactions [148]. The radical pool, which is responsible for chain propagation, branching, and termination, is mainly determined by the H_2/O_2 reaction mechanism which involves the production of the hydroperoxyl radical, HO_2 and hydrogen peroxide, H_2O_2 in one of the initiation reactions. Formaldehyde, CH_2O, is formed after the attack of O-atoms on the olefins that are generated in the earlier steps of the reaction mechanism [32]. It is from this step onwards that the oxidation of methyl radicals, formaldehyde, methylene, etc. produces carbon monoxide, which eventually gets oxidized to carbon dioxide [32]. Therefore, looking at the concentrations of HO_2, H_2O_2 and CH_2O during the compression stroke can give insights into the reactivity of the fuel under different RCM configurations and diluent gas compositions.

The plots in Figure 5-5 show that by the end of compression, HO_2, H_2O_2 and CH_2O mole fraction in the case of CR=11.7 with nitrogen as diluent is higher as compared to CR=17.1 with nitrogen as diluent. This implies that the fuel is more reactive at the end of compression in the lower compression ratio case relative to the higher compression ratio case. Also, the HO_2, H_2O_2 and CH_2O formed at the EOC when argon is used as the diluent are less by an order of magnitude relative to when nitrogen is used as a diluent. This again implies that the mixture is more reactive at the EOC when nitrogen is used as a diluent which results in a shorter IDT. Although the plots shown here are for a compressed temperature of 850 K, similar trends were observed at other

conditions as well: CR=11.7 with nitrogen as diluent had the highest concentration of radicals and CR=17.1 with nitrogen as diluent had the lowest concentration. Also, it can be seen that the HO_2, H_2O_2 and CH_2O radicals production starts a 1–2 milliseconds earlier in the case of CR=11.7 with nitrogen as a diluent, relative to CR=17.1 and this was observed at all compressed temperatures; which may again contribute to the higher reactivity of the mixture. In the case when argon was used as the diluent, the production of these radicals starts later as compared to when nitrogen was used for the same compression ratio of 11.7, again implying that fuel is comparatively more reactive when nitrogen is used as a diluent. However, the mole fraction of these species was not high enough to reflect a chemical heat release during the compression period. The effect that this radical formation has on ignition delay depends on the concentration and the time of production of these species, which in turn depends on the initial temperature. The higher the initial temperature, the earlier the generation and the higher the concentration of these species, the more reactive the mixture will be by the end of compression, which will lead to shorter ignition delay times.

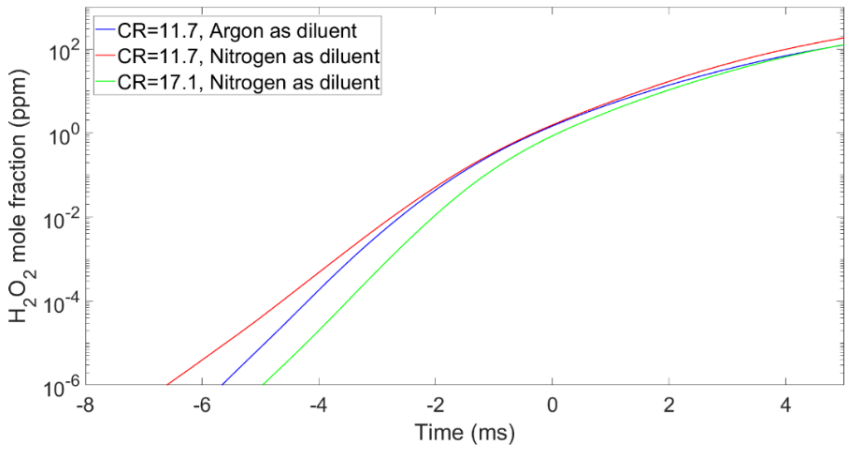

(a)

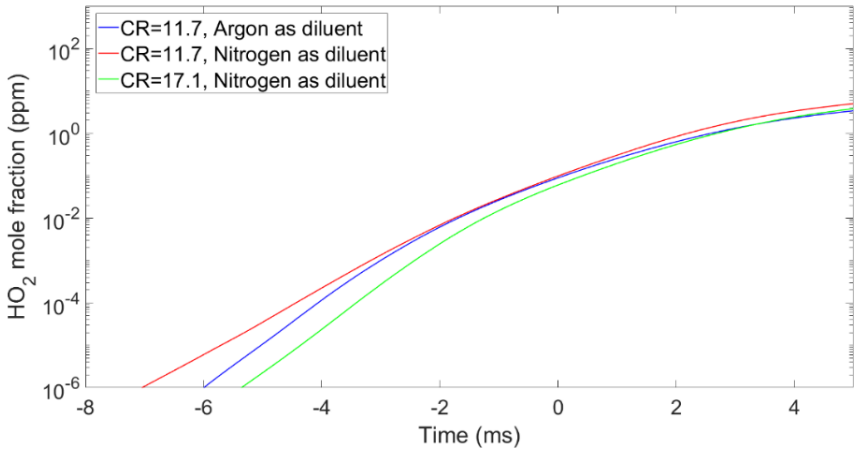

(b)

Figure 5-5: Evolution of (a) H_2O_2 mole fraction, (b) HO_2 mole fraction and (c) CH_2O mole fraction for different combinations of compression ratio and diluent gas using the mechanism by Zhang et al. [140], at compressed conditions of 20 bar and 850 K.

Figure 5-5 (cont'd)

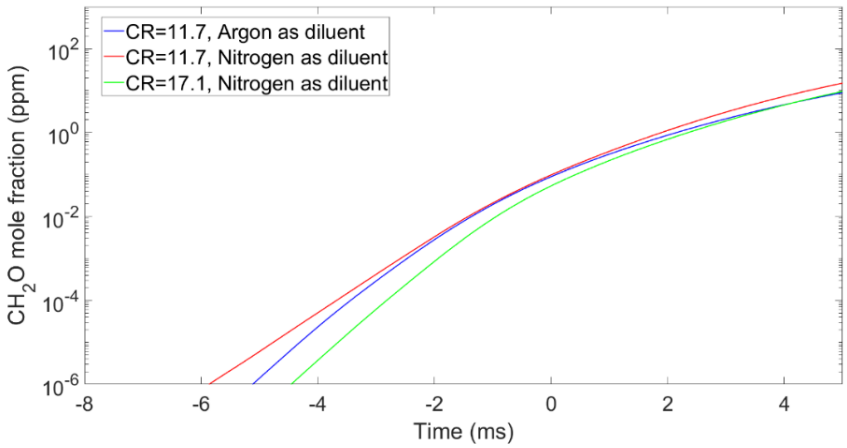

(c)

5.2. Comparison of Results with Literature

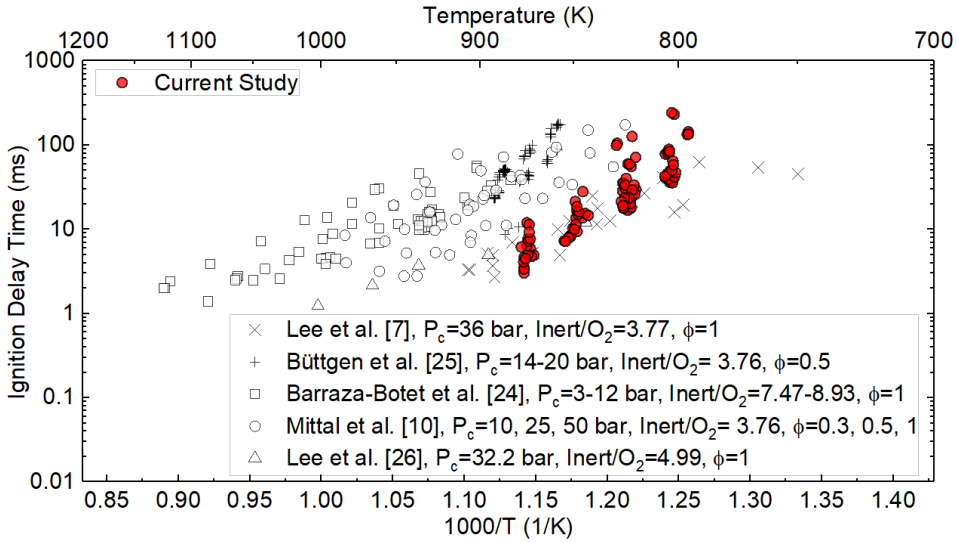

Figure 5-6: Summary of IDT results for stoichiometric mixtures of ethanol studied in the current work and in the past, adapted from [24].

Figure 5-6 depicts a summary of IDT data for stoichiometric mixtures of ethanol obtained from past RCM studies together with the results from the current study (shown as red dots). It should be noted that all of the data shown in Figure 5-6 is presented as it was reported in the literature and no scaling was used for the literature data or for the data from the current study, in

the creation of this figure. The data shown in the plot was obtained only from RCMs and was reported in the works of Mittal et al. [10], Lee et al. [7], Barazza Botet et al. [24], Büttgen et al. [25] and Lee et al. [26]. In Figure 5-7, the original data is scaled to ϕ=1.0, a compressed pressure of 20 bar and inert/oxygen of 3.76 using Equation 5-2, which was developed for data that spans the conditions of =0.3–1.0, P_c =2.5 bar-50 bar, molar dilution of inert/oxygen= 3.76 −8.93 and T_c =750 K–1150 K. The quality of the correlation at representing the data is reasonable as indicated by the R2 value of 0.853. The correlation is based on the kinetic mechanism of Zhang et al. [140], which was used in the numerical analysis portion of this study and is also plotted in Figure 5-7. The model predictions agree well with Equation 5-2 and the normalized data set. The extended data set collapses well to a single trendline. The results of the current work are also in good overall agreement with previous studies, especially after normalizing. Although normalization based on equivalence ratio, pressure, amount of oxygen, etc. can be used to better compare the ignition delay data from different RCMs, a considerable scatter in the data is still observed. Barazza-Botet et al. [24] also did regression analysis for stoichiometric mixtures of ethanol and air accounting for past data from RCMs and shock tubes. The R2 value was 0.967 implying that the quality of the correlation at representing the data was excellent, but a scatter was observed in the plot for temperatures less than 900 K. These scatters imply that there are factors other than the varying diluent/oxygen ratio, equivalence ratio and compressed pressure that affect the ignition delay even at identical conditions. These factors are presumed to have a greater effect on ignition delay at low temperatures. Therefore, normalization in turn leads to the necessity to understand the effect of these other factors on the ignition delay.

$$\tau = 1.08e^{-07}P_c^{-2.12}\left[\frac{Inert}{O_2}\right]^{-0.34}\phi^{-2.1}\exp\left[\frac{21879.39}{T_c}\right] \quad (5\text{-}2)$$

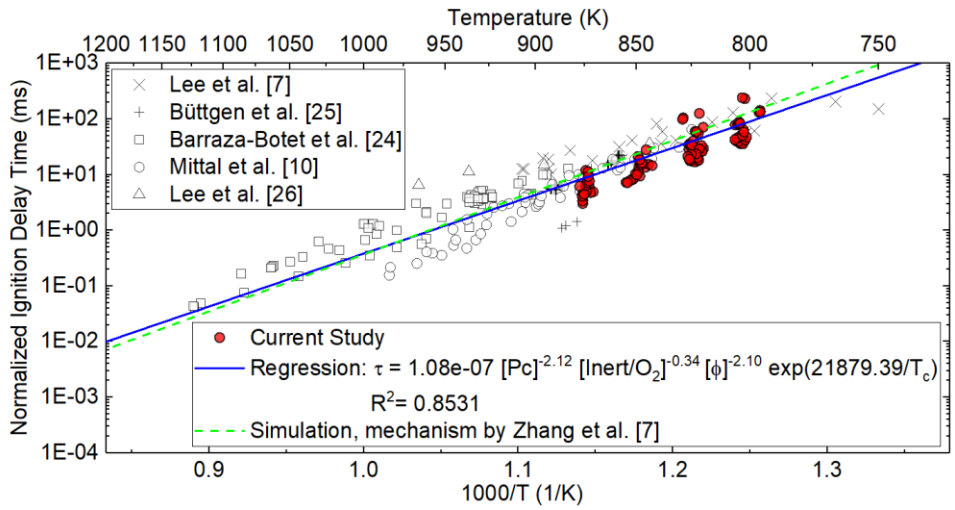

Figure 5-7: Normalized ethanol ignition delay time with respect to P_c =20 bar, Inert/O_2=3.76 and ϕ= 1; studied in this work and available in the literature [7,10,24–26]. Model predictions (green dashed line) based on the reaction mechanism by Zhang et al. [140] and Equation 5-2 (solid blue line) are also shown.

In an effort to help correlate the effect of changing compression ratios and diluent gas composition to ignition delay, a regression analysis was done on the experimental and simulation data obtained in this study. Since the only variables in this study were compression ratio and diluent gas composition, the regression analysis was done considering the surface area-to-volume ratio and the heat capacity, $C_{p,\,mix}$, of the diluent mixture at compressed conditions, as the variables. The experimental and simulation data were then normalized using Equation 5-4, for a surface area-to-volume ratio of 265.43m^{-1} which was calculated for CR=17.1 with the piston at TDC and for $C_{p,\,mix}$ of 31.64 J/(mol-K) which is the heat capacity of nitrogen in the range of 800 K–875 K. If the diluent mixture consists of a variety of gases, the heat capacity of the mixture can be calculated as:

$$C_{p,mix} = \Sigma \left(\chi_a . C_{p,a}\right) \tag{5-3}$$

where χ_a is the mole fraction of gas 'a' in the mixture of diluent gases and $C_{p,\,a}$ is the heat capacity of the gas 'a' in J/(mol-K) at compressed conditions.

$$\tau = 1.38e^{-14} \frac{Surface\ Area}{Volume}^{2.69}_{TDC} [C_{p,mix}]_{TDC}^{-3.84} \exp\left[\frac{27882.77}{Tc}\right] \quad (5\text{-}4)$$

The resulting curve-fit is shown in Figure 5-8, along with the normalized experimental and simulation ignition delay times. The quality of the correlation at representing the data was excellent, as indicated by the R2 value of 0.96. However, this correlation does not account for the increased radicals generated at the end of EOC in the lower CR case which may be the reason for the scatter at higher temperatures as the difference in radical production was greater at higher temperatures.

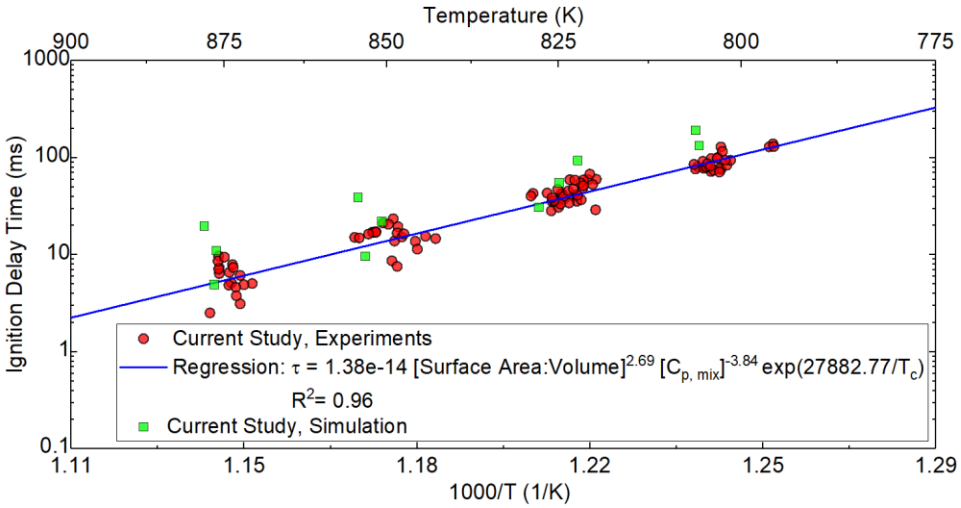

Figure 5-8: Normalized ethanol ignition delay time with respect to surface area-to-volume ratio=265.43m^{-1} and $C_{p,mix}$ of 31.64 J/(mol-K). Scaled model predictions (green squares) based on the reaction mechanism by Zhang et al. [140] and Equation 5-4 (solid blue line) are also included.

5.3. 3-D CFD Analysis

As can be observed from the images in Figure 4-6, Figure 4-7 and Figure 4-10 a single flame kernel develops at the top and propagates towards the bottom, in tests conducted with both the mixture preparation methods. This implies that this behavior of flame propagation is not mixture preparation dependent and some other factors are at work. On consulting with Dr. Patton Allison, a couple of factors were suspected to be the cause of this behavior: minor deformities or

asymmetry in the piston that could cause changes in the boundary layer which in turn would affect the spatial distribution of the mixture temperature and/or the heating bands causing temperature gradients in the combustion chamber. As a remedy, two heating bands located on the head flanges, since a major contribution to the temperature gradient when the piston is at TDC would be from these two bands, were rotated and tests were run, but the flame propagation behavior remained unchanged. Next, the piston was rotated and the connecting rods were centered so that the piston would be located exactly in the center of the combustion chamber and not translate off-center. These changes also did not affect the flame origination and propagation behavior. Temperature measurements performed by Griffiths et al. [149], have observed that the gas in the central region is colder than that in the "toroidal" zone surrounding it because a cold plug of gas is swept across the piston face and is able to penetrate the center of adiabatically heated core gas once the piston has reached TDC. The cold plug of gas across the piston face is due to the piston being in contact with a relatively colder connecting rod that is surrounded by oil in the hydraulic chamber, causing it to be a temperature which is lower than that at which the walls are maintained since the piston is not in direct physical contact with the heated walls. The temperature difference after only 1 ms post-compression, between the gas at the center and that in the toroid surrounding it is approximately 40 K [149]. In an experimental study of turbulence effect on combustion propagation in 1-hexene/air mixtures by Guibert et al. [150] combustion propagation was observed to spread in a front-like manner from an initial single spot located in the upper right corner. Walton et al. [28] also observed reaction fronts originating at different locations on the periphery of the test volume. Both, Guibert et al. [150] and Walton et al. [28] attributed the combustion propagation behavior to temperature inhomogeneities due to the cold plug of gas being pushed across the adiabatic core by the piston after TDC. The ethanol flame propagation behavior consistently

observed in this study also complements the explanation provided by Griffiths [149]. However, the focus of the current study is to investigate the consistent top-to-bottom flame propagation behavior observed in the experimental studies.

In an RCM configuration, while the cylinder walls are heated with the help of heating bands controlled by the feedback provided by thermocouples and a well-insulated combustion chamber, the piston stays in contact with a relatively cooler connecting rod that is surrounded by oil in the hydraulic chamber. As a result, a temperature gradient is observed within the RCM as the gas mixture near the piston has a lower initial temperature than desired as compared to the volume of the gas mixture located near the cylinder head. This is confirmed by looking at the thermocouple located near the piston, which reads about 50-60 degrees lower temperature compared to the desired initial temperature to be maintained, as shown in Figure 5-9. A part of the process of using the DTC technique to prepare the fuel-air mixture is allowing a wait time of 5 minutes to ensure fuel evaporation and mixing. It is suspected that during this wait time, a convection flux is set up due to buoyancy and non-uniform temperature boundary conditions causing the existing temperature inhomogeneity to be extended further into the combustion chamber, with the cooler and hence more dense gas settling along the bottom surface of the cylinder.

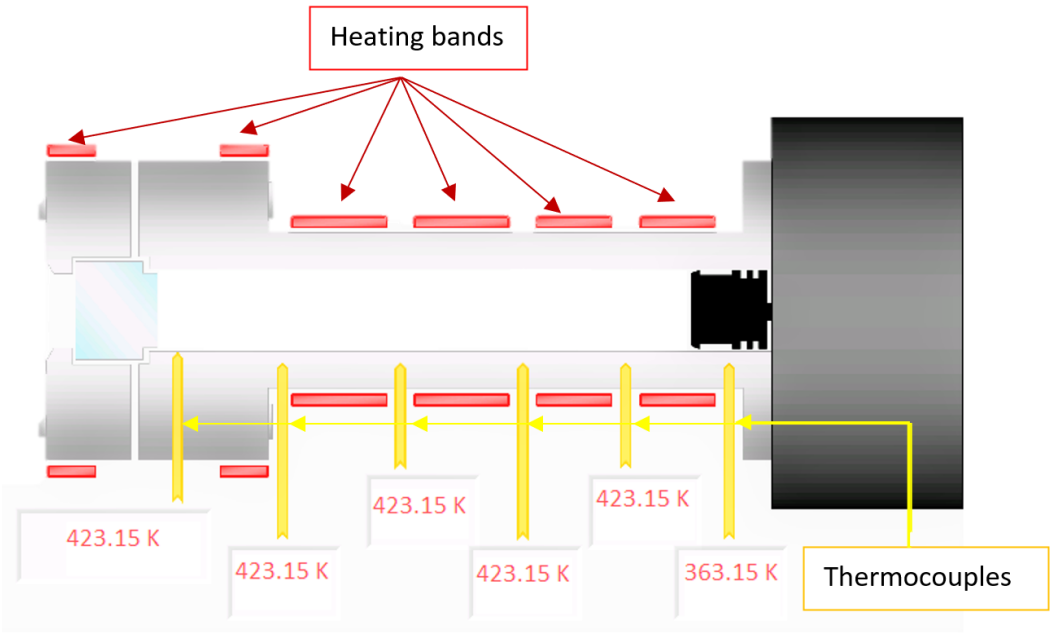

Figure 5-9: LabView virtual instrument used to control and monitor the combustion chamber temperature.

This literature review shows that there have been limited to no computational studies on the effect that the cooler piston and buoyancy can have on the initial temperature field due to convective flux. Studies utilizing uniform thermal boundary conditions and focusing on temperature distribution inside the RCM have previously been completed [128,131,151–154] using 2-D axisymmetric approach. Since these studies considered uniform thermal boundary conditions, buoyancy was assumed to have a negligible effect on the temperature distribution inside the RCM. Furthermore, the main focus of most of the above-mentioned studies has been on the end of compression and post-compression times. Nevertheless, comparing the results from the current study to the studies in the literature [128,131,151–154] can help to better understand the impact of not only buoyancy but also of non-uniform wall temperatures. It can be concluded that the results in the literature obtained using uniform boundary conditions and 2-D axisymmetry (not considering buoyancy) are similar to those obtained in this study using non-uniform thermal boundary conditions and not considering buoyancy. The focus of the current study is on the effect

of both non-uniform thermal boundary conditions and buoyancy. It is suspected that the non-uniform temperature boundary conditions, the effect of buoyancy and the characterization of the flow field before the start of compression are essential to study the transfer of the initial temperature inhomogeneities to the TDC. Therefore, the objectives of this study are: (1) to initialize the fluid velocity and temperature fields in the combustion chamber of the MSU RCM using 3D CFD analysis and not 2-D axisymmetry, and (2) to compare the initial and post-compression temperature field predictions for the cases with buoyancy and without buoyancy. The no buoyancy case serves primarily as a baseline for comparing the role of buoyancy in further influencing the temperature inhomogeneities.

5.3.1. Results and Discussion

5.3.1.1. Description of test cases

In an attempt to reproduce the experimental results, the reactive simulations are conducted for the stoichiometric composition of ethanol and air (species mass fractions for ethanol/O_2/N_2 = 0.10 / 0.21 / 0.69) and for the desired compressed conditions of 20 bar and 825 K, using a geometric compression ratio of 11.7. Ethanol is considered to be fully vaporized in the mixture and buoyancy is applied to all the gases components. The initial conditions needed to achieve the desired compressed conditions were the same as those maintained in the experiments, i.e., 1.14 bar and 423.15 K. Two cases are considered, one in which buoyancy is considered acting vertically downward, i.e., perpendicular to the axis of the RCM, and one in which buoyancy is neglected. The no buoyancy case serves primarily as a baseline for comparing the role of buoyancy in further influencing the temperature inhomogeneities.

The combustion chamber is the primary focus within the numerical domain for this analysis. Figure 5-10 shows planes A and B, which are selected for post-processing. Plane A is the

symmetry plane. Plane B is the plane inside the main chamber parallel to and midway between the piston head and the cylinder head. Moreover, in order to show the distribution of selected flow field variables inside the combustion chamber, three lines are selected. As shown in Figure 5-10, line C (red) is midway between the piston head and plane B, line D (green) is located at the middle of the combustion chamber after EOC and line E (blue) is midway between plane B and the cylinder head.

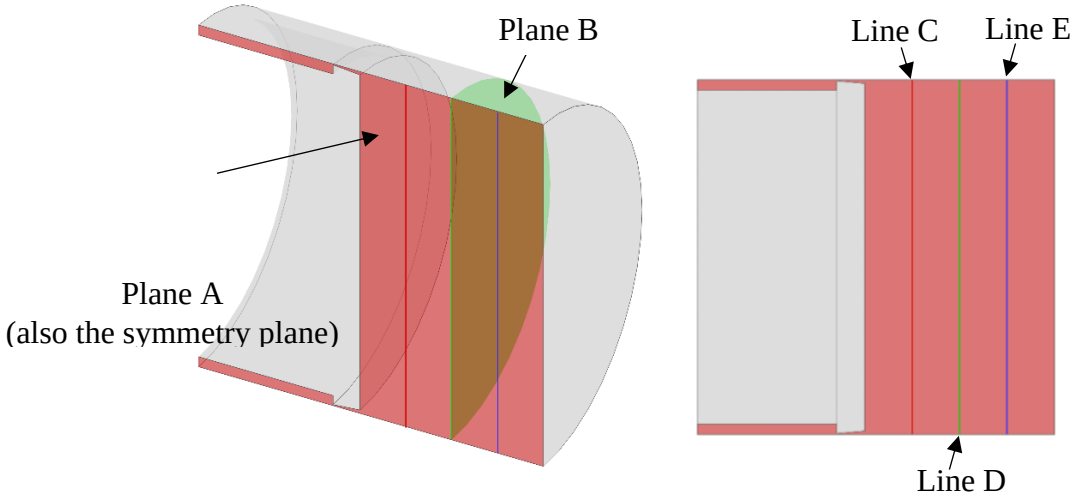

Figure 5-10: Depiction of the planes and lines within the computational domain to analyze the distribution of flow field variables.

5.3.1.2. Steady-State Results

Results of the steady-state velocity and temperature fields based on the differing boundary temperatures for the two cases are discussed in this section. Figure 5-11 (a) and Figure 5-12 show the steady-state solutions for the initial gas temperature fields in the case of buoyancy acting and buoyancy being neglected, respectively. Referring to the case with buoyancy in Figure 5-11 (a), the hot gas rises due to buoyancy directed against buoyancy and flows down along the cold piston, forming eddies with anti-clockwise rotations within the reaction chamber. The non-uniform distribution of streamlines, see Figure 5-11 (b), implies that the flow flux or convection is stronger in the outer region than in the center region, especially near the piston and along the bottom of the

reaction chamber. Furthermore, since the system heat transfer occurs more in the upper part of the chamber, the temperature stratification is gradually formed. As a result, the gas in the upper part is hotter than the lower part, which leads to the temperature being highest in the top right corner. This implies that the highest temperature of the gas is in the top half of the combustion chamber and near the centerline of the 2-inch diameter bore. The temperature inhomogeneity is observed in about half the length of the combustion chamber, especially at the bottom.

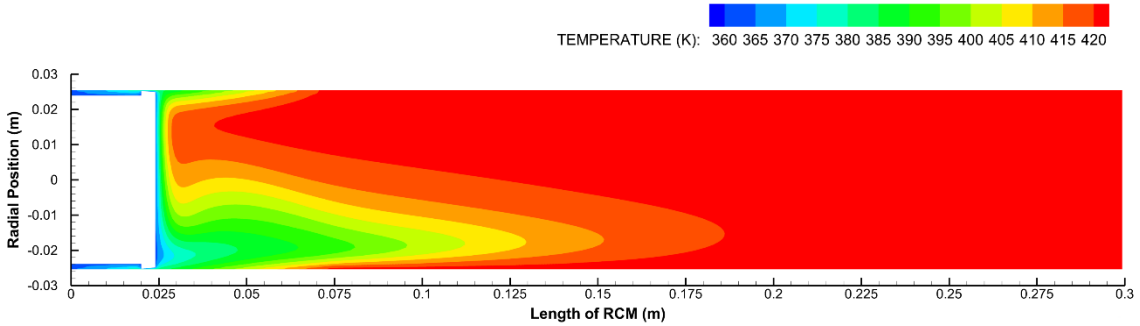

(a)

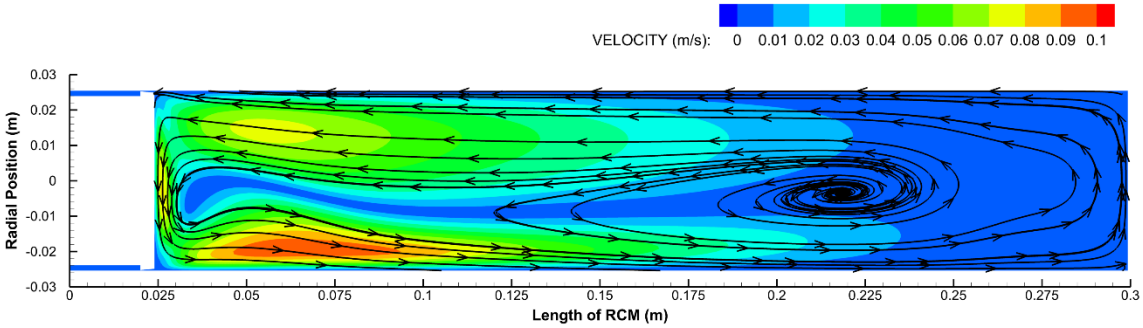

(b)

Figure 5-11: (a) Initial temperature (K) and (b) velocity fields (m/s) as a result of steady-state simulations in the case of buoyancy acting vertically downwards.

As shown in Figure 5-12 in the no buoyancy case, a gradient in temperature stemming from the 60 K cooler temperature of the piston to about a quarter of the length of the reaction chamber is observed. In the absence of buoyancy, despite the non-isothermal boundary conditions, no flow flux is observed in this case and the field is axisymmetric. The steady-state temperature and

velocity fields covering the entire domain for each case were then initialized as the temperature and velocity fields in the RCM before the compression stroke.

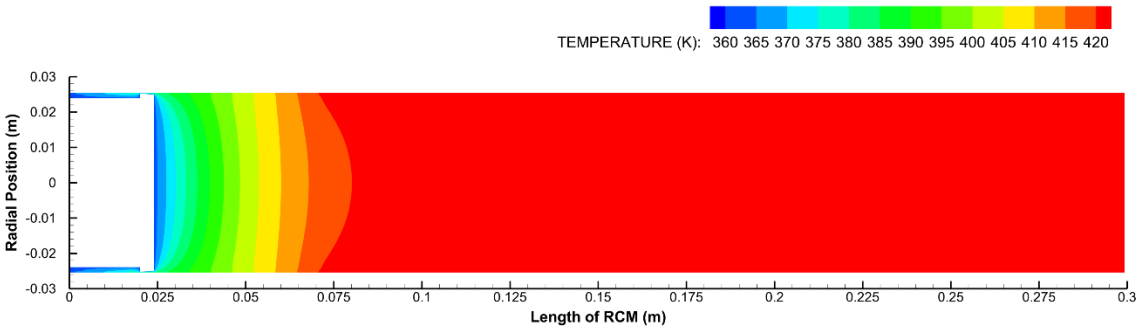

Figure 5-12: Initial temperature field as a result of steady-state simulations in the case of no buoyancy.

5.3.1.3. Transient Results

The results of the RCM compression simulations are presented in this section. The results display the gas temperature and the velocity vector field as well as the OH distribution at the TDC or the EOC (t = 0 ms), and also at the following times after TDC: 20 ms, 40 ms and 1 ms before the start of ignition in the respective cases.

5.3.1.3.1. Post-compression

Figure 5-13 shows total temperature contours on planes A and B at the 0 ms (EOC), 20 ms and 40 ms post-compression times and also for 1 ms before ignition for the buoyancy case, Figure 5-13 (a) and for the no buoyancy case, Figure 5-13 (b). Each of the test cases is distinguished by the structure of the vortices and hence the thickness of the thermal boundary layer. The general behavior observed in previous CFD studies is also seen for the no buoyancy case, where a cool toroidal vortex is formed at TDC. In the case without buoyancy, the toroidal vortex contracts towards the centerline of the RCM, as can be seen in the temperature contour images at 20 ms, 40 ms and 1 ms before ignition. However, in the case with buoyancy, the bottom half of the toroidal vortex moves faster than the top half, the vortex ring contracts towards the top of the main chamber

(vertically offset from the center in the radial direction along the piston surface). In both cases, the vortex ring also penetrates axially into the core gas region. The temperature gradient in the vortices formed in both cases remains similar. The effect of the non-uniform boundary temperature in terms of a reduction in gas temperature in and around the vortex is clearly noticeable in the temperature fields of both cases. Additionally, the added effect of buoyancy is also visible.

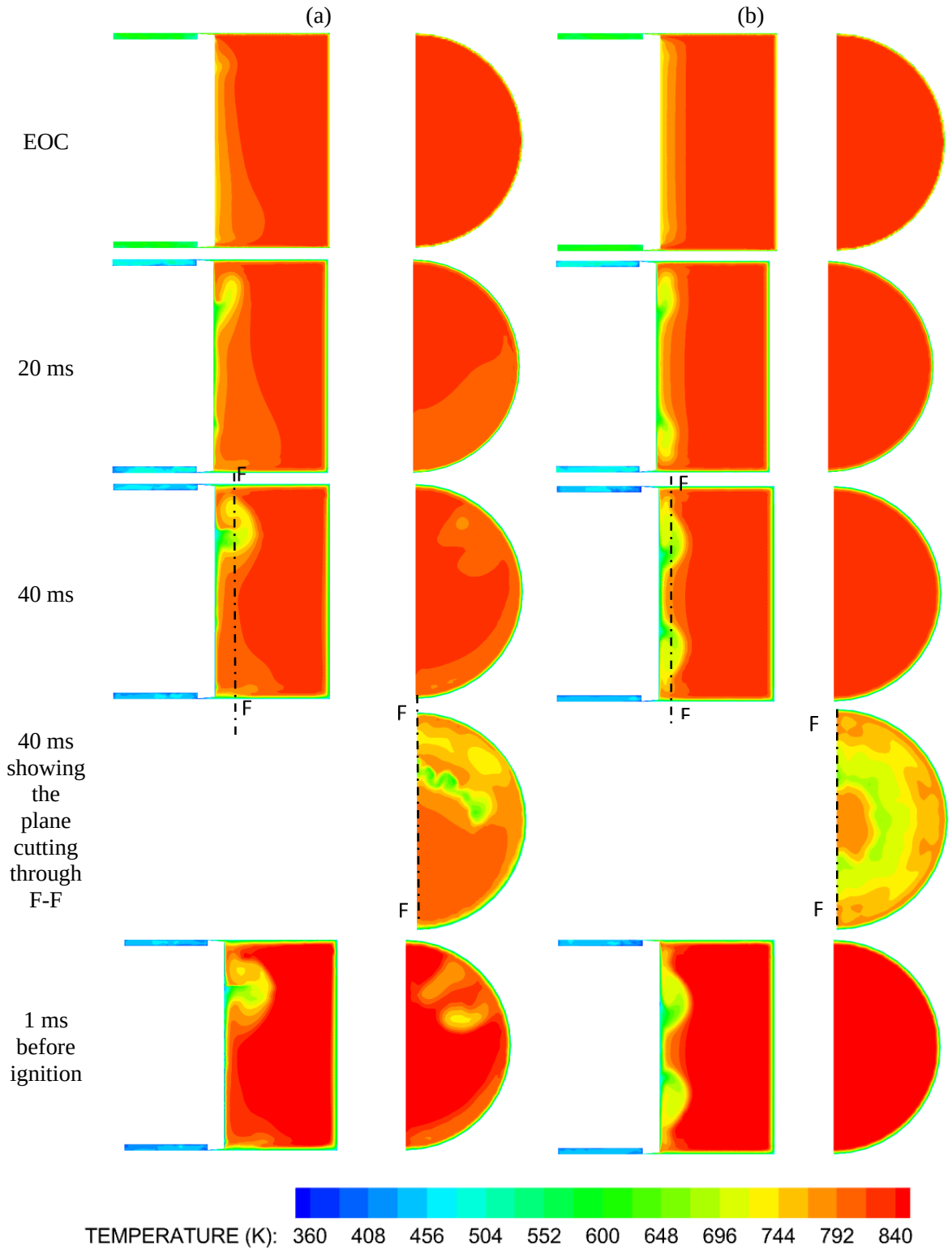

Figure 5-13: Total temperature distributions for (a) with buoyancy and (b) without buoyancy, during post-compression times on planes A and B. At 40ms for both cases, the total temperature distribution on a plane cutting through F-F is also shown to better visualize and compare the vortex rings.

The peak compressed temperatures were identical in both cases, despite the variation in the initial gas temperature fields. This implies that the temperature of the volume of the gas located farthest from the cool-piston crown is not influenced by mixing with the cool vortex during the post-compression period, also ensuring that the adiabatic core hypothesis is still valid.

Figure 5-14 shows the comparison of the distribution of total temperature along line C (midway between the piston head and line D), line D (at the middle of the combustion chamber) and line E (midway between line D and cylinder head) for the case with buoyancy (a) and without buoyancy (b).

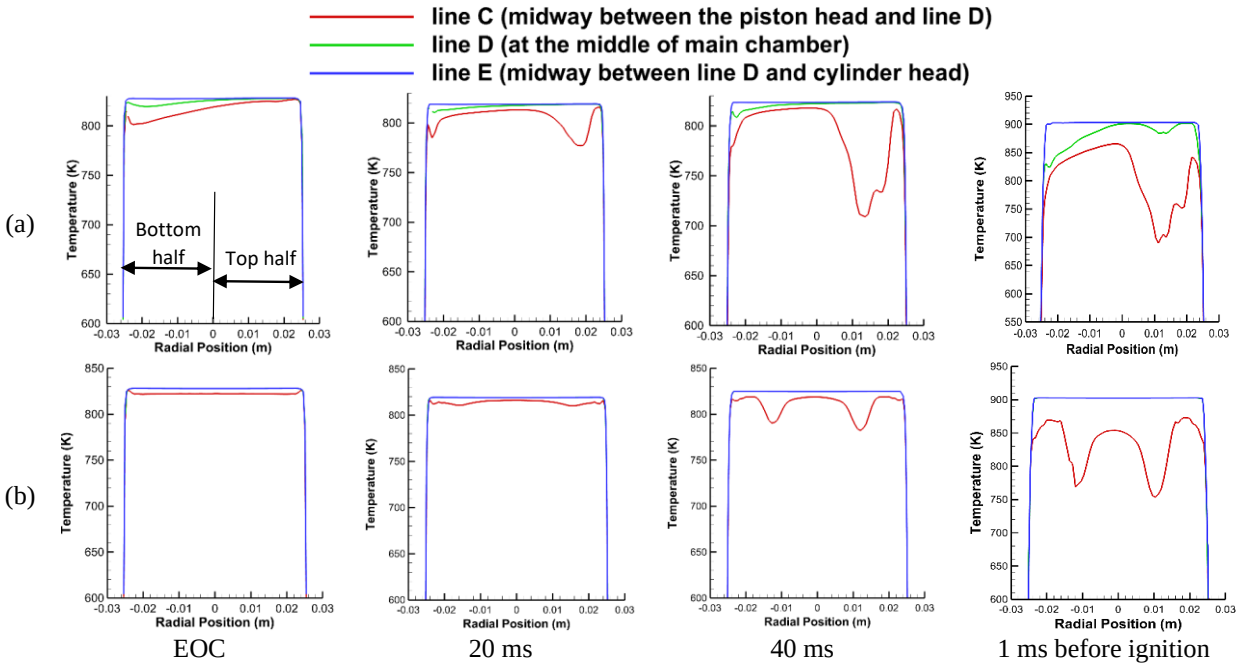

Figure 5-14: Comparison of computed temperature distribution along line C (red), D (green) and E (blue) for, (a) the case with buoyancy and (b) the case without buoyancy at post-compression times of 0 ms, 20 ms, 40 ms and 1 ms before ignition. (Note: For (b) the blue (line E) and green (line D) lines overlap at all time-steps shown).

Figure 5-14 (b) shows that for the case without buoyancy there is a well-controlled temperature distribution along lines D and E for up to 1 ms before ignition. For the condition with

buoyancy, the temperature distribution along line E is homogeneous but along line D, there is a non-uniform and asymmetric distribution of temperature due to the non-uniform thickness of the boundary layer. A gradient varying radially of about 10 K is observed at EOC and up to 40 ms along line D which is at the middle of the main chamber, with hotter gas located in the top region. As the vortex penetrates axially, the temperature distribution along line D starts to distort as can be observed 1 ms before ignition along line D in Figure 5-13 (a) and Figure 5-14 (a). However, the temperature along the line D remains homogeneous and is of the same magnitude as that at line E in the case without buoyancy. A lower magnitude of temperature is observed along line C, located near the piston face, in both cases. A maximum radial gradient of about 30 K at EOC in the case with buoyancy is observed. In comparison, a uniform 10 K gradient in the case without buoyancy is observed. As time progresses post-compression, the mixing effects of the roll-up vortex can be observed along line C as the temperature gradient starts to distort. A higher magnitude of mixing is observed to take place in the case with buoyancy as a gradient of ~100 K is observed at 40 ms near the piston face in the top half of the main chamber radially, where the vortex is located. This observation is also in agreement with results by Mittal et al. [3]. More enhanced mixing is observed, and the thermal stratification is exacerbated due to the enhanced reactivity in the hotter region, as a maximum temperature gradient of ~200 K is observed near the piston face. In the case without buoyancy, a maximum temperature gradient of ~40 K is observed at 40 ms and increases to 140 K at 1 ms before ignition.

These results indicate that a non-uniform thermal boundary layer is formed due to variation in the initial gas temperature fields that also affects the magnitude of the temperature gradient and the extent to which the gradient is observed in the main chamber post-compression. For the case with buoyancy, except in the top half of the main chamber (line E), a temperature gradient is

observed, not only radially but also axially. A ~90 K change in temperature is observed at EOC over an axial distance of approximately 0.01 m from the piston surface. On the other hand, in the case without buoyancy, the same temperature gradient is observed over a distance of about 0.005 m at EOC. The presence of a thick thermal boundary layer can significantly influence the ignition characteristics. The extent of the high-temperature gas region governs the heat release rate during the ignition event. A thick thermal boundary layer would deplete the high-temperature gas region resulting in a slower heat release event during ignition, as shown in Figure 5-15. It can be observed that in the case with buoyancy, the peak heat release rate is about 3 times lower as compared to the case without buoyancy. Moreover, the heat release takes place over a slightly longer period of time in the case without buoyancy (13.45 ms) as compared to the case with buoyancy (12.24 ms). Nevertheless, the integrated heat release in both the cases is more or less similar (660 ± 3 J).

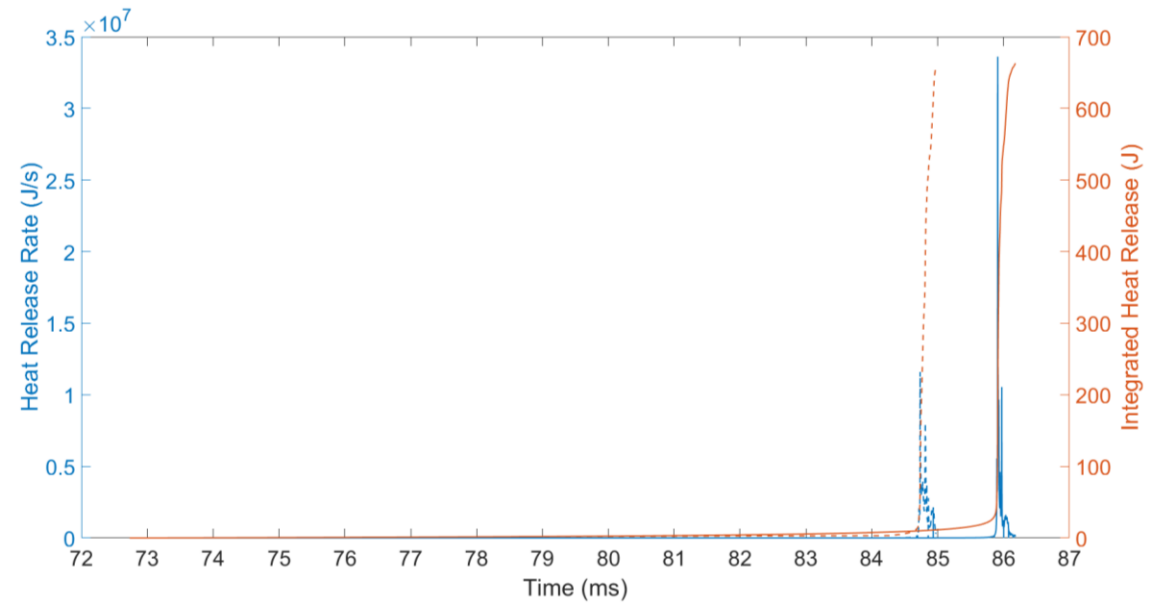

Figure 5-15: Comparison of heat release rates during the ignition event for the two cases (Note: the plots are aligned so that the heat release starts at the same time in both the cases. Solid lines are case without buoyancy and dashed lines are case with buoyancy).

Furthermore, the extent of the high-temperature gas region will also control the production and the diffusive transport of intermediate species such as OH, H_2O_2, HO_2, etc. However,

buoyancy did not lead to any spatial distribution in the equivalence ratio of the mixture as a result of diffusive transport. Figure 5-16 depicts the distribution of OH on planes A and B, 1 ms before ignition. The figure also shows the distribution of OH along lines C (red, close to the piston face), D (green, center of the combustion chamber) and E (blue, close to the cylinder head). It can be observed that OH is produced in volumetrically less quantity in the case of buoyancy as compared to the one without buoyancy. Additionally, in the case with buoyancy, more OH is produced in the top half of the combustion chamber, both axially and radially. In the case without buoyancy, there is a well-controlled homogeneous distribution of OH, except near the piston face where the distribution is perturbed due to the temperature gradients in the vortex.

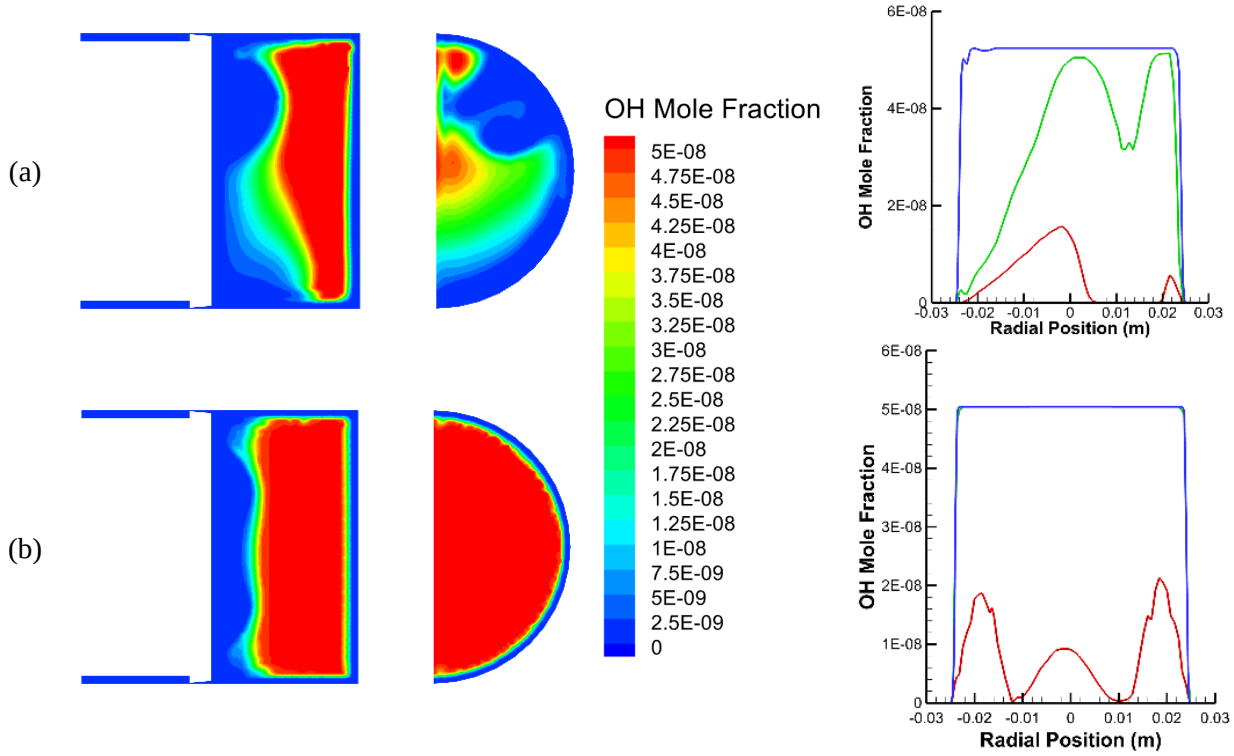

Figure 5-16: OH distributions for (a) with buoyancy and (b) without buoyancy, 1 ms before ignition. Also shown is the comparison of OH distribution along lines C, D and E. (Note: For OH Mole Fraction line plot of (b), the blue (line E) and green (line D) lines overlap).

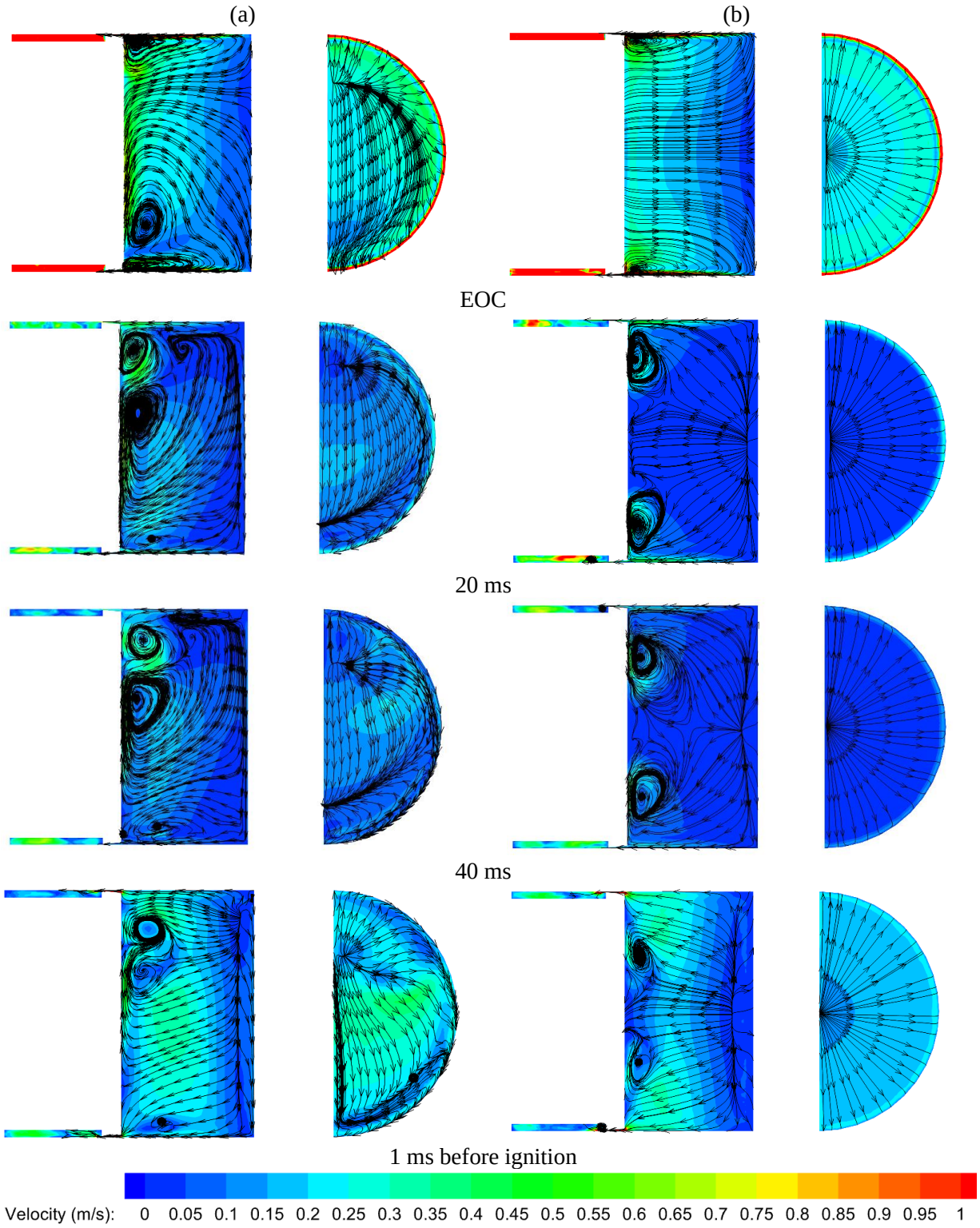

Figure 5-17: Distribution of velocity vectors and corresponding instantaneous streamlines on planes A and B during post-compression times.

Figure 5-17 shows velocity vector distribution (plane A and B) for 0, 20 and 40 ms post-compression times. The figure shows that the magnitude of velocity within the combustion chamber has relatively small values during the post-compression time compared to the average piston speed of ~12 m/s. There is a flow of maximum velocity magnitude of about 1.5 m/s from the combustion chamber to the entrance of the crevice, at the EOC. The velocity vector distribution near the chamber walls indicates that the flow direction is from the main chamber to the crevice entrance during all post-compression times. This illustrates the ability of the crevice to capture the boundary layer flow during compression and post-compression. While a large amount of boundary layer flow is captured during compression, there is still a small roll-up vortex formed on the piston face at EOC as seen on plane A for both cases. In both cases, the toroidal vortex formed begins to move towards the centerline. However, in the case with buoyancy, the bottom part of the toroidal vortex moves up along the piston at a faster rate than the top part. The movement of the toroidal vortex towards the centerline also begins earlier in the case with buoyancy (at EOC) as compared to the case without buoyancy (at 20 ms). The symmetry breaking of the vortex ring and the earlier movement is caused by buoyancy. The effect of gravity produces the same sign of vorticity along the bottom half of the vortex ring, which adds to the torque. In the case without buoyancy, the toroidal vortex symmetrically contracts towards the centerline of the RCM. However, in the case with buoyancy, since the bottom half of the toroidal vortex moves faster, the vortex ring contracts towards the top of the main chamber (vertically offset from the center in the radial direction along the piston surface). In both cases, the vortex ring also penetrates axially into the core gas region.

5.3.1.3.2. Ignition

The effect of temperature inhomogeneities due to buoyancy on predicted ignition delay is examined by comparing the ignition delay times. The results are summarized in Table 5-2 and

indicate that both the simulated ignition delays are similar. Therefore, it can be concluded that the ignition delay is minimally affected by the inhomogeneities. However, it does affect the location of ignition and the ignition behavior itself, as is explained in this section.

Table 5-2: Comparison of ignition delays obtained from the buoyancy and no buoyancy cases.

Ignition Delay Time (ms) with buoyancy	**Ignition Delay Time (ms) without buoyancy**
54.4	53.4

As illustrated in Figure 5-18 (a), a temperature rise and a maximum OH concentration are localized in the top half (both axially and radially) of the main chamber for the case with buoyancy. Whereas, in the case without buoyancy, the temperature rise and maximum OH concentration are localized in the core of the end-gas located in the center of the combustion chamber. As discussed in the previous section, these are the regions of highest temperature and OH concentration. Therefore, it is expected that the ignition would start at these locations in both cases.

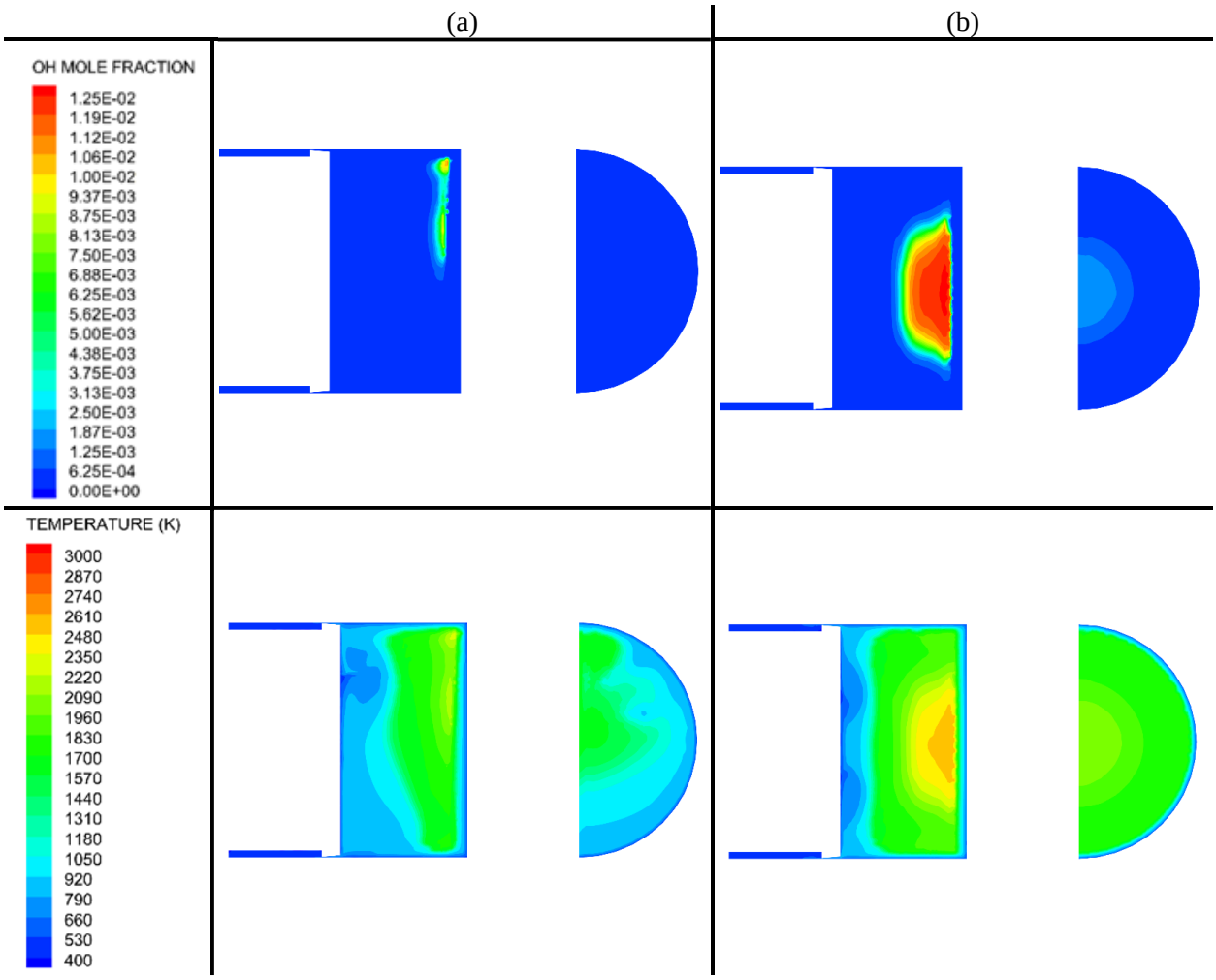

Figure 5-18: OH Mole Fraction (top) and temperature (bottom) at the auto-ignition time in (a) case with buoyancy and (b) case without buoyancy.

Figure 5-19 shows the progression of the flame front represented by the temperature iso-surface in (a) the simulated case with buoyancy, (b) the simulated case without buoyancy and (c) as observed in experiments. Due to larger temperature gradients in the axial direction because of the cooler piston than radially in the case with buoyancy (Figure 5-14), we see a flame originating at the top and propagating downwards in the radial direction while staying in the top axial half of the main chamber. In the case without buoyancy, the flame originates at the center of the combustion chamber and propagates radially outwards, again remaining in the top axial half of the

main chamber. As ignition progresses, the entire volume of the combustion chamber is consumed. The agreement is good when comparing the results simulated with buoyancy to the experimental data. This implies that it is the initial temperature inhomogeneity due to buoyancy and non-isothermal boundary conditions that causes the top to bottom flame propagation behavior that was observed in the experimental studies.

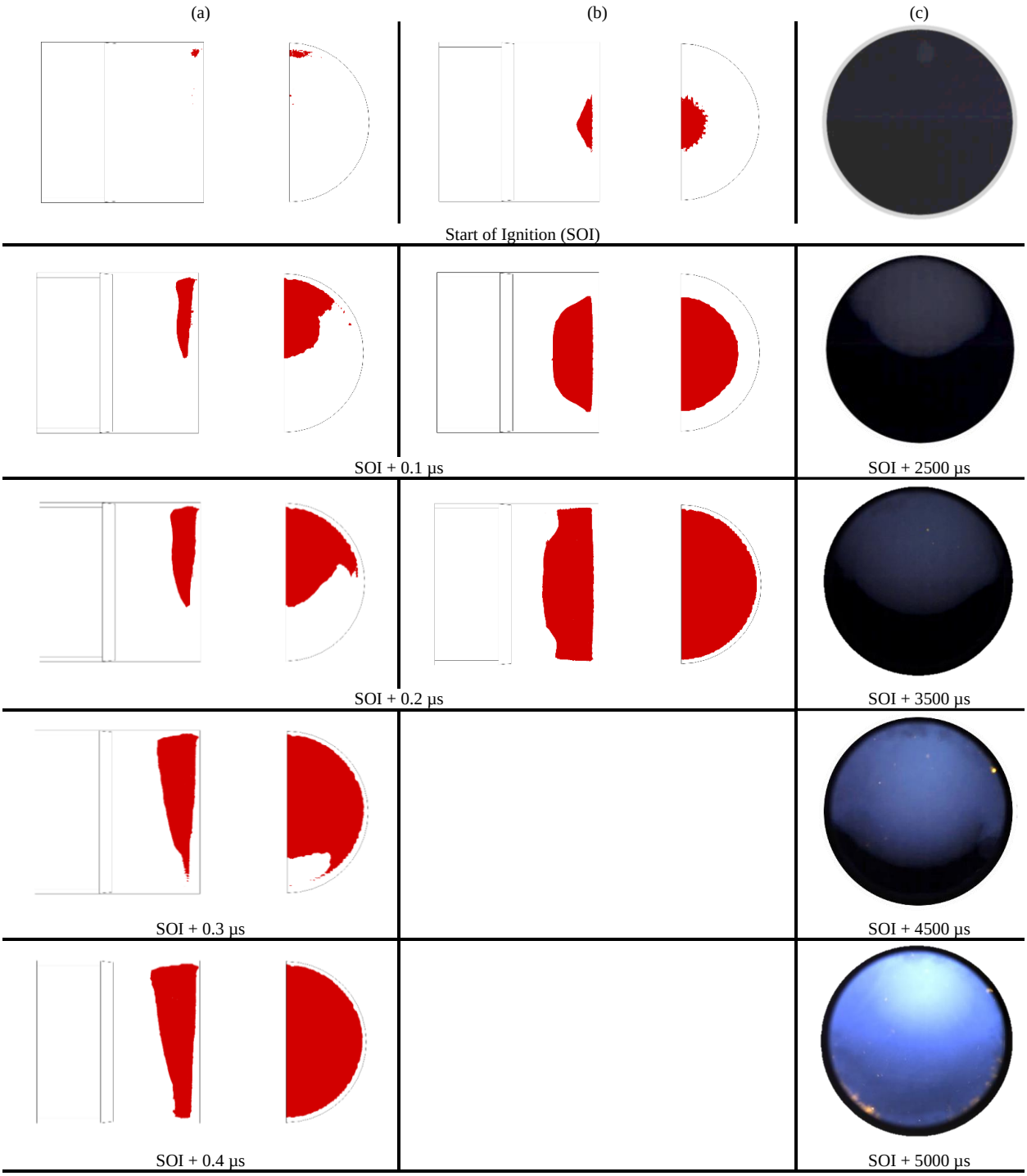

Figure 5-19: Temperature iso-surface in (a) simulated case with buoyancy, (b) simulated case without buoyancy and (c) as observed in experiments.

5.4. Chapter Summary

The experimental results were supplemented with 0-D simulations which made use of volume profiles of the corresponding configurations of compression ratio and diluent gas. Three mechanisms were used to verify this behavior and all three gave similar results.:

- Using a particular volume profile and eliminating heat losses results in identical IDTs across the three cases of varying compression ratio and diluent gas composition.
- In addition to the thermal effects affecting the ignition delay in the case of diluent gas composition, third-body collision efficiencies were also found to affect the ignition delay at all temperatures. Higher third-body collision coefficient resulted in shorter ignition delay.
- H_2O_2 and HO_2 mole fractions were formed in relatively higher concentrations by the EOC in the case of CR=11.7 with nitrogen as the diluent which implies that the mixture is chemically more active by the EOC and results in shortest IDTs, followed by the CR=17.1 with nitrogen as diluent case and finally the CR=11.7 with argon as the diluent case had the longest IDT. This trend was also observed in the experimental data. These low-temperature reactions, however, did not take place on a scale large enough to contribute a considerable amount of chemical heat release during the compression period. The reason for the mixture being chemically more active by the EOC can be attributed to the higher initial pressure and temperature needed to attain the same compressed conditions using a lower compression ratio and a diluent gas that has higher heat capacity.

CFD simulations were used to analyze the effect of non-uniform RCM boundary temperatures, with and without buoyancy, on the temporal evolution of compressed-gas temperature and velocity fields and also on the ignition characteristics. Computational results under laminar conditions and

non-isothermal boundary conditions with buoyancy considered, closely reproduce the features of the ethanol auto-ignition that are observed in the experiments. The creviced piston is still found to provide a homogeneous reacting core located away from the piston head and the post-compression temperature can still be accurately predicted based on the adiabatic core hypothesis in both cases. The simulation results indicate that the temperature field during compression and post-compression is sensitive to non-uniform gas temperature present at the start of an experiment and is also influenced by buoyancy. Steady-state simulations for a cool-piston with a temperature gradient applied to the cylinder wall and without buoyancy revealed the presence of an axisymmetric dome-shaped temperature gradient over the crown of the piston. For the case with buoyancy, the temperature gradient was asymmetric and penetrated further into the bottom half volume of the combustion chamber at BDC. The inhomogeneities in temperature are compressed to a spatial region near the piston during the compression stroke, and a significant temperature gradient can develop across this thermal boundary layer, both radially and axially. The effect of buoyancy causes more severe and asymmetric temperature gradients as compared to the case without buoyancy, with the hotter gas located in the axial and radial top half of the combustion chamber. The symmetry breaking of the vortex ring at the EOC due to the earlier upwards movement of the bottom half of the toroidal vortex is caused by buoyancy. The effect of gravity produces the same sign of vorticity along the bottom half of the vortex ring, which adds to the torque causing it to move upwards earlier and faster than the top half. In the case without buoyancy, the toroidal vortex symmetrically contracts towards the centerline of the RCM. The non-uniform boundary temperatures also led to thermal and species stratification as depicted by the compressed-gas temperature fields and OH concentrations for both cases. However, the ignition delay time predictions were not susceptible to this.

As a next step in examining the effect of test variables on IDTs, it is important to examine the effect that these factors would have on a variety of different fuels, particularly those that exhibit two-stage ignition delay and a negative temperature coefficient region.

Chapter 6. EXPERIMENTAL RESULTS – ISO-OCTANE

6.1. Introduction

Once a strong fundamental understanding of the factors causing discrepancies in ignition delay measurements of a simple fuel like ethanol was achieved, the study then moved on to a more complex fuel, iso-octane, which exhibits two-stage ignition delay and has a pronounced NTC region. In the regression analysis done for the ethanol data, it was found that the R2 value was 0.967; implying that the quality of the correlation at representing the data was excellent. However, a scatter was observed in the plot for temperatures less than 900 K, which in turn implies that there are factors other than the varying diluent/oxygen ratio, equivalence ratio and compressed pressure that affect the ignition delay even at identical conditions. These factors are presumed to have a greater effect on ignition delay at low temperatures. Therefore, normalization, in turn, leads to the necessity to understand the effect of these other factors on the ignition delay. The motivation of the current study is to expand on the ethanol study and determine the impacts of some of the facility dependent effects studied in the previous chapter on the two-stages of ignition and also in the NTC region. Additionally, the study also tries to investigate factors other than those studied previously, responsible for causing a discrepancy in the measured auto-ignition delay data. Following the study on understanding the effect of test variables on the single-stage ignition delay of ethanol, in this chapter, the the effect of changing compression ratio on the ignition delay times of iso-octane was examined. This work focuses on how the method used to achieve a certain compressed condition, in the form of varying compression ratio, influences ignition delay. More specifically, the current study focuses directly on the influence of the rate of heat loss and the t_{50}, a parameter dependent on the compression time.

6.2. Test Conditions

Experiments were conducted for iso-octane/oxygen/nitrogen mixtures of ϕ = 1.3 over a temperature range of 675 K-900 K and at a pressure of 20 bar. A constant diluent/oxygen ratio of 3.76 was maintained to simulate normal air. In order to study the effects of post-compression heat losses, a given compressed condition was achieved using two different compression ratios. The different compression ratios of the MSU RCM were assessed to cover the temperature range of interest without having to alter the diluent gas composition. However, the whole temperature range of 675 K - 900 K could not be achieved using a single compression ratio. Therefore, a total of 5 compression ratios were used to cover the compressed temperature range and to compare the ignition delay times at a given compressed condition, as can be observed in Table 6-1. The resulting compressed conditions are similar to those prevailing in piston engines. As the compression ratio is increased, the need for higher initial pressure and temperature to achieve a certain compressed condition decreases. This further helps in lowering the fuel partial pressure requirement in order for it to completely evaporate and enables sufficient time for mixing within the combustion chamber. The iso-octane used for the experiments was obtained from Sigma-Aldrich while all gases were supplied by Airgas.

Table 6-1: Test Conditions for which ignition delay times were measured and predicted.

	Molar Composition			**P_c (bar)**	**T_c (K)**	**CR**
	Iso-octane	O_2	N_2			
1	1.0	9.6	36.2	20	690	9.6
						6.8
2					710	9.6
						6.8
3					735	13.8
						9.6
4					760	17.1
						13.8
5					780	17.1
						13.8
						9.6
6					800	17.1
						13.8
						12.7
						12.5
7					835	17.1
						12.7
						12.5
8					850	17.1
						13.8
						12.7
						12.5
9					880	17.1
						12.5

As discussed in Chapter 1, exhaustive research has been done on the influence of varying diluent/buffer gas composition on the auto-ignition of iso-octane. While the current study used only nitrogen as the buffer gas, this study focuses on the effect that changing the compression ratio would have on iso-octane ignition delay measurements, which is an alternate method to varying diluent gas composition, to achieve the compressed conditions. As mentioned in Chapter 1, this emphasizes the difficulties in comparing experimental results when compressed temperatures and pressures are used as the only reference, as a large scatter can be observed across data sets for the same compressed conditions. This study presents one of the contributing factors, other than the buffer gas composition, to that scatter.

6.3. Data Interpretation

The ignition delay times reported in this work were limited to between 3 ms and 100 ms. The higher limit was set based on the study of Mittal et al. [71] where it was reported that beyond 100 ms, the adiabatic core assumption starts losing its validity; while the lower limit for ignition delay times was set to 3 ms to avoid the influence of pre-compression reactions [4]. No pressure scaling was used while reporting the ignition delay times because the achieved compressed pressures were within ± 0.5 bar of the desired pressure. At each compressed condition, a minimum of two non-reactive tests and three combustion tests were performed. A clean combustion chamber protocol was developed in the ethanol study to avoid multiple flame kernels and the slight pressure rises that were observed in some preliminary tests. The protocol involved regular cleaning of the combustion chamber after each set of 3 tests at a given compressed condition and also conducting oxygen runs in between individual tests. In order to obtain accurate measurements by preventing contamination through substances accumulated in oil layers, O-rings, impurities from previous

runs and other surfaces, the protocol was also followed for the current study. The total ignition delay times were reproducible within ± 10% of the mean value.

A typical pressure trace encountered in this study is shown in Figure 6-1. The measured pressure and evaluated temperature at the end of compression (t = 0) are P_c = 19.96 bar and T_c = 689.2 K, respectively for CR = 9.6. The duration of the compression stroke is approximately 31 ms. The first-stage ignition delay time (τ_1) is defined as the time from the end of the compression stroke (t = 0 ms) to the point of the maximum pressure rise rate due to first-stage ignition activity. The second-stage ignition delay time (τ_2) is defined as the time duration between the end of τ_1 and the maximum rate of pressure rise due to the second stage of ignition. The total ignition delay time (τ) is referred to as $\tau = \tau_1 + \tau_2$ or is defined as the time from the end of compression stroke to the maximum rate of pressure rise due to the second stage of ignition (inflection point, (dP/dt)max). End of compression (EOC) is the time when dP/dt first becomes negative after the start of compression and corresponds to the maximum of the pressure trace (P_c) prior to ignition. The corresponding nonreactive pressure trace is also shown as a dashed blue line in Figure 6-1. A non-reactive pressure trace was completed for each experiment to ensure that no significant heat release occurred during the compression stroke. The non-reactive experiments were conducted at initial conditions identical to those at which the reactive tests were carried out, except that the oxygen in the mixture was substituted by nitrogen to eliminate oxidation reactions while maintaining a comparable heat capacity ratio. Additionally, Figure 6-1 also depicts another typical parameter, t_{50}, defined as the time for the last 50% of the pressure rise to occur [1]. The t_{50} reflects the time a mixture spends at elevated conditions before the constant-volume test conditions are attained. This implies that low t_{50} values are desirable to prevent fuel reactivity during the compression period, which is necessary for the adiabatic core hypothesis to be valid. Moreover, lower t_{50} also reduces

the uncertainties related to the determined thermodynamic state for a particular compressed condition.

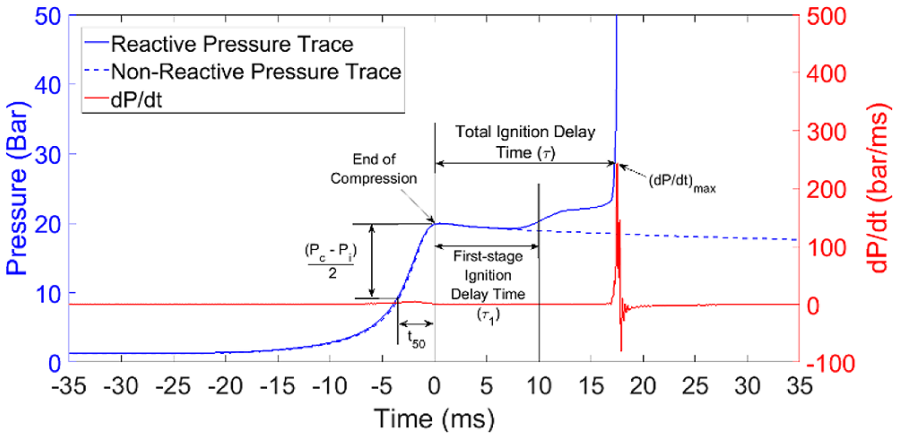

Figure 6-1: Typical pressure trace for a reactive and nonreactive case at 20 bar and 690 K for rich iso-octane and air mixture (ϕ = 1.3).

6.4. Effect of post-compression heat loss on the First-Stage Ignition Delay

Figure 6-2 shows the variation in the measured first-stage and total ignition delays using different compression ratios, with three measurements shown at each point. The measurements indicate that varying the compression ratio has an insignificant influence on the first-stage ignition delay, where the difference is less than 24%.

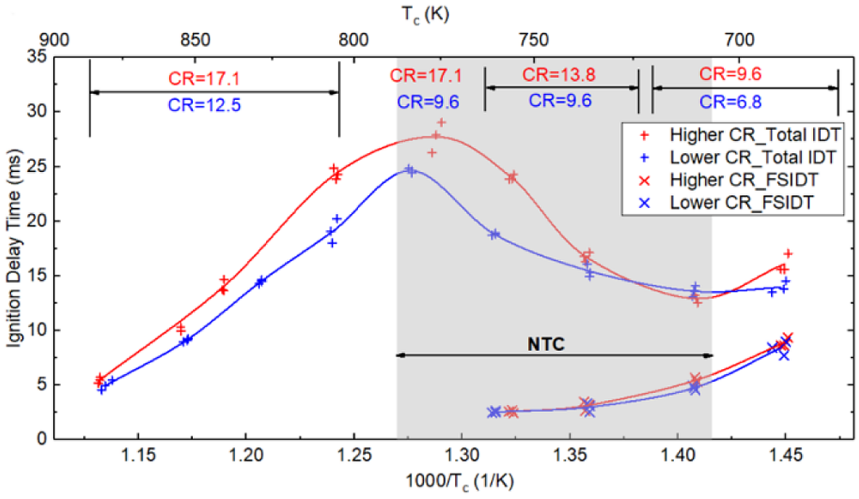

Figure 6-2: Ignition delay time vs 1000/T (K) for high and low compression ratios at 20 bar compressed pressure and ϕ = 1.3.

Figure 6-3 compares the typical non-reactive pressure traces of the iso-octane experiments using the different compression ratios that were used to achieve the corresponding compressed conditions. Due to variations in the initial pressure and temperature required to achieve the same compressed conditions when using different compression ratios, the pressure-time history of each compression ratio was different. In general, higher compression ratios exhibited a faster pressure drop post-compression due to the shorter clearance length at TDC (used to achieve the higher compression ratio), which resulted in higher surface area-to-volume ratio and led to higher post-compression heat losses.

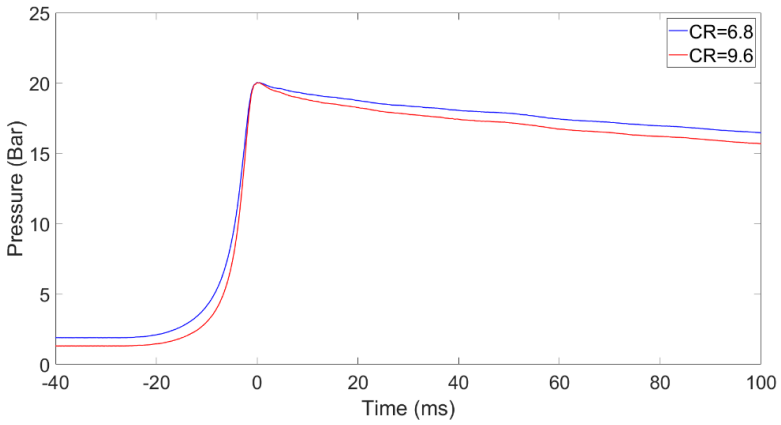

(a)

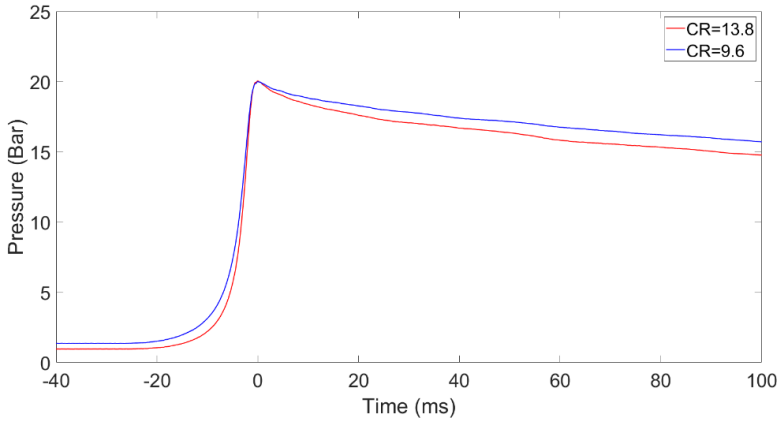

(b)

Figure 6-3: Non-reactive pressure traces for the different compression ratios that were used to achieve compressed conditions of 20 bar and (a) T_c = 710 K, (b) T_c = 760 K, (c) T_c = 780 K and (d) T_c = 800 K (also note the decrease in compression time for the higher compression ratios).

Figure 6-3 (cont'd)

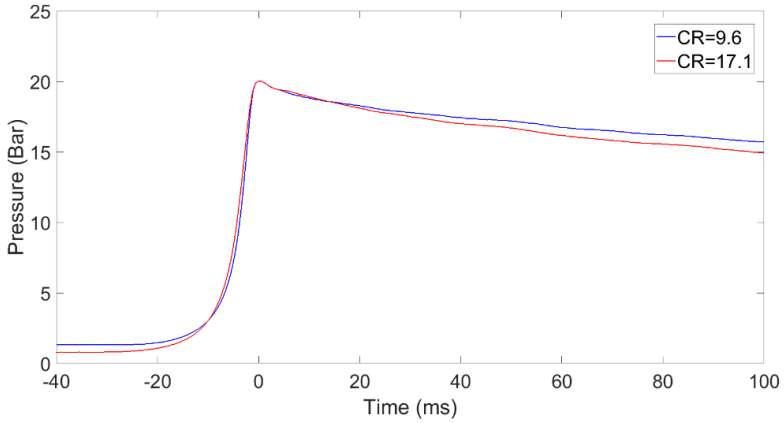

(c)

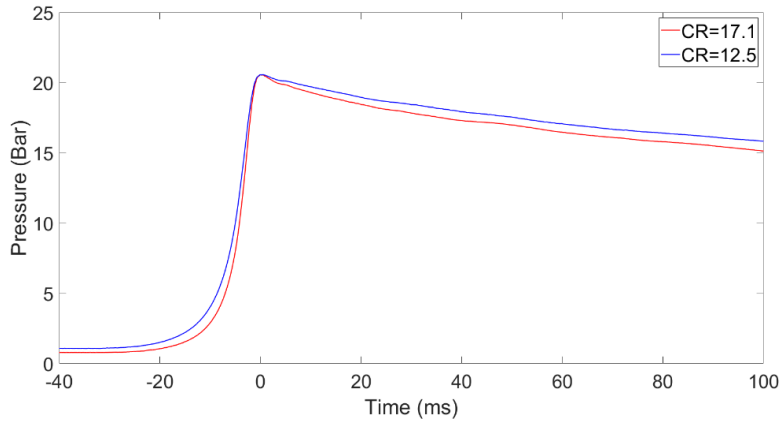

(d)

From Table 6-2 it can be observed that as the surface area-to-volume ratio increases, the rate of pressure drop post-compression also increases, which is also reflected in Figure 6-3. Figure 6-3 also shows that the higher compression ratios of CR = 9.6 for T_c = 690 K and 710 K, CR = 13.8 for T_c ranging from 735 K - 800 K and CR = 17.1 for T_c from 800 K - 900 K, always had a higher post-compression drop in pressure, which is representative of heat losses, as a result of the higher surface area-to-volume ratio as compared to the corresponding lower compression ratios cases. For compression ratios with similar surface area-to-volume ratio (see Table 2, CR = 9.6 and 12.5, and CR = 13.8 and 17.1), the rate of drop in pressure was also similar. The average percentage

reduction in the surface area-to-volume ratio, achieved by reducing the compression ratio for the three pairs of compression ratios was 21.6 ± 1.8% and the average percentage reduction in the rates of pressure drop between the pairs of compression ratios was 18.8 ± 2.4%. However, the pair of CR = 13.8 and 9.6 had the biggest reduction in pressure drop rate (22.8%), whereas the pairs of CR = 12.5 and 17.1 had the least reduction in pressure drop rate (15.1%). This is because the pair of CR = 13.8 and 9.6 has the biggest drop in the surface area-to-volume ratio (23.4%), whereas the reduction in the surface area-to-volume ratio for CR = 12.5 and 17.1 was the least with 20%.

Table 6-2: RCM configuration and initial conditions needed to achieve the desired compressed conditions, using different compression ratios.

CR	Surface Area: Volume Ratio (m^{-1})	rate of pressure drop post compression (±0.001 bar/ms)	P_i (±0.05 bar)	T_c (±9 K)	T_i (±5 deg. C)	Compression Time (±0.5 ms)	Clearance (m)	Stroke (m)
6.8	163.61	0.035	1.91	690	130	30	0.032	0.203
				710	145			
9.6	203.39	0.044	1.32	690	95	30	0.021	0.203
				710	110			
				735	120			
				760	140			
				780	150			
12.5	211.96	0.045	1.06	800	145	32	0.020	0.254
				835	160			
				850	175			
				880	190			
12.7	248.41	0.049	1.06	800	145	30	0.015	0.203
				835	160			
				850	175			
13.8	265.43	0.057	0.97	735	100	30	0.013	0.203
				760	110			
				780	120			
				800	135			
				850	165			
17.1	265.43	0.053	0.8	780	100	32	0.013	0.254
				800	115			
				835	130			
				850	140			
				880	165			

Although the effects of changing compression ratio on the first-stage ignition delay are minimal, considerable differences in the pressure and temperature rise rates as a result of the first-stage ignition heat release are observed due to the difference in the surface area-to-volume ratio, as shown in Figure 6-4 and Figure 6-5. These two figures depict typical reactive pressure traces of iso-octane experiments showing the first-stage ignition delay with the different pairs of compression ratios. As mentioned earlier, compression ratios having higher surface area-to-volume ratio cause higher rates of post-compression heat losses and thus exhibit lower pressure and temperature rise during the heat release of the first-stage ignition, as compared to the corresponding compression ratio cases with lower surface area-to-volume ratio. For CR = 6.8, as shown in Figure 6-4 (a), the total pressure rise due to the first-stage heat release is about 3.3 bar whereas for the corresponding higher compression ratio (CR = 9.6), the total pressure rise is about 2.9 bar. However, for T_c = 710 K, the total pressure rise due to the first-stage heat release in both the compression ratios was similar, as can be seen in Figure 6-4 (b). As a result, the total ignition delay times were also similar, with the added fact that the short duration of the second-stage ignition delay allows less time for post-compression heat losses to influence the total ignition delay time. This effect is discussed in more detail in the next section.

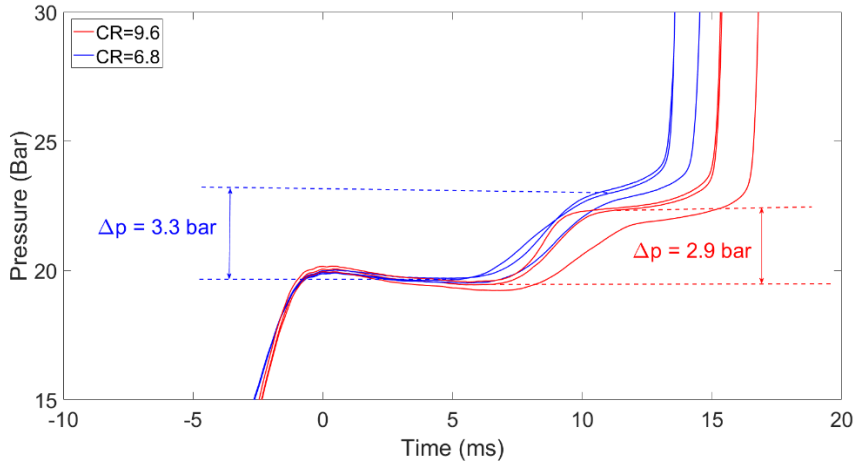

(a)

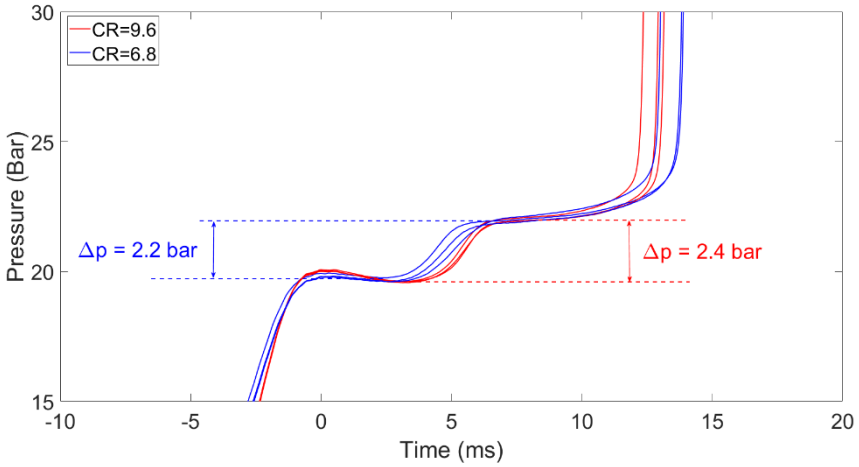

(b)

Figure 6-4: Comparison of the pressure traces obtained using CR = 9.6 (red) and CR = 6.8 (blue), representing the difference in ignition delay for the same compressed conditions of 20 bar pressure and (a) T_c = 690 K and (b) T_c = 710 K.

In general, changing the compression ratio demonstrated only a slight impact on the first-stage ignition delay duration. Nevertheless, it influenced the rise in temperature and pressure after the first-stage ignition, which noticeably impacted the consequent ignition event, as is presented next.

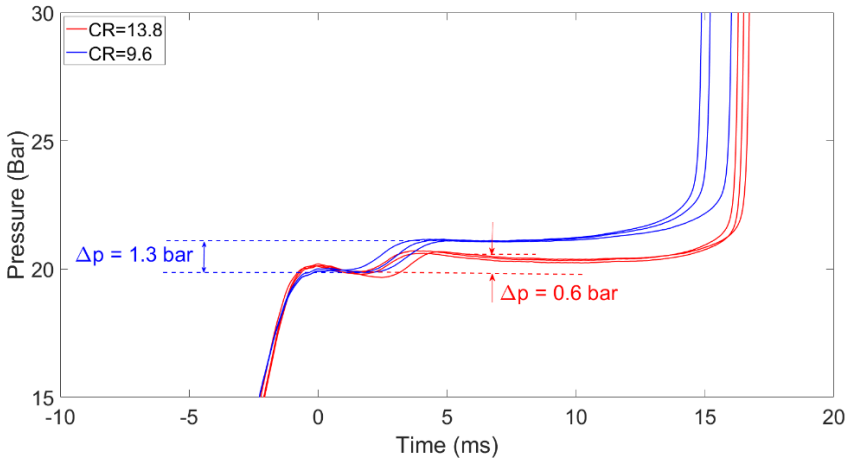

(a)

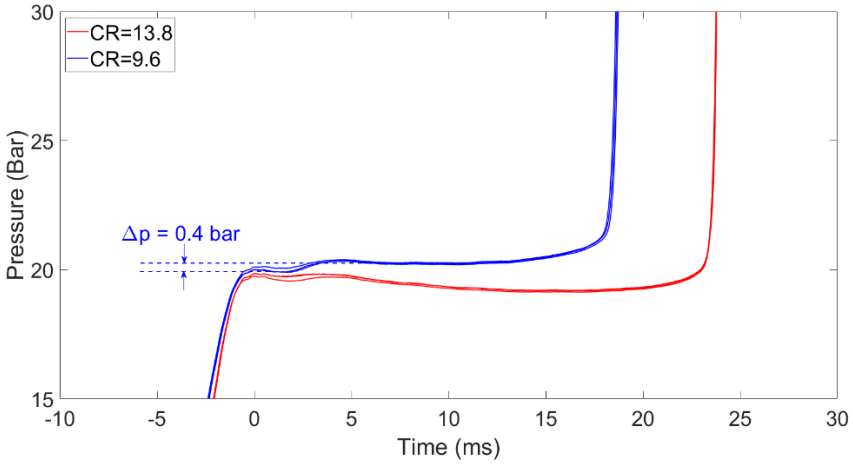

(b)

Figure 6-5: Comparison of the pressure traces obtained using different compression ratios, representing the difference in ignition delay for the same compressed conditions of 20 bar pressure and (a) T_c = 735 K, (b) T_c= 760 K and (c) T_c= 780 K.

Figure 6-5 (cont'd)

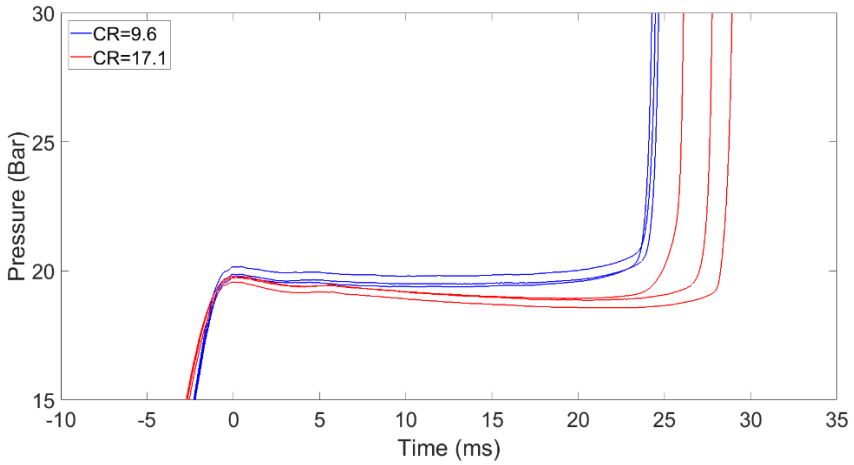

(c)

6.5. Effect of post-compression heat loss on Total Ignition Delay

As the results show, the second stage ignition is mainly coupled to the first-stage ignition via the heat release from the first-stage. Figure 6-2 and Table 6-3 show the experimental results of the ignition delays of iso-octane. It can be seen that the experimental data indicate NTC behavior over the temperature range studied. For low temperatures of 690 K - 735 K, there is hardly any sensitivity to the change in compression ratio. As can be seen in Figure 6-4, the difference in pressure rise due to the heat release from the first-stage of ignition for the two compression ratios is minimal at 690 K and similar at 710 K. The reason for similar total ignition delay times at T_c = 690 K and 710 K between the two compression ratios is the shorter second stage ignition delay at these temperatures, see Table 6-3, that allows less time for the post-compression heat loss to affect the second stage ignition. In the NTC region, for temperatures greater than 710 K and where two-stage ignition delay was observed (760 K $\geq T_c >$ 710 K), the difference between the total ignition delay for the two different compression ratios increased as T_c increased. The larger surface area-to-volume ratio in compression ratios cause greater post-compression heat losses. Higher post-

compression heat losses cause a smaller pressure rise due to the first-stage ignition, which in turn leads to a less reactive species pool. The lower reactivity extends the second stage of ignition, which also allows for the post-compression heat losses to further influence the ignition process, thereby causing a longer total ignition delay time at higher compression ratios. As the ignition delay time increases with T_c in the NTC region, the longer second stage ignition at higher temperatures allows more time for the post-compression heat losses to influence the total ignition delay time. As a result, the difference in total ignition delay times from the two compression ratios also increases with an increase in T_c.

Table 6-3: Summary of experimental results.

T_c (K)	**CR**	**t_{50} (ms)**	**First-stage Ignition Delay (ms)**	**Second Stage Ignition Delay (ms)**	**Total Ignition Delay (ms)**
690.4 ± 1.1	6.8	4.9	8.39 ± 0.5	5.6 ± 0.7	14.0 ± 0.4
	9.6	4.0	8.9 ± 0.3	7.2 ± 0.8	16.1 ± 0.7
710.3 ± 0.4	6.8	5.0	4.8 ± 0.2	8.8 ± 0.4	13.6 ± 0.4
	9.6	4.0	5.5 ± 0.2	7.4 ± 0.3	12.9 ± 0.3
736.3 ± 0.6	9.6	3.9	3 ± 0.3	12.5 ± 0.6	15.5 ± 0.5
	13.8	3.3 ± 0.2	3.1 ± 0.3	13.6 ± 0.5	16.7 ± 0.3
758.2 ± 2.3	9.6	4.1	2.5 ± 0.1	16.3 ± 0.1	18.8 ± 0.1
	13.8	3.3 ± 0.2	2.6 ± 0.1	21.4 ± 0.2	24.0 ± 0.2
779.9 ± 3.7	9.6	3.9			24.6 ± 0.2
	17.1	4.4 ± 0.1			27.7 ± 1.1
805.9 ± 0.8	12.5	5.0			19.1 ± 0.9
	17.1	4.3 ± 0.1			24.4 ± 0.4
834.7 ± 6.0	12.5	5.5 ± 0.3			14.5 ± 0.2
	17.1	4.6 ± 0.1			16.7 ± 0.4
854.0 ± 1.0	12.5	5.1 ± 0.1			9.1 ± 0.1
	17.1	4.2			10.1 ± 0.2
882.2 ± 1.7	12.5	4.9			5.0 ± 0.4
	17.1	4.6 ± 0.1			5.4 ± 0.2

For temperatures greater than 760 K where two-stage ignition delay was not observed, the total ignition delay times measured using the higher compression ratios were longer as compared to those measured using the lower compression ratio. It is also clear from Figure 6-2, Figure 6-5, and Figure 6-6 that, outside the NTC region, i.e. for compressed temperatures of 780 K and onwards, the difference in ignition delay times for different compression ratios but the same compressed conditions reduces as T_c increases. For T_c = 880 K, the ignition delay times obtained using both compression ratios collapsed around a single value. A similar trend was observed by the in the ethanol study, where the difference in ignition delay times across two compression ratios reduced as T_c increased. Since the ignition delay time reduces with increasing T_c, the shorter total ignition delay times allow less time for the post-compression heat losses to affect the ignition process. The trend is also in line with the trend observed within the NTC region; as the temperature increased, the second stage ignition delay also increased (Table 6-3) and so did the difference between the total ignition delay times from the different compression ratios. Longer second stage ignition delays allow longer duration for the post-compression heat losses to affect the total ignition delay times. As mentioned earlier, at high temperature the total ignition delay times are only minimally affected by post-compression heat losses because the auto-ignition occurs in the early stages of the post-compression process, where the effect of heat loss is minimal. This reasoning is also applicable to the first-stage ignition delay time being minimally affected by the compression ratio; since both, the first-stage ignition delay from 690 K-750 K and the total ignition delay from 850 K-900 K have a similar order of magnitude.

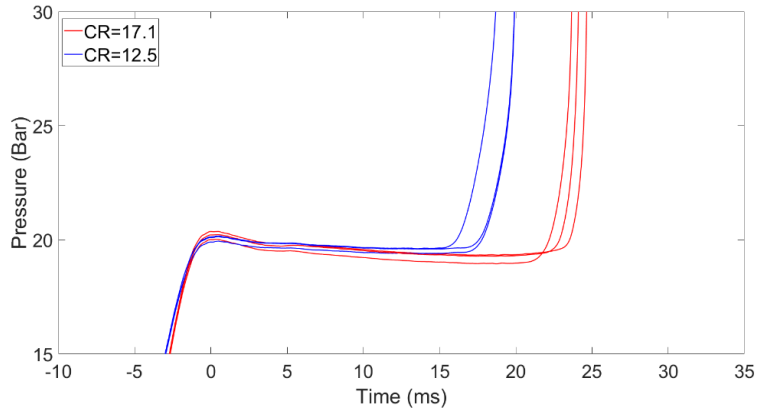

(a)

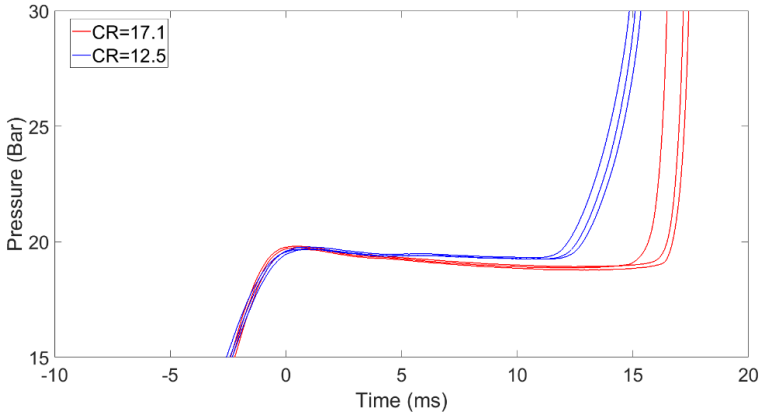

(b)

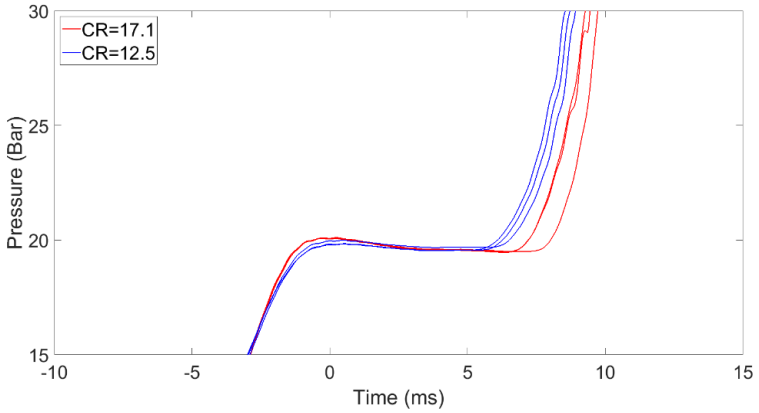

(c)

Figure 6-6: Plot comparing the pressure traces obtained using CR=17.1 (red) and CR=12.5 (blue), representing the difference in ignition delay for same compressed conditions of 20 bar pressure and (a) T_c = 800 K, (b) T_c= 835 K, (c) T_c= 850 K and (d) T_c= 880 K.

Figure 6-6 (cont'd)

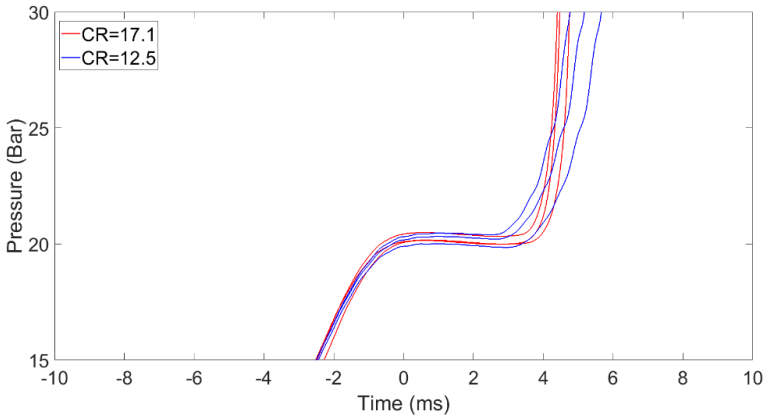

(d)

6.6. Effect of t_{50} on ignition delay

The volumetric compression period of the experiment is crucial in achieving a desired compressed condition with minimal reactivity before the desired condition is reached. A typical parameter, t_{50}, defined as the time for the last 50% of the pressure rise to occur, can be used to evaluate the compression phase [1]. The t_{50} times represent the amount of time a mixture spends at elevated state conditions before the constant-volume test conditions are achieved. This implies that low t_{50} values are desirable in order to prevent fuel reactivity during the compression period and also to reduce uncertainties related to the determined thermodynamic state for a particular compressed condition. The t_{50} times are tabulated in Table 6-3 and it can be observed that in most cases, lower compression ratios have longer t_{50} times as compared to the corresponding higher compression ratios, at a given test condition. Longer t_{50} times indicate that the mixture spends more time at elevated conditions and gets more reactive by the end of compression, leading to shorter total ignition delay times.

While post-compression heat loss is the major factor affecting the ignition delay times, there are other contributing factors that are also suspected. As can be inferred from Table 6-2, the lower

compression ratio cases need a higher initial pressure and temperature to achieve the same compressed conditions, as compared to their corresponding higher compression ratios. Also, the lower compression ratios had relatively longer compression times as compared to the corresponding higher compression ratio counterparts used to achieve the same compressed condition. Higher initial pressure and temperature, along with longer compression times, increases the potential for low-temperature reactions to occur during the compression stroke, which can result in shorter ignition delay times. It was shown in the ethanol study that the higher pressure and temperature initial conditions required for the lower compression ratio case, combined with the longer compression time caused shorter ignition delay times for ethanol. In the studies on ethanol, two compression ratios of 11.7 and 17.1 were used over the entire temperature range from 800 K to 875 K and it was found that the ignition delay times using CR = 17.1 were consistently longer than those obtained using CR = 11.7. The lower temperature and pressure initial conditions, higher surface area-to-volume ratio (SA/V) ratio and shorter t_{50} times (4.3 ± 0.2 ms in CR = 17.1 vs 5.2 ± 0.1 ms in CR = 11.7) contributed to the longer ignition delay times obtained using CR = 17.1 as compared to CR = 11.7, at the same compressed conditions. However, when argon was used as a diluent with CR = 11.7, despite the lower initial temperature and pressure conditions needed to achieve the same compressed conditions, the t_{50} times using argon (5.1 ± 0.2 ms) were found to be the same as those obtained using nitrogen as the diluent (5.2 ± 0.1 ms) for the same compression ratio. This is due to the lower thermal capacity of argon as compared to nitrogen that allows the mixture to heat up faster. The lower thermal capacity of argon also led to greater post-compression heat losses due to faster cooling as compared to nitrogen, which in turn resulted in longer ignition delay times at identical compressed conditions.

Based on the analysis of the experimental results in this study, it is suspected that the effect of compression ratio on the ignition delay times is primarily manifested due to the change in the surface area-to-volume ratio. With the help of non-reactive pressure traces, the post-compression pressure drop was evaluated and found to be similar if the surface area-to-volume ratio is similar, despite the difference in the compression ratio (CR = 13.8 and 17.1, see Table 6-2). In an effort to show that the different ignition behaviors presented in this study are not caused by the change of chamber geometry, experiments were conducted at identical compressed conditions using CR = 13.8 and CR = 17.1 and the results are plotted in Figure 6-7. By employing CR = 13.8 and 17.1, the TDC volume and geometry remain consistent. It is observed that for T_c = 780 K, the ignition delay times are identical using the two compression ratios. However, the results start to slightly deviate as T_c increases, with shorter ignition delays times observed for the higher compression ratio (CR = 17.1) and maximum percentage deviation of 16%.

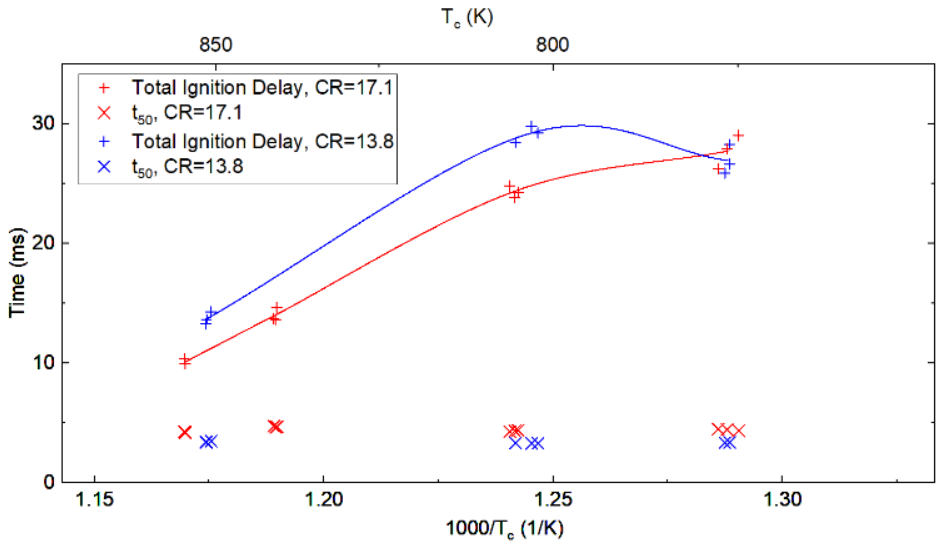

Figure 6-7: Ignition delay time vs 1000/T (K) for the two compression ratios (CR=13.8 and 17.1) with identical surface area-to-volume ratio at 20 bar compressed pressure and ϕ = 1.3.

Looking at the t_{50} times in Figure 6-7, it is observed that the mixture spends about a millisecond longer at elevated conditions when CR = 17.1 as compared to when CR = 13.8. This

can contribute to shorter ignition delays in the higher compression ratio case. Despite the identical surface area-to-volume ratio at TDC and lower initial conditions maintained in the higher compression ratio case, the total ignition delay times with CR = 17.1 were shorter than with CR = 13.8. These results suggest that the ignition delay times are more sensitive to the volumetric compression process than the initial conditions. This implies that the compression period plays a crucial role in the ignition delay times and that RCMs should be designed to ensure t_{50} times are as low as possible.

It has been established that different compression ratios can have identical surface area-to-volume ratio and yet result in different ignition delay measurements at identical test conditions. The initial conditions and compression process also affect the ignition delay times and therefore similar compression ratios may not necessarily result in identical ignition delay measurements as different compression ratios can vary in compression time and surface area-to-volume ratio. In order to isolate the compression ratio, tests were carried out at similar compression ratios of 12.5 and 12.7 and results are plotted in Figure 6-8.

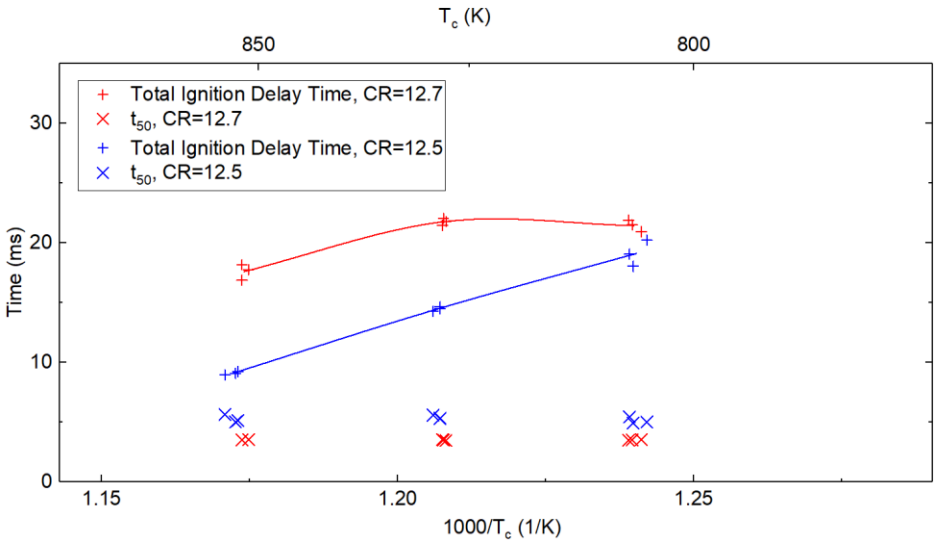

Figure 6-8: Ignition delay time vs 1000/T (K) for the two similar compression ratios (CR=12.5 and 12.7) with identical initial conditions at 20 bar compressed pressure and ϕ = 1.3.

The configuration now differed in terms of surface area-to-volume ratio and compression time, while maintaining the same initial conditions. From Table 6-2 it can be seen that CR = 12.7 has a greater surface area-to-volume ratio and hence the mixture experiences a slightly greater rate of pressure drop post-compression, as can also be seen in Figure 6-9. Moreover, the faster rate of compression in CR = 12.7 can also be observed in Figure 6-9. From Figure 6-8, it can be inferred that the t_{50} times for CR = 12.7 are about 1.5 ms shorter than that of CR = 12.5. From Figure 6-8, the ignition delay times using CR = 12.7 are longer than those obtained using CR = 12.5, despite the identical initial conditions. The greater post-compression heat losses and shorter t_{50} times of CR = 12.7 as compared to CR = 12.5 together contribute to affecting the ignition delay times. In this case, the t_{50} times seem to play a bigger role in influencing the ignition delay times because even at the high temperature of T_c = 850 K, there is a substantial difference (a deviation of 32%) between the ignition delay times measured using the two compression ratios. This is one of the contributing reasons as to why different facilities report different ignition delay times at identical compressed conditions, even when employing similar compression ratios.

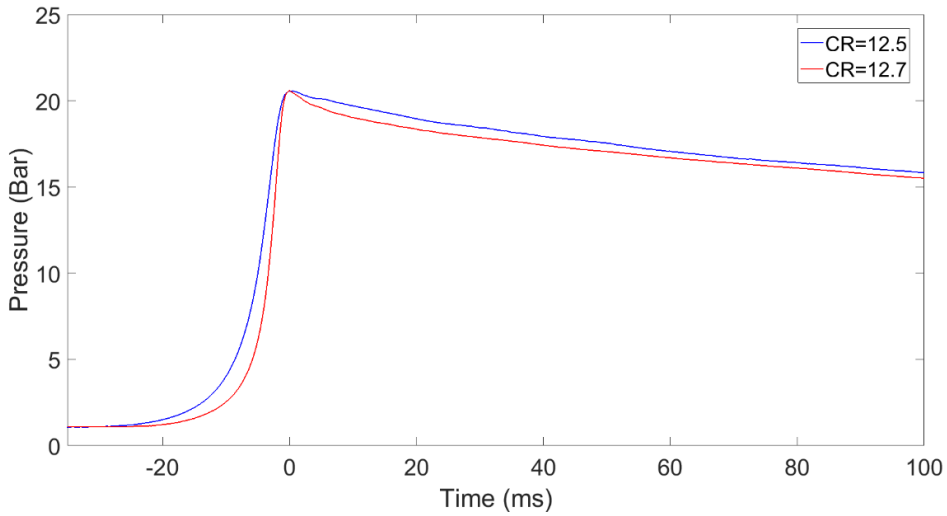

Figure 6-9: Non-reactive pressure trace for similar compression ratios of 12.5 and 12.7 used to achieved test conditions of 20 bar and 850 K (also note the decrease in compression time for CR=12.7).

In order to isolate the influence of t_{50} times, two compression ratios of 12.7 and 13.8 were chosen, which had identical t_{50} and compression times in this study. However, CR = 13.8 had greater surface area-to-volume ratio as compared to CR = 12.7, see Table 6-2. As a result of which, as can be inferred from Figure 6-10, CR = 13.8 had longer ignition delay times at T_c = 800 K as compared to CR = 12.7. Despite the slightly lower temperature and pressure initial conditions required when using CR = 13.8, the t_{50} times were calculated to be the same as in the case of CR = 12.7. This may be attributed to the smaller clearance volume for CR = 13.8 that enables the mixture to heat up at a faster rate. However, due to a greater rate of pressure drop post-compression in CR = 13.8 (0.057 bar/ms vs 0.049 bar/ms) as observed in the non-reactive pressure traces shown in Figure 6-11, the total ignition delay times using CR = 13.8 were longer as compared to those obtained using CR = 12.7 at T_c = 800 K. Nevertheless, at higher T_c of 850 K, the ignition delay times had a maximum of 13% deviation between the two compression ratios, as can be observed in Figure 6-10.

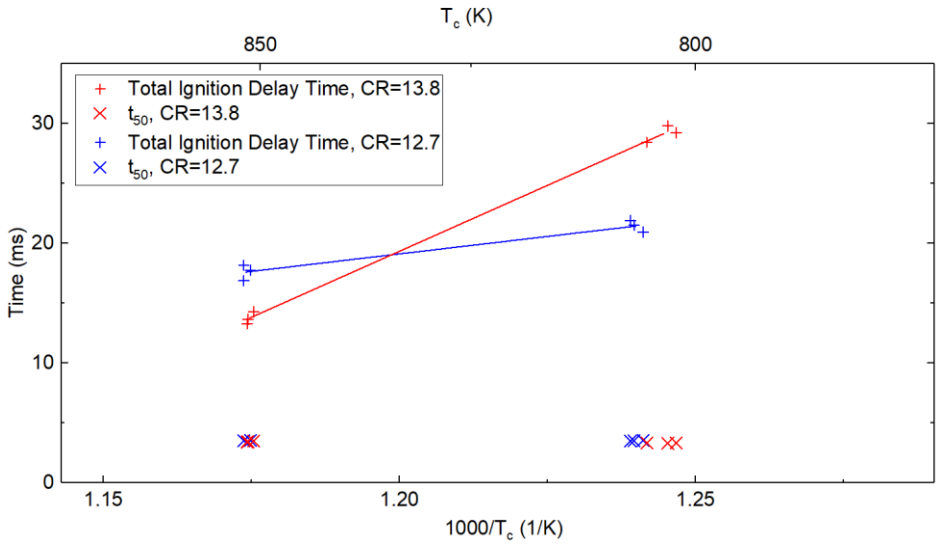

Figure 6-10: Ignition delay time vs 1000/T (K) for the two compression ratios (CR=13.8 and 12.7) with identical t_{50} times at 20 bar compressed pressure and ϕ = 1.3.

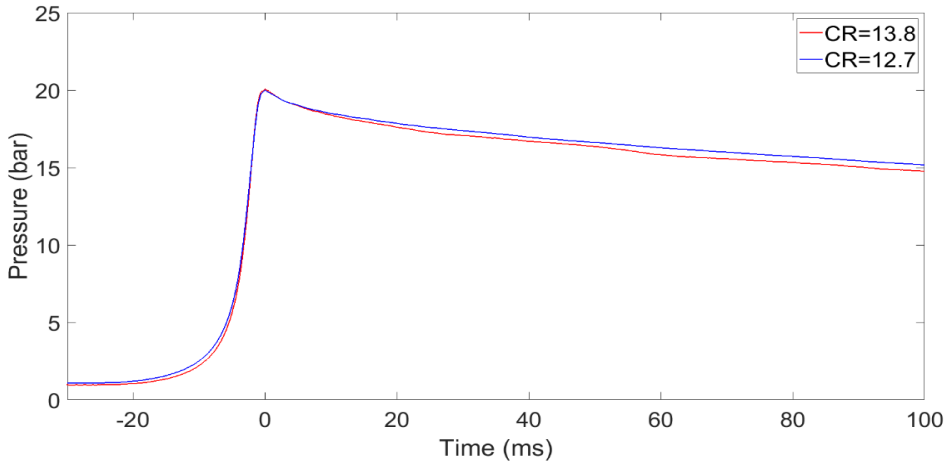

Figure 6-11: Non-reactive pressure trace for compression ratios of 12.7 and 13.8 with similar t_{50} times used to achieve test conditions of 20 bar and 850 K.

For the case where the surface area-to-volume ratio was kept constant (CR = 13.8 and 17.1), an average reduction in 22 ± 2% of t_{50} times led to an average increase of 28 ± 8% in total ignition delay times at 850 K ≥ T_c ≥ 800 K. On the other hand, keeping the t_{50} times constant (CR = 12.7 and 13.8); a reduction of 6% in SA/V ratio leads to an increase in the total ignition delay time of 36% at T_c = 800 K. It can be said that the ignition delay times are more sensitive to post-compression heat losses which are in turn dependent on surface area-to-volume ratio. However, more in-depth sensitivity analysis needs to be carried out over a broader range of temperature. Furthermore, for a given compression ratio, different fuels may have different t_{50} times and rates of post-compression heat losses because of the difference in chemical kinetics and thermodynamics of the mixtures. However, the effects studied in this work would still translate well to different fuels as the ignition is found to be limited more by post-compression heat losses as compared to the t_{50} times. In other words, shorter t_{50} times and greater post-compression heat losses would lead to longer ignition delay times at identical compressed conditions; as was observed for ethanol as well as iso-octane.

Table 6-4: Comparison of total ignition delay and t_{50} times from compression ratios having similar SA/V ratio (CR=13.8 and 17.1), similar CR (CR= 12.5 and 12.7) and similar t_{50} times (CR=12.7 and 13.8).

T_c (K)	CR	t_{50} (ms)	Total Ignition Delay (ms)
779.9 ± 3.7	13.8	3.4	26.9 ± 1.0
	17.1	4.4 ± 0.1	27.7 ± 1.1
806.2 ± 1.1	12.7	3.5	21.4 ± 0.4
	13.8	3.3	29.2 ± 0.6
	17.1	4.3 ± 0.1	24.4 ± 0.4
828.3 ± 0.5	12.7	3.5	21.8 ± 0.2
853.2 ± 1.35	12.7	3.5	17.6 ± 0.5
	13.8	3.4	13.7 ± 0.4
	17.1	4.2	10.1 ± 0.2

6.7. Comparison of Results with Literature

Iso-octane has been studied previously in numerous RCMs, [1,28,62,64–66,69–72,74,75] and a selection of this data for stoichiometric mixtures of iso-octane and air at different pressures and levels of dilution is shown in Figure 6-12. In order to validate the results from the current study, the data obtained from the literature has been overlaid with data obtained from the current study. As seen in Figure 6-12, the NTC region appears around 700-850K for isooctane at 20 bar for air levels of dilution. This region is well captured by the current tests and a reasonable agreement is obtained over the temperature range. At 850K and 900K, the current data has slightly shorter ignition delay times, which is likely due to the fact that for these temperatures the wall temperatures used was higher, as seen in Table 6-2, in the 130-170°C range and most of the reported work shown in Figure 6-12 uses varying buffer gas composition in order to achieve higher

compressed gas temperature. This may have resulted in lower heat loses in the current RCM experiments and hence shortened the total delay time.

It should be noted that a relatively small scatter in the first-stage ignition delay data can be observed across facilities. This confirms the findings of the current study that the factors responsible for the discrepancy minimally affect the first-stage ignition delay time due to their smaller magnitude. However, the temperature and pressure rise due to the first-stage ignition is affected by these factors, which in turn leads to a bigger discrepancy in the second-stage ignition and eventually, the total ignition delay times.

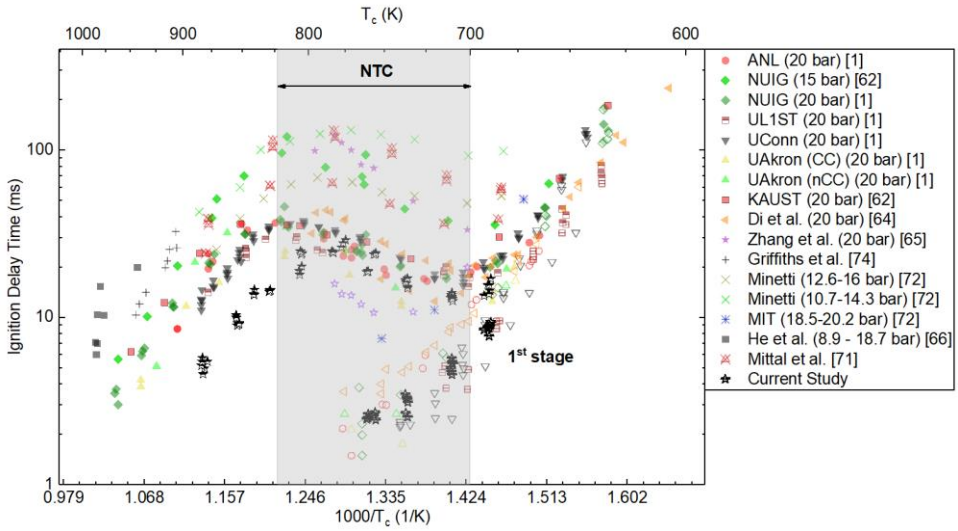

Figure 6-12: Results comparing several RCM ignition delay data for stoichiometric mixtures of iso-octane and air at different levels of dilution, as reported in [1,62,64–66,71,72,74].

6.8. Chapter Summary

This study provides experimental data to examine the effects of changing compression ratio on low to intermediate temperature ignition processes of a key reference fuel, iso-octane, using a rapid compression machine. The experimental results confirm that varying the compression ratio has a significant impact on ignition delay at conditions exhibiting single as well as two-stage ignition within and outside the NTC region, for temperatures greater than 710 K. The effect of

compression ratio on ignition delay is manifested due to the change in initial conditions, compression and t_{50} times and the SA/V ratio. However, the post-compression heat loss had minimal impact on the first-stage ignition at any of the compressed conditions studied. Differences in the surface area-to-volume ratio due to the changing compression ratio cause differences in the heat release and the pressure and temperature rise during the first-stage ignition, which affects the overall ignition delay. Furthermore, longer t_{50} times indicate that the mixture spends more time at elevated conditions and is more reactive by the end of compression, leading to shorter total ignition delay times. The experimental data indicates that the overall ignition delay can differ by up to 32% between compression ratios, with compression ratios having higher surface area-to-volume ratios and shorter t_{50} times resulting in longer overall ignition delay times. For the compression ratios employed and the temperature range of $850\ K \geq T_c \geq 800\ K$, it was observed that keeping the SA/V ratio constant and varying the compression ratio had a smaller effect on ignition delay times as compared to when the t_{50} times were kept constant and the compression ratio was varied. This implies that the post-compression heat losses (and hence the SA/V ratio) have a greater influence on ignition delay times as compared to the t_{50} times and the initial conditions. However, in the case of two-stage ignition delay, if the second stage ignition delay is short enough, the total ignition delay was found to be similar across both compression ratios. For temperatures greater than 780 K, single-stage ignition was observed, and it was seen that the difference in ignition delay across compression ratios decreased as T_c increased. This is because comparatively less time is allowed for the post-compression heat losses to affect the total ignition delay. The effects studied in this work would translate well to similarly reactive fuels since the ignition is found to be limited more by post-compression heat losses (thermal effect) as compared to the t_{50} times which affect the fuel reactivity. This study suggests that the RCM configuration, in terms of surface area-to- volume

ratio, t_{50} times, piston configuration, compression duration, diluent gas composition, compression ratio, etc., must be mentioned in detail and should be considered when assessing the fuel reactivity and reporting ignition delay data. Ideally, minimizing t_{50} times and post-compression heat losses are desirable in order to obtain and compare the auto-ignition delay measurements accurately. While trying to compare data across facilities, care should be taken to have similar t_{50} times and SA/V ratio. In this way, a much better comparison of experimental data can be achieved.

Chapter 7. NUMERICAL RESULTS – ISO-OCTANE

7.1. Introduction

In the iso-octane experiments, it was observed that changing the compression ratio did not have a large effect on the first-stage ignition delay (FSID) times, but it did affect the total ignition delay times considerably, at identical compressed conditions. However, experimental limitations made it infeasible to cover the entire temperature range using any of the compression ratios, which in turn did not provide enough data to study the effects of various facility-dependent factors on ignition comprehensively. Simulations, therefore, help to conduct an extensive study at conditions that are not experimentally feasible. Efforts were made to study the sensitivity of ignition delay to t_{50} and post-compression heat losses, in order to determine which parameter has a larger effect on the ignition delay and therefore, the strongest influence on data discrepancy. This study helps in determining the parameters that need to be specified when reporting ignition delay measurements to ensure accurate interpretation; and, at the same time, establish the factors that have minimal influence on the measurements.

7.2. Description of test cases

Simulations were conducted for iso-octane/oxygen/nitrogen mixtures with ϕ = 1.3 over a temperature range of 675 K–900 K and at a pressure of 20 bar. A constant diluent/oxygen ratio of 3.76 was maintained to simulate normal air. In order to study the effects of post-compression heat losses and initial conditions, a given compressed condition was achieved using five different compression ratios of 6.8, 9.6, 12.5, 12.7 and 17.1. This implies that five different volume profiles were developed from the corresponding experimental non-reactive pressure traces. The volumetric compression ratios used in the current study are identical to those used in the experimental study. Experimental results at different compression ratios were compared with simulations using various

mechanisms available in the literature. Two iso-octane mechanisms developed by Lawrence Livermore National Laboratory (LLNL), version 2 [60] and version 3 [155,156], were considered. Additionally, a recent iso-octane mechanism by Atef et al. [62], which is based on versions 2 and 3, was also used. The iso-octane version 2.0 mechanism by Curran et al. was developed based on the low- and high-temperature reaction pathways and rate rules proposed earlier for the LLNL n-heptane model [157]; however, some modifications were made to better predict experimental iso-octane reactivity. Mehl et al. [155,156] (version 3) further developed the low-temperature reaction mechanism for iso-octane oxidation of version 2.0 to better predict low-temperature heat release in HCCI engines. The mechanism by Curran et al. (version 2) and Mehl et al. (version 3) was further updated by Atef et al. to cover the low-intermediate temperature range of 600–800 K and lean conditions. All the three models were tested against data of ignition delay times, JSR oxidation speciation data, premixed laminar flame speeds, counterflow flame ignition data, and shock tube pyrolysis speciation data available in the literature.

The isooctane version 2.0 mechanism over-predicted the ignition delay times for temperatures between 675 K and 725 K, while it under-predicted at temperatures between 725 K and 825 K, which constitutes the NTC region. The mechanism by Atef et al. also under-predicted the ignition delay times in the NTC region of 725 K to 825 K. Both version 2 and the mechanism by Atef et al. had a reasonable agreement with experiments for temperatures of 850 K and 875 K. Due to the range of compression ratios used, which resulted in varying post-compression heat losses and compression times, no single mechanism reasonably predicted ignition delay times for all the compression ratios and at all test conditions. However, it was observed that the iso-octane version 3 mechanism (874 species and 3796 reactions) gave predictions that were in reasonable agreement

with the experimental results at most conditions, as can be seen in Figure 7-1. Based on this result, this mechanism was used for further investigations in this study.

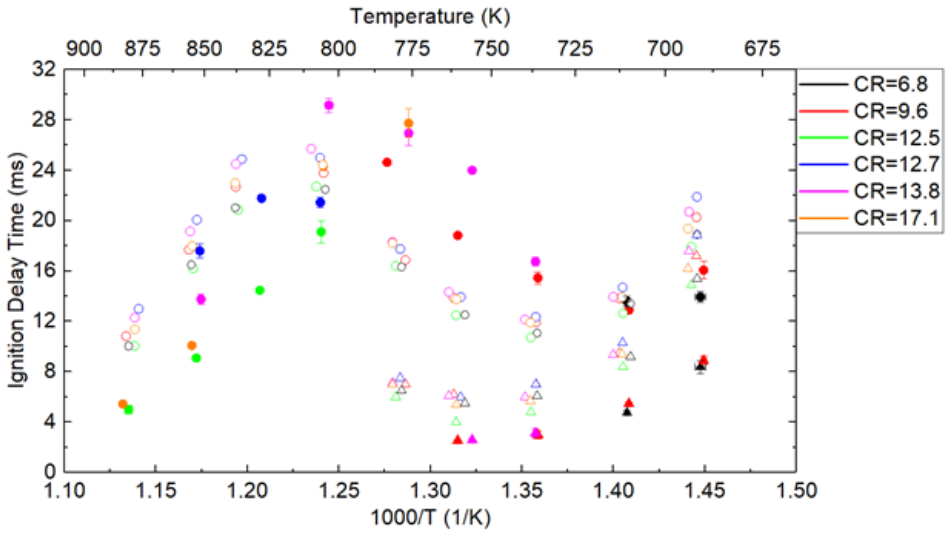

Figure 7-1: Comparison of model predicted ignition delay times using the isooctane mechanism version 3 with experimental data, for various compression ratios. Filled markers are experimental data, and outline markers are simulation data. Circles are total ignition delay time, and triangles are first-stage ignition delay time.

7.3. Effect of initial conditions and compression time

Table 7-1 summarizes the initial conditions and RCM configuration of different compression ratios that were used for the simulations. The values of initial conditions, t_{50} and compression times are in good agreement with those determined from the experiments. The trend of increasing pressure drop rates post-compression for compression ratios with a greater surface area-to-volume ratio is also observed here, even though a linear volume expansion profile was fit. For compression ratios with similar surface-area-to-volume ratio (see Table 6-2, CR = 9.6 and 12.5, and CR = 13.8 and 17.1), the pressure drop rate was also similar.

Table 7-1: RCM configuration and initial conditions needed to achieve the desired compressed conditions (T_c = 675 K – 900 K, P_c = ~20 bar), using different compression ratios.

CR	**T_i (deg. C)**	**P_i (bar)**	**AVERAGE t_{50} (± 0.04 ms)**	**Rate of pressure drop, post-compression (bar/ms)**	**Compression Time (ms)**
6.80	127 to 257	1.895 to 1.935	5.28	0.0376	30
9.60	91 to 213	1.29 to 1.33	3.97	0.0433	30
12.50	73 to 187	1.04 to 1.08	5.68	0.0448	32
12.70	72 to 186	1.04 to 1.08	3.49	0.0492	30
17.10	47 to 154	0.75 to 0.79	4.41	0.0521	32

In order to simplify the quantification of the effect of post-compression heat loss on the ignition delay times, a linear, instead of a polynomial, curve fitting was done to the volume expansion profile derived from the experimental non-reactive pressure curve. Starting from the end of compression and ending at 100 ms, the pressure drop rate for a simulated non-reactive case was kept identical to that of the corresponding experimental non-reactive pressure curve. The volume profiles with linear expansion profiles will be referred to as the original volume profiles when comparing the ignition delay results obtained from different adjusted volume profiles. From Table 7-1, it can be observed that the compression times for the compression ratios considered for this study are either 30 or 32 ms. Although a difference of 2 ms in compression time might not be enough to cause a discrepancy in ignition delay times at a given condition, compression duration can have a considerable effect on ignition delay time measurements due to preignition reactions in the later phases of compression. This is especially problematic for highly reactive fuels or test

conditions. In an effort to study the effect of compression time, three new volume profiles were created for CR = 12.7 since it had the lowest t_{50}. The volume profiles were created such that the compression times were 20 ms with identical t_{50} (~3.5 ms), 40 ms with identical t_{50} and 40 ms with t_{50} = 6.9 ms, as shown in Table 7-2. The compression times and t_{50} were selected such that they were in the typical operating range of conventional RCMs. The volume expansion profile remained unaltered, implying that the post-compression heat loss remained identical across the cases.

Table 7-2: Summary of the compression times and t_{50} for the simulated models at CR=12.7.

Compression time (ms)	t_{50} **(ms)**	**Post-compression pressure drop rate (bar/ms)**
20	3.5	0.0492
30	3.5	
40	3.5	
40	6.9	

Looking at the results in Figure 7-2 and Table 7-3, it can be seen that as long as the post-compression heat losses and t_{50} remain the same, the reduction or extension of compression time by 10 ms has a negligible effect on the first-stage as well as the total ignition delay times. The total and first-stage ignition delay times for compression times of 20 ms, 30 ms and 40 ms exactly overlap. However, in the case of 40 ms compression time with extended t_{50} (= 6.9 ms), the first-stage ignition delay times were shortened by as much as 26% and the total ignition delay times were shortened by as much as 12%, especially at conditions for which the ignition delay time was short. This discrepancy exists because the longer t_{50} of 6.9 ms allows the fuel-air mixture to spend more time at elevated temperatures and pressures, leading to reaction initiation during the compression stroke. The effect of t_{50} will be discussed in more detail in the following sub-sections.

As can be observed from Table 7-1, lower compression ratios require higher initial temperature and pressure to be maintained in order to achieve a given set of compressed conditions. The higher initial temperature and pressure may affect the chemical heat release during compression, which in turn may affect the ignition delay times. To study the effect of initial conditions on the ignition delay times, the volume profiles of all the compression ratios were adjusted so as to maintain the same value of t_{50} (~3.5 ms) and post-compression pressure drop (~0.0376 bar/ms), while maintaining compression times identical to the corresponding original volume profiles. In doing so, the ignition delay times can be compared across the six compression ratios as they would differ only in terms of initial conditions. In the case of originally predicted total ignition delay times, the percentage deviation from the mean across the six compression ratios was in the range of 3.2% to 6.6% and the percentage variation from the mean in first-stage ignition delay ranged between 4.6% and 8.7%. When the adjusted volume profiles were used to predict the ignition delay times, the percentage deviation from the mean for the total ignition delay times was brought down to between 1.1% and 3.5%. Also, the percentage deviation from the mean for the first-stage ignition delay times was reduced to between 3.7% and 5.4%. A summary of the results comparing the first-stage and total ignition delay times for different compression times and initial conditions is tabulated in the supplemental material. The main observations from these results are as follows:

- Compression time has a negligible effect on the first-stage and the total ignition delay times, as long as the post-compression heat loss and t_{50} are identical.
- After maintaining similar t_{50} and post-compression heat loss across the six compression ratios, the percentage deviation in the total and first-stage ignition delay times was reduced from about 9% to less than 5%. This reduction implies that initial conditions play a minimal role in affecting the first-stage and also the total ignition delay times.

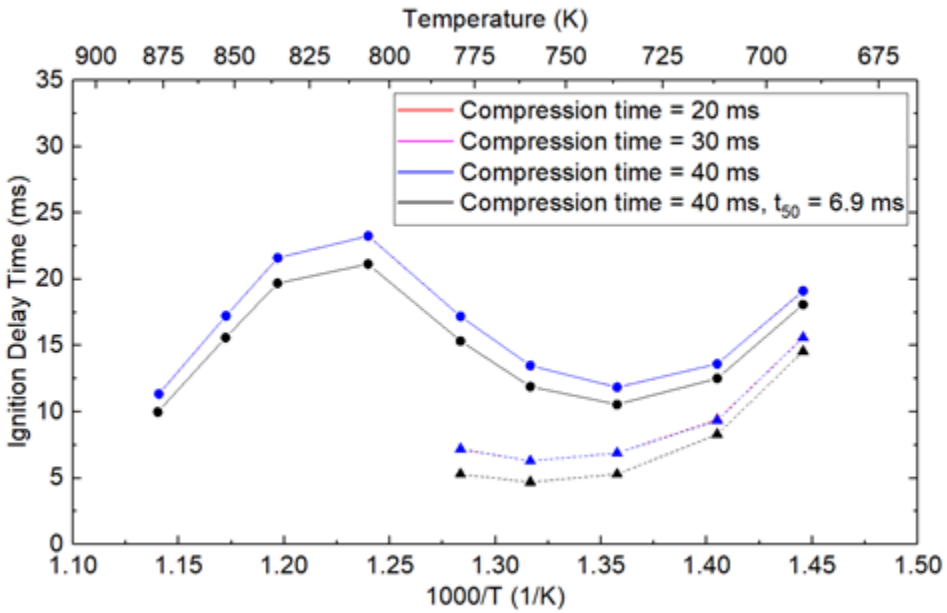

Figure 7-2: Comparison of ignition delay times obtained from volume profiles with various compression times at CR = 12.7. Circles are total ignition delay times and triangles are first-stage ignition delay times.

Table 7-3: Ignition delay times obtained from volume profiles with various compression times at CR = 12.7.

	Compression time = 20, 30 and 40 ms, t_{50} = ~3.5 ms		**Compression time = 40 ms, t_{50} = ~6.9 ms**	
T_c (±0.2 K)	**FSID (ms)**	**Total IDT (ms)**	**FSID (ms)**	**Total IDT (ms)**
691.7	15.6	19.1	14.6	18.1
711.7	9.4	13.6	8.3	12.5
736.6	6.9	11.9	5.3	10.6
759.6	6.3	13.5	4.7	11.9
779.1	7.2	17.2	5.3	15.3
806.6		23.3		21.1
835.5		21.6		19.7
853.0		17.2		15.6
876.8		11.3		10.0

Based on the analysis of the experimental results, it was observed that the effect of compression ratio on the ignition delay times is manifested due to the change in initial conditions, compression and t_{50} times, and the surface area-to-volume ratio. Looking at the results summarized earlier, the compression time and initial conditions play a minimal role in affecting the first-stage as well as the total ignition delay times. The surface-area-to-volume ratio, in turn, governs the post-compression heat losses, in addition to the insulation around the RCM. It was also observed in the experiments that despite the similar post-compression heat losses across two compression ratios, there was still a discrepancy in measured ignition delay data. This implies that an additional factor plays a role in influencing the ignition delay times, which was later found out to be the t_{50}. Therefore, it can be concluded that, at identical compressed conditions for different configurations of the RCM, t_{50} and post-compression heat loss are the factors that most significantly influence the ignition delay times. Results supporting this are discussed in detail, with supporting figures, in the following subsections.

In order to isolate the effects of post-compression heat loss and t_{50} times and to quantitatively demonstrate the contributions of each of these parameters in influencing the ignition delay times, two sets of volume profiles were created for each compression ratio. For the first set of volume profiles, the post-compression volume profile for each compression ratio was adjusted to match the pressure drop in the case of CR = 6.8 (0.0376 bar/ms) since it had the lowest rate of pressure drop. This enabled comparing the originally predicted ignition delay times to the ignition delay times obtained using the reduced post-compression heat loss profile while keeping the t_{50} identical for each compression ratio. For the second set of volume profiles, the volume profiles during the compression stroke were adjusted to achieve a minimum t_{50} of about 3.5 ms. This allowed for the comparison of the originally predicted ignition delay times with the ignition delay

times obtained using the reduced t_{50} while maintaining the same original post-compression heat loss.

7.4. Effect on first-stage ignition

7.4.1. Effect of t_{50}

In order to study the sensitivity of ignition delay times on t_{50} times, the volume profiles during the compression stroke were adjusted to achieve a t_{50} of about 3.5 ms. However, the compression time was kept the same as the original for each compression ratio. Doing this for each compression ratio enabled the effect of t_{50} on ignition delay times to be studied over a wide range of t_{50} values. The reduction in t_{50} varied from 13% in the case of CR = 9.6 to 43% in the case of CR = 12.5. By keeping the post-compression volume profile unaltered, the effect of t_{50} on the ignition delay times could be isolated.

Figure 7-3 shows the effect of t_{50} on the first-stage ignition delay. As can be seen in Figure 7-3 (a), reduction in t_{50} results in longer first-stage ignition delay times. This trend can be observed for all the compression ratios and at all the compressed conditions for which the first-stage ignition delay can be measured. In an effort to quantify the effects of t_{50} and post-compression heat loss, for each compression ratio, changes in first-stage and total ignition delay times due to change in t_{50} and post-compression heat loss with respect to the originally predicted first-stage and total ignition delay times were calculated. The effect of t_{50} on the first-stage ignition, $\eta t_{50,\text{first-stage}}$, is then calculated by normalizing the difference in the first-stage ignition delay due to the change in t_{50} with respect to the originally predicted FSID. While the effect of post-compression heat loss on first-stage ignition delay, $\eta_{\text{post-compression heat loss,first-stage,}}$ is calculated by normalizing the difference in FSID due to the change in post-compression pressure drop with respect to the originally predicted FSID.

$$\eta_{t50} = \frac{\tau_{reduced\ t50} - \tau_{original}}{\tau_{original}} \tag{7-1}$$

$$\eta_{post-compression\ heat\ loss} = \frac{\tau_{reduced\ heat\ loss} - \tau_{original}}{\tau_{original}} \tag{7-2}$$

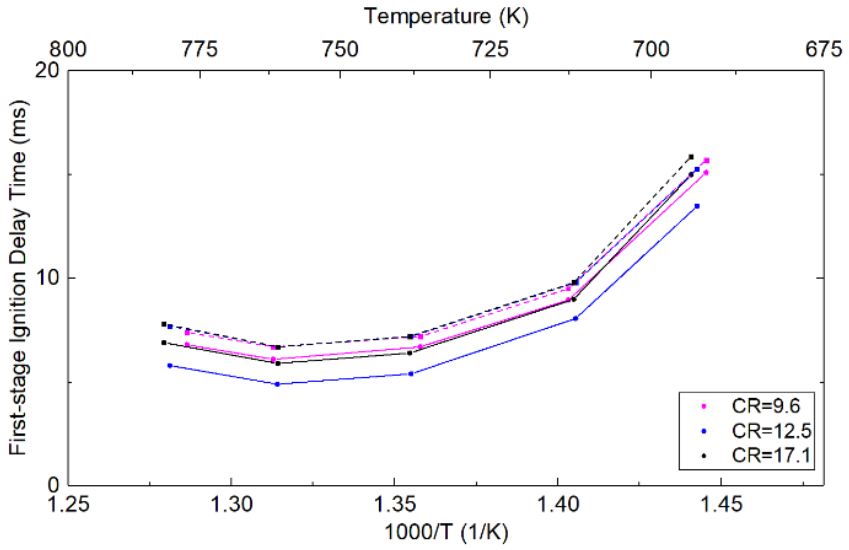

(a)

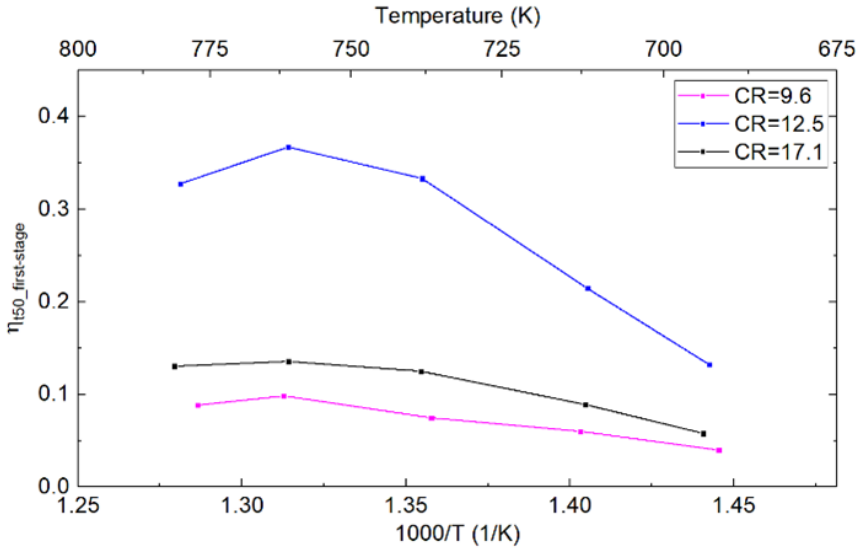

(b)

Figure 7-3: (a) Comparison of first-stage ignition delay time obtained from the altered t_{50} volume profiles (dashed) with those obtained from the original volume profile (solid). (b) Effect of t_{50} on the first-stage ignition delay time.

It can be observed from Figure 7-3 (b) that the t_{50} effect (solid lines) remains negative across the whole temperature range and for all the compression ratios, implying that a reduction in t_{50} leads to longer first-stage ignition delay times. CR = 12.5 has the highest magnitude of t_{50} effect at all temperatures due to a bigger reduction in t_{50} (43%), while CR = 9.6 has the smallest magnitude of t_{50} effect due to the lowest reduction in t_{50} (13%). It can also be observed that as the first-stage ignition delay decreases with increasing temperature, the effect of t_{50} increases for all compression ratios. This implies that shorter first-stage ignition delays are influenced more by changes in the t_{50}. In other words, conditions at which the fuel is more reactive will be influenced more by changes in the t_{50}. This discrepancy exists because a longer t_{50} results in increased reaction initiation during the compression stroke. Longer t_{50} indicates that the mixture spends more time at elevated conditions enabling more reactivity by the end of compression, leading to shorter total ignition delay times. However, the chemical heat release during the t_{50} is not substantial enough to render time zero at the top dead center to be a poor choice, as can be seen in Figure 7-4 (a). For brevity, only heat release data for CR = 17.1 and at T_c = 780 K is shown in Figure 7-4. However, the observations stated are applicable to all of the compression ratios and compressed conditions studied. Figure 7-4 (a) also shows that, although minimal, the heat release starts about 1 ms earlier in the case of longer t_{50} (solid lines) as compared to the reduced t_{50} model predictions. As a result, by the end of compression, the heat release rate and accumulated heat release for the case with longer t_{50} is about five times that of the case with reduced t_{50}. This, in turn, leads to earlier initiation of the reactions resulting in the first-stage ignition, as is represented by the heat release rate and accumulated heat release plot in Figure 7-4 (b).

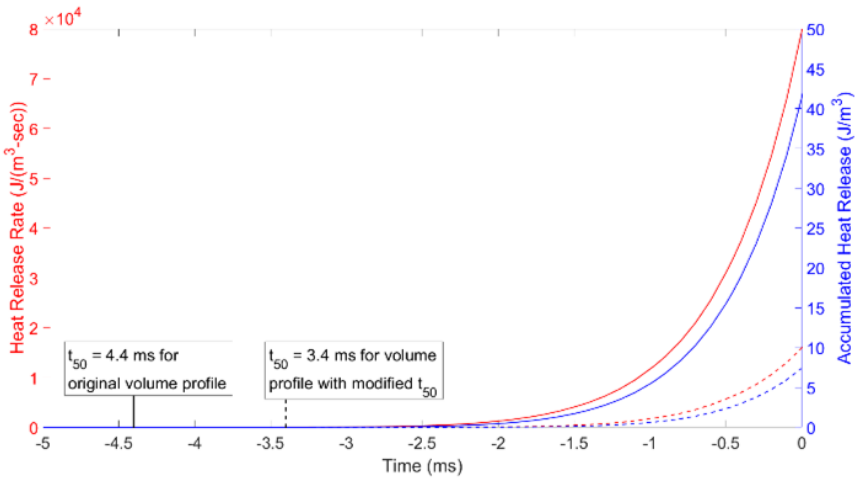

(a)

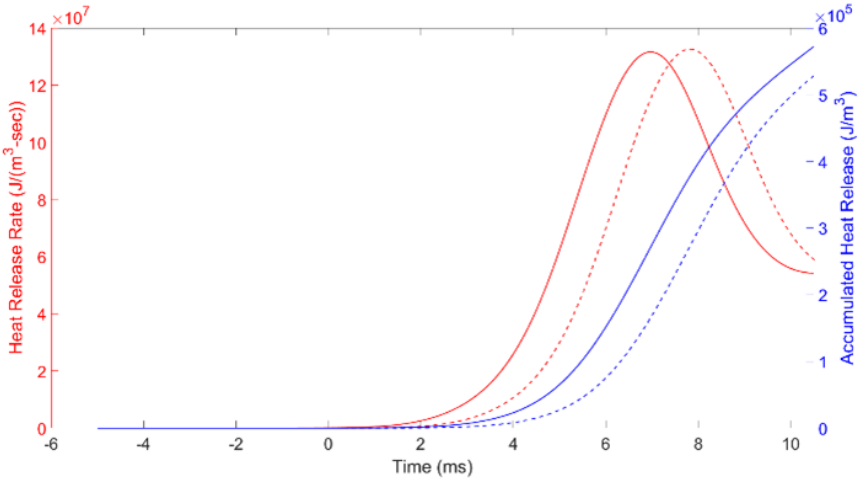

(b)

Figure 7-4: (a) Heat release rate and accumulated heat release from t_{50} until EOC (t= 0) (b) Heat release rate and accumulated heat release during the first-stage ignition. CR = 17.1, T_c = 780 K. Solid lines are predictions from the original volume profile and dashed lines are for the altered t_{50} volume profile.

However, both cases exhibit similar first-stage heat release duration. Consequently, the overall accumulated heat release during the first-stage ignition is also similar. As a result, the pressure and temperature rise due to the first-stage ignition is almost identical (<8% difference),

which in turn leads to similar second stage ignition delay times, the results of which are shown in Figure 7-5 for CR = 17.1.

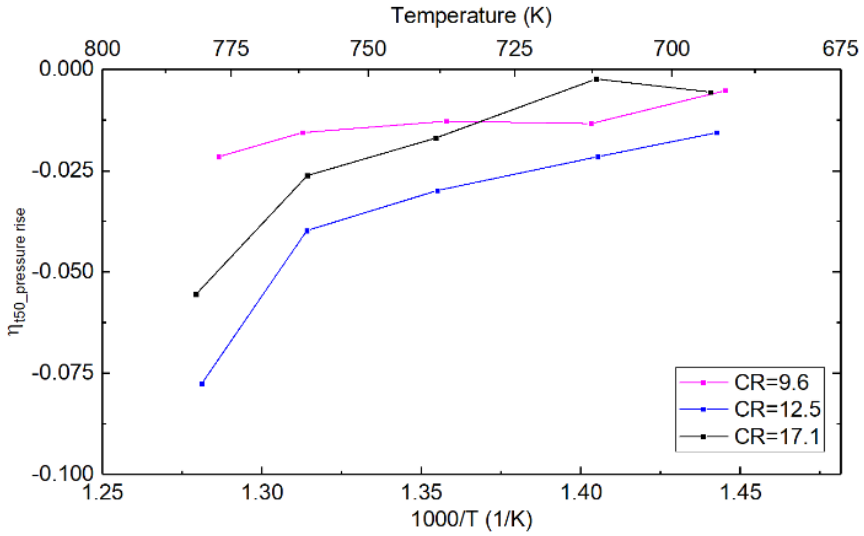

(a)

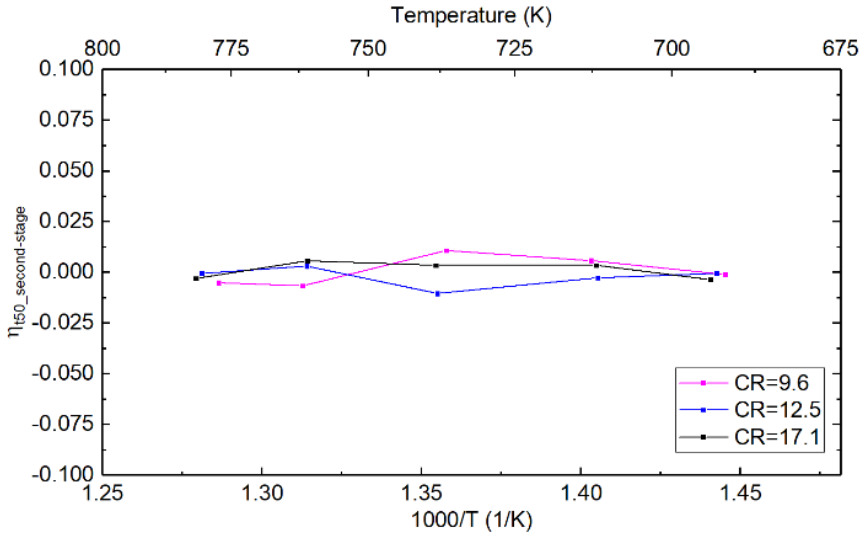

(b)

Figure 7-5: (a) Effect of t_{50} on pressure rise due to the first-stage ignition. (b) Effect of t_{50} on second stage ignition delay.

7.4.2. Effect of post-compression heat loss

The post-compression volume profiles were altered for each compression ratio to match the pressure drop rate for the CR = 6.8 case since it had the lowest pressure drop rate, and therefore the lowest heat loss, which is desirable when reporting ignition delay times. Comparing the model predictions from altered post-compression volume profiles with those obtained from the original volume profiles isolates the effect of post-compression heat loss on ignition delay since the t_{50} remains identical. The reduction in post-compression heat loss varied from 14% in the case of CR = 9.6 to 29% for the case of CR = 17.1.

Post-compression heat loss has a minimal effect on first-stage ignition delay time, especially at temperatures for which the delay time is short. Referring to Figure 7-6 (b), only for CR = 17.1, a considerable effect of post-compression heat loss on first-stage ignition delay is observed, with the highest effect observable at T_c = 690 K. This is because CR = 17.1 has the largest reduction in post-compression pressure drop rate (29%) and the first-stage ignition delay time is the longest at T_c = 690 K. The effect remains more or less constant in the range of 760 K ≥ T_c ≥ 710 K for CR = 17.1. However, as T_c increases further, the first-stage ignition delay time collapses around the same value. As can be observed from Figure 7-6 (a), the first-stage ignition delay time reduces as T_c increases. Therefore, shorter first-stage ignition delay times allow less time for the post-compression heat losses to have an effect. The dashed lines in Figure 7-3 (a) represent the model predictions for reduced t_{50} volume profiles. Since the t_{50} was identical and only the post-compression heat loss varied across the compression ratios, the first-stage ignition delay times converge with an increase in temperature.

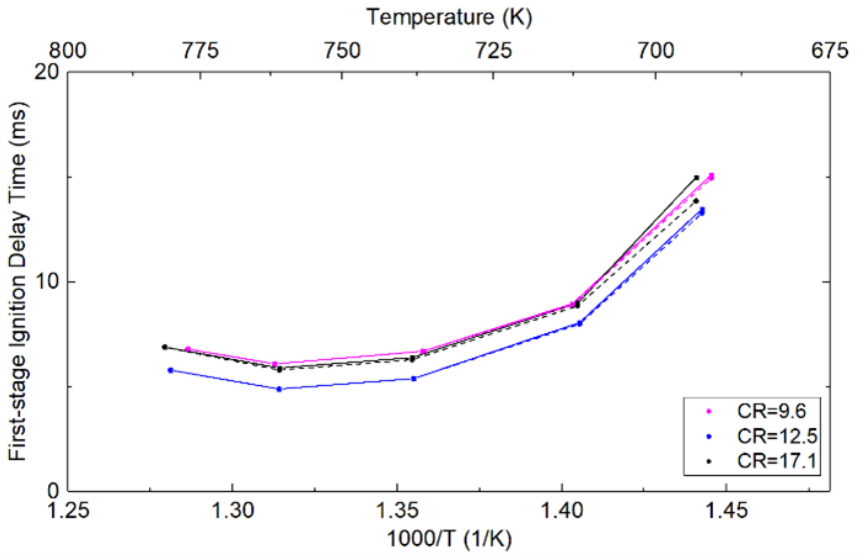

(a)

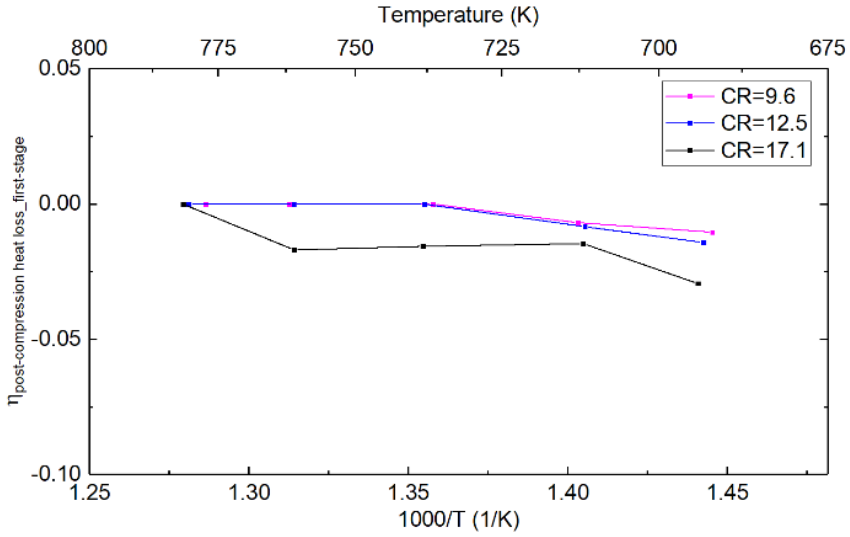

(b)

Figure 7-6: (a) Comparison of first-stage ignition delay time obtained from altered post-compression volume profiles (dashed) with those obtained from the original volume profile (solid). (b) Effect of post-compression heat loss on the first-stage ignition delay time.

Although the effect of post-compression heat loss on the first-stage ignition delay is minimal, considerable differences in the pressure and temperature rise rates are observed as a result of the first-stage ignition heat release, as shown in Figure 7-7 and Figure 7-8. The heat release rate

and accumulated heat release as a function of time are shown in Figure 7-7. For brevity, heat release data for only CR = 17.1 and at T_c = 780 K is shown in Figure 7-7. However, the observations stated are applicable to all the tested compression ratios and compressed conditions. The start and duration of heat release for both the original and altered volume profiles are identical. The pressure and temperature subsequent to the first-stage ignition are controlled by the accumulated heat release, mixture heat capacity and the post-compression heat losses, with the post-compression heat losses being the dominant factor provided that the mixture heat capacity remains the same.

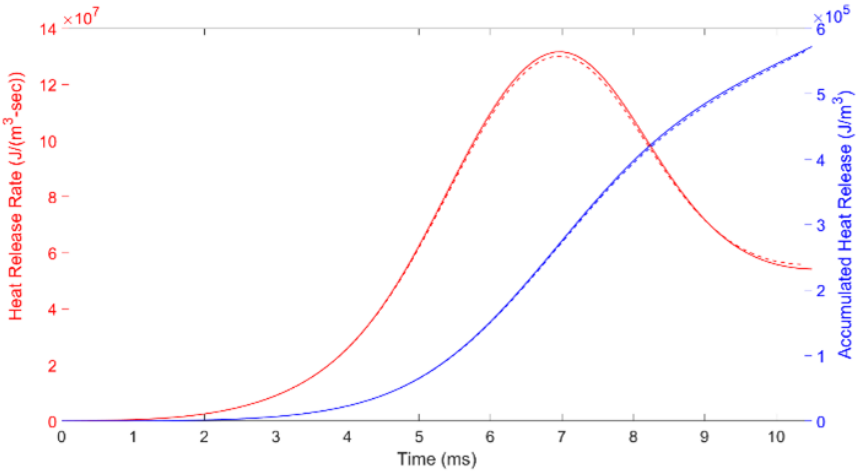

Figure 7-7: Heat release rate and accumulated heat release during the first-stage of ignition. CR = 17.1, T_c = 780 K. Solid lines are predictions from the original volume profile and dashed lines are for the altered post-compression pressure drop rate volume profile.

Therefore, although the accumulated heat release is similar in both cases since the pressure drop rate in the original volume profile is greater, a lower rise in pressure and temperature is observed after the first-stage of ignition. The larger surface-area-to-volume ratio due to the compression ratio contributed to greater post-compression heat losses. The higher post-compression heat losses lead to a smaller pressure and temperature rise due to the first-stage of ignition, which in turn leads to a less reactive species pool. The lower reactivity also extends the second stage of ignition delay. Figure 7-8 (a) depicts that with an increase in temperature, the effect

of post-compression heat loss on the first-stage of ignition pressure rise also increases; with an increase in pressure of as much as 22% for CR = 17.1 at T_c = 780 K when the rate of pressure drop post-compression is reduced by 29%. As a result, the second-stage ignition delay is shorter, as can be seen in Figure 7-8 (b). To summarize the effect of t_{50} and post-compression heat loss on the first-stage ignition:

- Reduction in t_{50} causes longer first-stage ignition delay times but has a minimal effect on the pressure and temperature rise due to the first-stage ignition. Consequently, the second stage ignition delay time is minimally affected as well.
- Reduction in post-compression heat loss causes an increase in pressure and temperature rise due to the first-stage ignition, which results in shorter second-stage ignition delay times. However, the first-stage ignition delay time is minimally impacted by post-compression heat loss.

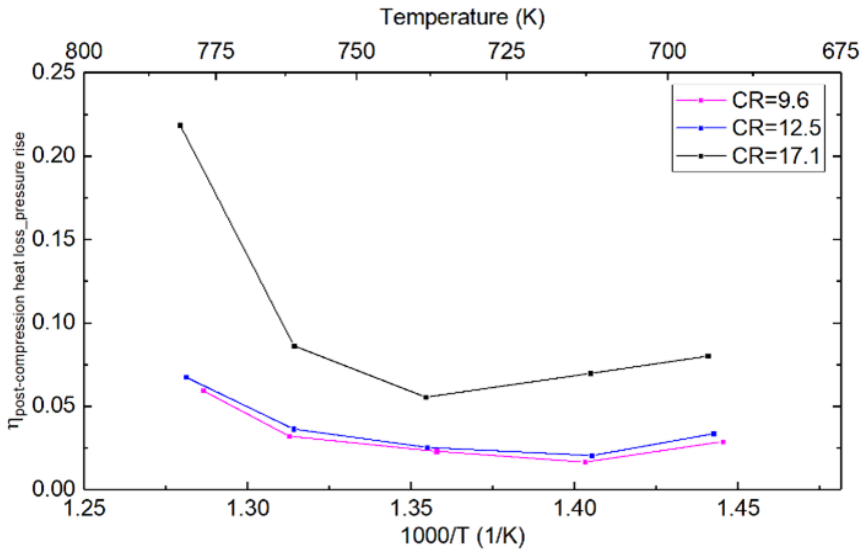

(a)

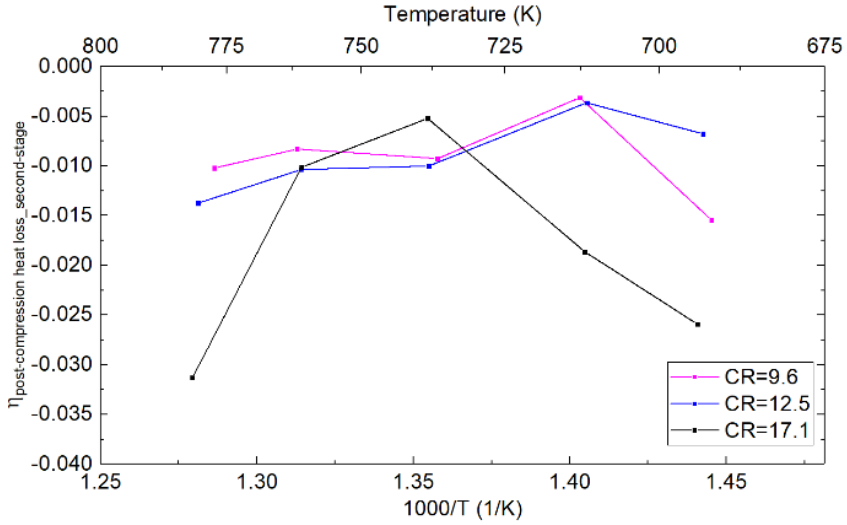

(b)

Figure 7-8: (a) Effect of post-compression heat loss on pressure rise due to the first-stage ignition. (b) Effect of post-compression heat loss on the second stage ignition delay.

7.5. Effect on total ignition delay times

7.5.1. Effect of t_{50}

The results show that the second stage ignition is mainly coupled to the first-stage ignition via the heat release from the first-stage. Figure 7-9 (a) compares the simulation results of the total

ignition delays obtained from the original volume profile with the reduced t_{50} model predictions and Figure 7-9 (b) quantifies the effect of t_{50} on total ignition delay times. It can be seen that the simulation data indicate NTC behavior over the temperature range studied. Generally, as was mentioned earlier, a reduction in t_{50} leads to an increase in the first-stage ignition delay. However, due to similar heat release during the first-stage ignition, the second-stage ignition delay is minimally affected as the rise in pressure and temperature during the first-stage ignition is similar. Consequently, the total ignition delay time for the reduced t_{50} cases is also longer for all compression ratios and compressed conditions, as can be observed in Figure 7-9 (a). It can also be observed from Figure 7-9 (b) that as the magnitude of the total ignition delay time reduces (736 K $\geq T_c \geq$ 690 K and 880 K $\geq T_c \geq$804 K), the effect of t_{50} increases. On the other hand, in the NTC region (804 K $\geq T_c \geq$736 K), where the ignition delay time increases with temperature, the effect of t_{50} reduces. This implies that even for the conditions at which two-stage ignition is not observed (880 K $\geq T_c \geq$804 K), longer t_{50} indicates that the mixture spends more time at elevated conditions causing earlier initiation of radical species production which results in shorter total ignition delay times. CR = 12.5 again has the highest magnitude of t_{50} effect at all temperatures due to a greater reduction in t_{50} (43%), while CR = 9.6 has the least magnitude of t_{50} effect due to the least reduction in t_{50} (13%). However, for all the compression ratios, the effect of t_{50} is the highest at conditions where the total ignition delay time is the shortest. To summarize, shorter ignition delay times, or in other words, conditions at which the fuel is highly reactive, are influenced more by changes in the t_{50}.

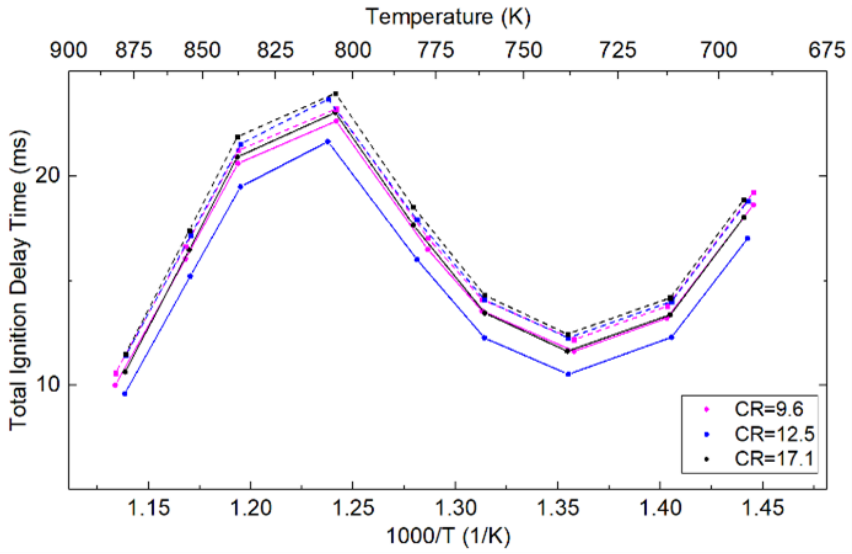

(a)

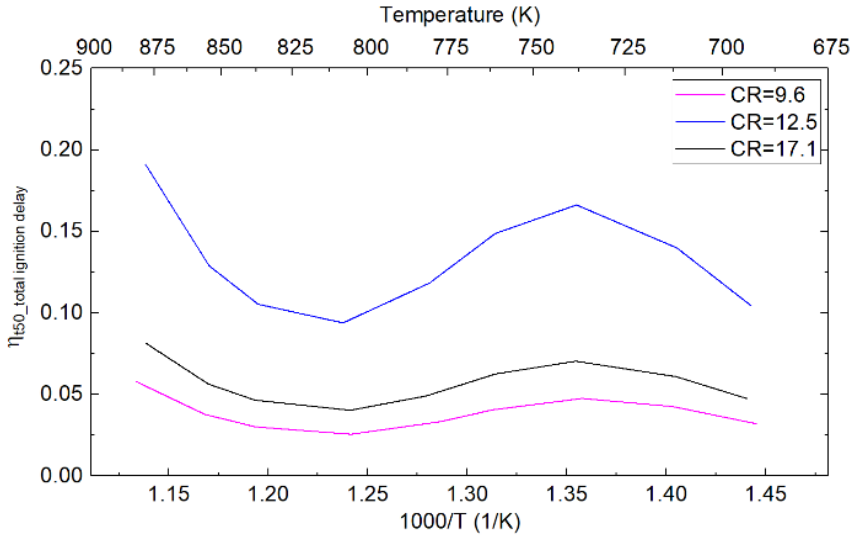

(b)

Figure 7-9: (a) Comparison of total ignition delay time obtained from the altered t_{50} volume profiles (dashed) with those obtained from the original volume profile (solid). (b) Effect of t_{50} on the total ignition delay time.

7.5.2. Effect of post-compression heat loss

Figure 7-10 (a) compares the simulation results for the total ignition delay times obtained from the original volume profile with those from the reduced post-compression pressure drop rate

of iso-octane. Figure 7-10 (b) quantifies the effect of post-compression heat loss on total ignition delay times. It can be seen that the simulation data indicate NTC behavior over the temperature range studied. As was already mentioned in Section 7.4.2, reduction in post-compression heat loss leads to an increase in the pressure and temperature rise during the first-stage of ignition. Consequently, the second-stage ignition delay is shortened and hence the total ignition delay time is also reduced, as can be observed in Figure 7-10 (a). It can also be observed from Figure 7-10 (b) that as the magnitude of the total ignition delay time reduces (736 K $\geq T_c \geq$ 690 K and 880 K $\geq T_c \geq$ 804 K), the effect of post-compression heat loss also reduces. On the other hand, in the NTC region (804 K $\geq T_c \geq$ 736 K), where the ignition delay time increases with temperature, the effect of post-compression heat loss increases. This implies that even for the conditions where two-stage ignition is not observed (880 K $\geq T_c \geq$ 804 K), longer ignition delay times will be more affected by post-compression heat losses. CR = 17.1 has the highest magnitude of post-compression heat loss effect at all temperatures due to a greater reduction in pressure drop rate post-compression (29%), while CR = 9.6 has the least magnitude of post-compression heat loss effect due to the least reduction in pressure drop rate (14%).

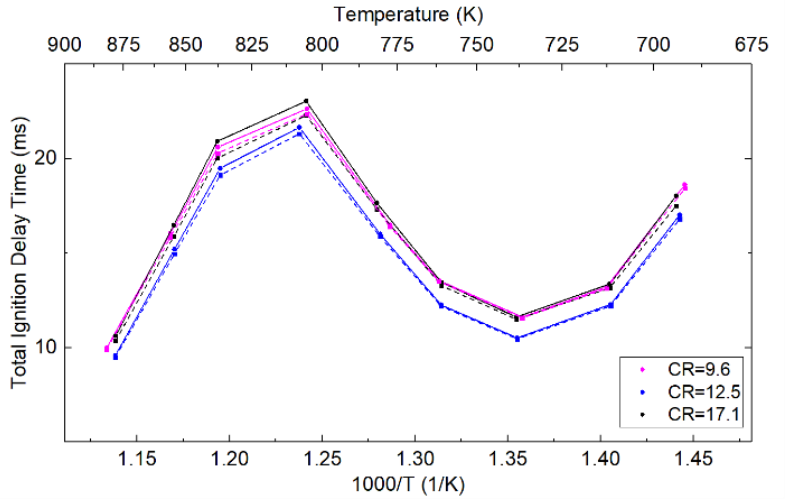

(a)

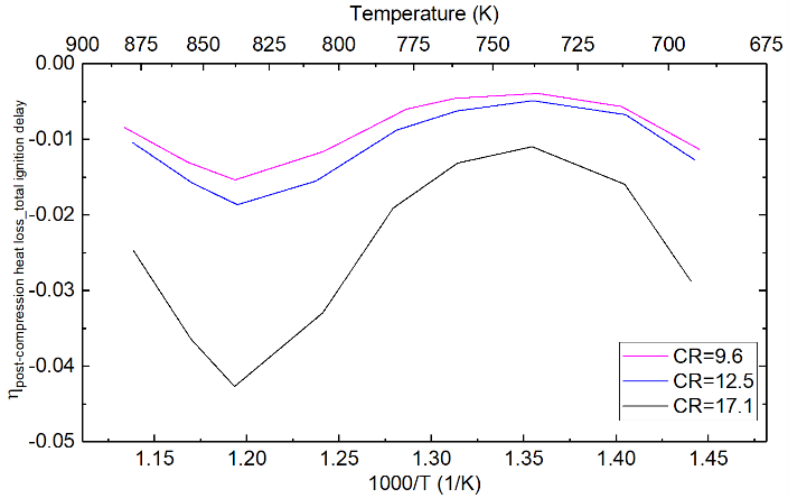

(b)

Figure 7-10: (a) Comparison of total ignition delay time obtained from the altered post-compression volume profiles (dashed) with those obtained from the original volume profile (solid). (b) Effect of post-compression heat loss on the total ignition delay time.

However, for all the compression ratios, the effect of post-compression heat loss is the highest at conditions where the total ignition delay time is the longest (T_c = 837 K). Shorter total ignition delay times allow less time for the post-compression heat losses to affect the ignition process. This reasoning is also applicable to the first-stage ignition delay time being minimally

affected by the heat losses; since both the first-stage ignition delay from 690 K-750 K and the total ignition delay from 850 K-900 K have similar magnitudes (~< 15 ms). The magnitude of the effect of post-compression heat losses on total ignition delay times is less compared to that of the effect of t_{50}, implying that total ignition delay times are more sensitive to changes in the t_{50}.

7.6. Sensitivity to equivalence ratio

Simulations were run using the same volume profiles generated earlier for equivalence ratios of 0.7 and 1.0, in addition to 1.3. The reduction in t_{50} and post-compression pressure drop rate for each equivalence ratio was kept identical. The effect of equivalence ratio on the first-stage and total ignition delay using the original volume profiles of CR = 12.5 is shown in Figure 7-11 (a) and (b) respectively. For the conditions investigated, as the equivalence ratio increases, the first-stage and total ignition delay times get shorter. The observed equivalence ratio effect is consistent with other studies on hydrocarbons [69,158–160]. The increase in reactivity with increasing equivalence ratio is because the N_2/O_2 ratio is kept constant and the fuel concentration is varied. Mixtures, in which the equivalence ratio is varied by changing the N_2/O_2 ratio and keeping the fuel concentration constant would observe an opposite trend where lean mixtures would become more reactive. In such a case, the increased reactivity is a result of the increase in oxygen levels leading to lower dilution levels [161].

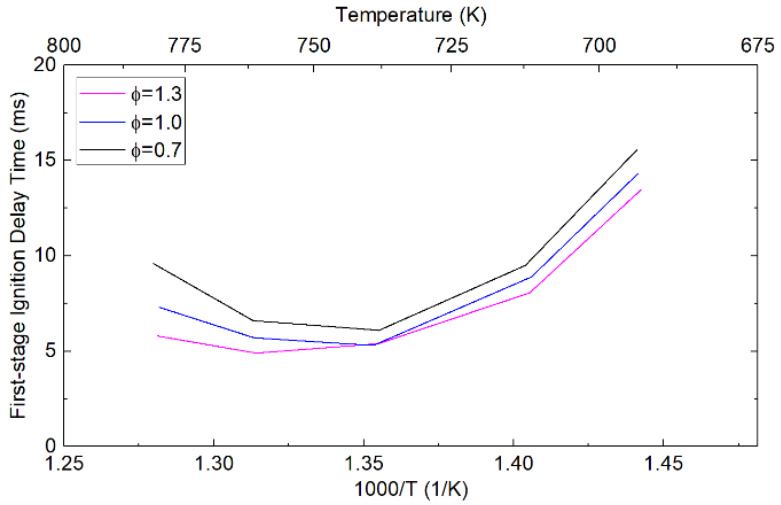

(a)

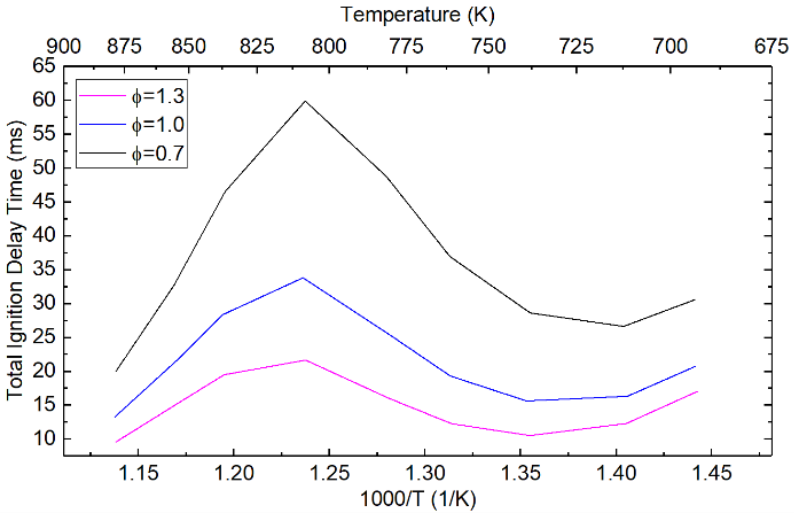

(b)

Figure 7-11: (a) First-stage ignition delay times for CR = 12.5 at different equivalence ratios with the original volume profiles. (b) Total ignition delay times for CR = 12.5 at different equivalence ratios with the original volume profiles. (c) Effect of t_{50} (solid lines) and post-compression heat losses (dashed lines) on first-stage ignition delay. (d) Effect of t_{50} (solid lines) and post-compression heat losses (dashed lines) on total ignition delay.

Figure 7-11 (cont'd)

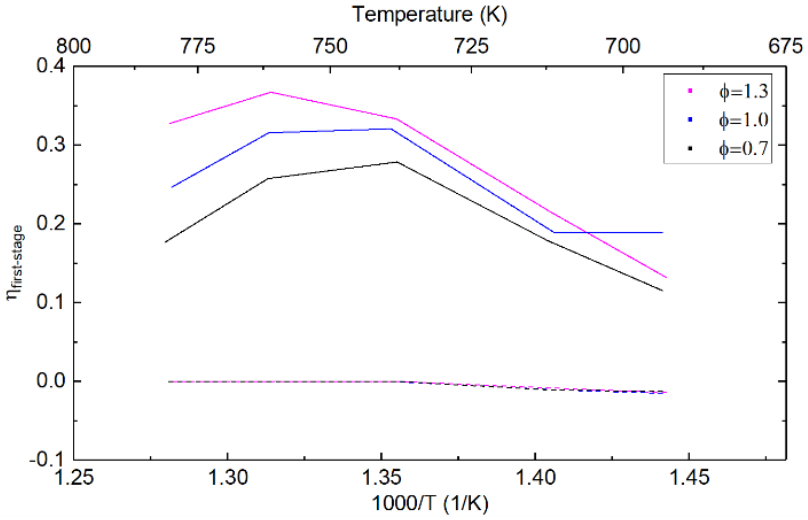

(c)

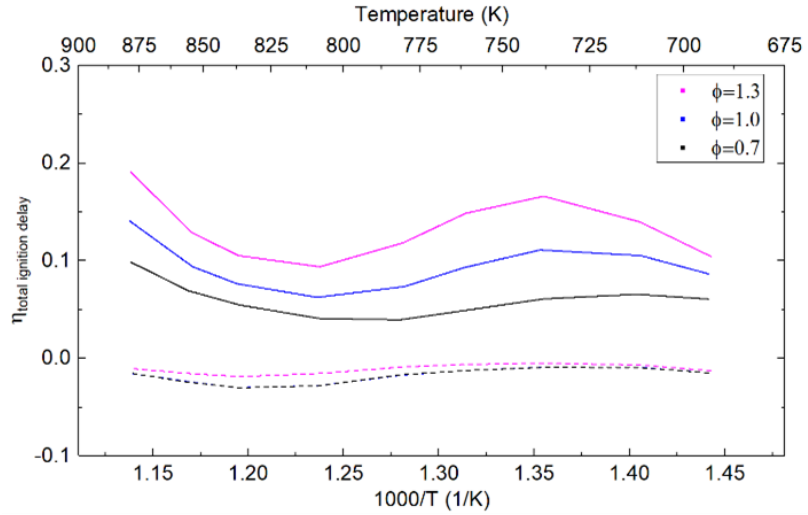

(d)

Figure 7-11 (c) and (d) quantify the effect of t_{50} and post-compression heat loss, which was also studied for the different equivalence ratios. Since ϕ=1.3 is the most reactive and has the shortest first-stage and total ignition delay times, it is impacted the most by t_{50} and the least by post-compression heat losses; followed by ϕ=1.0 and 0.7. The first-stage ignition delay is again minimally impacted by post-compression heat losses because of the short duration, which allows less time for the post-compression heat loss to influence the ignition process. Since ϕ=0.7 has the

longest total ignition delay times, a greater effect of post-compression heat loss is seen. However, overall, the effect of t_{50} has greater importance than that of post-compression heat loss for all of the equivalence ratios tested.

7.7. Sensitivity to diluent gases

Simulations were also completed with identical volume profiles to those described previously but with the nitrogen (N_2) replaced by argon (Ar) in one case and by carbon dioxide (CO_2) in the second. The reduction in the t_{50}, post-compression pressure drop rate and diluent/O_2 ratio for each diluent gas mixture was kept identical.

The effect of using various diluent gases on the first-stage and total ignition delay times using the original volume profiles of CR = 9.6 is shown in Figure 7-12 (a) and (b) respectively. Overall, the results show that the diluent gases have little impact on the first-stage ignition delay time. However, differences in the heat capacity of the diluent gas cause a difference in the first-stage heat release, and the subsequent pressure and temperature rise during the first-stage ignition, which significantly affected the overall ignition delay. Since CO_2 has the highest heat capacity, the mixture undergoes the least rise in pressure and temperature during the first-stage ignition and hence, longer total ignition delay times are observed. The opposite was observed for Ar. For temperatures greater than 800 K, the difference in total ignition delay times reduces. The observed effect of diluent gases is consistent with other published hydrocarbon data [64,65,68].

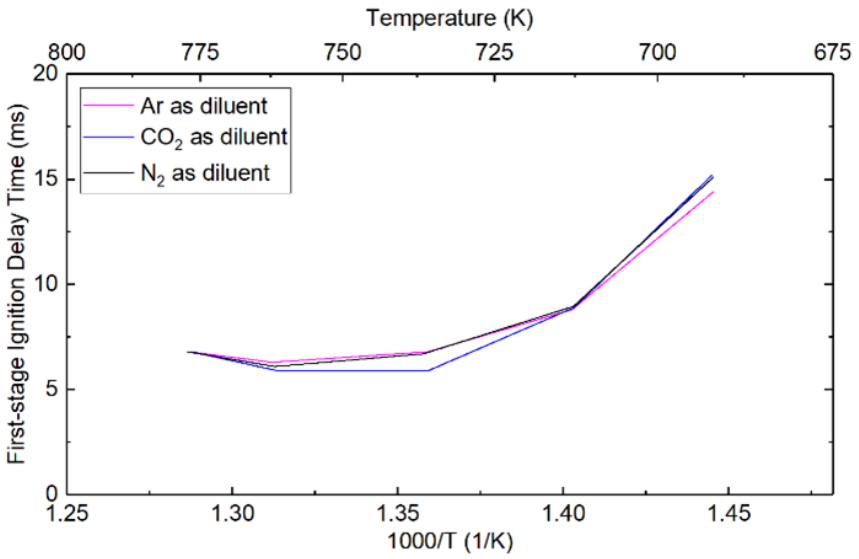

(a)

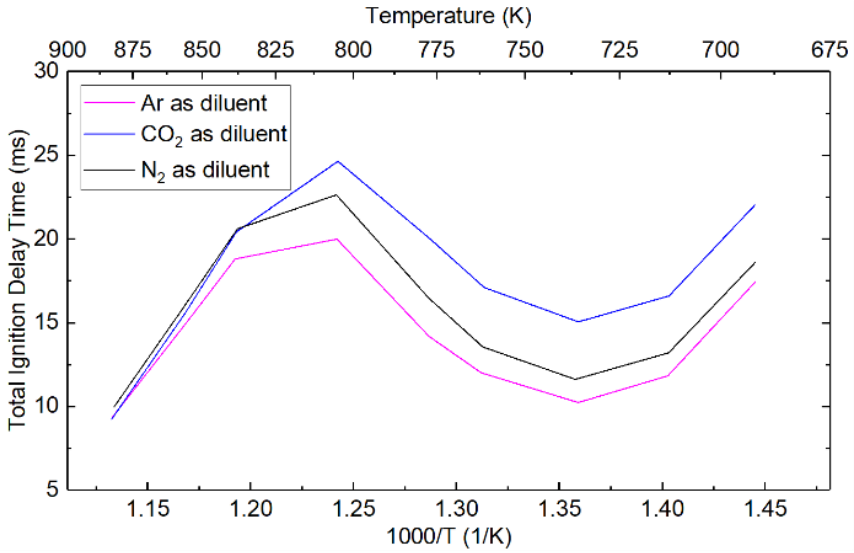

(b)

Figure 7-12: (a) First-stage ignition delay times for CR = 9.6 using different diluent gases with the original volume profiles. (b) Total ignition delay times for CR = 9.6 using different diluent gases with the original volume profiles.

Figure 7-13 (a) and (b) quantify the effect of t_{50} on the first-stage and total ignition delay times respectively, for the different diluent gases. All three diluent gases are impacted by t_{50} similarly in regards to the first-stage ignition delay time. As expected and was observed earlier,

the magnitude of the effect of t_{50} in each diluent gas mixture increases with temperature due to the increased reactivity of the fuel. However, looking at the effect of t_{50} on total ignition delay times in Figure 7-13 (b), it can be observed that the mixture with Ar is most affected, followed by N_2 and CO_2. This implies that although the first-stage ignition delay time is impacted similarly, the influence of t_{50} on the second-stage of ignition differs across the diluent gas mixtures. Sensitivity analysis published previously by several authors [64,65,162] has confirmed that in the low-temperature region (650–750 K), isomerization reactions of RO_2 and $QOOHO_2$ dominate the first-stage of ignition for iso-octane. Furthermore, none of these reactions involve third bodies. Thus, a similar effect of t_{50} across the different diluent gases on the first-stage ignition is expected. As was observed in Section 7.4.1 for the N_2 mixture, t_{50} minimally affects the second-stage ignition delay time; the same is applicable to Ar and CO_2 mixtures as well. As a result, the total ignition delay times of the three diluent mixtures are also identically affected due to a similar reduction in t_{50}. Over the entire temperature range, the Ar mixture is slightly more affected and the CO_2 mixture is the least affected by t_{50}. Since Ar is more reactive due to its lower thermal heat capacity, it has shorter ignition delay times over the entire temperature range. Consequently, it is comparatively more affected by a similar reduction in t_{50}. Referring to Figure 7-13 (b), the maximum percentage deviation from mean of $\eta_{t50,\text{ total ignition delay}}$ for the three diluent gas mixtures is ~14%. The large discrepancy in the effect of t_{50} is mainly due to CO_2 also acting as a reactant in some of the elementary reactions. If just the Ar and N_2 mixtures are considered, the maximum percentage deviation from the mean of $\eta_{t50,\text{ total ignition delay}}$ for the two diluent gas mixtures drops down to ~5%.

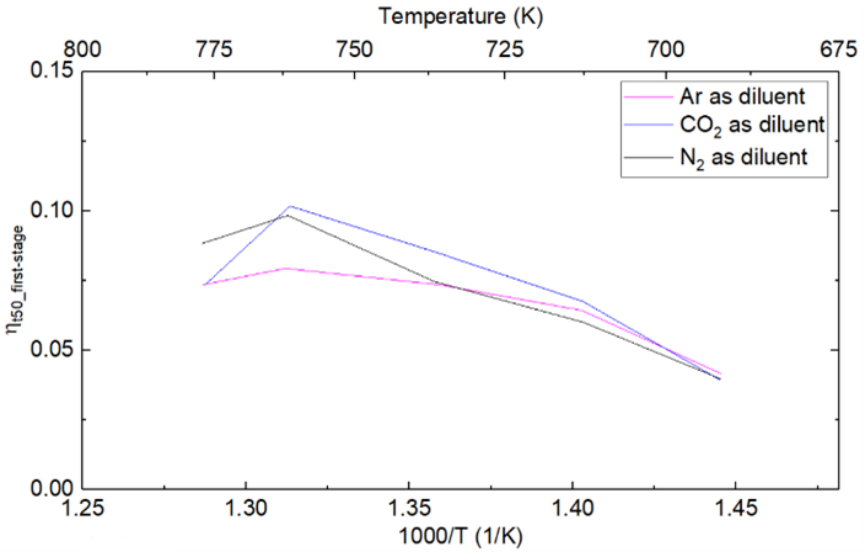

(a)

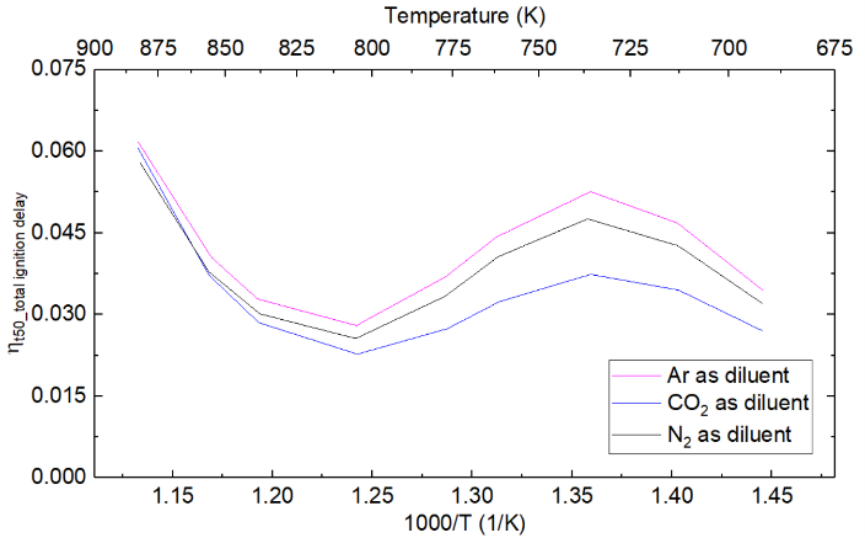

(b)

Figure 7-13: (a) Effect of t_{50} on first-stage ignition delay using different diluent gas mixtures. (b) Effect of t_{50} on total ignition delay using different diluent gas mixtures.

Figure 7-14 (a) and (b) quantify the effect of post-compression heat loss on the first-stage and total ignition delay times, respectively, for the different diluent gases. The first-stage ignition delay is again minimally impacted by post-compression heat losses because of the short duration, which allows less time for the post-compression heat loss to influence the ignition process. Overall,

the post-compression heat loss has a similar effect on total ignition delay for all the diluent gas mixtures. However, in the NTC region, a minor difference in effect on each diluent gas is observed, which is majorly due to the difference in thermal capacities of the diluent gases. Since the Ar mixture has the shortest total ignition delay times, it is the least affected by post-compression heat loss and the opposite is applicable to the CO_2 mixture. As temperature further increases, the effect of post-compression heat loss across the different diluent gas mixtures normalizes and reaches a maximum value at around T_c = 825 K, where the total ignition delay times are the longest. Beyond 825 K, the effect of post-compression heat loss starts to reduce, as expected due to the shorter ignition delay times, for all the diluent gas mixtures as $\eta_{\text{post-compression heat loss, total ignition delay}}$ tends to zero.

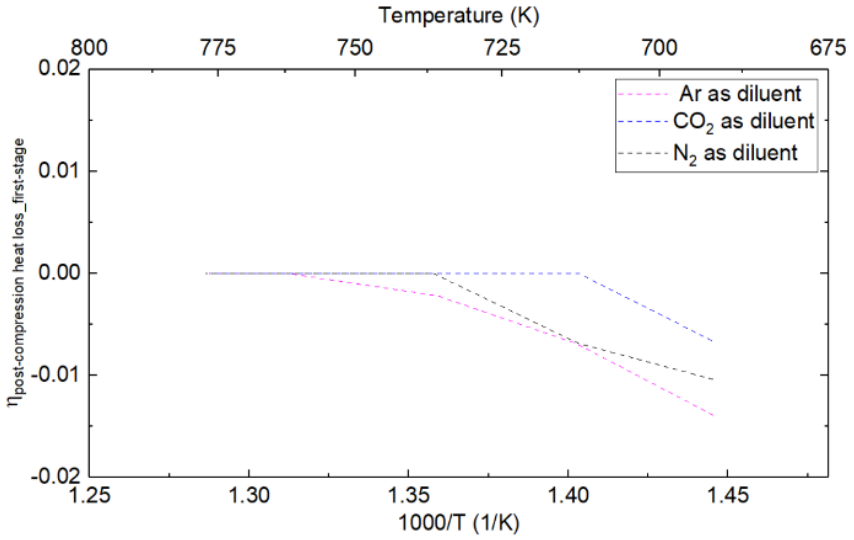

(a)

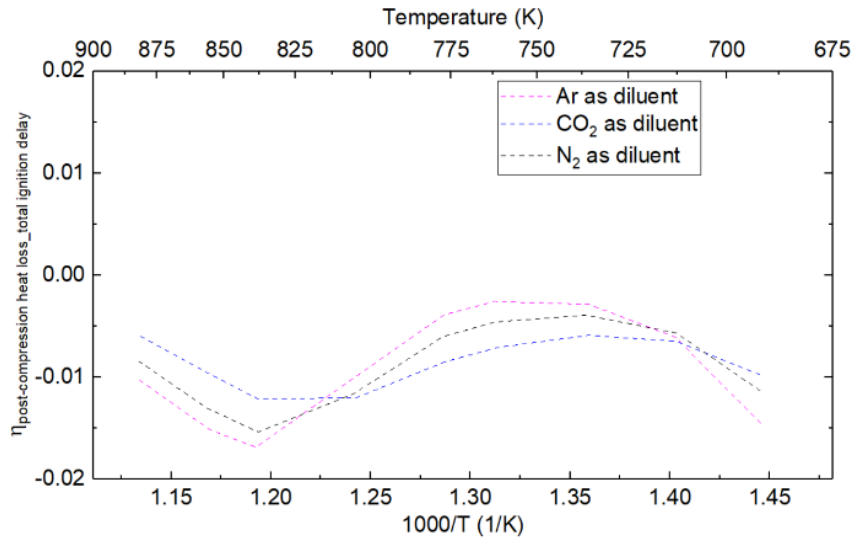

(b)

Figure 7-14: (a) Effect of post-compression heat loss on first-stage ignition delay using different diluent gas mixtures. (b) Effect of post-compression heat loss on total ignition delay using different diluent gas mixtures.

To summarize, post-compression heat loss and t_{50} have a similar effect on each of the different diluent gas mixtures. However, the effect of t_{50} has greater importance than that of post-compression heat loss for all of the diluent gas mixtures tested.

7.8. Chapter Summary

A simulation-based study to evaluate the influence of changing compression ratio on ignition delay times measured in an RCM is successfully carried out. Furthermore, an investigation on whether the evaluated effects are more prominent in a particular equivalence ratio mixture and in a particular diluent gas mixture is performed. A comprehensive set of test conditions was simulated to consider how fuel reactivity and ignition behavior coupled with the RCM's configuration would result in unique ignition delay times. The simulation results have led to the following conclusions:

- Compression time has a negligible effect on the first-stage as well as the total ignition delay times, as long as the post-compression heat loss and t_{50} are identical.
- The reduction in percentage deviation of total and first-stage ignition delay times from about 9% to less than 5%, after maintaining similar t_{50} and post-compression heat loss across the six compression ratios, implies that initial conditions play a minimal role in affecting the first-stage and also the total ignition delay times.
- Post-compression heat losses have minimal impact on the first-stage ignition at any of the compressed conditions studied. However, differences in the rate of pressure drop post-compression cause differences in the heat release and the pressure and temperature rise during the first-stage ignition, which affects the second-stage ignition and hence the total ignition delay.
- Longer t_{50} times indicate that the mixture spends more time at elevated conditions and is more reactive by the end of compression, leading to shorter first-stage and total ignition delay times. Longer t_{50} causes earlier initiation of radicals production, thereby shortening the ignition delay time.

- Conditions at which there is no two-stage ignition and the ignition delay time is comparatively longer are more affected by post-compression heat losses than by t_{50}. This is because comparatively more time is allowed for the post-compression heat losses to affect the ignition process. However, the magnitude of the effect of post-compression heat loss remains less than that of t_{50} across all compression ratios, compressed conditions and equivalence ratios that were tested.
- The higher the reactivity of the fuel, the more sensitive it will be to changes in t_{50}. This is supported by studying the effects on ignition delay for varying equivalence ratios. Since ϕ=1.3 is the most reactive and has the shortest first-stage and total ignition delay times, it is impacted the most by t_{50} and the least by post-compression heat losses; followed by ϕ=1.0 and 0.7.
- The above-listed effects are also observed in similar magnitudes when the diluent gas in the mixture (N_2) is replaced with Ar or CO_2.

It can be concluded that t_{50} and post-compression heat loss are the factors that most significantly influence the ignition delay times. However, the finding of t_{50} influencing ignition delay more than post-compression heat loss is inconsistent with the observations made in the experimental study. This discrepancy may be due to the mass transfer between gases in the main combustion chamber and the crevice volume where the amount of mass transfer can vary as a function of the end of compression conditions, which in turn are dependent on compression time and t_{50}. Additionally, some of the energy released in the first-stage of ignition is also expended as expansion work against the boundary layer in the test section. The aforementioned effects, in addition to the coupling between pre-ignition energy release, heat loss, and temperature distribution within the RCM, are not modeled in 0-D CHEMKIN simulations.

Chapter 8. CONCLUSIONS

This dissertation identifies and evaluates the influence of various parameters on the auto-ignition delay times obtained at identical compressed conditions using a Rapid Compression Machine. This chapter concludes the work presented in this thesis. Since the findings are already summarized at the end of each chapter, the conclusions that answer the research questions posed in the introductory chapter are presented here. Furthermore, recommendations are suggested for future modeling and experimental work, which may aid in a better understanding of the discrepancy causing factors.

8.1. Conclusions of research

The main goal of this research was to identify the factors that cause a discrepancy in auto-ignition delay measurements from RCMs, at identical compressed conditions. These factors are identified in the previously posed research questions which involved mixture preparation methods, compression ratios and diluent gas composition. Answers to the research questions previously posed are presented.

- **What are the reasons behind the discrepancies in measured auto-ignition delay data at identical compressed conditions? Which components of RCM testing have the strongest connection to the data discrepancy?**

  The ignition characteristics are investigated by changing the mixture preparation method, compression ratio and diluent gas composition. Changing the compression ratio, in turn, changes many other operating parameters, such as initial conditions required to achieve the same compressed conditions, compression time, surface-area-to-volume ratio and t_{50}. The influence of each of these parameters on the ignition delay times was isolated and studied.

For a given compression ratio, the mixture preparation method, initial conditions and compression time had a negligible effect on ignition delay times, as long as the post-compression heat loss and t_{50} were kept identical. This implies that surface-area-to-volume ratio and t_{50} are the factors that primarily influence the ignition delay times when the compression ratio is varied.

Diluent gas composition was another major factor causing a discrepancy in data because it altered the post-compression heat losses.

- **Do the post-compression heat loss and t_{50} have a larger impact on ignition delay times at certain equivalence ratios?**

The higher the reactivity of the fuel, the more sensitive it will be to changes in t_{50}. This was supported by numerically studying the effects on ignition delay for varying equivalence ratios of iso-octane and air. Since ϕ=1.3 was the most reactive and has the shortest first-stage and total ignition delay times, it was impacted the most by t_{50} and the least by post-compression heat losses; followed by ϕ=1.0 and 0.7. Post-compression heat losses were also observed to affect the ignition delay times; however, the effect of t_{50} was more significant.

- **Do the post-compression heat loss and t_{50} affect ignition delay times more for a particular diluent gas?**

The effects of t_{50} and post-compression heat loss on iso-octane ignition delay times were observed in similar magnitudes for a given equivalence ratio when the diluent gas in the mixture (N_2) was replaced with Ar or CO_2. In other words, t_{50} affects the ignition delay time of an iso-octane/oxygen/nitrogen mixture by the same amount as in an iso-octane/oxygen/argon or iso-octane/oxygen/carbon dioxide mixture.

- **Do the post-compression heat loss and t50 affect the first stage of the two-stage ignition process? Does a given factor affect a particular stage more than the other?**

  Post-compression heat losses have minimal impact on the first-stage ignition at any of the compressed conditions studied. However, differences in the rate of pressure drop post-compression cause differences in the heat release and the pressure and temperature rise during the first-stage ignition, which affects the second-stage ignition and hence the total ignition delay.

  Longer t_{50} times indicate that the mixture spends more time at elevated conditions and is more reactive by the end of compression, leading to shorter first-stage and total ignition delay times. Longer t_{50} causes earlier initiation of radical production, thereby shortening the ignition delay time.

- **Is this discrepancy also observed during numerical analysis of RCM experiments? What other factors can potentially contribute other than those observed experimentally?**

  The experimental results were supplemented with 0-D simulations which made use of volume profiles of the corresponding configurations of compression ratio and diluent gas. The numerical results also complemented the experimental results well.

  In addition to the thermal effects on the ignition delay, in the case of diluent gas composition, third-body collision efficiencies were also found to affect the ignition delay at all temperatures. Higher third-body collision coefficient resulted in shorter ignition delay.

As a result of longer t_{50}, radicals such as H_2O_2, HO_2 and CH_2O were at higher concentrations by the end of compression, implying that the mixture was more chemically reactive, resulting in shorter ignition delay times.

The CFD simulation results indicate that the temperature field during compression and post-compression is sensitive to non-uniform gas temperature present at the start of an experiment and is also influenced by buoyancy. The non-uniform boundary temperatures also led to thermal and species stratification as depicted by the compressed-gas temperature fields and OH concentrations. As a result, the computational results closely reproduced the features of the ethanol auto-ignition that were observed in the experiments. However, the ignition delay time predictions were not susceptible to this.

8.2. Recommendation for Future Work

During this research, a number of factors causing a discrepancy in auto-ignition delay data were identified, both experimentally and numerically. Over the course of completing this work, a number of potential future research ideas have emerged. Continuing work in these areas would enable a greater understanding of the discrepancy causing factors and would facilitate the comparison of ignition delay results across RCM facilities and within a single facility. From a numerical standpoint, considering the discrepancy causing factors would enable the development of models that could provide better predictions over a wider range of equivalence ratios, diluent gas compositions and RCM configurations. Suggestions for further experimental and modeling work include:

- **Further study of the effects of t_{50} and post-compression heat loss on ignition delay with multi-zone and CFD Modelling**

The numerical finding of t_{50} influencing ignition delay more than post-compression heat loss is inconsistent with the observations made in the experimental study of iso-octane. This discrepancy may be due to the mass transfer between gases in the main combustion chamber and the crevice volume where the amount of mass transfer can vary as a function of the end of compression conditions, which in turn are dependent on compression time and t_{50}. Additionally, some of the energy released in the first-stage of ignition is also expended as expansion work against the boundary layer in the test section. The aforementioned effects, in addition to the coupling between pre-ignition energy release, heat loss, and temperature distribution within the RCM, are not modeled in 0-D CHEMKIN simulations. For this reason, for better comparison and understanding of the effects of t_{50} and post-compression heat loss on ignition delay, either multi-zone models coupling the RCM physics with the heat release [108,163–165] or CFD simulations need to be used. Furthermore, a linear post-compression heat loss rate does not accurately capture the actual rate of heat loss occurring in RCM experiments. This assumption would influence the temporal and spatial temperature profile and, in turn, the ignition delay times; since the reaction rates have a highly non-linear temperature dependence. With the basic understanding from this study, the analysis can now be made more complex by fitting a polynomial curve to the post-compression profile which would more accurately capture the heat loss rate observed in the RCM experiments.

- **More accurate 3-D CFD Analysis**

Due to the considerably increased computational cost of simulating half the geometry of the RCM and considering mixture-averaged diffusion coefficients, adaptive mesh refinement was used to balance the simulation time and the accuracy of the simulations. Moreover, it was determined from 1-D flame simulations that in order to capture the thin radical layers, a mesh size

of about 4 microns would be needed which was infeasible to obtain given the limited resources. Therefore, more accurate reacting flow physics analysis can be conducted using more refined mesh. However, the use of such a fine mesh will not alter the solution before the ignition event. As such, the very fine mesh resolution needed during the ignition process is deemed unnecessary for the presented investigations on temperature distribution leading up to the ignition event.

- **Study of the effects of initial temperature inhomogeneities and buoyancy on the combustion of a two-stage ignition fuel**

Limited experimental studies have been done imaging the two-stage ignition process of iso-octane. Therefore, optical experiments of iso-octane at conditions where two-stage ignition is observed would not only provide insights into the ignition characteristics of iso-octane but would also help understand the effect of initial temperature inhomogeneities and buoyancy on the ignition process. It is suspected that the non-uniform boundary conditions and buoyancy would have a more prominent effect on fuels that exhibit NTC behavior and two-stage ignition. Neglecting buoyancy and validating mechanisms in such cases might lead to inaccurate and inconsistent predictions of the mechanism. More accurate predictions can be made using 3D-CFD and the non-uniform temperature boundary conditions along with buoyancy. For instance, the comparatively lower temperature in the vortex region would provide the main contribution to hot ignition under some NTC conditions and have the potential to influence the timing of hot ignition during RCM experiments strongly. While chemistry occurring outside the vortex will drive the first-stage of ignition where initial temperature non-uniformities have little effect, the main ignition chemistry occurs in the vortex region, which was observed to be different in the buoyancy and no buoyancy cases. It would be interesting to see the effect of the break in the symmetry of the vortex ring due to buoyancy on the first-stage ignition and how the aerodynamics change after the first-stage

ignition. The total ignition delay results (i.e., first and second stage) obtained under such conditions have been shown to be extremely sensitive to non-uniformities in the initial temperature [107,166]. Hence, it is also suspected that considering the effect of buoyancy would strongly influence the total ignition delay data. Mechanism validations and the validity of 0-D simulations based on the approach of adiabatic volume expansion in predicting ignition delay needs to be further examined by comparing to the 3-D CFD simulations with buoyancy for varying compressed conditions in the NTC region.

- **Validating the adiabatic core hypothesis considering initial temperature inhomogeneities and buoyancy at different compressed pressures**

  It is a well-known fact that the creviced piston is more efficient in suppressing the roll-up vortex at higher compressed pressures [3]. However, a study with buoyancy acting and initial non-uniformities in the temperature field needs to be done at different compressed pressures to validate the adiabatic core hypothesis at these compressed conditions.

APPENDIX

APPENDIX

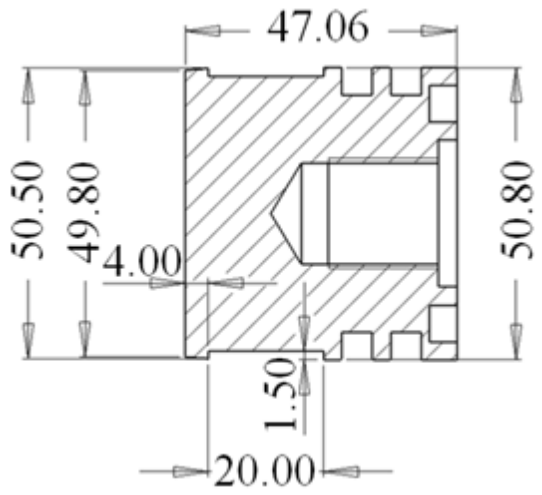

Figure A-1: MSU creviced piston with dimensions (in mm)

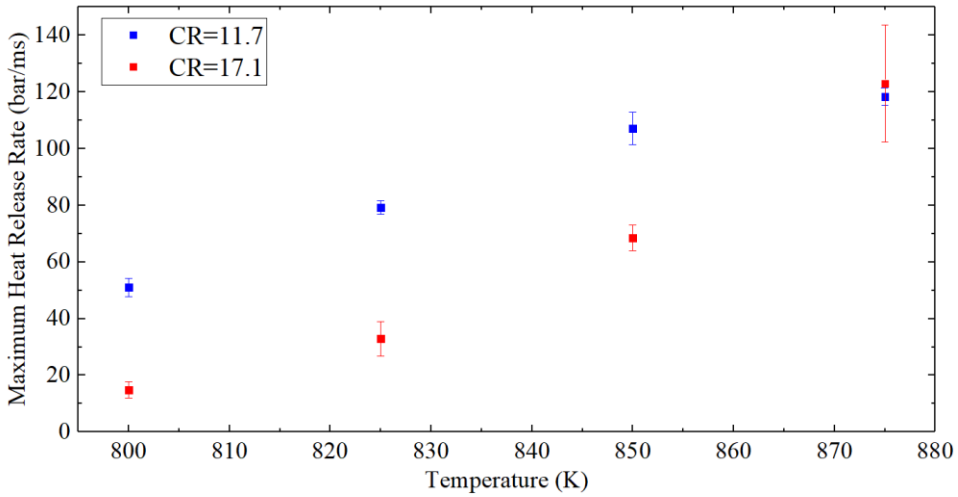

Figure A-2: Comparison of Maximum Heat Release Rates at different compression ratios using Mixing Tank

BIBLIOGRAPHY

BIBLIOGRAPHY

1. Goldsborough, S.S., Hochgreb, S., Vanhove, G., Wooldridge, M.S., Curran, H.J., and Sung, C.-J., "Advances in rapid compression machine studies of low- and intermediate-temperature autoignition phenomena," *Progress in Energy and Combustion Science* 63:1–78, 2017, doi:10.1016/j.pecs.2017.05.002.

2. Mittal, G., "A rapid compression machine-design, characterization, and autoignition investigations," PhD Thesis, CASE WESTERN RESERVE UNIVERSITY, 2006.

3. Mittal, G. and Sung, C.J., "Aerodynamics inside a rapid compression machine," *Combustion and Flame* 145(1–2), 2006, doi:10.1016/j.combustflame.2005.10.019.

4. Javed, T., Ahmed, A., Lovisotto, L., Issayev, G., Badra, J., Sarathy, S.M., and Farooq, A., "Ignition studies of two low-octane gasolines," *Combustion and Flame* 185, 2017, doi:10.1016/j.combustflame.2017.07.006.

5. Bradley, D., Lawes, M., and Materego, M., "Interpretation of Auto-ignition Delay Times Measured in Different Rapid Compression Machines," 2015.

6. Goldsborough, S.S., "A chemical kinetically based ignition delay correlation for iso-octane covering a wide range of conditions including the NTC region," *Combustion and Flame* 156(6), 2009, doi:10.1016/j.combustflame.2009.01.018.

7. Lee, C., Vranckx, S., Heufer, K.A., Khomik, S.V., Uygun, Y., Olivier, H., and Fernandes, R.X., "On the chemical kinetics of ethanol oxidation: Shock tube, rapid compression machine and detailed modeling study," *Zeitschrift Fur Physikalische Chemie* 226(1), 2012, doi:10.1524/zpch.2012.0185.

8. Heufer, K.A. and Olivier, H., "Determination of ignition delay times of different hydrocarbons in a new high pressure shock tube," *Shock Waves* 20(4), 2010, doi:10.1007/s00193-010-0262-2.

9. Cancino, L.R., Fikri, M., Oliveira, A.A.M., and Schulz, C., "Measurement and chemical kinetics modeling of shock-induced ignition of ethanol-air mixtures," *Energy and Fuels* 24(5), 2010, doi:10.1021/ef100076w.

10. Mittal, G., Burke, S.M., Davies, V.A., Parajuli, B., Metcalfe, W.K., and Curran, H.J., "Autoignition of ethanol in a rapid compression machine," *Combustion and Flame* 161(5), 2014, doi:10.1016/j.combustflame.2013.11.005.

11. Gülder, Ö.L., "Laminar burning velocities of methanol, ethanol and isooctane-air mixtures," *Symposium (International) on Combustion* 19(1):275–281, 1982, doi:10.1016/S0082-0784(82)80198-7.

12. Egolfopoulos, F.N., Du, D.X., and Law, C.K., “A study on ethanol oxidation kinetics in laminar premixed flames, flow reactors, and shock tubes,” *Symposium (International) on Combustion* 24(1), 1992, doi:10.1016/S0082-0784(06)80101-3.

13. Kasper, T.S., Oßwald, P., Kamphus, M., and Kohse-Höinghaus, K., “Ethanol flame structure investigated by molecular beam mass spectrometry,” *Combustion and Flame* 150(3), 2007, doi:10.1016/j.combustflame.2006.12.022.

14. Saxena, P. and Williams, F.A., “Numerical and experimental studies of ethanol flames,” *Proceedings of the Combustion Institute* 31 I(1), 2007, doi:10.1016/j.proci.2006.08.097.

15. Natarajan, K. and Bhaskaran, K.A., “An Experimental and Analytical Investigation of High Temperature Ignition of Ethanol,” *Proceedings of the 13th Internatinal Symposium on Shock Tubes and Waves*, 1981.

16. Dunphy, M.P. and Simmie, J.M., “High-temperature oxidation of ethanol. Part 1.-Ignition delays in shock waves,” *Journal of the Chemical Society, Faraday Transactions* 87(11), 1991, doi:10.1039/FT9918701691.

17. Curran, H.J., Dunphy, M.P., Simmie, J.M., Westbrook, C.K., and Pitz, W.J., “Shock tube ignition of ethanol, isobutene and MTBE: Experiments and modeling,” *Symposium (International) on Combustion* 24(1), 1992, doi:10.1016/S0082-0784(06)80094-9.

18. Li, J., Kazakov, A., and Dryer, F.L., “Ethanol pyrolysis experiments in a variable pressure flow reactor,” *International Journal of Chemical Kinetics* 33(12):859–867, 2001, doi:10.1002/kin.10009.

19. Li, J., Kazakov, A., and Dryer, F.L., “Experimental and Numerical Studies of Ethanol Decomposition Reactions,” *The Journal of Physical Chemistry A* 108(38):7671–7680, 2004, doi:10.1021/jp0480302.

20. Haas, F.M., Chaos, M., and Dryer, F.L., “Low and intermediate temperature oxidation of ethanol and ethanol-PRF blends: An experimental and modeling study,” *Combustion and Flame* 156(12), 2009, doi:10.1016/j.combustflame.2009.08.012.

21. Leplat, N., Dagaut, P., Togbé, C., and Vandooren, J., “Numerical and experimental study of ethanol combustion and oxidation in laminar premixed flames and in jet-stirred reactor,” *Combustion and Flame* 158(4), 2011, doi:10.1016/j.combustflame.2010.12.008.

22. Frassoldati, A., Cuoci, A., Faravelli, T., and Ranzi, E., “Kinetic modeling of the oxidation of ethanol and gasoline surrogate mixtures,” *Combustion Science and Technology* 182(7), 2010, doi:10.1080/00102200903466368.

23. Barraza-Botet, C.L. and Wooldridge, M.S., “Combustion chemistry of iso-octane/ethanol blends: Effects on ignition and reaction pathways,” *Combustion and Flame* 188, 2018, doi:10.1016/j.combustflame.2017.10.011.

24. Barraza-Botet, C.L., Wagnon, S.W., and Wooldridge, M.S., "Combustion chemistry of ethanol: Ignition and speciation studies in a rapid compression facility," *Journal of Physical Chemistry A* 120(38), 2016, doi:10.1021/acs.jpca.6b06725.

25. Büttgen, R.D., Raffius, T., Grünefeld, G., Koß, H.J., and Heufer, A., "High-speed imaging of the ignition of ethanol at engine relevant conditions in a rapid compression machine," *Proceedings of the Combustion Institute* 37(2), 2019, doi:10.1016/j.proci.2018.05.001.

26. Lee, D., Hochgreb, S., and Keck, J.C., "Autoignition of alcohols and ethers in a rapid compression machine," *SAE Technical Papers*, 1993, doi:10.4271/932755.

27. Noorani, K.E., Akih-Kumgeh, B., and Bergthorson, J.M., "Comparative high temperature shock tube ignition of C1-C4 primary alcohols," *Energy and Fuels* 24(11), 2010, doi:10.1021/ef1009692.

28. Walton, S.M., He, X., Zigler, B.T., Wooldridge, M.S., and Atreya, A., "An experimental investigation of iso-octane ignition phenomena," *Combustion and Flame* 150(3), 2007, doi:10.1016/j.combustflame.2006.07.016.

29. Walton, S.M., He, X., Zigler, B.T., and Wooldridge, M.S., "An experimental investigation of the ignition properties of hydrogen and carbon monoxide mixtures for syngas turbine applications," *Proceedings of the Combustion Institute* 31 II(2), 2007, doi:10.1016/j.proci.2006.08.059.

30. Mansfield, A.B. and Wooldridge, M.S., "High-pressure low-temperature ignition behavior of syngas mixtures," *Combustion and Flame* 161(9), 2014, doi:10.1016/j.combustflame.2014.03.001.

31. Mansfield, A.B., Wooldridge, M.S., Di, H., and He, X., "Low-temperature ignition behavior of iso-octane," *Fuel* 139, 2015, doi:10.1016/j.fuel.2014.08.019.

32. Stephen R. Turns, "An Introduction to Combustion, Concepts and Applications, Third Edition," 2011.

33. Heywood, J., "Internal Combustion Engine Fundamentals," McGraw-Hill, 1988.

34. Pitz, W.J., Cernansky, N.P., Dryer, F.L., Egolfopoulos, F.N., Farrell, J.T., Friend, D.G., and Pitsch, H., "Development of an experimental database and chemical kinetic models for surrogate gasoline fuels," *SAE Technical Papers*, 2007, doi:10.4271/2007-01-0175.

35. Farrell, J.T., Cernansky, N.P., Dryer, F.L., Law, C.K., Friend, D.G., Hergart, C.A., McDavid, R.M., Patel, A.K., Mueller, C.J., and Pitsch, H., "Development of an experimental database and kinetic models for surrogate diesel fuels," *SAE Technical Papers*, 2007, doi:10.4271/2007-01-0201.

36. Colket, M., Edwards, T., Williams, S., Cernansky, N.P., Miller, D.L., Egolfopoulos, F., Lindstedt, P., Seshadri, K., Dryer, F.L., Law, C.K., Friend, D., Lenhert, D.B., Pitsch, H., Sarofim, A., Smooke, M., and Tsang, W., "Development of an experimental database and kinetic

models for surrogate jet fuels," *Collection of Technical Papers - 45th AIAA Aerospace Sciences Meeting*, 2007, doi:10.2514/6.2007-770.

37. Oehlschlaeger, M.A., Davidson, D.F., Herbon, J.T., and Hanson, R.K., "Shock Tube Measurements of Branched Alkane Ignition Times and OH Concentration Time Histories," *International Journal of Chemical Kinetics* 36(2), 2004, doi:10.1002/kin.10173.

38. Davidson, D.F., Gauthier, B.M., and Hanson, R.K., "Shock tube ignition measurements of iso-octane/air and toluene/air at high pressures," *Proceedings of the Combustion Institute* 30(1), 2005, doi:10.1016/j.proci.2004.08.004.

39. Shen, H.P.S., Vanderover, J., and Oehlschlaeger, M.A., "A shock tube study of iso-octane ignition at elevated pressures: The influence of diluent gases," *Combustion and Flame* 155(4), 2008, doi:10.1016/j.combustflame.2008.06.001.

40. Hartmann, M., Gushterova, I., Fikri, M., Schulz, C., Schießl, R., and Maas, U., "Auto-ignition of toluene-doped n-heptane and iso-octane/air mixtures: High-pressure shock-tube experiments and kinetics modeling," *Combustion and Flame* 158(1):172–178, 2011, doi:10.1016/j.combustflame.2010.08.005.

41. Fieweger, K., Blumenthal, R., and Adomeit, G., "Self-ignition of S.I. engine model fuels: A shock tube investigation at high pressure," *Combustion and Flame* 109(4), 1997, doi:10.1016/S0010-2180(97)00049-7.

42. Fieweger, K., Blumenthal, R., and Adomeit, G., "Shock-tube investigations on the self-ignition of hydrocarbon-air mixtures at high pressures," *Symposium (International) on Combustion* 25(1), 1994, doi:10.1016/S0082-0784(06)80803-9.

43. Malewicki, T., Comandini, A., and Brezinsky, K., "Experimental and modeling study on the pyrolysis and oxidation of iso-octane," *Proceedings of the Combustion Institute* 34(1), 2013, doi:10.1016/j.proci.2012.06.137.

44. Davis, S.G. and Law, C.K., "Laminar flame speeds and oxidation kinetics of iso-octane-air and n-heptane-air flames," *Symposium (International) on Combustion*, 1998, doi:10.1016/S0082-0784(98)80442-6.

45. Bradley, D., Hicks, R.A., Lawes, M., Sheppard, C.G.W., and Woolley, R., "The measurement of laminar burning velocities and Markstein numbers for iso-octane-air and iso-octane-n-heptane-air mixtures at elevated temperatures and pressures in an explosion bomb," *Combustion and Flame* 115(1–2), 1998, doi:10.1016/S0010-2180(97)00349-0.

46. Galmiche, B., Halter, F., and Foucher, F., "Effects of high pressure, high temperature and dilution on laminar burning velocities and Markstein lengths of iso-octane/air mixtures," *Combustion and Flame* 159(11), 2012, doi:10.1016/j.combustflame.2012.06.008.

47. Kelley, A.P., Liu, W., Xin, Y.X., Smallbone, A.J., and Law, C.K., "Laminar flame speeds, non-premixed stagnation ignition, and reduced mechanisms in the oxidation of iso-octane," *Proceedings of the Combustion Institute* 33(1), 2011, doi:10.1016/j.proci.2010.05.058.

48. Van Lipzig, J.P.J., Nilsson, E.J.K., De Goey, L.P.H., and Konnov, A.A., “Laminar burning velocities of n-heptane, iso-octane, ethanol and their binary and tertiary mixtures,” *Fuel* 90(8), 2011, doi:10.1016/j.fuel.2011.04.029.

49. Kumar, K., Freeh, J.E., Sung, C.J., and Huang, Y., “Laminar flame speeds of preheated iso-octane/O2/N2 and n-heptane/O2/N2 mixtures,” *Journal of Propulsion and Power* 23(2), 2007, doi:10.2514/1.24391.

50. Kwon, O.C., Hassan, M.I., and Faeth, G.M., “Flame stretch interactions of premixed fuel-vapor O sub 2 N sub 2 flames,” *Journal of Propulsion and Power* 16(3), 2000.

51. Huang, Y., Sung, C.J., and Eng, J.A., “Laminar flame speeds of primary reference fuels and reformer gas mixtures,” *Combustion and Flame* 139(3), 2004, doi:10.1016/j.combustflame.2004.08.011.

52. Ji, C., Sarathy, S.M., Veloo, P.S., Westbrook, C.K., and Egolfopoulos, F.N., “Effects of fuel branching on the propagation of octane isomers flames,” *Combustion and Flame* 159(4), 2012, doi:10.1016/j.combustflame.2011.12.004.

53. Liu, N., S. Mani Sarathy, Westbrook, C.K., and Egolfopoulos, F.N., “Ignition of non-premixed counterflow flames of octane and decane isomers,” *Proceedings of the Combustion Institute* 34(1), 2013, doi:10.1016/j.proci.2012.05.040.

54. Blouch, J.D. and Law, C.K., “Non-premixed ignition of n-heptane and iso-octane in a laminar counterflow,” *Proceedings of the Combustion Institute* 28(2), 2000, doi:10.1016/S0082-0784(00)80567-6.

55. Dagaut, P., Reuillon, M., and Cathonnet, M., “High pressure oxidation of liquid fuels from low to high temperature. 1. n-heptane and iso-octane.,” *Combustion Science and Technology* 95(1–6), 1993, doi:10.1080/00102209408935336.

56. Lignola, P.G., Di Maio, F.P., Marzocchella, A., Mercogliano, R., and Reverchon, E., “JSFR combustion processes of n-heptane and isooctane,” *Symposium (International) on Combustion* 22(1), 1989, doi:10.1016/S0082-0784(89)80174-2.

57. Danna, A., Mercogliano, R., Barbella, R., and Ciajolo, A., “Low temperature oxidation chemistry of iso-octane under high pressure conditions,” *Combustion Science and Technology* 83(4–6), 1992, doi:10.1080/00102209208951833.

58. Chen, J.S., Litzinger, T.A., and Curran, H.J., “The diluted stoichiometric oxidation of iso-octane in the intermediate temperature regime at elevated pressures,” *Combustion Science and Technology* 172(1), 2001, doi:10.1080/00102200108935838.

59. Dryer, F.L. and Brezinsky, K., “A Flow Reactor Study of the Oxidation of n-Octane and Iso-Octane,” *Combustion Science and Technology* 45(3–4), 1986, doi:10.1080/00102208608923850.

60. Curran, H.J., Gaffuri, P., Pitz, W.J., and Westbrook, C.K., “A comprehensive modeling study of iso-octane oxidation,” *Combustion and Flame* 129(3), 2002, doi:10.1016/S0010-2180(01)00373-X.

61. Mehl, M., Pitz, W.J., Westbrook, C.K., and Curran, H.J., “Kinetic modeling of gasoline surrogate components and mixtures under engine conditions,” *Proceedings of the Combustion Institute* 33(1), 2011, doi:10.1016/j.proci.2010.05.027.

62. Atef, N., Kukkadapu, G., Mohamed, S.Y., Rashidi, M.A., Banyon, C., Mehl, M., Heufer, K.A., Nasir, E.F., Alfazazi, A., Das, A.K., Westbrook, C.K., Pitz, W.J., Lu, T., Farooq, A., Sung, C.J., Curran, H.J., and Sarathy, S.M., “A comprehensive iso-octane combustion model with improved thermochemistry and chemical kinetics,” *Combustion and Flame* 178, 2017, doi:10.1016/j.combustflame.2016.12.029.

63. Glaude, P.A., Conraud, V., Fournet, R., Battin-Leclerc, F., Côme, G.M., Scacchi, G., Dagaut, P., and Cathonnet, M., “Modeling the oxidation of mixtures of primary reference automobile fuels,” *Energy and Fuels* 16(5), 2002, doi:10.1021/ef020025e.

64. Di, H., He, X., Zhang, P., Wang, Z., Wooldridge, M.S., Law, C.K., Wang, C., Shuai, S., and Wang, J., “Effects of buffer gas composition on low temperature ignition of iso-octane and n-heptane,” *Combustion and Flame* 161(10), 2014, doi:10.1016/j.combustflame.2014.04.014.

65. Zhang, P., Ji, W., He, T., He, X., Wang, Z., Yang, B., and Law, C.K., “First-stage ignition delay in the negative temperature coefficient behavior: Experiment and simulation,” *Combustion and Flame* 167, 2016, doi:10.1016/j.combustflame.2016.03.002.

66. He, X., Donovan, M.T., Zigler, B.T., Palmer, T.R., Walton, S.M., Wooldridge, M.S., and Atreya, A., “An experimental and modeling study of iso-octane ignition delay times under homogeneous charge compression ignition conditions,” *Combustion and Flame* 142(3), 2005, doi:10.1016/j.combustflame.2005.02.014.

67. Würmel, J., Silke, E.J., Curran, H.J., Ó Conaire, M.S., and Simmie, J.M., “The effect of diluent gases on ignition delay times in the shock tube and in the rapid compression machine,” *Combustion and Flame* 151(1–2), 2007, doi:10.1016/j.combustflame.2007.06.010.

68. Wagnon, S.W. and Wooldridge, M.S., “Effects of buffer gas composition on autoignition,” *Combustion and Flame* 161(4), 2014, doi:10.1016/j.combustflame.2013.09.022.

69. Chinnathambi, P., Wadkar, C., and Toulson, E., “Impact of CO2 dilution on ignition delay times of iso-octane at 15% and 30% dilution levels in a rapid compression machine,” *SAE Technical Papers*, 2019, doi:10.4271/2019-01-0569.

70. Park, P. and Keck, J.C., “Rapid compression machine measurements of ignition delays for primary reference fuels,” *SAE Technical Papers*, 1990, doi:10.4271/900027.

71. Mittal, G. and Sung, C.J., “A rapid compression machine for chemical kinetics studies at elevated pressures and temperatures,” *Combustion Science and Technology* 179(3), 2007, doi:10.1080/00102200600671898.

72. Minetti, R., Carlier, M., Ribaucour, M., Therssen, E., and Sochet, L.R., "Comparison of oxidation and autoignition of the two primary reference fuels by rapid compression," *Symposium (International) on Combustion* 26(1), 1996, doi:10.1016/S0082-0784(96)80283-9.

73. Park, P. and Keck, J.C., "Rapid Compression Machine Measurements of Ignition Delay Times for PRD Mixtures," *SAE International Congress & Exposition* 99:11–23, 1990.

74. Griffiths, J.F., Halford-Maw, P.A., and Mohamed, C., "Spontaneous ignition delays as a diagnostic of the propensity of alkanes to cause engine knock," *Combustion and Flame* 111(4), 1997, doi:10.1016/S0010-2180(97)00004-7.

75. Tanaka, S., Ayala, F., Keck, J.C., and Heywood, J.B., "Two-stage ignition in HCCI combustion and HCCI control by fuels and additives," *Combustion and Flame* 132(1–2), 2003, doi:10.1016/S0010-2180(02)00457-1.

76. He, X., Walton, S.M., Zigler, B.T., Wooldridge, M.S., and Atreya, A., "Experimental investigation of the intermediates of isooctane during ignition," *International Journal of Chemical Kinetics* 39(9), 2007, doi:10.1002/kin.20254.

77. Dooley, S., "Autoignition measurements and a validated detailed kinetic model for the combustion of the model biodiesel methyl butanoate," PhD Thesis, National University of Ireland, Galway, 2008.

78. Minetti, R., Ribaucour, M., Carlier, M., and Sochet, L.R., "Autoignition delays of a series of linear and branched chain alkanes in the intermediate range of temperature," *Combustion Science and Technology* 113–114, 1996, doi:10.1080/00102209608935493.

79. Vanhove, G., Petit, G., and Minetti, R., "Experimental study of the kinetic interactions in the low-temperature autoignition of hydrocarbon binary mixtures and a surrogate fuel," *Combustion and Flame* 145(3), 2006, doi:10.1016/j.combustflame.2006.01.001.

80. He, X., Zigler, B.T., Walton, S.M., Wooldridge, M.S., and Atreya, A., "A rapid compression facility study of OH time histories during iso-octane ignition," *Combustion and Flame* 145(3), 2006, doi:10.1016/j.combustflame.2005.12.014.

81. Mittal, G. and Sung, C.J., "Homogeneous charge compression ignition of binary fuel blends," *Combustion and Flame* 155(3), 2008, doi:10.1016/j.combustflame.2008.05.003.

82. Yahyaoui, M., Djebaïli-Chaumeix, N., Dagaut, P., Paillard, C.E., and Gail, S., "Experimental and modelling study of gasoline surrogate mixtures oxidation in jet stirred reactor and shock tube," *Proceedings of the Combustion Institute* 31 I(1), 2007, doi:10.1016/j.proci.2006.07.179.

83. Sakai, Y., Ozawa, H., Ogura, T., Miyoshi, A., Koshi, M., and Pitz, W.J., "Effects of Toluene Addition to Primary Reference Fuel at High Temperature," 2007-01–4104, 2007, doi:10.4271/2007-01-4104.

84. Kahandawala, M.S.P., Corera, S.A.P., Williams, S., Carter, C.D., and Sidhu, S.S., "Investigation of kinetics of iso-octane ignition under scramjet conditions," *International Journal of Chemical Kinetics* 38(3), 2006, doi:10.1002/kin.20155.

85. Davidson, D.F. and Hanson, R.K., "Interpreting shock tube ignition data," *International Journal of Chemical Kinetics* 36(9), 2004, doi:10.1002/kin.20024.

86. Chinnathambi, P., Wadkar, C., Amit, S., Soumya, G., Estefanous, A., Lurun, Z., and Toulson, E., "Impact of CO2 dilution on ignition delay times of full blend gasolines in a rapid compression machine."

87. Sung, C.-J. and Curran, H.J., "Using rapid compression machines for chemical kinetics studies," *Progress in Energy and Combustion Science* 44:1–18, 2014, doi:10.1016/j.pecs.2014.04.001.

88. Kéromnès, A., "Rapid Compression Machines," in: Battin-Leclerc, F., Simmie, J. M., and Blurock, E., eds., *Cleaner Combustion*, Springer London, London, ISBN 978-1-4471-5306-1: 163–181, 2013, doi:10.1007/978-1-4471-5307-8_7.

89. Mittal, G., Chaos, M., Sung, C.J., and Dryer, F.L., "Dimethyl ether autoignition in a rapid compression machine: Experiments and chemical kinetic modeling," *Fuel Processing Technology* 89(12), 2008, doi:10.1016/j.fuproc.2008.05.021.

90. Würmel, J. and Simmie, J.M., "CFD studies of a twin-piston rapid compression machine," *Combustion and Flame* 141(4), 2005, doi:10.1016/j.combustflame.2005.01.015.

91. Lee, D. and Hochgreb, S., "Rapid compression machines: Heat transfer and suppression of corner vortex," *Combustion and Flame* 114(3–4), 1998, doi:10.1016/S0010-2180(97)00327-1.

92. Mittal, G., Raju, M.P., and Sung, C.J., "Vortex formation in a rapid compression machine: Influence of physical and operating parameters," *Fuel* 94, 2012, doi:10.1016/j.fuel.2011.08.034.

93. Mittal, G., Raju, M.P., and Sung, C.J., "CFD modeling of two-stage ignition in a rapid compression machine: Assessment of zero-dimensional approach," *Combustion and Flame* 157(7), 2010, doi:10.1016/j.combustflame.2010.02.019.

94. Lodier, G., Merlin, C., Domingo, P., Vervisch, L., and Ravet, F., "Self-ignition scenarios after rapid compression of a turbulent mixture weakly-stratified in temperature," *Combustion and Flame* 159(11):3358–3371, 2012, doi:10.1016/j.combustflame.2012.07.006.

95. Grogan, K.P., Scott Goldsborough, S., and Ihme, M., "Ignition regimes in rapid compression machines," *Combustion and Flame* 162(8):3071–3080, 2015, doi:10.1016/j.combustflame.2015.03.020.

96. Ihme, M., "On the role of turbulence and compositional fluctuations in rapid compression machines: Autoignition of syngas mixtures," *Combustion and Flame* 159(4):1592–1604, 2012, doi:10.1016/j.combustflame.2011.11.022.

97. Yousefian, S., Quinlan, N.J., and Monaghan, R.F.D., “Simulation of turbulent flow in a rapid compression machine: Large Eddy Simulation and computationally efficient alternatives for the design of ignition delay time experiments,” *Fuel* 234:30–47, 2018, doi:10.1016/j.fuel.2018.06.117.

98. Im, H.G., Pal, P., Wooldridge, M.S., and Mansfield, A.B., “A Regime Diagram for Autoignition of Homogeneous Reactant Mixtures with Turbulent Velocity and Temperature Fluctuations,” *Combustion Science and Technology* 187(8):1263–1275, 2015, doi:10.1080/00102202.2015.1034355.

99. Pal, P., Valorani, M., Arias, P.G., Im, H.G., Wooldridge, M.S., Ciottoli, P.P., and Galassi, R.M., “Computational characterization of ignition regimes in a syngas/air mixture with temperature fluctuations,” *Proceedings of the Combustion Institute* 36(3):3705–3716, 2017, doi:10.1016/j.proci.2016.07.059.

100. Yousefian, S., Gauthier, F., Morán-Guerrero, A., Richardson, R.R., Curran, H.J., Quinlan, N.J., and Monaghan, R.F.D., “Simplified approach to the prediction and analysis of temperature inhomogeneity in rapid compression machines,” *Energy and Fuels* 29(12), 2015, doi:10.1021/ef501961s.

101. Mittal, G. and Bhari, A., “A rapid compression machine with crevice containment,” *Combustion and Flame* 160(12), 2013, doi:10.1016/j.combustflame.2013.06.027.

102. Mittal, G. and Gupta, S., “Computational assessment of an approach for implementing crevice containment in rapid compression machines,” *Fuel* 102, 2012, doi:10.1016/j.fuel.2012.07.026.

103. Mittal, G., Raju, M.P., and Bhari, A., “A numerical assessment of the novel concept of crevice containment in a rapid compression machine,” *Combustion and Flame* 158(12), 2011, doi:10.1016/j.combustflame.2011.04.013.

104. Bourgeois, N., Goldsborough, S.S., Jeanmart, H., and Contino, F., “CFD simulations of Rapid Compression Machines using detailed chemistry: Evaluation of the ‘crevice containment’ concept,” *Combustion and Flame* 189, 2018, doi:10.1016/j.combustflame.2017.10.033.

105. Yousefian, S., Quinlan, N.J., and Monaghan, R.F.D., “Simulation of turbulent flow in a rapid compression machine: Large Eddy Simulation and computationally efficient alternatives for the design of ignition delay time experiments,” *Fuel* 234, 2018, doi:10.1016/j.fuel.2018.06.117.

106. Bourgeois, N., Jeanmart, H., Winckelmans, G., Lamberts, O., and Contino, F., “How to ensure the interpretability of experimental data in Rapid Compression Machines? A method to validate piston crevice designs,” *Combustion and Flame* 198, 2018, doi:10.1016/j.combustflame.2018.09.030.

107. Bourgeois, N., Goldsborough, S.S., Vanhove, G., Duponcheel, M., Jeanmart, H., and Contino, F., “CFD simulations of Rapid Compression Machines using detailed chemistry: Impact

of multi-dimensional effects on the auto-ignition of the iso-octane," *Proceedings of the Combustion Institute* 36(1), 2017, doi:10.1016/j.proci.2016.08.064.

108. Ezzell, J., Wilson, D., and Allen, C., "On the influence of initial conditions and facility effects on rapid compression machine data," *Fuel* 245, 2019, doi:10.1016/j.fuel.2019.01.146.

109. Gentz, G., Thelen, B., Toulson, E., Litke, P., and Hoke, J., "Combustion Visualization, Performance, and CFD Modeling of a Pre-Chamber Turbulent Jet Ignition System in a Rapid Compression Machine," *SAE International Journal of Engines* 8(2):538–546, 2015, doi:10.4271/2015-01-0779.

110. Allen, C., Toulson, E., Edwards, T., and Lee, T., "Application of a novel charge preparation approach to testing the autoignition characteristics of JP-8 and camelina hydroprocessed renewable jet fuel in a rapid compression machine," *Combustion and Flame* 159(9), 2012, doi:10.1016/j.combustflame.2012.03.019.

111. Gentz, G., Gholamisheeri, M., and Toulson, E., "A study of a turbulent jet ignition system fueled with iso-octane: Pressure trace analysis and combustion visualization," *Applied Energy* 189, 2017, doi:10.1016/j.apenergy.2016.12.055.

112. Allen, C., Valco, D., Toulson, E., Edwards, T., and Lee, T., "Ignition behavior and surrogate modeling of JP-8 and of camelina and tallow hydrotreated renewable jet fuels at low temperatures," *Combustion and Flame* 160(2), 2013, doi:10.1016/j.combustflame.2012.10.008.

113. Allen, C., "Advanced rapid compression machine test methods and surrogate fuel modeling for bio-derived jet and diesel fuel autoignition," PhD Thesis, Michigan State University, 2012.

114. Chinnathambi, P., "Experiments on the effects of dilution and fuel composition on ignition of gasoline and alternative fuels in a rapid compression machine," PhD Thesis, Michigan State University, 2019.

115. Horning, D.C., "A study of the high-temperature autoignition and thermal decomposition of hydrocarbons," PhD Thesis, Stanford University, 2001.

116. Darcy, D., Nakamura, H., Tobin, C.J., Mehl, M., Metcalfe, W.K., Pitz, W.J., Westbrook, C.K., and Curran, H.J., "A high-pressure rapid compression machine study of n-propylbenzene ignition," *Combustion and Flame* 161(1), 2014, doi:10.1016/j.combustflame.2013.08.001.

117. Yaws, C., "Chemical Properties Handbook: Physical, Thermodynamics, Environmental Transport, Safety & Health Related Properties for Organic & Inorganic Chemical," McGraw-Hill Education, 1998.

118. Weber, B.W., Kumar, K., Zhang, Y., and Sung, C.J., "Autoignition of n-butanol at elevated pressure and low-to-intermediate temperature," *Combustion and Flame* 158(5), 2011, doi:10.1016/j.combustflame.2011.02.005.

119. Kumar, K., Mittal, G., and Sung, C.J., "Autoignition of n-decane under elevated pressure and low-to-intermediate temperature conditions," *Combustion and Flame* 156(6), 2009, doi:10.1016/j.combustflame.2009.01.009.

120. Das, A.K., Sung, C.J., Zhang, Y., and Mittal, G., "Ignition delay study of moist hydrogen/oxidizer mixtures using a rapid compression machine," *International Journal of Hydrogen Energy* 37(8), 2012, doi:10.1016/j.ijhydene.2012.01.111.

121. Griffiths, J.F., Jiao, Q., Schreiber, M., Meyer, J., and Knoche, K.F., "Development of thermokinetic models for autoignition in a CFD Code: Experimental validation and application of the results to rapid compression studies," *Symposium (International) on Combustion* 24(1), 1992, doi:10.1016/S0082-0784(06)80212-2.

122. Mittal, G., Sung, C.-J., and Yetter, R.A., "Autoignition of H2/CO at elevated pressures in a rapid compression machine," *International Journal of Chemical Kinetics* 38(8):516–529, 2006, doi:10.1002/kin.20180.

123. Mittal, G. and Sung, C.J., "Autoignition of toluene and benzene at elevated pressures in a rapid compression machine," *Combustion and Flame* 150(4), 2007, doi:10.1016/j.combustflame.2007.04.014.

124. Mittal, G. and Sung, C.J., "Autoignition of methylcyclohexane at elevated pressures," *Combustion and Flame* 156(9), 2009, doi:10.1016/j.combustflame.2009.05.009.

125. Weber, B.W., Sung, C.J., and Renfro, M.W., "On the uncertainty of temperature estimation in a rapid compression machine," *Combustion and Flame* 162(6), 2015, doi:10.1016/j.combustflame.2015.03.001.

126. Birch, K., "Good Practice Guide Estimating Uncertainties Testing," *Measurement*, 2003.

127. Würmel, J. and Simmie, J.M., "CFD studies of a twin-piston rapid compression machine," *Combustion and Flame* 141(4):417–430, 2005, doi:10.1016/j.combustflame.2005.01.015.

128. Mittal, G. and Sung, C.-J., "Aerodynamics inside a rapid compression machine," *Combustion and Flame* 145(1–2):160–180, 2006, doi:10.1016/j.combustflame.2005.10.019.

129. Mittal, G., Raju, M.P., and Sung, C.J., "Computational fluid dynamics modeling of hydrogen ignition in a rapid compression machine," *Combustion and Flame* 155(3), 2008, doi:10.1016/j.combustflame.2008.06.006.

130. Goldsborough, S.S. and Potokar, C.J., "The influence of crevice flows and blow-by on the charge motion and temperature profiles within a rapid compression expansion machine used for chemical kinetic (HCCI) studies," SAE Technical Papers, 2007.

131. Mittal, G., Raju, M.P., and Sung, C.-J., "Computational fluid dynamics modeling of hydrogen ignition in a rapid compression machine," *Combustion and Flame* 155(3):417–428, 2008, doi:10.1016/j.combustflame.2008.06.006.

132. Mittal, G., Raju, M.P., and Sung, C.-J., “Vortex formation in a rapid compression machine: Influence of physical and operating parameters,” *Fuel* 94:409–417, 2012, doi:10.1016/j.fuel.2011.08.034.

133. Senecal, P., Richards, K., Pomraning, E., Lee, D., and Rothbauer, R., “CONVERGE CFD Software,” 2008.

134. Lu, T.F. and Law, C.K., “Strategies for mechanism reduction for large hydrocarbons: n-heptane,” *Combustion and Flame* 154(1–2), 2008, doi:10.1016/j.combustflame.2007.11.013.

135. He, Z., Jing, Q., Zhu, L., Zhang, W., and Huang, Z., “The effects of different intake charge diluents on the combustion and emission characteristics of a spark ignition natural gas engine,” *Applied Thermal Engineering* 89, 2015, doi:10.1016/j.applthermaleng.2015.06.072.

136. Marinov, N.M., “A Detailed Chemical Kinetic Model for High Temperature Ethanol Oxidation,” *International Journal of Chemical Kinetics* 31(2–3), 1999, doi:10.1002/(sici)1097-4601(1999)31:3<183::aid-kin3>3.0.co;2-x.

137. Li, J., Chaos, M., Kazakov, A., Dryer, F., and Haas, F., “Personal communication: Ethanol Model v1. 0,” Princeton University, 2009.

138. Kéromnès, A., Metcalfe, W.K., Heufer, K.A., Donohoe, N., Das, A.K., Sung, C.J., Herzler, J., Naumann, C., Griebel, P., Mathieu, O., Krejci, M.C., Petersen, E.L., Pitz, W.J., and Curran, H.J., “An experimental and detailed chemical kinetic modeling study of hydrogen and syngas mixture oxidation at elevated pressures,” *Combustion and Flame* 160(6), 2013, doi:10.1016/j.combustflame.2013.01.001.

139. Metcalfe, W.K., Burke, S.M., Ahmed, S.S., and Curran, H.J., “A hierarchical and comparative kinetic modeling study of C1 - C2 hydrocarbon and oxygenated fuels,” *International Journal of Chemical Kinetics* 45(10):638–675, 2013, doi:10.1002/kin.20802.

140. Zhang, Y., El-Merhubi, H., Lefort, B., Le Moyne, L., Curran, H.J., and Kéromnès, A., “Probing the low-temperature chemistry of ethanol via the addition of dimethyl ether,” *Combustion and Flame* 190, 2018, doi:10.1016/j.combustflame.2017.11.011.

141. Burke, U., Somers, K.P., O’Toole, P., Zinner, C.M., Marquet, N., Bourque, G., Petersen, E.L., Metcalfe, W.K., Serinyel, Z., and Curran, H.J., “An ignition delay and kinetic modeling study of methane, dimethyl ether, and their mixtures at high pressures,” *Combustion and Flame* 162(2), 2015, doi:10.1016/j.combustflame.2014.08.014.

142. Zhou, C.W., Li, Y., Burke, U., Banyon, C., Somers, K.P., Ding, S., Khan, S., Hargis, J.W., Sikes, T., Mathieu, O., Petersen, E.L., AlAbbad, M., Farooq, A., Pan, Y., Zhang, Y., Huang, Z., Lopez, J., Loparo, Z., Vasu, S.S., and Curran, H.J., “An experimental and chemical kinetic modeling study of 1,3-butadiene combustion: Ignition delay time and laminar flame speed measurements,” *Combustion and Flame* 197, 2018, doi:10.1016/j.combustflame.2018.08.006.

143. Burke, S.M., Metcalfe, W., Herbinet, O., Battin-Leclerc, F., Haas, F.M., Santner, J., Dryer, F.L., and Curran, H.J., "An experimental and modeling study of propene oxidation. Part 1: Speciation measurements in jet-stirred and flow reactors," *Combustion and Flame* 161(11), 2014, doi:10.1016/j.combustflame.2014.05.010.

144. Burke, S.M., Burke, U., Mc Donagh, R., Mathieu, O., Osorio, I., Keesee, C., Morones, A., Petersen, E.L., Wang, W., DeVerter, T.A., Oehlschlaeger, M.A., Rhodes, B., Hanson, R.K., Davidson, D.F., Weber, B.W., Sung, C.J., Santner, J., Ju, Y., Haas, F.M., Dryer, F.L., Volkov, E.N., Nilsson, E.J.K., Konnov, A.A., Alrefae, M., Khaled, F., Farooq, A., Dirrenberger, P., Glaude, P.A., Battin-Leclerc, F., et al., "An experimental and modeling study of propene oxidation. Part 2: Ignition delay time and flame speed measurements," *Combustion and Flame* 162(2), 2015, doi:10.1016/j.combustflame.2014.07.032.

145. Zhou, C.W., Li, Y., O'Connor, E., Somers, K.P., Thion, S., Keesee, C., Mathieu, O., Petersen, E.L., DeVerter, T.A., Oehlschlaeger, M.A., Kukkadapu, G., Sung, C.J., Alrefae, M., Khaled, F., Farooq, A., Dirrenberger, P., Glaude, P.A., Battin-Leclerc, F., Santner, J., Ju, Y., Held, T., Haas, F.M., Dryer, F.L., and Curran, H.J., "A comprehensive experimental and modeling study of isobutene oxidation," *Combustion and Flame* 167, 2016, doi:10.1016/j.combustflame.2016.01.021.

146. Li, Y., Zhou, C.W., and Curran, H.J., "An extensive experimental and modeling study of 1-butene oxidation," *Combustion and Flame* 181, 2017, doi:10.1016/j.combustflame.2017.03.023.

147. Li, Y., Zhou, C.W., Somers, K.P., Zhang, K., and Curran, H.J., "The oxidation of 2-butene: A high pressure ignition delay, kinetic modeling study and reactivity comparison with isobutene and 1-butene," *Proceedings of the Combustion Institute* 36(1), 2017, doi:10.1016/j.proci.2016.05.052.

148. Li, J., Kazakov, A., Chaos, M., and Dryer, F.L., "Chemical kinetics of ethanol oxidation," *5th US Combustion Meeting 2007*, 2007.

149. Griffiths, J.F., Clarkson, J., Macnamara, J.P., and Whitaker, B.J., "Temperature fields during the development of combustion in a rapid compression machine," *Combustion and Flame* 125(3):1162–1175, 2001, doi:10.1016/S0010-2180(01)00236-X.

150. Guibert, P., Keromnes, A., and Legros, G., "An experimental investigation of the turbulence effect on the combustion propagation in a rapid compression machine," *Flow, Turbulence and Combustion* 84(1), 2010, doi:10.1007/s10494-009-9225-z.

151. Goldsborough, S.S. and Potokar, C.J., "The Influence of Crevice Flows and Blow-By on the Charge Motion and Temperature Profiles Within a Rapid Compression Expansion Machine Used for Chemical Kinetic (HCCI) Studies," 2007-01–0169, 2007, doi:10.4271/2007-01-0169.

152. Griffiths, J.F., Piazzesi, R., Sazhina, E.M., Sazhin, S.S., Glaude, P.-A., and Heikal, M.R., "CFD modelling of cyclohexane auto-ignition in an RCM," *Fuel* 96:192–203, 2012, doi:10.1016/j.fuel.2011.12.059.

153. Bourgeois, N., Goldsborough, S.S., Vanhove, G., Duponcheel, M., Jeanmart, H., and Contino, F., "CFD simulations of Rapid Compression Machines using detailed chemistry: Impact of multi-dimensional effects on the auto-ignition of the iso-octane," *Proceedings of the Combustion Institute* 36(1):383–391, 2017, doi:10.1016/j.proci.2016.08.064.

154. Mittal, G., Raju, M.P., and Sung, C.-J., "CFD modeling of two-stage ignition in a rapid compression machine: Assessment of zero-dimensional approach," *Combustion and Flame* 157(7):1316–1324, 2010, doi:10.1016/j.combustflame.2010.02.019.

155. Mehl, M., Pitz, W.J., Sjöberg, M., and Dec, J.E., "Detailed kinetic modeling of low-temperature heat release for PRF fuels in an HCCI engine," *SAE Technical Papers*, 2009, doi:10.4271/2009-01-1806.

156. Mehl, M., Curran, H.J., Pitz, W.J., and Westbrook, C.K., "Chemical kinetic modeling of component mixtures relevant to gasoline," United States, 2009.

157. Curran, H.J., Gaffuri, P., Pitz, W.J., and Westbrook, C.K., "A Comprehensive Modeling Study of n-Heptane Oxidation," *Combustion and Flame* 114(1):149–177, 1998, doi:10.1016/S0010-2180(97)00282-4.

158. Griffiths, J.F., Halford-Maw, P.A., and Rose, D.J., "Fundamental features of hydrocarbon autoignition in a rapid compression machine," *Combustion and Flame* 95(3), 1993, doi:10.1016/0010-2180(93)90133-N.

159. Healy, D., Curran, H.J., Simmie, J.M., Kalitan, D.M., Zinner, C.M., Barrett, A.B., Petersen, E.L., and Bourque, G., "Methane/ethane/propane mixture oxidation at high pressures and at high, intermediate and low temperatures," *Combustion and Flame* 155(3), 2008, doi:10.1016/j.combustflame.2008.07.003.

160. Gallagher, S.M., Curran, H.J., Metcalfe, W.K., Healy, D., Simmie, J.M., and Bourque, G., "A rapid compression machine study of the oxidation of propane in the negative temperature coefficient regime," *Combustion and Flame* 153(1–2), 2008, doi:10.1016/j.combustflame.2007.09.004.

161. Somers, K.P., Simmie, J.M., Gillespie, F., Conroy, C., Black, G., Metcalfe, W.K., Battin-Leclerc, F., Dirrenberger, P., Herbinet, O., Glaude, P.A., Dagaut, P., Togbé, C., Yasunaga, K., Fernandes, R.X., Lee, C., Tripathi, R., and Curran, H.J., "A comprehensive experimental and detailed chemical kinetic modelling study of 2,5-dimethylfuran pyrolysis and oxidation," *Combustion and Flame* 160(11), 2013, doi:10.1016/j.combustflame.2013.06.007.

162. Zhao, P. and Law, C.K., "The role of global and detailed kinetics in the first-stage ignition delay in NTC-affected phenomena," *Combustion and Flame* 160(11), 2013, doi:10.1016/j.combustflame.2013.06.009.

163. Wilson, D. and Allen, C., "Application of a multi-zone model for the prediction of species concentrations in rapid compression machine experiments," *Combustion and Flame* 171, 2016, doi:10.1016/j.combustflame.2016.05.018.

164. Goldsborough, S.S., Mittal, G., and Banyon, C., “Methodology to account for multi-stage ignition phenomena during simulations of RCM experiments,” *Proceedings of the Combustion Institute* 34(1), 2013, doi:10.1016/j.proci.2012.05.094.

165. Goldsborough, S.S., Banyon, C., and Mittal, G., “A computationally efficient, physics-based model for simulating heat loss during compression and the delay period in RCM experiments,” *Combustion and Flame* 159(12), 2012, doi:10.1016/j.combustflame.2012.07.010.

166. Griffiths, J.F., Piazzesi, R., Sazhina, E.M., Sazhin, S.S., Glaude, P.-A., and Heikal, M.R., “CFD modelling of cyclohexane auto-ignition in an RCM,” *Fuel* 96:192–203, 2012, doi:10.1016/j.fuel.2011.12.059.